



HAL
open science

**Structures actives dans un fluide visqueux :
modélisation, analyse mathématique et simulations
numériques**

Fabien Vergnet

► **To cite this version:**

Fabien Vergnet. Structures actives dans un fluide visqueux: modélisation, analyse mathématique et simulations numériques. Equations aux dérivées partielles [math.AP]. Université Paris Saclay (COMUE), 2019. Français. NNT : 2019SACLS169 . tel-02194265

HAL Id: tel-02194265

<https://theses.hal.science/tel-02194265v1>

Submitted on 25 Jul 2019

HAL is a multi-disciplinary open access archive for the deposit and dissemination of scientific research documents, whether they are published or not. The documents may come from teaching and research institutions in France or abroad, or from public or private research centers.

L'archive ouverte pluridisciplinaire **HAL**, est destinée au dépôt et à la diffusion de documents scientifiques de niveau recherche, publiés ou non, émanant des établissements d'enseignement et de recherche français ou étrangers, des laboratoires publics ou privés.

NNT : 2019SACLS169

THÈSE DE DOCTORAT

de

L'UNIVERSITÉ PARIS-SACLAY

École doctorale de mathématiques Hadamard (EDMH, ED 574)

Établissement d'inscription : Université Paris-Sud

Laboratoire d'accueil : Laboratoire de mathématiques d'Orsay, UMR 8628 CNRS

Spécialité de doctorat : Mathématiques appliquées

Fabien VERGNET

Structures actives dans un fluide visqueux : modélisation, analyse mathématique et simulations numériques

Soutenue publiquement le : 3 juillet 2019

Après avis des rapporteurs :

ALEXEI LOZINSKI (Université de Franche-Comté)

PHILIPPE PONCET (Université de Pau et des Pays de l'Adour)

Jury de soutenance :

FRANÇOIS ALOUGES (École Polytechnique)

ASTRID DECOENE (Université Paris-Sud)

CÉLINE GRANDMONT (INRIA de Paris)

ALEXEI LOZINSKI (Université de Franche-Comté)

SÉBASTIEN MARTIN (Université Paris Descartes)

BERTRAND MAURY (Université Paris-Sud)

PHILIPPE PONCET (Université de Pau et des Pays de l'Adour)

Président du jury

Codirectrice de thèse

Examinatrice

Rapporteur

Codirecteur de thèse

Codirecteur de thèse, Invité

Rapporteur

Structures actives dans un fluide visqueux :
modélisation, analyse mathématique et
simulations numériques

Fabien Vergnet
Laboratoire de mathématiques d'Orsay
Université Paris Sud, Université Paris Saclay

Thèse soutenue publiquement le 3 juillet 2019

Remerciements

En tout premier lieu, je tiens à exprimer ma profonde gratitude envers mes directeur·rice-s de thèse, Astrid Decoene, Sébastien Martin et Bertrand Maury. Merci pour la confiance que vous m'avez accordée en me confiant cet ambitieux projet de recherche. J'ai énormément appris à vos côtés et je vous remercie pour votre présence, vos conseils et votre enthousiasme. Votre curiosité scientifique et votre ouverture d'esprit resteront une source d'inspiration pour moi.

Une partie de ma thèse a été réalisé en collaboration avec Céline Grandmont. Je te remercie pour tout le temps que tu m'a consacré et les conseils que tu m'as prodigués. J'ai particulièrement apprécié nos discussions et séances de travail et j'espère que ta rigueur et ton intuition mathématique auront un peu déteint sur moi.

Je remercie sincèrement Alexei Lozinski et Philippe Poncet pour l'attention qu'ils ont portée à mes travaux en acceptant de rapporter cette thèse, ainsi que François Alouges et Céline Grandmont qui m'ont fait l'honneur de participer à mon jury.

Pendant ces quelques années, j'ai eu la chance de travailler dans un environnement particulièrement amical et bienveillant. Pour cela, je tiens à remercier toutes celles et ceux qui ont contribué à rendre ce quotidien si agréable. Au laboratoire de mathématiques d'Orsay, je remercie toutes les personnes que j'ai eu le plaisir de côtoyer, notamment les membres de l'équipe ANEDP. En particulier, je remercie Jean-François Babadjian, Blanche Buet, Filipa Caetano, Patrick Gérard, Benjamin Graille, Bernard Héron, Danielle Hilhorst, Jean-Baptiste Lagaert, Hugo Leclerc, Quentin Mérigot, Jean-Marie Mirebeau, Frédéric Rousset, Julien Sabin et Filippo Santambrogio. Au laboratoire de mathématiques appliquées de l'université Paris Descartes, je remercie Rémy Abergel, Flora Alarcon, Andrés Almansa, Étienne Birmelé, Olivier Bouaziz, Michel Boynard, Marc Briant, Thierry Cabanal-Duvillard, Antoine Chambaz, Magali Champion, Fabienne Comte, Maya de Buhan, Manon Defosseux, Julie Delon, Nathalie Eisenbaum, Anne Estrade, Joan Glaunès, Christine Graffigne, Bérénice Grec, Georges Koepfler, Raphaël Lachieze-Rey, Pierre Latouche, Rachid Lounes, Eric Luçon, Nicolas Meunier, Lionel Moisan et Vittorio Perduca.

Les résultats obtenus dans cette thèse sont en partie le fruit de nombreuses discussions et je remercie toutes les personnes qui ont eu la gentillesse de m'accorder un peu de leur temps. En particulier, merci à Sergio Chibbaro, Franz Chouly, Sylvain Faure, Loic Gouarin, Corrado Maurini, Konstantin Pankrashkin, Annie Raoult et Marcela Szopos.

Cette thèse n'aurait pas été possible sans le soutien de l'école doctorale Jacques Hadamard, c'est pourquoi je tiens à remercier Frédéric Lagoutière, Stéphane Nonnenmacher et Frédéric Paulin.

Pour leur aide au quotidien, leur dynamisme et leur efficacité, je remercie également les équipes informatiques et administratives. En particulier, merci à Olivier Chaudet, Jérémy Gosse, Mathilde Rousseau et Estelle Savinien au LMO ainsi qu'à Christophe Castellani, Sandrine Fallu, Marie-Hélène Gbaguidi et Azedine Mani, Arnaud Meunier,

Maureen Némorin, Max Paisley et Isabelle Valero au MAP5.

Un grand merci à tous mes ami.e.s doctorant.e.s, post-doctorant.e.s et stagiaires pour votre enthousiasme permanent ; je n'ai pas vu le temps passer à vos côtés. Merci à tous les doctorants du MAP5, anciens et actuels, pour votre bonne humeur et ces déjeuners-débats sur la terrasse : Sinda, Pierre-Louis, Antoine B., Ismaël, Valentin, Julie, Anton, Nicolas, Antoine H., Claire, Arthur Leclaire, Arthur Leroy, Anne-Sophie, Cambyse, Juliana, Léo, Mariano, Pierre, Ousmane, Vincent et Alexandre. Je remercie tout particulièrement mes collègues de l'équipe modélisation, Andrea, Alessandro, Christèle et Loïc. Nous étions peu mais nous étions bien. Merci également à celles et ceux avec qui j'ai partagé le bureau 750, du stage de M2 à aujourd'hui : Charlotte, Florian, Gwen, Vivien, Warith, Allan, Maud, Safa, Alkéos, Jean, Matias et Yen. Nos discussions éclectiques et passionnées resteront parmi mes meilleurs souvenirs du laboratoire. Enfin, j'ai une pensée toute particulière pour mes co-bureau d'Orsay. Merci à Fatima, Pierre, Guillaume, Clémentine, Samer, Magda, Perla, Hugo, Guilherme, Antonin, Paul, Anthony et Clément. Merci pour cette ambiance amicale et chaleureuse et pour tous ces bons moments passés ensemble.

Bien que mes remerciements seront toujours en deçà de la dette véritablement due, je souhaite remercier mes ami.e.s et ma famille qui me soutiennent depuis toutes ces années et qui se reconnaîtront. Merci à mes camarades de Centrale (ou presque) avec qui j'ai vécu tant d'agréables moments. Merci à mes amis d'enfance, qui ont toujours été présents à mes côtés. Merci à toute ma famille, sans qui cette aventure aurait été bien difficile. Merci à Marie, Adélaïde, Justine et Marc.

Enfin, mes remerciements les plus sincères vont à la France. Cette thèse, entièrement financée par le ministère de l'enseignement supérieur et de la recherche, n'est que le témoignage de l'attention toute particulière dont j'ai pu profiter en tant que citoyen français.

Sommaire

1	Introduction	1
2	A continuum active structure model for the interaction of cilia with a viscous fluid	29
3	Existence and uniqueness for a quasi-static interaction problem between a viscous fluid and an active structure	63
4	A smooth extension method for transmission problems	89
5	Conclusion et perspectives	133
A	Proofs of theorems related to the smooth extension method	137
B	Transformation of the Stokes equations into the reference configuration	149
	Bibliography	157
	Contents	165
	List of Figures	169
	List of Tables	173

Chapitre 1

Introduction

Le but de cette thèse est l'étude mathématique de l'interaction entre des structures élastiques allongées et actives (modélisant typiquement des cils ou des flagelles) et un fluide visqueux. Ce sujet est abordé sous trois aspects. Le premier est celui de la modélisation de ces structures actives dans le contexte de la théorie des milieux continus et en prenant en compte les effets hydrodynamiques du fluide de façon directe et précise. En particulier nous considérons les équations aux dérivées partielles qui régissent les deux milieux fluide et solide et les couplons par des conditions de transmission physiques à l'interface fluide-structure. Le deuxième aspect est celui de l'étude mathématique du système fluide-structure résultant de cette modélisation. Dans ce manuscrit l'existence et l'unicité de solutions à des problèmes fluide-structure quasi-statiques et stationnaires (pour l'étude de problèmes discrétisés en temps) sont prouvées sous certaines hypothèses de petitesse, notamment concernant l'activité interne des structures considérées. Enfin, le troisième aspect est celui de la simulation numérique directe de ces phénomènes. Pour cela, nous nous plaçons dans le contexte de la méthode des éléments finis. Une méthode itérative sur maillages conformes est d'abord considérée pour la simulation de structures actives dans un fluide visqueux puis, une méthode sur maillages non conformes qui préserve l'ordre optimal de convergence est développée pour quelques modèles de problèmes de transmission.

Dans ce chapitre introductif, nous nous consacrons à la présentation du contexte et des motivations de cette étude. Après un bref aperçu de la vie à faible nombre de Reynolds, un monde étrange où les effets inertiels sont presque inexistant, nous nous arrêtons sur plusieurs modèles développés depuis les années 1950 pour modéliser l'interaction entre les cils et flagelles eucaryotes et le fluide visqueux environnant. De cet état de l'art nous ferons alors le constat suivant. Un nombre impressionnant de travaux traitent de la modélisation de l'activité interne des cils et les résultats, quel que soit le modèle utilisé, sont souvent très réalistes. Néanmoins, la modélisation de l'interaction fluide-structure est, en revanche, régulièrement délaissée, nombre d'auteurs se concentrant davantage sur l'approximation de l'action du cil sur le fluide ainsi que de la rétro-action du fluide sur le cil, cette dernière n'étant d'ailleurs par toujours considérée. Dans cette thèse, nous avons donc cherché à réconcilier la modélisation des moteurs internes des cils et l'interaction avec le fluide environnant, afin de construire un modèle qui représente au mieux la complexité de ce système biologique et hydrodynamique.

1.1 Sur la vie à bas nombre de Reynolds

À l'échelle du micromètre, les lois physiques qui régissent les déplacements de micro-organismes dans un fluide sont bien différentes de celles qui agissent à l'échelle humaine.

Alors qu'un poisson utilise essentiellement les effets inertiels pour "glisser" dans l'eau entre deux battements de nageoires, les bactéries, spermatozoïdes et autres organismes munis de cils ou de flagelles microscopiques, vivent dans un monde régi par les effets purement visqueux. En mécanique des fluides, cette différence de régime se met en évidence au travers du nombre de Reynolds, que nous allons maintenant introduire.

1.1.1 Mécanique des fluides à bas nombre de Reynolds

Pour un fluide newtonien incompressible de masse volumique $\rho > 0$ et de viscosité $\mu > 0$ constantes, soumis à des forces volumiques extérieures f , sa vitesse u et sa pression p vérifient les équations de Navier-Stokes

$$\begin{aligned} \rho \left(\frac{\partial u}{\partial t} + u \cdot \nabla u \right) - \mu \Delta u + \nabla p &= f, \\ \operatorname{div}(u) &= 0, \end{aligned}$$

auxquelles il convient d'ajouter des conditions aux limites et des conditions initiales appropriées. Considérons un nageur immergé dans le fluide, de taille et vitesse caractéristiques L et U . Il est alors possible d'adimensionner ces équations de Navier-Stokes, en introduisant les variables sans dimensions \tilde{u} , \tilde{p} , \tilde{t} et \tilde{f} , définies par

$$\tilde{u} = \frac{u}{U}, \quad \tilde{p} = \frac{L^2 p}{\mu U}, \quad \tilde{t} = \frac{U t}{L}, \quad \tilde{f} = \frac{L f}{\mu U}.$$

On obtient les équations de Navier-Stokes adimensionnées :

$$\begin{aligned} \operatorname{Re} \left(\frac{\partial \tilde{u}}{\partial \tilde{t}} + \tilde{u} \cdot \nabla \tilde{u} \right) - \Delta \tilde{u} + \nabla \tilde{p} &= \tilde{f}, \\ \operatorname{div}(\tilde{u}) &= 0, \end{aligned}$$

où Re est le nombre de Reynolds, définie par

$$\operatorname{Re} = \frac{\rho L U}{\mu}.$$

Ce nombre de Reynolds peut d'abord s'interpréter comme le rapport entre le terme d'inertie des équations de Navier-Stokes, qui se comporte comme $\rho u \cdot \nabla u$, et le terme visqueux, $\mu \Delta u$. Un faible nombre de Reynolds (typiquement $\operatorname{Re} < 1$) correspond donc à un régime où les effets visqueux du fluide dominent les effets inertiels.

Deuxièmement, le nombre de Reynolds peut également se définir en termes de rapport de forces s'exerçant sur le solide immergé dans le fluide. Les contraintes visqueuses que le fluide impose au solide sont données par le tenseur des contraintes du fluide, noté $\sigma_f = \mu(\nabla u + \nabla u^T) - pI$, où I est la matrice identité. Nous en déduisons alors les forces visqueuses qui s'exercent sur le solide par intégration du tenseur des contraintes sur la surface du solide S :

$$f_{\text{visqueuses}} = \int_S \sigma_f n,$$

où n est le vecteur unitaire normale à la surface S . Par analyse dimensionnelle, il vient pour les forces visqueuses $f_{\text{visqueuses}} \sim \mu U L$. D'un autre côté les forces inertiels, sont données par la masse du solide multipliée par son accélération, c'est-à-dire $f_{\text{inertiels}} \sim \rho U^2 L^2$. On remarque alors que le nombre de Reynolds peut également s'écrire

$$\operatorname{Re} = \frac{f_{\text{inertiels}}}{f_{\text{visqueuses}}}.$$

Avec cette définition, un faible nombre de Reynolds est alors caractéristique d'un régime dans lequel les forces inertielles qui s'exercent sur le solide sont faibles par rapport aux forces visqueuses.

Une troisième interprétation d'un régime à bas nombre de Reynolds peut être faite en termes de distance parcourue par le solide à cause des effets inertiels. Supposons qu'un nageur de masse m immergé dans le fluide s'arrête brusquement de nager. Il va alors subir une décélération qui dépend de sa masse et des forces de résistance du fluide qui s'exercent sur lui. À bas nombre de Reynolds ces forces se résument aux forces visqueuses, comme nous l'avons vu précédemment. La décélération du solide est donc proportionnelle à $\frac{f_{visqueuse}}{m}$ et sa distance parcourue est de l'ordre de $d \sim \frac{m}{\rho L^2} \text{Re}$, qui peut également s'écrire en fonction de la masse volumique du solide ρ_s :

$$d \sim \frac{\rho_s L}{\rho} \text{Re}.$$

Le nombre de Reynolds peut donc être interprété comme la distance adimensionnée parcourue par le solide lorsqu'il s'arrête de nager, relativement à sa taille caractéristique L .

Considérons par exemple de l'eau ($\rho \approx 10^3 \text{kg} \cdot \text{m}^{-3}$ et $\mu \approx 10^{-3} \text{kg} \cdot \text{m}^{-1} \cdot \text{s}^{-1}$ à 25°C). Pour un nageur humain ($L \approx 1\text{m}$ et $U \approx 1\text{m} \cdot \text{s}^{-1}$), le nombre de Reynolds sera de l'ordre de 10^6 , alors que pour une bactérie ($L \approx 10\mu\text{m}$ et $U \approx 100\mu\text{m} \cdot \text{s}^{-1}$), il sera plutôt de l'ordre de 10^{-4} . Pour un nombre de Reynolds aussi petit il convient alors d'étudier la limite $\text{Re} = 0$, pour laquelle les équations de Navier-Stokes prennent la forme des équations de Stokes :

$$\begin{aligned} -\mu \Delta u + \nabla p &= f, \\ \text{div}(u) &= 0. \end{aligned}$$

La prédominance de ces effets visqueux, qui se traduit mathématiquement par la linéarité et la stationnarité des équations de Stokes, a pour conséquence que toutes les stratégies de nage qui nous semblent familières à notre échelle sont inefficaces à l'échelle microscopique. À titre d'exemple, Ludwig ([Ludwig, 1930]) mit en évidence en 1930 qu'un micro-rameur (un micro-robot possédant deux bras qui battent symétriquement de chaque côté de son corps) est incapable de se déplacer efficacement dans un fluide où les effets visqueux sont prédominants, méthode pourtant bien adaptée à notre échelle, où les effets inertiels sont prépondérants. Au contraire, dans une série d'expériences menées dans les années 1960, Taylor ([Taylor, 1967]) illustra l'efficacité de la nage hélicoïdale à faible nombre de Reynolds, que l'on retrouve chez certains micro-organismes. Afin de se déplacer efficacement à bas nombre de Reynolds, ces micro-organismes ont donc dû mettre au point des techniques beaucoup plus sophistiquées. Deux propriétés importantes ont notamment été mises en évidence par Purcell, dont la première peut se formuler de la façon suivante :

Propriété 1.1 ([Purcell, 1977]). *Pour un solide qui se déforme dans un fluide de Stokes entre deux instants, la distance parcourue par le nageur entre ces deux instants ne dépend pas de la vitesse de déformation mais dépend uniquement de la séquence des déformations.*

Cette propriété est due à l'absence d'effets inertiels dans le fluide à bas nombre de Reynolds, qui se traduit par une réponse instantanée du fluide aux changements de formes du micro-nageurs. Cela signifie en particulier que l'étude des battements d'un cil dans un fluide visqueux peut être abordée uniquement d'un point de vue géométrique. La deuxième propriété mise en évidence par Purcell est le fameux *théorème de la coquille Saint-Jacques* :

Théorème 1.1 (dit de la coquille Saint-Jacques [Purcell, 1977]). *Si un solide se déforme dans un fluide de Stokes avec une séquence de déformations périodique et qui, de plus, est identique par inversion du temps (on parle alors de déformations réciproques), alors le solide n'est pas capable de se déplacer en moyenne.*

Ce résultat est caractéristique des fluides à faible nombre de Reynolds et est dû à la linéarité et la stationnarité des équations de Stokes. En effet, leur linéarité implique que si u est une solution associée à des forces externes f , alors $-u$ est une solution associée aux forces $-f$. De plus, la stationnarité des équations de Stokes se traduit par une réponse instantanée du fluide aux déformations du micro-nageur. Ainsi, inverser les forces revient à inverser les lignes de courant de la vitesse du fluide et le système retourne dans son état initial. En conséquence, la nage de micro-organismes se doit de briser la symétrie temporelle des équations de Stokes en adoptant des déformations non-réciproques. Dans son article, Purcell illustre cette propriété avec une coquille saint-Jacques qui cherche à se déplacer uniquement en ouvrant et en fermant sa coquille. Dans ce cas, une séquence périodique de déformations est donnée par l'ouverture puis la fermeture de la coquille et il s'agit bien de déformations réciproques au sens où une inversion du temps donne exactement la même séquence de déformations. Alors, la coquille saint-Jacques n'est pas capable de nager avec un déplacement net puisqu'elle revient toujours à sa position initiale après une période de déformations. Bien sûr, une vraie coquille saint-Jacques utilise énormément les effets inertiels pour se déplacer et nage donc dans un régime où le nombre de Reynolds est élevé, pour lequel le théorème de Purcell ne s'applique pas. Néanmoins, ce théorème montre que pour se déplacer efficacement, les micro-nageurs doivent engendrer des déformations non réciproques et c'est bien ce qu'on observe dans la nature, avec des battements asymétriques, des ondulations ou des mouvements hélicoïdaux, que nous allons présenter dans la suite.

Dans cette étude, nous nous intéressons exclusivement aux organismes dont le mouvement est produit par des cils et des flagelles mais précisons tout de même que d'autres moyens de locomotion existent. Nous pouvons par exemple citer le cas du *spriroplasma*, une bactérie hélicoïdale qui se déplace par contraction de son cytosquelette ([Berg, 2002]).

1.1.2 Zoologie des déformations des cils et flagelles

Ces structures allongées que sont les cils et les flagelles sont présentes aussi bien chez les végétaux que chez les champignons ou les animaux et apparaissent comme un mécanisme de transport universel à l'échelle microscopique. Dans la Figure 1.1 sont représentées quelques micro-organismes possédant des cils et des flagelles (dans le disque central) entourées des congénères de leurs espèces respectives. Procaryotes ou eucaryotes, protozoaires, algues ou champignons, la propulsion à l'aide de cils ou de flagelles se retrouve à toutes les échelles de la biosphère, des bactéries jusqu'aux poumons des mammifères. Le terme *flagelle* est souvent utilisé pour désigner les structures très allongées qui interviennent dans la nage de certains organismes (comme chez les spermatozoïdes ou chez la bactérie *Eschirichia coli*) et qui ont parfois un mouvement hélicoïdal, alors que le terme cil est généralement employé pour des structures moins longues dont les déformations consistent en un battement asymétrique (comme chez l'algue *Chlamydomonas reinhardtii* ou les cils bronchiques). Néanmoins, ces deux définitions ne sont pas mutuellement exclusives et nous ne ferons donc pas de différence entre cils et flagelles dans cette thèse, où l'appellation *cil* sera souvent privilégiée. Ce qui nécessite cependant une distinction, ce sont les différences de déformations observées entre les cils procaryotes, qui sont de simples filaments mis en rotation par un moteur externe, et les cils eucaryotes, qui possèdent une structure bien plus complexe et se déforme grâce à des moteurs internes situés tout le long de leur structure.

L'exemple type de micro-nageur procaryote est celui de la bactérie *Eschirichia coli*. Son système de propulsion est constitué de plusieurs filaments inertes, d'un diamètre d'environ 20nm et d'une longueur de $10\mu\text{m}$, entraînés dans un mouvement hélicoïdal par un moteur rotatif. L'accroche entre les filaments et le moteur s'effectue à l'aide d'un crochet. Lorsque le moteur se met en marche les filaments se mettent à tourner dans le sens horaire



FIGURE 1.1 – Aperçu général de quelques micro-organismes possédant des cils ou des flagelles et autres organismes associés. Image tirée de [Lighthill, 1976]. Les micro-organismes possédant des cils sont représentés à l'intérieur du cercle au centre de la figure.

et s'entremêlent pour former comme un câble de filaments, ce qui permet à la bactérie de se propulser à quelques $25 - 35 \mu\text{m} \cdot \text{s}^{-1}$. Quand le moteur s'arrête, les filaments se séparent et la bactérie se met à vaciller avant de repartir dans une autre direction. D'autres bactéries comme *Caulobacter crescentus* ne possèdent qu'un seul filament accroché à son moteur rotatif, qui peut tourner dans les deux sens, lui permettant à la fois de se propulser ou de se tracter dans le fluide environnant.

Les cils eucaryotes sont plus épais que les flagelles de bactéries, avec un diamètre d'environ 200nm. Leur longueur peut en revanche varier de $5 \mu\text{m}$ pour les cils bronchiques à plusieurs dizaines, voir centaines de micromètres pour les flagelles de spermatozoïdes. La principale caractéristique des cils eucaryotes est de pouvoir se déformer d'eux-mêmes avec des mouvements parfois très différents suivant les espèces. Par exemple, les spermatozoïdes de nombreux organismes vivants sont constitués d'une tête contenant le matériel génétique propulsé par un flagelle, dont les mouvements peuvent être planaires ou hélicoïdaux suivant les espèces. *Chlamydomonas reinhardtii* (Figure 1.2b), est une micro-algue qui possède deux flagelles qui lui permettent de nager avec un mouvement semblable à celui de la brasse. La paramécie (*Paramecium*) est un organisme couvert de cils qui se déplace à des vitesses de l'ordre de $500 \mu\text{m} \cdot \text{s}^{-1}$ ([Tawada and Oosawa, 1972]). Enfin, les cils bronchiques (Figure 1.2a), présents sur les parois des bronches des mammifères, battent avec un mouvement asymétrique et de façon synchronisée, mettant en mouvement les fluides environnant (comme le mucus bronchique). Ce mouvement asymétrique peut se décomposer en deux phases : une phase dite *effective* pendant laquelle le cil bat en restant le plus droit possible afin de pousser au maximum le fluide dans sa direction de battement et une phase dite *de récupération* pendant laquelle le cil retourne à sa position initiale en se courbant le plus possible afin de limiter son action sur le fluide. Comme nous le verrons dans la prochaine section, plusieurs études ont mis en évidence que cette stratégie était parfaitement adaptée au transport du fluide environnant dans la direction de battement du cil lors de sa phase effective. Ce phénomène est d'ailleurs d'une importance capitale dans le bon fonctionnement du système respiratoire, puisqu'il permet de nettoyer les poumons de toutes les impuretés qui ont pu être respirées.

Étant donné leur caractère universel et leur implication dans de nombreux phénomènes biologiques et physiques, les cils eucaryotes ont été au cœur de nombreux travaux scientifiques dont le but est la compréhension des mécanismes internes permettant cette diversité de déformations.

1.1.3 Mécanismes de déformation des cils eukaryotes

Les cils motiles eucaryotes ont une structure étonnamment semblable au vu des nombreux mouvements que l'on observe chez différentes espèces. Les principaux composants des cils sont les *microtubules*, des structures filamentaires couramment présentes dans les cellules eucaryotes, qui peuvent se représenter comme de longs cylindres d'un diamètre d'environ 25nm. L'agencement de plusieurs de ces microtubules forme un cytosquelette cylindrique appelé *axonème*, entouré d'une membrane plasmique ; le tout forme le cil eucaryote. La coupe transversale d'un cil est représentée dans la Figure 1.3, où l'on observe une structure caractéristique des cils eucaryotes, que l'on retrouve souvent sous le nom de structure "9+2" dans la littérature. Au centre se trouve une paire de microtubules entourée d'une gaine de protection, qui forment l'axe centrale de l'axonème. En périphérie de la structure se trouvent neuf doublets de microtubules (formés de deux microtubules couramment nommés A et B), reliés à l'axe central par des connexions radiales qui rigidifient la structure afin que la section reste circulaire. Les doublets de microtubules sont également reliés entre eux par des filaments élastiques appelés *nexine* qui contribuent aussi à la rigidité de la section,

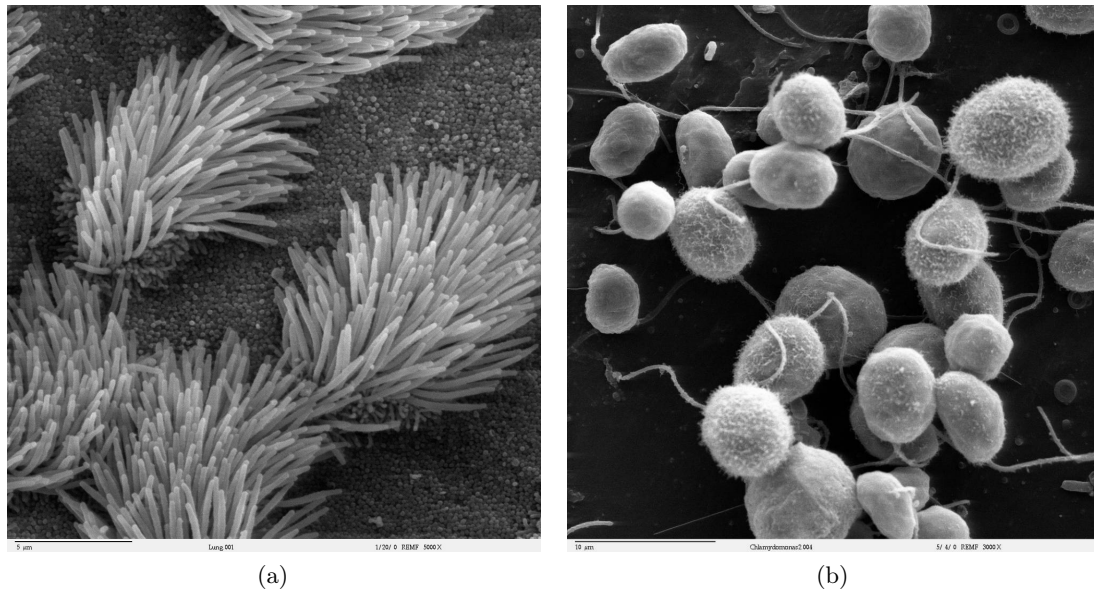


FIGURE 1.2 – Cils bronchiques (a) et *Chlamydomonas reinhardtii* (b).

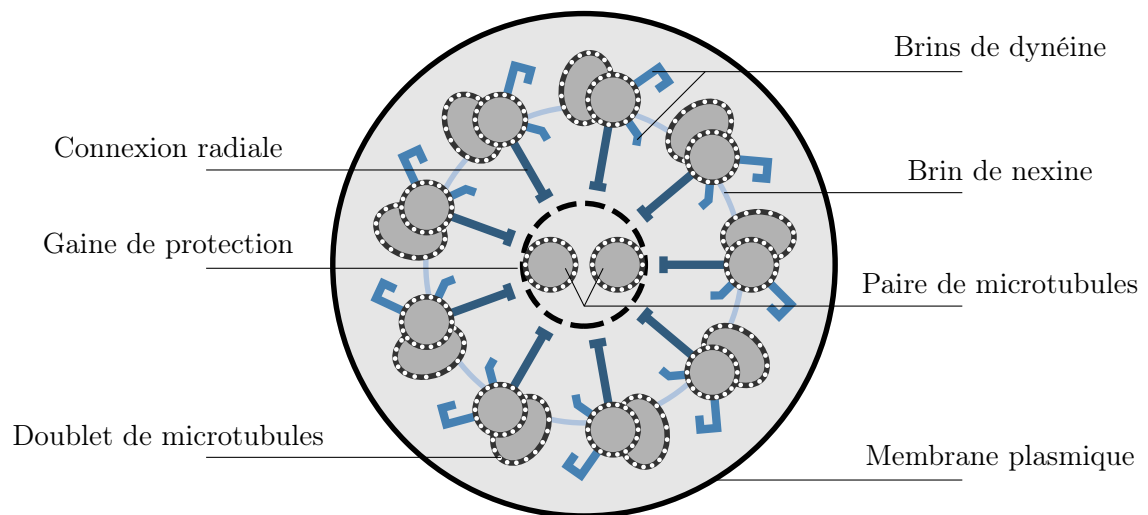


FIGURE 1.3 – Schéma représentant la coupe transversale d'un cil eucaryotes.

tout en laissant une certaine mobilité à la structure. Les déformations des cils proviennent d'un effet de cisaillement qui a lieu entre deux doublets de microtubules adjacents et dont une autre protéine, la *dynéine*, est responsable. Des brins de dynéine sont synthétisés par les microtubules A et migrent vers les microtubules B des doublets voisins pour s'y accrocher. C'est alors la succession d'accrochages et de décrochages de ces protéines tout le long des microtubules qui génère un mouvement de cisaillement entre les deux doublets de microtubules. Comme ces doublets sont ancrés à leur base, il en résulte un mouvement de courbure, qui entraîne toute la structure. Ce phénomène de migration et d'accrochage des brins de dynéine a lieu tout le long des neuf doublets de microtubules et est à l'origine des diverses déformations que l'on observe chez les cils eucaryotes. Néanmoins, la nature précise (aussi bien spatiale que temporelle) de ce phénomène de contrôle interne dont la dynéine et le moteur nous est encore inconnue.

1.1.4 Motivations et applications

Les raisons d'étudier les cils eucaryotes et leurs interactions avec le fluide environnant sont nombreuses. Hormis l'incroyable diversité des mécanismes de nage de ces micro-organismes et la beauté des problèmes mathématiques qui en ressortent, qui justifient déjà l'intérêt des chercheurs pour ce problème, les applications médicales et industrielles sont presque illimitées.

Les cils et flagelles sont présents dans presque tous les organes des êtres humains ([Wheatley et al., 1996]) et participent activement à de nombreux processus biologiques comme au fonctionnement du système respiratoire, au transport du fluide cérébro-spinal et aux mécanismes de reproduction. Un dysfonctionnement de motilité de ces structures ou une modification des propriétés physiques du fluide environnant peuvent donc avoir des conséquences désastreuses sur la santé ou la reproduction d'un individu. La dyskinésie ciliaire primitive est une maladie génétique qui provoque un défaut de motilité chez les cils, ce qui peut engendrer de mauvais fonctionnements du système respiratoire, du système rénale et être à l'origine de l'infertilité ([Afzelius and Eliasson, 1983]). Dans le système respiratoire, des maladies comme l'asthme ([Laitinen et al., 1985]) ou la grippe ([Camner et al., 1983]) entraînent une réduction du nombre de cils bronchiques, ce qui met en déroute le transport des fluides environnants. La mucoviscidose est une maladie génétique affectant les épithéliums glandulaires de nombreux organes et qui entraîne notamment une augmentation de la viscosité des mucus présents dans les voies respiratoires et digestives. Avec l'augmentation de la viscosité du fluide, l'action des cils sur le transport du fluide est alors plus limitée. La modélisation, l'étude mathématique et la simulation numérique de ces structures actives en interaction avec des fluides visqueux pourraient aider à mieux comprendre le rôle que jouent les cils dans ces différentes maladies.

En ingénierie, la conception de micro-nageurs artificiels est également un enjeu majeur, notamment pour des applications médicales. Plusieurs modèles de micro-robots théoriques ont été proposés et étudiés mathématiquement ([Taylor, 1967], [Purcell, 1977], [Alouges and Di Fratta, 2018]) et récemment, le premier prototype de micro-nageur artificiel a été construit ([Dreyfus et al., 2005]). De quelques micromètres, il est composé d'un filament paramagnétique attaché à un globule rouge, qui se déforme sous l'action d'un champ magnétique externe et permet le transport du globule rouge. En particulier, de tels micro-robots pourraient permettre le transport de médicaments et le traitement localisé de certaines maladies.

1.2 Modélisation mathématique des cils et flagelles

1.2.1 Le modèle historique de Taylor

En 1951, Taylor se posa la question de savoir comment est-ce qu'un micro-organisme est capable de nager en utilisant uniquement les forces visqueuses ([Taylor, 1951]). Il étudia alors un problème de Stokes dont les conditions aux limites sont données par les déformations d'une surface plane infinie, représentant le flagelle d'un micro-nageur (vu en deux dimensions). En considérant que la surface se déforme par la propagation d'une onde transverse de faible amplitude et que la vitesse du fluide est nulle loin de la structure, Taylor mit en évidence le déplacement à vitesse constante de la structure dans la direction opposée à la direction de propagation de l'onde. Le cas où le fluide est présent des deux côtés de la surface est également étudié et mène à la même conclusion. Dans cet article, Taylor réalise un développement limité de la condition limite (car l'amplitude est considérée petite) et résout le problème de Stokes ordre par ordre, ce qui est possible grâce à la linéarité des équations de Stokes. Les généralisations de ce travail, pionnier dans l'étude de la nage des micro-organismes, sont nombreuses. Dans [Taylor, 1952], le cas d'un cylindre infini déformé par la propagation d'une onde transverse est considéré. Ici, la différence est qu'il faut tenir compte du rayon du cylindre dans le développement limité de la condition limite, mais les résultats sur la vitesse de déplacement du micro-nageur sont similaires. Ce travail est intéressant pour la modélisation de micro-nageurs car il permet de reproduire des déformations réalistes de flagelles en trois dimensions (comme des mouvements hélicoïdaux) par superposition d'ondes transverses déphasées. Dans [Blake, 1971a], les cas de la surface infinie et du cylindre infini déformés par la propagation d'ondes transverses et longitudinales sont également traités.

Une extension du travail de Taylor à des objets de tailles finies a été abordée par Lighthill afin de modéliser la nage de micro-organismes recouverts de cils, comme la paramécie ([Lighthill, 1952]). Le micro-nageur est modélisé par une sphère déformable dont les déformations sont dues à la propagation d'une onde sur sa surface. L'auteur suppose en fait que les cils à la surface de la paramécie sont si denses que leurs sommets forment une surface oscillante : c'est la *modèle de l'enveloppe*. Par suite, une amélioration des résultats de Lighthill est proposée dans [Blake, 1971b].

Dans tous ces travaux, les déformations des cils sont imposées et l'interaction avec le fluide est prise en compte de façon approchée en supposant les déformations d'assez faible amplitude, afin d'obtenir une estimation de la vitesse de nage du solide en fonction du scénario de déformations prescrit comme une condition limite du problème fluide.

1.2.2 Les débuts de l'étude du mouvement des cils

Lorsque les déformations sont plus importantes d'autres approximations ont été développées au fil des années, comme la *resistive force theory* et la *slender body theory*. La *resistive force theory* suppose que la force locale exercée par le cil sur le fluide est proportionnelle à la vitesse locale du cil et que le coefficient de proportionnalité est donné par le coefficient de traînée. Pour des structures élancées comme les cils, qui possèdent une longueur bien supérieure à leur épaisseur, une approximation de ce coefficient de traînée peut être obtenue en approchant les cils par une succession d'ellipsoïdes et en utilisant la propriété de linéarité des équations de Stokes. Ainsi, la force exercée par un cil sur le fluide peut-être modélisée par une force linéique placée le long de l'axe centrale du cil dont l'intensité est proportionnelle à la vitesse du cil. Cette idée, développée dans [Gray and Hancock, 1955], a ensuite été reprise dans plusieurs travaux afin d'étudier la propulsion de micro-organismes et les battements

asymétriques des cils. Néanmoins, Lighthill met en évidence dans [Lighthill, 1976] que l'hypothèse de proportionnalité entre la force locale engendrée par le cil et sa vitesse locale n'est pas valide à bas nombre de Reynolds, puisque la prédominance des effets visqueux produit des interactions hydrodynamiques à longue portée, qui ne sont pas prises en compte par la *resistive force theory*.

La *slender body theory*, initiée dans [Hancock, 1953], revisitée dans [Lighthill, 1976] et [Shen et al., 1975], puis améliorée dans [Johnson, 1977], permet de prendre en compte les interactions à longue distance. Comme dans la *resistive force theory*, l'idée est d'approcher l'action du cil sur le fluide par une force linéique bien choisie. Dans le cas de la *slender body theory*, cette force vérifie cette fois une équation intégrale qui prend en compte les effets non locaux dus aux effets visqueux. Une comparaison entre la *resistive force theory* et la *slender body theory* est réalisée dans [Johnson and Brokaw, 1979] : la *slender body theory* permet d'obtenir des résultats plus réalistes en tenant compte des déformations locales des structures. Néanmoins, la *slender body theory* peut être plus difficile à mettre en place, puisqu'elle nécessite parfois la résolution d'une équation intégrale afin d'obtenir les intensités des forces ponctuelles associées à la vitesse du cil.

Ces deux méthodes permettent notamment d'obtenir de façon approchée la vitesse et la pression d'un fluide soumis aux effets des déformations de cils et flagelles, dont les déplacements sont imposés. Formellement, on peut remplacer l'action du cil sur le fluide par une distribution de forces ponctuelles (des forces de Dirac) dont l'intensité est à déterminer. Avec la *resistive force theory*, considérant l'hypothèse que les forces locales engendrées par les cils sont proportionnelles à leurs vitesses locales, les intensités de ces forces ponctuelles sont alors entièrement déterminées par la vitesse locale du cil. Si l'on souhaite utiliser la *slender body theory*, l'obtention des intensités des forces ponctuelles nécessite par contre de prendre en compte les déformations locales du cils ou de résoudre une équation intégrale, dont la solution peut être approchée numériquement par la résolution d'un système linéaire. Ensuite, par linéarité des équations de Stokes, la vitesse et la pression du fluide qui résultent de l'action de ces forces de Dirac sont données par la superposition de solutions fondamentales associées, que nous allons expliciter. Soit f_0 une force ponctuelle (vectorielle) appliquée en un point x_0 du fluide, la solution fondamentale des équations de Stokes associée à cette force de Dirac est alors donnée par

$$\begin{aligned} u(x, f_0) &= \frac{1}{8\pi\mu} \left(\frac{1}{|x - x_0|} I + \frac{1}{|x - x_0|^3} (x - x_0) \otimes (x - x_0) \right) f_0, \\ p(x, f_0) &= \frac{1}{4\pi|x - x_0|^3} (x - x_0) \cdot f_0, \end{aligned}$$

où I est la matrice identité et l'opérateur \otimes représente le produit tensoriel entre deux vecteurs. La solution fondamentale en vitesse, u , est communément appelée *Stokeslet* associée au Dirac f_0 et au point x_0 . Ainsi, la vitesse du fluide engendrée par les effets additionnés de toutes les forces ponctuelles dues aux cils est la somme de toutes les Stokeslets engendrées individuellement par chaque force ponctuelle. Comme nous le verrons dans la prochaine sous-section, cette méthode des Stokeslets a donné lieu à de nombreux travaux numériques concernant l'étude des mouvements des cils dans des fluides visqueux.

1.2.3 Modèles à mouvement imposé

Avec les développements de la *resistive force theory*, de la *slender body theory* et de la méthode des Stokeslets, de nombreux travaux se sont intéressés à la modélisation et la simulation numérique de cils ou flagelles à mouvements imposés interagissant avec un fluide visqueux. Dans [Dresdner et al., 1980], la nage d'un micro-nageur ne possédant qu'un

flagelle est étudié. Les déformations du flagelle sont imposées et deux motifs sont étudiés : d'abord des déformations sinusoïdales, puis des déformations dont l'amplitude augmente en s'éloignant de la tête du micro-nageur, qui représentent de façons plus réalistes les ondulations observées pour certains flagelles de spermatozoïdes. L'interaction avec le fluide environnant est prise en compte par la méthode des Stokeslets et l'intensité des forces ponctuelles est obtenue par la *slender body theory* en résolvant une équation intégrale par une méthode itérative. Par des méthodes similaires, des déformations hélicoïdales du flagelle d'un micro-nageur sont étudiées dans [Higdon, 1979].

Dans [Fulford and Blake, 1986], les auteurs étudient le transport mucociliaire dans les poumons, c'est-à-dire l'interaction entre les cils bronchiques et le fluide environnant. À partir d'observations expérimentales ([Sanderson and Sleight, 1981]), ils proposent une paramétrisation du battements des cils sous la forme d'une série de Fourier tronquée dont les coefficients sont obtenus par la méthode des moindres carrés. Les cils sont modélisés par des filaments en une dimension dont la distribution de forces est approchée en utilisant la *resistive force theory* et les effets sur le fluide sont étudiés numériquement en considérant jusqu'à cent cils battant dans le fluide. Plus récemment cette paramétrisation des cils bronchiques a été utilisée dans [Ding et al., 2014], afin d'étudier les effets de transport et de mélange du fluide engendrés par l'activité des cils. Pour la résolution numérique, l'effet de chaque cil sur le fluide est approché par une distribution de forces ponctuelles régularisées dont la taille de la zone d'application est de l'ordre du diamètre d'un cil. La vitesse et la pression du fluide sont toujours approchées par la superposition de solutions particulières aux équations de Stokes, appelées ici *Stokeslets régularisées*, associées à ces forces ponctuelles régularisées, dont l'intensité est obtenue par la *slender body theory* (pour la méthode des Stokeslets régularisées voir [Cortez, 2001]).

Dans [Lacouture, 2016], l'auteur utilise également la paramétrisation des cils bronchiques de [Fulford and Blake, 1986] en considérant une distribution de forces ponctuelles sur les cils dont l'intensité est obtenue par la *slender body theory*. Dans ce travail, la méthode des Stokeslets n'est pas utilisée mais un problème de Stokes (en bi-fluide) soumis à des forces de Dirac est résolu de façon directe par la méthode des éléments finis. L'analyse numérique du problème est menée par des estimations d'erreurs locales et des résultats de convergence locale quasi-optimale sont obtenus. Des applications au transport mucociliaire sont également étudiées numériquement en considérant des forêts de plusieurs centaines de cils.

D'autres auteurs se sont également intéressés à la résolution du problème d'interaction fluide-structure sans approcher les effets des cils sur le fluide par des forces ponctuelles (comme c'est le cas avec la méthode des Stokeslets) mais plutôt en imposant la continuité des vitesses au travers de l'interface fluide-structure. En effet, cette condition est une condition de transmission physique et usuelle pour des problèmes fluide-structure avec des fluide visqueux. Néanmoins les déplacements des cils sont toujours imposés et l'action du fluide sur les cils n'est toujours pas prise en compte.

Dans [Chatelin, 2013] et [Chatelin and Poncet, 2016] le cil est modélisé par un cylindre en trois dimensions dont les déplacements le long de l'axe central vérifient une équation d'advection en une dimension. La paramétrisation du cil ainsi obtenue est qualitativement proche de la paramétrisation de [Fulford and Blake, 1986], définie à partir de données expérimentales. Le fluide entourant les cils est modélisé par un fluide newtonien à faible nombre de Reynolds dont la viscosité est variable et dépend de la concentration d'une protéine présente dans le fluide. La vitesse et la pression du fluide vérifient les équations de Stokes et la viscosité du fluide vérifie une équation de convection-diffusion. La condition de continuité des vitesses entre les cils et le fluide est prise en compte par pénalisation dans les

équations de Stokes et la résolution numérique de ce problème est réalisée par des méthodes utilisant un algorithme de transformée de Fourier rapide (FFT). Ces méthodes permettent une étude détaillée de l'influence des différents paramètres du modèle sur l'efficacité du transport du fluide par les battements des cils.

Dans [Dauplain et al., 2008], les cils sont modélisés par des filaments en une dimension et la méthode des frontières immergées ([Peskin, 2002]) est utilisée afin d'imposer la condition de continuité des vitesses au travers de l'interface fluide-structure. Comme dans la méthode des Stokeslets, il s'agit d'introduire une distribution de forces dans le problème fluide, mais qui dépend cette fois de la différence entre la vitesse du cil et la vitesse du fluide en un point donné du cil. Ici en particulier, cette méthode des frontières immergées est très semblable à une méthode de pénalisation sur la vitesse du fluide. Il est important de remarquer que dans cette étude les équations de Navier-Stokes sont considérées à la place des équations de Stokes, pour des raisons techniques concernant le solveur fluide utilisé. C'est également le cas dans [Chateau et al., 2017], où les équations modélisant le fluide sont résolues avec la méthode de Boltzmann sur réseau qui ne permet pas de traiter les équations de Stokes. Dans ce travail, les cils sont représentés comme des structures en une dimension qui battent dans un bi-fluide et dont les déformations sont imposées et proviennent de la résolution de l'équation d'advection introduite dans [Chatelin, 2013]. Néanmoins, une amélioration, qui permet de considérer (en partie) la rétro-action du fluide sur les cils, est proposée. Cette modification consiste à moduler la vitesse des cils en fonction des efforts exercés par le fluide environnant. Cependant, l'action du fluide sur les cils n'est pas complètement prise en compte car seules les vitesses de déformations des cils sont modifiées ; leur séquence de déformations reste, en revanche, toujours la même. Numériquement, les effets des cils sur le fluide sont pris en compte en imposant la continuité des vitesses fluide et structure par la méthode des frontières immergées, tandis que la rétro-action du fluide sur un cil est prise en compte en modifiant la vitesse du cil par une vitesse qui dépend de la force exercée par le fluide sur le cil. Cette modification de la vitesse du cil est modulée par un paramètre qui contrôle l'intensité de la rétro-action : plus ce paramètre est petit moins les cils sont soumis aux effets du fluide environnant. Dans cette étude, des effets de synchronisation sont mis évidence entre les battements des cils et les effets sur le transport du fluide environnant sont étudiés.

Pour finir, rappelons que tous les travaux présentés dans cette sous-section considèrent des cils dont les déformations sont imposées et ne subissent aucunement les effets du fluide environnant (dans [Chateau et al., 2017] la vitesse des cils est modifiée par l'action du fluide environnant mais le cycle de déformations est imposé). Néanmoins, la modélisation de l'activité interne des cils eucaryotes a également été au centre de nombreux travaux scientifiques, qui ont permis de comprendre davantage les mécanismes d'interaction hydrodynamiques qui entrent en jeu dans ce système.

1.2.4 Modélisation de l'activité interne des cils

À notre connaissance, Machin fut le premier à étudier mathématiquement les mécanismes de déformations internes des cils eucaryotes. Dans son travail précurseur de 1958 ([Machin, 1958]), un cil est modélisé comme un filament élastique immergé dans un fluide visqueux dont le déplacement vérifie une équation de poutre en une dimension. Le fluide environnant n'est pas modélisé, mais son action sur le cil est prise en compte de façon approchée en utilisant les forces données par la *resistive force theory*, qui viennent contrebalancer les forces élastiques du cil. L'idée novatrice de Machin est de modéliser l'activité du cil par l'ajout d'un moment de courbure actif dans les équations du déplacement du cil. Comme expliqué dans son article, ce moment de courbure peut être vu comme l'action d'éléments contractiles

situés de part et d'autre de la structure et qui, en se contractant ou en s'allongeant, déforme le cil. Cette idée de modéliser l'activité des cils par les déformations élastiques d'éléments contractiles est d'ailleurs au centre de notre étude, comme nous le verrons au Chapitre 2.

Ce mécanisme de contractilité a été repris dans [Brokaw, 1966], où un cil est modélisé par une paire de filaments contractiles verticaux ancrés à leur base et reliés par des ressorts horizontaux répartis tout le long des filaments. Ces deux filaments peuvent se contracter ou s'allonger. Comme ils sont reliés l'un à l'autre et ancrés au sol, si l'un des deux filaments se contracte l'autre est entraîné avec lui et cette action engendre la déformation de toute la structure dans un mouvement de courbure. Comme dans [Machin, 1958], ce travail met en évidence que des mécanismes de contractilité locaux peuvent engendrer des déformations à l'échelle de toute la structure du cil. Un modèle similaire en trois dimensions pour un cil de longueur infinie est développé dans [Lubliner and Blum, 1971] en considérant une géométrie proche de la structure de l'axonème du cil eucaryote (la structure "9 + 2"). Dans cet article, le mécanisme de contraction des filaments est contrôlé par une équation différentielle modélisant la propagation d'une entité chimique supposée induire la contraction des filaments. Les effets de la viscosité du fluide sur les déformations de la structure sont étudiées, ce qui n'avait pas été pris en compte dans [Brokaw, 1966], et il est observé que la vitesse de propagation de l'onde diminue avec l'augmentation de la viscosité du fluide. Ce travail est néanmoins limité à des déformations de faible amplitude.

Par suite, plusieurs modèles ont été proposés afin d'expliquer, dans le cas de grandes déformations, l'origine des mécanismes de battements des cils eucaryotes. Le cil est modélisé par une poutre dont les déplacements vérifient une équation en une dimension, obtenue à partir d'un bilan des forces s'exerçant sur le cil : les forces venant du fluide environnant, les forces élastiques provenant de la composante passive de la structure et les forces dues à l'activité du cil. Les effets du fluide sont généralement pris en compte de façon approchée en utilisant la *resistive force theory* ou la *slender body theory*. Les forces élastiques dépendent des modèles considérés et peuvent inclure de la résistance à l'élongation et de la résistance à la flexion. Quant à l'activité interne des cils, elle est modélisée par des forces de cisaillement, qui représentent les mouvements de cisaillement qui sont observés entre deux doublets de microtubules à la périphérie de l'axonème. Cependant, les mécanismes de contrôle agissant sur ces forces de cisaillement diffèrent suivant les modèles.

Dans [Brokaw, 1971], l'activité du cil est décrite par des forces de cisaillement qui sont contrôlées par la courbure locale de la structure. Ce modèle a donné lieu à une classe de modèles pour les cils eucaryotes, que l'on nomme *modèles à contrôle par courbure* (*curvature-controlled models* en anglais) et qui ont été étudiés par exemple dans [Brokaw, 1972], [Hines and Blum, 1978] et [Brokaw, 1985]. Avec ce modèle, les déformations planaires comme les ondulations des flagelles de spermatozoïdes sont bien reproduites. En revanche, les battements de cils bronchiques ou de paramécie ne le sont pas car ce modèle n'est pas capable de générer des séquences de battements pendant lesquelles une partie du cil est droite (c'est-à-dire à courbure nulle). Néanmoins, une extension de ce modèle dans [Brokaw, 2002] a mis en évidence la capacité de cette classe de modèles à générer des mouvements hélicoïdaux.

La deuxième classe de modèles engendrée par ces modèles de poutres est celle des *modèles auto-oscillants* (*self-oscillatory models* en anglais), qui supposent qu'un cil est un filament élastique entouré d'éléments contractiles qui ont des propriétés d'élasticité particulières : leur tension réagit à des changements de longueur avec un retard en temps. Ce modèle a été introduit dans [Machin, 1958] et [Machin, 1963], puis étudié également dans [Brokaw, 1975] et dans [Brokaw, 2005]. Dans ces articles, il a été mis en évidence que ces modèles reproduisent assez fidèlement les déformations observées chez les flagelles et les

cils, mais uniquement en introduisant un terme de viscosité dans les équations modélisant la structure élastique.

Parmi ces modèles de poutres, une autre approche est employée dans [Gueron and Levit-Gurevich, 1998] où l'activité interne des cils est également modélisée par des forces de cisaillement, mais dont le scénario est déterminé à partir de données expérimentales. Ce modèle plus phénoménologique permet néanmoins d'observer des déformations similaires aux déformations des cils bronchiques ou des cils de paramécie par exemple. La vitesse et la pression du fluide sont approchées à l'aide de la méthode des Stokeslets et la rétro-action du fluide sur le cil est prise en compte au travers de la *slender body theory*. Concernant l'activité du cil, les forces de cisaillement sont imposées dans les deux phases de battement du cil (la phase effective et la phase de récupération), néanmoins, le passage d'une phase à l'autre se fait par un critère purement géométrique, qui porte sur la courbure ou l'inclinaison de la structure. Les résultats obtenus sont également cohérents avec les expériences : les auteurs observent une décroissance de la fréquence de battement lorsque la viscosité du fluide augmente ainsi que des phénomènes de synchronisation entre deux cils.

Bien d'autres résultats existent concernant ces modèles de poutres actives pour les cils eucaryotes, mais aujourd'hui encore aucun n'est assez satisfaisant pour modéliser toute la diversité des déformations des cils eucaryotes. Pour les lecteurs intéressés, un aperçu détaillé de ces différentes méthodes est donné dans [Murase, 1992].

Plus récemment, plusieurs travaux se sont intéressés à la modélisation des mécanismes internes des cils en prenant en compte la paire centrale de microtubules, les neuf doublets de microtubules et les différentes protéines qui constituent la structure des cils eucaryotes.

Dans [Dillon and Fauci, 2000] une description discrète de la structure du cil est proposée en deux dimensions d'espace. Un cil est composé de deux microtubules qui consistent chacun en deux filaments élastiques reliés par un nombre fini de connexions élastiques diagonales très rigides. Les deux microtubules sont également reliés entre eux par un nombre fini de ressorts, représentant les brins de nexine, assez élastiques pour permettre le cisaillement des deux structures. Les brins de dynéine, moteurs des déformations sont modélisés par des ressorts donc la longueur de référence est plus petite que la distance entre les deux microtubules. Ces brins de dynéine n'ont pas de position fixe dans la structure. Ils s'attachent au microtubule voisin, se contractent et se détachent suivant un scénario géométrique qui engendre du cisaillement entre les deux microtubules. À l'interface fluide-structure, (c'est-à-dire sur les deux filaments les plus à l'extérieur de la structure) la continuité des vitesses fluide et structure est imposée. Numériquement, cette condition est traitée à l'aide de la méthode des frontières immergées. Il en résulte que les déformations engendrées sont qualitativement proches de celles observées par exemple dans les battements asymétriques des cils bronchiques. Ce modèle est également utilisé dans [Dillon et al., 2003] pour la modélisation des déformations de flagelles de spermatozoïdes, dans [Yang et al., 2008] pour l'étude de la synchronisation entre quelques cils et dans [Lukens et al., 2010] pour l'étude du transport et du mélange induit par un cil dans le fluide environnant.

Un modèle en trois dimensions d'espace est construit dans [Gueron and Levit-Gurevich, 2001] avec une représentation précise de la structure "9+2". Les doublets de microtubules et la paire de microtubules centrale sont modélisés par des filaments élastiques vérifiant une équation de poutre similaire à celle introduite dans [Gueron and Levit-Gurevich, 1998]. Les actions des connexions radiales (entre les doublets de microtubules et la paire de microtubules centrale), des brins de nexine (entre doublets de microtubules) et des brins de dynéine (entre doublets de microtubules également) sont modélisées par des distributions de forces volumiques élastiques. L'activité du cil est prise en compte au travers d'un modèle mécanico-chimique qui modélise l'attachement et le détachement des brins de dynéine au

doublet de microtubules voisin. La vitesse et la pression du fluide sont obtenues en utilisant la méthode des Stokeslets et la rétro-action du fluide sur le cil provient de la *slender body theory*. Un travail similaire est réalisé dans [Mitran, 2007] à la différence que le scénario de forces lié à l'action des brins de dynéine est imposé et que le problème fluide est plus détaillé et est résolu de manière directe avec la méthode des volumes finis. Dans ces deux travaux, les déformations des structures observées sont assez proches des déformations réelles des cils et des effets de synchronisation sont observés entre cils.

Enfin, une approche complètement différente est de laisser les cils adapter leurs déformations afin de trouver le battement le plus efficace d'un point de vue énergétique. Cette méthode a notamment été étudiée dans [Osterman and Vilfan, 2011] et [Eloy and Lauga, 2012] pour l'étude des déformations des cils bronchiques et dans [Lauga and Eloy, 2013] pour celle des flagelles de spermatozoïdes. Dans ces trois articles les déformations obtenues sont semblables aux déformations des cils et flagelles réels.

1.2.5 Étude mathématique de problèmes d'interaction fluide-structure avec structures actives

Comme nous l'avons vu, dans la majorité des travaux cités précédemment l'interaction fluide-structure entre les cils et le fluide visqueux n'est pas complètement prise en compte. En effet, soit le problème fluide est résolu de façon approchée, soit l'action du fluide sur la structure n'est pas (ou partiellement) considérée. Du point de vue de l'analyse mathématique, il en résulte que le problème d'interaction fluide-structure pour les cils et flagelles dans sa généralité la plus complète, c'est-à-dire avec une modélisation à la fois de l'activité interne des cils et d'un couplage fluide-structure fort, est un problème ouvert. Néanmoins, quelques résultats d'existence et d'unicité existent pour d'autres problèmes qui font également intervenir des structures actives et des fluides homogènes, visqueux et incompressibles.

Pour un solide autopropulsé de forme constante se déplaçant dans un fluide homogène et incompressible modélisé soit par les équations de Stokes, soit par les équations de Navier-Stokes non inertielles, Galdi démontre dans [Galdi, 1999] un résultat d'existence pour ce problème d'interaction fluide-structure stationnaire. Pour cela, l'auteur se place dans le référentiel du solide et impose la vitesse du fluide sur l'interface fluide-structure comme étant égale à la vitesse d'autopropulsion du micro-nageur. Dans ce référentiel, la vitesse du fluide loin du solide correspond alors à la vitesse de déplacement du micro-nageur dans le référentiel du laboratoire, qui résulte à la fois de l'autopropulsion du nageur et des interactions hydrodynamiques avec le fluide. Du point de vue de la théorie du contrôle, Galdi met également en évidence l'existence d'un espace de contrôle pour la vitesse d'autopropulsion qui permet de lier la vitesse de nage du micro-nageur à sa vitesse d'autopropulsion distribuée sur l'interface fluide-structure. Pour une vitesse de nage donnée, il prouve l'existence d'une unique vitesse d'autopropulsion qui minimise le travail nécessaire pour propulser le solide.

Pour un solide déformable, le problème de la nage d'un poisson dans un fluide modélisé par les équations de Navier-Stokes en deux dimensions d'espace est étudié dans [San Martín et al., 2008]. Dans cet article, et ce sera d'ailleurs le cas également dans les articles que nous citerons dans ce paragraphe, le déplacement de la structure est divisé en deux parties : une partie sous forme de mouvement rigide, qui résulte de l'interaction avec le fluide environnant, et une partie sous forme de déformations, qui est imposée. Avec ce formalisme, un résultat d'existence et d'unicité de solutions fortes globales en temps (tant que le solide ne touche pas le bord du domaine) est ainsi prouvé. Pour le même modèle mais en trois dimensions d'espace, un résultat d'existence et d'unicité de solutions faibles globales en temps (tant

que le solide ne touche pas le bord du domaine) est établi dans [Nečasová et al., 2011]. Dans [Court, 2017], avec des hypothèses de régularité plus faibles sur les déformations imposées à la structure, un résultat d’existence et d’unicité de solutions fortes est prouvé, localement en temps pour toutes données et globalement en temps (tant que le solide ne touche pas le bord du domaine) pour des données petites.

Pour un solide élastique dont les déformations ne sont pas imposées mais résultent de l’interaction entre l’activité interne et les propriétés élastiques de la structure d’une part et les effets visqueux du fluide environnant d’autre part, aucune étude mathématique n’a, à notre connaissance, été réalisée.

1.2.6 Positionnement de la thèse

Les travaux regroupés dans cette thèse portent sur l’étude de problèmes d’interaction fluide-structure mettant en jeu des structures allongées, élastiques et actives, capables de se déformer d’elles-mêmes grâce à des moteurs internes, et un fluide newtonien homogène et incompressible. Comme nous l’avons vu précédemment, les modèles mathématiques et méthodes numériques utilisés pour étudier ce système sont nombreux et variés. Néanmoins, pour comprendre davantage les mécanismes biologiques et hydrodynamiques qui entrent en jeu dans ce phénomène de transport à l’échelle microscopique, il est nécessaire de développer des modèles où l’interaction fluide-structure est prise en compte de manière complète.

Afin d’essayer de répondre à cette problématique, nous proposons un modèle pour les cils qui s’inscrit dans le cadre de la mécanique des milieux continus. Ce développement se base sur des modèles popularisés en bio-mécanique ([Payan and Ohayon, 2017]) et qui n’ont, à notre connaissance, ni été étudiés mathématiquement, ni été utilisés pour la modélisation de micro-organismes. Avec ce modèle d’*élasticité active*, le cil est représenté en deux ou trois dimensions d’espace et son interaction avec le fluide environnant s’effectue au niveau de l’interface fluide-structure, au travers de conditions de transmission physiques qui y sont imposées. En particulier, des conditions usuelles sont la continuité de la vitesse et la continuité de la composante normale des contraintes surfaciques.

Le système d’équations aux dérivées partielles couplées obtenu, avec les équations de l’élasticité active d’une part et les équations de Stokes d’autre part, est ensuite étudié mathématiquement. Pour le problème stationnaire, issu de la discrétisation en temps des équations, des résultats d’existence et d’unicité de solutions faibles sont démontrés sous une hypothèse de petitesse concernant l’activité interne de la structure. Pour le problème quasi-statique, lorsque l’évolution des domaines fluide et structure est continue en temps, un résultat d’existence et d’unicité de solutions fortes locales en temps est prouvé, à condition que les données du problème soient suffisamment petites.

Du point de vue de la résolution numérique, nous nous plaçons dans le contexte de la simulation directe, à l’aide de la méthode des éléments finis. Les méthodes numériques considérées dans cette thèse sont de deux natures. Premièrement nous développons une méthode à maillage conforme qui permet la résolution précise du problème. Pour cela la formulation faible des équations fluide et structure est réécrite sous forme d’un problème point-selle, dans lequel les conditions de transmission à l’interface fluide-structure sont traitées par multiplicateurs de Lagrange. Sous cette forme, le problème est alors approché numériquement à l’aide d’éléments finis usuels. Deuxièmement, nous présentons une méthode à maillage non conforme pour la résolution de quelques problèmes de transmission, qui a l’avantage de s’affranchir de tous les problèmes de remaillage liés aux grands déplacements de la structure et qui, de plus, préserve l’ordre de convergence optimal de la méthode des éléments finis à maillage conforme.

1.3 Résultats principaux

1.3.1 Chapitre 2 : un modèle de mécanique des milieux continus pour la modélisation de l'interaction de cils avec un fluide visqueux

Dans le Chapitre 2, nous présentons les équations de l'*élasticité active*, popularisées en bio-mécanique (voir [Payan and Ohayon, 2017]), que nous adaptons pour la modélisation de cils eucaryotes battant dans un fluide à faible nombre de Reynolds. Notons Ω_s l'ouvert de dimension n (typiquement deux ou trois), borné et de frontière lipschitzienne, dont la fermeture représente le domaine de l'espace occupé par le cil dans sa position de référence, et supposons que sa frontière est divisée en deux parties disjointe Γ et Γ_s . En introduisant d_s , le déplacement de la structure, le problème de l'élasticité active avec des conditions aux limites de Dirichlet s'écrit alors :

$$\left\{ \begin{array}{l} \text{pour tout } t \geq 0, \text{ trouver } d_s(t) : \Omega_s \rightarrow \mathbb{R}^n \text{ tel que} \\ -\text{div}((I + \nabla d_s(t))(\Sigma_s(d_s(t)) - \Sigma^*(t))) = f_s(t), \quad \text{dans } \Omega_s, \\ d_s(t) = 0, \quad \text{sur } \Gamma_s. \end{array} \right. \quad (1.1)$$

De plus, il convient d'ajouter des conditions aux limites sur la frontière Γ lorsque ce problème d'élasticité est couplé à un problème fluide. Comme dans les équations non linéaires de l'élasticité, nous retrouvons le second tenseur de Piola-Kirchhoff, Σ_s , qui modélise les contraintes élastiques (passives) internes de la structure, ainsi que des forces volumiques extérieures, f_s , qui s'exercent sur le cil. Dans cette thèse nous nous restreignons à l'étude de solides élastiques dont la loi de comportement est donnée par la loi de Saint Venant-Kirchhoff,

$$\begin{aligned} \Sigma_s(d_s(t)) &= 2\mu_s E(d_s(t)) + \lambda_s \text{tr}(E(d_s(t)))I, \\ E(d_s(t)) &= \frac{1}{2}(\nabla d_s(t) + \nabla d_s(t)^T + \nabla d_s(t)^T \nabla d_s(t)), \end{aligned} \quad (1.2)$$

où μ_s et λ_s sont les coefficients de Lamé et I est la matrice identité. Ici, nos équations diffèrent des équations de l'élasticité classiques par l'ajout d'un tenseur de *contraintes actives*, noté Σ^* . Pour la modélisation des cils eucaryotes, ces contraintes actives sont écrites comme des contraintes de cisaillement afin de modéliser les forces internes dues à l'activité des de la dynéine. Avec des scénarios en temps bien choisis pour le tenseur Σ^* , qui dépend de l'espace et du temps, nous sommes alors capables de reproduire des déformations réalistes de cils ou de flagelles. Des exemples sont présentés dans la Sous-section 2.2.4. Le caractère bien-posé du problème d'élasticité active stationnaire avec des conditions aux limites de Dirichlet non-homogènes (sur Γ et Γ_s) est étudié dans la Section 3.4.

Dans la Section 2.3, notre modèle fluide-structure est introduit en couplant les équations de l'élasticité active avec les équations de Stokes, qui modélisent le fluide visqueux, homogène et incompressible environnant. Les conditions de couplage usuelles pour ce type de problèmes sont la continuité des vitesses fluide et structure au travers de l'interface Γ (car le fluide est considéré visqueux) et la continuité de la composante normale des contraintes surfaciques. La principale difficulté dans l'écriture et l'étude de problèmes fluide-structure réside dans le fait que les deux problèmes ne sont pas définis dans les mêmes configurations. En effet, le problème d'élasticité est écrit dans le domaine de référence de la structure alors que les équations de Stokes sont classiquement définies dans le domaine courant, c'est-à-dire dans le domaine déformé à un instant donné. De plus, cette déformation du domaine fluide, que l'on notera Φ , dépend du déplacement de la structure.

Notons Ω_f l'ouvert borné, connexe et de frontière lipschitzienne dont la fermeture représente le domaine occupé par le fluide. Sa frontière est divisée en deux parties : Γ , l'interface

fluide-structure et Γ_f , où sont appliquées diverses conditions aux limites. Introduisons l'opérateur de trace de Ω_s sur l'interface Γ , noté γ_Γ , et \mathcal{R} , un opérateur de relèvement de Γ dans Ω_f . La déformation du domaine fluide à un instant $t \geq 0$ peut alors s'écrire

$$\Phi(d_s(t)) = \mathcal{I} + \mathcal{R}(\gamma_\Gamma(d_s(t))), \quad \text{dans } \Omega_f,$$

en supposant que le relèvement $\mathcal{R}(\gamma_\Gamma(d_s(t)))$ est nul sur la frontière extérieure Γ_f . Avec ces notations, les équations de Stokes s'écrivent alors, à un instant $t \geq 0$, dans le domaine fluide déformé $\Phi(d_s(t))(\Omega_f)$,

$$\begin{aligned} -\operatorname{div}(\sigma_f(u_f(t), p_f(t))) &= f_f(t), & \text{dans } \Phi(d_s(t))(\Omega_f), \\ \operatorname{div}(u_f(t)) &= 0, & \text{dans } \Phi(d_s(t))(\Omega_f), \end{aligned}$$

où σ_f représente le tenseur des contraintes du fluide, et auxquelles il convient d'ajouter des conditions aux limites sur la frontière extérieure déformée $\Phi(d_s(t))(\Gamma_f)$.

Concernant les conditions de transmission à l'interface fluide-structure, il convient, par changement de variables dans les équations de Stokes, de les écrire sur Γ , c'est-à-dire dans la configuration de référence du système. Il vient alors

$$\begin{aligned} \frac{\partial d_s(t)}{\partial t} &= w_f(t), & \text{sur } \Gamma, \\ (I + \nabla d_s(t))(\Sigma_s(d_s(t)) - \Sigma^*(t))n_s &= \Pi_f(w_f(t), q_f(t))n_s, & \text{sur } \Gamma, \end{aligned} \quad (1.3)$$

où w_f , q_f et Π_f représentent réciproquement la vitesse du fluide, la pression du fluide et les contraintes du fluide, toutes trois écrites dans la configuration de référence. Le vecteur n_s est le vecteur unitaire normal à la frontière de Ω_s .

Dans la Sous-section 2.3.3, après une discrétisation en temps du problème fluide-structure défini précédemment, nous introduisons et étudions la formulation faible du problème stationnaire associé, en se restreignant pour la structure à un problème d'élasticité linéarisée. Pour une discrétisation en temps $(t_k)_{k \in \mathbb{N}}$ à intervalle constant $\delta t > 0$, nous définissons les inconnues du problème discrétisées en temps, pour tout $k \in \mathbb{N}$,

$$d_s^k = d_s(t_k), \quad u_f^k = u_f(t_k), \quad p_f^k = p_f(t_k), \quad \Omega_f^k = \Phi(d_s^{k-1})(\Omega_f), \quad \text{et} \quad \Gamma_f^k = \Phi(d_s^{k-1})(\Gamma_f).$$

Nous introduisons également les espaces fonctionnels

$$\begin{aligned} V_s &= \{v \in (H^1(\Omega_s))^n; \gamma_{\Gamma_s}(v) = 0\}, \\ W_u &= \left\{ (v_f, v_s) \in V_f^k \times V_s; \gamma_\Gamma(v_f \circ \Phi(d_s^{k-1})) = \gamma_\Gamma(v_s) \right\}, \\ W_d &= \left\{ (v_f, d_s) \in V_f^k \times V_s; \delta t \gamma_\Gamma(v_f \circ \Phi(d_s^{k-1})) + d_s^{k-1} = \gamma_\Gamma(d_s) \right\}, \end{aligned}$$

où V_f^k est un sous-espace de Hilbert de $(H^1(\Omega_f^k))^n$ pour la vitesse du fluide, qui contient les conditions aux limites de Dirichlet considérées. La formulation faible du problème d'interaction fluide-structure stationnaire, avec structure active, s'écrit alors

$$\left\{ \begin{array}{l} \text{trouver } (u_f^k, d_s^k) \in W_d \text{ et } p_f^k \in L^2(\Omega_f^k) \text{ tels que} \\ \int_{\Omega_f^k} \sigma_f(u_f^k, p_f^k) : \nabla v_f + \int_{\Omega_s} (\sigma_s(d_s^k) - \nabla d_s^k \Sigma_k^*) : \nabla v_s \\ \qquad \qquad \qquad = \int_{\Omega_f^k} f_f^k \cdot v_f + \int_{\Omega_s} f_s^k \cdot v_s - \int_{\Omega_s} \Sigma_k^* : \nabla v_s, \quad \forall (v_f, v_s) \in W_u, \\ \int_{\Omega_f^k} q_f \operatorname{div}(u_f^k) = 0, \quad \forall q_f \in L^2(\Omega_f^k), \end{array} \right. \quad (1.4)$$

où σ_s est le tenseur des contraintes élastiques linéarisées et f_f^k , f_s^k et Σ_k^* sont les données du problème discrétisées en temps. Nous démontrons alors le résultat d'existence et d'unicité qui suit.

Théorème 1.2. *Soit $k \geq 0$. Supposons que f_f^k appartient à $(L^2(\Omega_f^k))^n$, f_s^k à $(L^2(\Omega_s))^n$, d_s^{k-1} à V_s et Σ_k^* à $(L^\infty(\Omega_s))^{n \times n}$. Si Σ_k^* vérifie la condition*

$$\|\Sigma^*\|_{L^\infty(\Omega_s)} < \mu_s, \quad (1.5)$$

alors il existe une unique solution au problème (1.4).

La preuve du Théorème 1.2 se fait en reformulant le problème (1.4) en “vitesse-vitesse”, à la place de la formulation en “vitesse-déplacement” introduite précédemment, ce qui est possible par linéarité du problème. Nous reconnaissons dans cette formulation un problème point-selle, dont l’étude consiste à montrer la continuité et la coercivité d’une forme bilinéaire, la continuité d’une forme linéaire et la surjectivité d’un opérateur linéaire et continu. En particulier, c’est la condition de petitesse (1.5) qui permet de prouver la coercivité de la forme bilinéaire. Le point technique de la preuve concerne la surjectivité de l’opérateur associé à la contrainte de divergence nulle de la vitesse du fluide, démontrée à l’aide d’un résultat de surjectivité concernant l’opérateur divergence et dû à Bogovskii ([Bogovski, 1979]).

Dans la Sous-section 2.3.4, nous introduisons une nouvelle formulation du problème, motivée par notre volonté d’approcher numériquement la solution de ce problème. Encore une fois, il s’agit d’un problème point-selle, mais dans lequel la contrainte d’incompressibilité de la vitesse du fluide et celle de l’égalité des vitesses sur l’interface fluide-structure sont traitées à l’aide de multiplicateurs de Lagrange. Ce problème s’écrit

$$\left\{ \begin{array}{l} \text{trouver } u_f^k \in V_f^k, p_f^k \in L^2(\Omega_f^k), d_s^k \in V_s \text{ et } \lambda^k \in \Upsilon \text{ tels que} \\ 2\mu_f \int_{\Omega_f^k} D(u_f^k) : D(v_f) - \int_{\Omega_f^k} p_f^k \operatorname{div}(v_f) \\ \qquad \qquad \qquad = \int_{\Omega_f^k} f_f^k \cdot v_f + \left(\lambda^k, v_f \circ \Phi(d_s^{k-1}) \right)_\Upsilon, \quad \forall v_f \in V_f^k, \\ \int_{\Omega_f^k} q_f \operatorname{div}(u_f^k) = 0, \quad \forall q_f \in L^2(\Omega_f^k), \\ \int_{\Omega_s} \sigma_s(d_s^k) : \nabla v_s - \int_{\Omega_s} (\nabla d_s \Sigma_k^*) : \nabla v_s = \int_{\Omega_s} f_s^k \cdot v_s - \left(\lambda^k, v_s \right)_\Upsilon, \quad \forall v_s \in V_s, \\ \left(\mu, \gamma_\Gamma(u_f^k \circ \Phi(d_s^{k-1})) - \frac{1}{\delta t} (\gamma_\Gamma(d_s^k) - \gamma_\Gamma(d_s^{k-1})) \right)_\Upsilon = 0, \quad \forall \mu \in \Upsilon, \end{array} \right. \quad (1.6)$$

où λ^k est le multiplicateur associé à la contrainte d’égalité des vitesses fluide et structure sur l’interface Γ et Υ est l’espace fonctionnel défini par

$$\Upsilon = (H_{00}^{1/2}(\Gamma))^n.$$

Sous la condition (1.5), nous démontrons que le problème (1.6) admet une solution unique. De plus, la vitesse et la pression du fluide ainsi que le déplacement de la structure sont également solutions du problème (1.4).

Précisons que cette formulation est introduite dans l’optique de la résolution numérique du problème d’interaction fluide-structure. En effet, comme nous pouvons l’observer dans le problème (1.6), la contrainte entre la vitesse du fluide et le déplacement de la structure n’est plus présente dans les espaces fonctionnels. Ainsi, la résolution numérique de ce problème point-selle est simple à implémenter car cette formulation est adaptée à l’utilisation de la méthode des éléments finis et de solveurs fluide et structure usuels.

Dans la Section 2.4, nous résolvons numériquement un problème similaire à (1.6), mais en considérant cette fois les équations non linéaires de l’élasticité active. Pour cela nous

utilisons l'algorithme d'Uzawa, une méthode itérative pour la résolution de problèmes point-selle. À chaque itération de l'algorithme, le multiplicateur de Lagrange pour la contrainte d'égalité des vitesses est explicite et les problèmes fluide et structure sont alors découplés. Le problème de Stokes est résolu sous forme mixte avec un solveur direct et des éléments finis P1b/P1, tandis que le problème d'élasticité est résolu avec un algorithme de Newton et des éléments finis P1. La méthode de résolution est détaillée dans la Sous-section 2.4.1. Deux études sont alors menées. Premièrement, dans la Sous-section 2.4.2, nous étudions le battement d'un cil dont les forces internes sont imposées et faisons varier la viscosité du fluide environnant. Nous mettons alors en évidence les effets d'une modification de la viscosité du fluide sur les déformations du cil, ce qui ne peut être observé si les déplacements de la structure sont imposés, comme par exemple dans [Lacouture, 2016] ou [Chatelin and Poncet, 2016]. De plus, en se déformant moins, le cil agit également moins sur le fluide environnant, dont la vitesse moyenne est alors de plus en plus faible avec l'augmentation de la viscosité du fluide. Deuxièmement, dans la Sous-section 2.4.3, nous étudions les battements de deux cils en faisant varier leur espacement et le déphasage entre leurs activités internes. Nous montrons alors que la capacité de deux cils à transporter le fluide environnant est très dépendante de ces deux paramètres.

1.3.2 Chapitre 3 : existence et unicité pour un problème fluide-structure quasi-statique mettant en jeu une structure active et un fluide visqueux

Le Chapitre 3 est consacré à la preuve d'un résultat d'existence et d'unicité pour le problème d'interaction fluide-structure quasi-statique, avec une structure active. En reprenant les notations introduites dans la section précédente, le domaine Ω_s est rempli d'un matériau élastique dont les mouvements sont modélisés par les équations non linéaires de l'élasticité active, définies par (1.1). De plus, ses comportements élastiques sont donnés par la loi de Saint Venant-Kirchhoff (1.2). D'autre part, le domaine Ω_f est rempli d'un fluide visqueux, homogène et incompressible dont la vitesse et la pression vérifient les équations de Stokes, écrites dans la configuration courante du domaine fluide. À la différence des études faites dans la Section 2.3, où l'évolution en temps est discrétisée et les problèmes étudiés à chaque instant sont stationnaires, nous nous intéressons ici au problème quasi-statique, c'est-à-dire au problème dont l'évolution est continue en temps. Dans ce cas, la déformation du domaine fluide, Φ , qui dépend du déplacement de la structure et donc aussi des forces internes de la structure, est également une inconnue du problème et le domaine courant du fluide n'est pas connu *a priori*. Afin de contourner cette difficulté nous réécrivons à chaque instant $t \geq 0$, par changement de variables, les équations de Stokes dans la configuration de référence du fluide, Ω_f . Il vient alors :

$$\begin{aligned} -\mu_f \operatorname{div}((F(d_s(t))\nabla)w_f(t)) + (G(d_s(t))\nabla)q_f(t) &= 0, & \text{dans } \Omega_f, \\ \operatorname{div}(G(d_s(t))^t w_f(t)) &= 0, & \text{dans } \Omega_f, \\ w_f(t) &= 0, & \text{sur } \Gamma_f, \end{aligned} \quad (1.7)$$

où les matrices $F(d_s(t))$ et $G(d_s(t))$ sont définies par

$$\begin{aligned} F(d_s(t)) &= (\nabla(\Phi(d_s(t))))^{-1} \operatorname{cof}(\nabla(\Phi(d_s(t)))), \\ G(d_s(t)) &= \operatorname{cof}(\nabla(\Phi(d_s(t)))). \end{aligned}$$

Pour tout $t \geq 0$, la matrice $F(d_s(t))$, est bien définie si la déformation du domaine fluide, Φ , est un C^1 -difféomorphisme. Dans la Section 3.2, nous montrons que c'est effectivement le

cas si le déplacement de la structure, $d_s(t)$, est suffisamment petit (voir le Lemme 3.2), c'est-à-dire s'il appartient à une boule

$$\mathcal{B}_{\mathcal{M}_0} = \{b \in H^3(\Omega_s); \|b\|_{H^3(\Omega_s)} \leq \mathcal{M}_0\},$$

avec \mathcal{M}_0 une constante réel strictement positive assez petite.

Dans ce chapitre, nous considérons certaines hypothèses géométriques sur les domaines Ω_s et Ω_f , indispensables pour obtenir des solutions régulières au problème fluide-structure :

- (H₁) Le domaine Ω est un ouvert connexe borné de \mathbb{R}^n ($n \in \{2, 3\}$) de forme toroïdale et de frontière de classe $C^{3,1}$, divisé en deux domaines Ω_f et Ω_s par une interface Γ .
- (H₂) L'interface Γ est non vide et n'intersecte pas le bord de Ω , i.e. $\bar{\Gamma} \cap \overline{\partial\Omega} = \emptyset$.
- (H₃) Les domaines Ω_f et Ω_s sont deux ouverts connexes bornés de formes toroïdales et de frontières de classe $C^{3,1}$.
- (H₄) Les frontières restantes sont nommées $\Gamma_f = \partial\Omega_f \setminus \Gamma$ et $\Gamma_s = \partial\Omega_s \setminus \Gamma$.

Le résultat principal du chapitre est alors le suivant.

Théorème 1.3. *Soient Ω_f et Ω_s des domaines de \mathbb{R}^n ($n \in \{2, 3\}$) définis par les hypothèses (H₁)-(H₄) et Γ_f , Γ_s et Γ leurs frontières. Soit $T > 0$. Supposons que les données du problème, les forces extérieures f_s dans $L^\infty(0, T; H^1(\Omega_s))$ et l'activité interne de la structure Σ^* dans $L^\infty(0, T; H^2(\Omega_s))$, vérifient la condition $f_s(0) = \text{div}(\Sigma^*(0))$. Nous introduisons également la solution d'un problème de Stokes, (w_f^0, q_f^0) , qui vérifie les équations*

$$\begin{aligned} -\mu_f \Delta w_f^0 + \nabla q_f^0 &= 0 && \text{dans } \Omega_f, \\ \text{div}(w_f^0) &= 0 && \text{dans } \Omega_f, \\ w_f^0 &= 0 && \text{sur } \Gamma_f, \\ \sigma_f(w_f^0, q_f^0) \cdot n_f &= -\Sigma^*(0) \cdot n_f && \text{sur } \Gamma. \end{aligned}$$

Enfin, pour un réel $\mathcal{M}_1 > 0$, nous définissons la boule $\mathcal{B}_{\mathcal{M}_1}$ telle que

$$\mathcal{B}_{\mathcal{M}_1} = \left\{ (\omega, \pi) \in L^2(0, T; H^3(\Omega_f) \cap H_{\Gamma_f}^1(\Omega_f)) \times L^2(0, T; H^2(\Omega_f)) \ ; \right. \\ \left. \|\omega - w_f^0\|_{L^2(0, T, H^3(\Omega_f))} + \|\pi - q_f^0\|_{L^2(0, T, H^2(\Omega_f))} \leq \mathcal{M}_1 \right\}.$$

Alors, si les données du problème f_s et Σ^* , le temps T et la constante \mathcal{M}_1 vérifient certaines conditions de petitesse (voir (3.13)-(3.17)), le problème fluide-structure quasi-statique, formé des équations (1.1), (1.2), (1.3) et (1.7), admet une unique solution (w_f, q_f, d_s) , avec (w_f, q_f) dans $\mathcal{B}_{\mathcal{M}_1}$ et d_s dans $L^\infty(0, T; \mathcal{B}_{\mathcal{M}_0} \cap H_{\Gamma_s}^1(\Omega_s))$.

La preuve de ce théorème est réalisée en utilisant une méthode de point-fixe de Banach. Pour cela, nous construisons une application \mathcal{S} , qui à tout couple vitesse-pression (ω, π) dans $\mathcal{B}_{\mathcal{M}_1}$ associe la solution d'un problème de Stokes, notée (w_f, q_f) , dans l'espace fonctionnel $L^2(0, T; H^3(\Omega_f)) \times L^2(0, T; H^2(\Omega_f))$, au travers d'une succession d'applications. En fait, l'application \mathcal{S} est la composition de plusieurs applications :

$$\mathcal{S} = \mathcal{O}_3 \circ \mathcal{O}_2 \circ \mathcal{O}_1,$$

(sous la condition (3.16)) et que \mathcal{S} est une contraction (sous la condition (3.17)). Cela nous permet alors d'appliquer le théorème de point-fixe de Banach qui nous donne l'existence et l'unicité d'une solution forte locale en temps au problème d'interaction fluide-structure avec structure active.

Enfin, dans la section Section 3.7 nous démontrons que ce résultat reste valide sans l'hypothèse $f_s(0) = \text{div}(\Sigma^*(0))$, considérée dans le Théorème 1.3, sur les données du problème au temps initial.

1.3.3 Chapitre 4 : une méthode de prolongement régulier pour la résolution numérique de problèmes de transmission

Le Chapitre 4 est dédié au développement d'une méthode numérique pour la résolution de problèmes de transmission sur maillages non conformes, qui préserve l'ordre de convergence optimal de la méthode des éléments finis. Dans cette thèse, nous nous restreignons en particulier aux problèmes de transmission s'écrivant comme un système de deux équations aux dérivées partielles elliptiques, linéaires et couplées par des conditions de transmission à l'interface séparant les deux milieux. Néanmoins, cette classe de problèmes reste large puisqu'elle concerne de nombreux phénomènes physiques et biologiques comme, par exemple, l'étude de la conduction dans des matériaux non homogènes, la modélisation d'écoulements multiphasiques à faible nombre de Reynolds et, bien sûr, l'étude de problèmes d'interaction fluide-structure faisant intervenir des micro-organismes.

Contrairement aux méthodes à maillages conformes (comme celle utilisée dans le Chapitre 2) qui nécessitent un remaillage des domaines si le déplacement de l'interface est important, les méthodes à maillages non conformes utilisent des maillages fixes pour lesquels aucune technique de remaillage n'est nécessaire. Un autre avantage de ces méthodes à maillages non conformes est de pouvoir utiliser des méthodes de résolution rapides, comme des techniques de transformée de Fourier sur maillages cartésiens par exemple. En contrepartie, puisque l'interface n'est pas représentée par le maillage, la vitesse de convergence en espace de ces méthodes est souvent dégradée par rapport à celle observée pour des méthodes à maillages conformes dans le contexte des éléments finis, à moins d'un traitement adéquat des conditions de transmission. Ici, nous proposons une méthode basée sur la reformulation du problème de transmission sous la forme d'un problème de contrôle, qui nous permet, pour la résolution numérique, d'utiliser des maillages non conformes, ainsi que des solveurs éléments finis usuels, sans perdre l'ordre de convergence optimal.

Considérons un domaine borné, connexe et de frontière lipschitzienne Ω , divisé en deux sous-domaines Ω_1 et Ω_2 par une interface Γ . Ces deux domaines sont également supposés avoir une frontière lipschitzienne et nous notons $\Gamma_1 = \partial\Omega_1 \setminus \Gamma$ et $\Gamma_2 = \partial\Omega_2 \setminus \Gamma$ leurs frontières extérieures, que nous supposons non vide pour le moment.

Dans la Section 4.2, nous présentons la *méthode de prolongement régulier* pour un problème de transmission de Laplace, qui s'écrit

$$\left\{ \begin{array}{ll} \text{trouver } u_1: \Omega_1 \rightarrow \mathbb{R} \text{ et } u_2: \Omega_2 \rightarrow \mathbb{R} \text{ tels que} & \\ \begin{array}{ll} -\mu_1 \Delta u_1 = f_1, & \text{dans } \Omega_1, \\ u_1 = 0, & \text{sur } \Gamma_1, \end{array} & (1.8a) \\ \begin{array}{ll} -\mu_2 \Delta u_2 = f_2, & \text{dans } \Omega_2, \\ u_2 = 0, & \text{sur } \Gamma_2, \end{array} & (1.8b) \\ \begin{array}{ll} u_1 = u_2, & \text{sur } \Gamma, \\ \mu_1 \nabla u_1 \cdot n_1 = -\mu_2 \nabla u_2 \cdot n_2, & \text{sur } \Gamma, \end{array} & (1.8c) \end{array} \right.$$

où $f_1 \in L^2(\Omega_1)$ et $f_2 \in L^2(\Omega_2)$ sont des forces extérieures, μ_1 et μ_2 sont des coefficients réels constants et strictement positifs et n_1 et n_2 sont les vecteurs unitaires normaux aux frontières $\partial\Omega_1$ et $\partial\Omega_2$, respectivement. Les équations (1.8c), sont les conditions de transmission sur Γ , qui représentent physiquement la continuité des champs au travers de l'interface et la continuité des contraintes normales. Le problème (1.8) admet une unique solution faible, notée (\bar{u}_1, \bar{u}_2) dans \mathcal{V} , avec

$$\begin{aligned}\mathcal{V} &= \{(v_1, v_2) \in V_1 \times V_2; v_1|_\Gamma = v_2|_\Gamma\}, \\ V_1 &= \{v_1 \in H^1(\Omega_1); v_1|_{\Gamma_1} = 0\}, \\ V_2 &= \{v_2 \in H^1(\Omega_2); v_2|_{\Gamma_2} = 0\}.\end{aligned}$$

Dans la Sous-section 4.2.1, nous introduisons le *problème de prolongement régulier* associé au problème de transmission de Laplace, qui consiste à trouver un contrôle $g : \Omega_2 \rightarrow \mathbb{R}$ dans V_2' (l'espace dual de V_2), tel que la solution du problème

$$\left\{ \begin{array}{ll} \text{trouver } u_1 : \Omega \rightarrow \mathbb{R} \text{ et } u_2 : \Omega_2 \rightarrow \mathbb{R} \text{ tels que} & \\ \begin{array}{ll} -\mu_1 \Delta u_1 = \overline{f_1}^\Omega + \overline{g}^\Omega, & \text{dans } \Omega, \\ u_1 = 0, & \text{sur } \partial\Omega, \end{array} & (1.9a) \\ \begin{array}{ll} -\mu_2 \Delta u_2 = f_2, & \text{dans } \Omega_2, \\ u_2 = 0, & \text{sur } \Gamma_2, \\ \mu_2 \nabla u_2 \cdot n_2 = -\mu_1 \nabla u_1 \cdot n_1, & \text{sur } \Gamma, \end{array} & (1.9b) \end{array} \right.$$

vérifie l'égalité :

$$(u_1|_{\Omega_1}, u_2) = (\bar{u}_1, \bar{u}_2). \quad (1.10)$$

Dans le problème (1.9), les fonctions $\overline{f_1}^\Omega$ et \overline{g}^Ω sont les extensions par zéro dans tout le domaine Ω des fonctions f_1 et g . Par rapport au problème (1.8), nous remarquons que le problème sur Ω_1 à été prolongé dans tout Ω et que la condition de transmission sur la contrainte normale est maintenant une condition aux limites de Neumann pour le problème sur Ω_2 . De plus, la condition d'égalité des champs au travers de la frontière Γ sera vérifiée si l'équation (1.10) est vérifiée par la solution du problème (1.9). Notons également que le problème (1.9) admet une unique solution faible dans $H_0^1(\Omega) \times V_2$ pour tout g dans V_2' , que nous notons (u_1^g, u_2^g) .

Sous cette forme, le problème de prolongement régulier est donc un problème de contrôle : il convient de trouver une fonction g dans V_2' qui nous permet de récupérer la solution du problème de transmission initial (\bar{u}_1, \bar{u}_2) . Un premier résultat concernant l'existence d'un tel contrôle est énoncé.

Théorème 1.4. *Soient f_1 dans $L^2(\Omega_1)$ et f_2 dans $L^2(\Omega_2)$. Il existe un contrôle g dans V_2' tel que la solution faible du problème (1.9) vérifie l'égalité (1.10).*

Pour démontrer ce résultat, nous partons de la solution du problème de transmission initial (\bar{u}_1, \bar{u}_2) et construisons une extension de \bar{u}_1 dans $H_0^1(\Omega)$. Le contrôle g est alors obtenu par identification après une intégration par parties des équations du problème faible de (1.9). Néanmoins, précisons que ce contrôle n'est pas unique car plusieurs extensions de \bar{u}_1 dans Ω sont possibles.

Du point de vue de la simulation numérique cette méthode est donc intéressante puisque, si nous connaissons un bon contrôle g , la solution du problème de transmission est obtenue en résolvant deux problèmes de Laplace séparément, par des solveurs éléments

finis usuels. De plus, si la solution du problème de transmission initial, (\bar{u}_1, \bar{u}_2) , est plus régulière (c'est-à-dire si $\bar{u}_1 \in H^2(\Omega_1) \cap V_1$ et $\bar{u}_2 \in H^2(\Omega_2) \cap V_2$), alors nous montrons que la méthode converge à l'ordre optimal. En effet, si dans la preuve du théorème (1.4) nous étendons la fonction \bar{u}_1 dans $H^2(\Omega) \cap H_0^1(\Omega)$ et non plus dans $H_0^1(\Omega)$, alors l'existence d'un contrôle g dans $L^2(\Omega)$ est assurée. Dans ce cas, la solution du problème (1.9) est dans $(H^2(\Omega) \cap H_0^1(\Omega)) \times (H^2(\Omega_2) \cap V_2)$ et la méthode des éléments finis converge à l'ordre optimal.

Dans ce but, nous prouvons dans la Sous-section 4.2.3 le résultat suivant, qui démontre la possibilité d'étendre \bar{u}_1 dans tout Ω en conservant sa régularité H^2 .

Théorème 1.5. *Soit $\Omega \in \mathbb{R}^n$ ($n \in \{2, 3\}$), un ouvert borné, connexe et dont la frontière, $\partial\Omega$, est lipschitzienne. Soit Γ une interface qui divise Ω en deux ouverts bornés, connexes et à frontières lipschitziennes, notés Ω_1 et Ω_2 . De plus, si $n = 3$, nous supposons que $\Gamma \cap \partial\Omega_2$ est une courbe de régularité C^2 . Considérons une fonction u_1 dans $H^2(\Omega_1) \cap V_1$. Si les frontières Γ et $\partial\Omega$ sont au moins de classe C^2 au voisinage de chaque élément de $\Gamma \cap \partial\Omega$ (deux points en deux dimensions d'espace et une courbe fermée en trois dimensions d'espace), il existe une extension de u_1 dans $H^2(\Omega) \cap H_0^1(\Omega)$ notée u , telle que $u = u_1$ dans Ω_1 .*

En deux dimensions d'espace, la preuve de ce résultat repose sur une décomposition bien choisie de la fonction u_1 en trois fonctions régulières définies dans Ω_1 . Chacune de ces fonctions est alors étendue à tout le domaine Ω séparément en utilisant, soit le théorème d'extension de Stein ([Adams and Fournier, 2003, Theorem 5.24]), loin des éléments de $\Gamma \cap \partial\Omega$, soit le théorème d'extension de Babič ([Babič, 1953]), dans un voisinage des éléments de $\Gamma \cap \partial\Omega$. La preuve peut ensuite être étendue de façon similaire en trois dimensions d'espace.

Il reste maintenant à savoir comment obtenir un contrôle g adéquat, permettant de retrouver la solution du problème de transmission de Laplace à partir de la résolution du problème (1.9). Dans la Sous-section 4.2.2, nous introduisons le problème de minimisation

$$\begin{cases} \text{trouver } g \text{ dans } V_2' \text{ qui minimise la fonctionnelle} \\ J(g) := \frac{1}{2} \int_{\Gamma} |u_1^g - u_2^g|^2, \end{cases} \quad (1.11)$$

et démontrons un résultat d'équivalence entre le problème de minimisation (1.11) et le problème de prolongement régulier.

Théorème 1.6. *Une fonction g dans V_2' est un minimiseur de J si et seulement si la solution (u_1^g, u_2^g) du problème faible associé à (1.9) vérifie l'égalité (1.10).*

De plus, nous montrons également que la fonctionnelle J est différentiable dans V_2' et donnons une formule explicite de son gradient, qui dépend de la solution à un problème de Laplace similaire au problème (1.9), appelé *problème adjoint*. Plus précisément, nous introduisons le *lagrangien* associé au problème de minimisation (1.11), défini de

$$V_2' \times (H_0^1(\Omega) \times V_2) \times (H_0^1(\Omega) \times V_2)$$

dans \mathbb{R} par

$$\begin{aligned} & \mathcal{L}(g, (v_s, v_2), (\lambda_1, \lambda_2)) \\ &= \frac{1}{2} \|v_1 - v_2\|_{L^2(\Gamma)}^2 + \mu_1 \int_{\Omega} \nabla v_1 \cdot \nabla \lambda_1 - \mu_1 \int_{\Omega_2} \nabla v_1|_{\Omega_2} \cdot \nabla \lambda_2 \\ &+ \mu_2 \int_{\Omega_2} \nabla v_2 \cdot \nabla \lambda_2 - \int_{\Omega_1} f_1 \lambda_1|_{\Omega_1} - \int_{\Omega_2} f_2 \lambda_2 - \langle g, \lambda_1|_{\Omega_2} \rangle_{V_2', V_2} \\ &+ \langle g, \lambda_2 \rangle_{V_2', V_2}. \end{aligned}$$

Les équations adjointes sont alors obtenues en annulant les différentielles du lagrangien \mathcal{L} par rapport à v_1 et v_2 évaluées en $(v_1, v_2) = (u_1^g, u_2^g)$:

$$\begin{aligned} \left\langle \frac{\partial \mathcal{L}}{\partial v_1}(g, (u_1^g, u_2^g), (\lambda_1, \lambda_2)), \delta v_1 \right\rangle_{H^{-1}(\Omega), H_0^1(\Omega)} &= 0, \quad \forall \delta v_1 \in H_0^1(\Omega), \\ \left\langle \frac{\partial \mathcal{L}}{\partial v_2}(g, (u_1^g, u_2^g), (\lambda_1, \lambda_2)), \delta v_2 \right\rangle_{V_2', V_2} &= 0, \quad \forall \delta v_2 \in V_2. \end{aligned} \quad (1.12)$$

Les variables adjointes, solutions de ces équations, sont alors notées λ_1^g et λ_2^g . Le gradient de J est lui obtenu en différentiant l'équation

$$\mathcal{L}(g, (u_1^g, u_2^g), (\lambda_1, \lambda_2)) = J(g), \quad \forall g \in V_2', \quad \forall (\lambda_1, \lambda_2) \in H_0^1(\Omega) \times V_2$$

par rapport à g . Nous montrons alors que le gradient de J s'exprime en fonction de λ_1^g et λ_2^g :

Théorème 1.7. *L'application qui à tout g dans V_2' associe $J(g)$ dans \mathbb{R} est différentiable et son gradient $\nabla J(g) \in V_2''$ est donné par*

$$\langle \nabla J(g), \delta g \rangle_{V_2'', V_2'} = \left\langle \delta g, \lambda_2^g - \lambda_{1|\Omega_2}^g \right\rangle_{V_2', V_2}, \quad \forall \delta g \in V_2', \quad (1.13)$$

où $(\lambda_1^g, \lambda_2^g)$ est solution des équations adjointes (1.12).

Pour la résolution numérique, la méthode à adopter est donc claire : nous effectuons une descente de gradient sur la fonctionnelle J en résolvant à chaque étape des problèmes de Laplace sur les domaines Ω et Ω_2 , discrétisés avec des maillages non conformes. À convergence, les fonctions u_1^g et u_2^g construites par ce procédé nous permettent alors de récupérer la solution du problème de transmission initial (\bar{u}_1, \bar{u}_2) . La procédure est détaillée dans l'Algorithme 1.1.

Algorithm 1.1 Implementation de la méthode de prolongement régulier

Choisir un contrôle initial g_0 .

$k = 0$.

tant que l'algorithme n'a pas convergé **faire**

Calculer la solution $(u_1^{g_k}, u_2^{g_k})$ du problème (1.9) avec $g = g_k$.

Calculer la solution $(\lambda_1^{g_k}, \lambda_2^{g_k})$ des équations adjointes (1.12) avec $g = g_k$.

Calculer le gradient $\nabla J(g_k) = \lambda_2^{g_k} - \lambda_{1|\Omega_2}^{g_k}$.

Mettre à jour le contrôle $g_{k+1} = g_k - \rho_k \nabla J(g_k)$, avec ρ_k un paramètre dépendant de la méthode de gradient choisie.

Mettre à jour le nombre d'itérations $k = k + 1$.

fin tant que

Le cas où le domaine Ω_2 est strictement inclus dans Ω , c'est-à-dire lorsque $\partial\Omega_2 = \Gamma$, est traité dans la Sous-section 4.2.4, où des résultats similaires sont obtenus.

Dans la Section 4.3, la méthode de prolongement régulier est testée numériquement et comparée à des méthodes éléments finis usuelles avec maillages conformes et non conformes. Pour cela, le contrôle g est obtenu par minimisation de la fonctionnelle J par une méthode de descente de gradient, que nous avons implémentée en FEniCS ([Logg et al., 2012]). En particulier, nous mettons en évidence l'ordre optimal de convergence en espace de notre

méthode, ce qui n'est pas le cas de la méthode des éléments finis usuelle avec des maillages non conformes.

Enfin, dans la Section 4.4, nous étendons notre méthode à deux autres problèmes de transmission : un problème de transmission de Stokes (Sous-section 4.4.1) et un problème d'interaction fluide-structure, avec une structure élastique passive dans un fluide de Stokes (Sous-section 4.4.2). Dans les deux cas, le problème de prolongement régulier associé au problème de transmission est introduit et nous montrons l'existence d'un contrôle tel que la condition d'égalité au travers de l'interface est vérifiée. Le problème de prolongement régulier est ensuite formulé sous la forme d'un problème équivalent de minimisation d'une fonctionnelle. Nous montrons que cette fonctionnelle est différentiable et donnons une formule explicite de son gradient. Nous résolvons ensuite ce problème de minimisation avec une méthode de descente de gradient, ce qui nous permet de récupérer la solution du problème de transmission initial.

Pour le problème d'interaction fluide-structure en particulier, nous considérons une structure élastique, passive, attachée à la paroi et immergée dans un fluide de Stokes en mouvement. Soumise aux forces hydrodynamiques du fluide, la structure va alors se déformer dans le sens de l'écoulement jusqu'à atteindre une position d'équilibre. Avec la méthode de prolongement régulier développée dans cette thèse, nous mettons notamment en avant la possibilité de mailler finement la structure tout en gardant un maillage plus grossier dans le domaine fluide sans dégrader la dynamique d'évolution du système, ce qui permet un gain de temps pour la résolution numérique de ce problème. Pour finir, cette méthode constitue une première étape pour la simulation numérique de structures actives dans un fluide visqueux en utilisant des maillages non conformes.

Chapter 2

A continuum active structure model for the interaction of cilia with a viscous fluid

2.1 Introduction

Cilia and flagella are motile elongated structures, involved in swimming and/or transport mechanisms that arise in many living organisms. Flagella are usually used by microswimmers such as sperm-cells, bacteria or algae for motility purpose at low Reynolds number, while cilia are generally involved in the transport of proteins, nutrients or dust inside bigger organisms. Such process, can be universally found in prokaryotic or eukaryotic systems, from bacteria to mammals. Focusing on the human body, cilia appear in several vital processes, such as the left-right asymmetry of the heart in the foetus, the transport of nutrients in the brain and the mucociliary transport. At the origin of all these mechanisms are two essential ingredients. The first one is the capacity for cilia and flagella to modify their shapes by generating active internal deformations and stresses, even without external load. The second one is the strong reciprocal interaction between these structures and the surrounding fluid. The problem we are interested in is the capacity of such microorganisms to deform themselves by mean of internal biological motors and to interact with the surrounding fluid. In the present chapter, we present a model for the actuation of elongated cilia-like structures, which fits within the framework of continuum mechanics, and study the fluid-structure interaction problem they are involved in.

Eukaryotic cilia (or flagella) are elongated deformable structures with a typical diameter between 0.1 and 0.3 μm , whereas the length of cilia can vary from 5 μm (in the lung [Fulford and Blake, 1986]), to 80 μm long (for the tail of spermatozoon in mice). Cilia are membrane-bounded structures composed of a microtubule cytoskeleton, called axoneme, consisting of a ring of nine doublets microtubules surrounding a central pair of microtubules. Outer doublets microtubules are linked to the central pair by radial proteins and to each other by nexin links, which strengthen the structure. Beating movements of cilia are induced by internal motors producing a bending in the whole structure, when two outer doublets microtubules slide with respect to one another. This sliding is produced by proteins, called dyneins, that are synthesized on one doublet microtubules and attach to the neighboring one. The radial connections resist the sliding and contribute to the bending of the structure, since the cilium is anchored at the bottom. This mechanism appears all along the length of a cilium and between all doublets microtubules, which contributes to the emergence of different sliding patterns and different shapes of deformation for the cilium. The precise

nature of the spatial and temporal control mechanisms regulating the various ciliary beats is still unknown ([Brokaw, 2001]). Further details on the internal structure and mechanisms of cilia can be found in [King and Pazour, 2009].

The presence of ciliary propulsion in almost all living organisms, from bacteria to mammals, has encouraged numerous scientists to model and study this universal phenomenon. The first work in that sense goes back to 1951 and is due to Taylor ([Taylor, 1951]), who initiated the mathematical study of microorganism propulsion. This work presents the swimming of an extensible sheet in a viscous fluid modeled by the Stokes equations. The author works in the rest frame of the sheet, whose deformations are modeled by the propagation of a wave of small amplitude. Thus, the unknown of the problem is the velocity of the fluid far from the sheet, which also represents the velocity of the sheet in the laboratory frame. Extensions to an infinite cylinder ([Taylor, 1952], [Blake, 1971a]) and to finite objects ([Lighthill, 1952], [Blake, 1971b]) have subsequently been studied. When the amplitude of deformations are large, the resistive force theory (also known as local drag theory) developed in the pioneering work of Gray and Hancock ([Gray and Hancock, 1955]), describes the cilia as several cylinders and uses the linear property of the Stokes equations to compute the flow induced in the fluid. A similar but more accurate method is the slender body theory, started by Hancock in [Hancock, 1953] and then improved by Lighthill in [Lighthill, 1976], which makes use of the long and thin geometry of cilia. It consists in modeling a cilium by a distribution of stokeslets and dipoles, which impose a force on the surrounding fluid. This method is also known as the sublayer method or the stokeslet method and has been extensively applied to the simulation of thin flagellar propulsion when the deformations of the structure are imposed (see for example [Dresdner et al., 1980], [Ding et al., 2014], [Lacouture, 2016]). More recently, the immersed boundary method has been used for the simulation of thin beating cilia in a Newtonian fluid in [Daughton et al., 2008]. Similarly to the sublayer method, the idea is to impose a distribution of forces in the fluid. However, in that case the force does not come from the slender body theory but is used to impose the equality of the fluid and solid velocities on the fluid-structure interface. In this work, the velocity of the structure is imposed and its action on the fluid is studied. A different approach is also considered in [Chatelin, 2013], where cilia are three-dimensional structures whose deformations are reproduced by solving a one-dimensional transport equation. The fluid velocity on the fluid-structure interface is imposed using a penalization method, thus no retro-action from the fluid to cilia is taken into account. In [Chateau et al., 2017], cilia are modeled by thin structures whose deformations are given by the same transport equation as in [Chatelin, 2013]. The equality of the fluid and solid velocities on the fluid-structure interface is imposed with the immersed boundary method and the action of the fluid on the structure is taken into account by changing the velocity of the structure, but cilia always follows the same beat pattern. In all works previously mentioned, the cyclic shape change of a cilium is imposed whereas its beatform is really an emergent property of a coupled system involving the internal mechanisms of the cilium, the elastic properties of the structure and the surrounding viscous fluid.

The first work that attempted to take into account the internal activity of cilia through local deformations is due to Machin in [Machin, 1958]. The cilium is considered as an elastic filament immersed in a viscous fluid, whose action on the structure is given by the resistive force theory. Moreover, the internal activity of the cilium is modeled by adding an active bending moment distributed all along the structure. With the active bending moment, wave-like displacements similar to those observed on flagella are observed whereas, with a passive elastic filament driven from its proximal end, the forms of the wave do not match the actual shapes of cilia. Thus Machin brought to light the importance of local

contractility in the deformation of cilia. In [Brokaw, 1966], a modification of this model is proposed, where the author considers two active filaments with regular cross-connections whose contractility is activated when the passive bending reach a critical value. In [Lubliner and Blum, 1971], a similar three-dimensional model is proposed with a more realistic geometry of the internal structure of a cilium. Subsequently, several class of models have been proposed such that curvature-controlled models ([Brokaw, 1972], [Hines and Blum, 1978], [Brokaw, 1985]) and self-oscillatory models ([Machin, 1963], [Brokaw, 2005]). A comprehensive review of these different models is presented in [Murase, 1992].

An other approach is presented in [Dillon and Fauci, 2000] and further studied in [Dillon and Fauci, 2000], [Yang et al., 2008] and [Lukens et al., 2010], where a discrete description of the axoneme is proposed in two space dimension. The cilium is composed of elastic filaments connected by a finite number of springs that represent nexin and dynein links. Then, the deformation of the structure is produced by the connection scenario of dynein links which depends on the geometry of the structure. At the fluid-structure interface the continuity of the velocity is considered and is treated numerically with the immersed boundary method. A similar model is considered in [Gueron and Levit-Gurevich, 2001] and [Mitran, 2007] in three dimension dimension, where a precise description of the “9+2” structure of the cilium is proposed. In both works, the emerging beating patterns are realistic.

Unlike all previous works on cilia and self-propelled microorganisms moving in a viscous fluid, we aim to model the behavior of active biological structures in the framework of continuum mechanics, without using a detailed description of their internal structure. The reasons for this study are twofold. First, since the chemical, biological and even mechanical processes for the internal activity of eukaryotic cilia are not yet completely understood, we do not intend to model the nexin and dynein links at the nanometric scale. Instead, we rather take into account the activity in a more phenomenological manner by mean of an internal stress. The context of two and three dimensional elasticity is particularly suitable to reproduce realistic deformations of cilia and flagella. Second, the framework of continuum mechanics enables to fully consider the fluid-structure interaction, which is one of the most important ingredient of the system and which is often neglected in other studies. The model that we develop in this chapter is suitable for both the mathematical study and the numerical simulation of the fluid-structure interaction with active structures and a viscous fluid.

The chapter is organized as follows. In Section 2.2 we present the equations of *active elasticity* that have been introduced in biomechanics for the study of biological tissues, but never used or mathematically studied for active microorganisms at low Reynolds number. Examples of activity scenarios are illustrated in Subsection 2.2.4. In Section 2.3, we couple the elasticity equations to the Stokes equations and study the fluid-structure interaction problem. For the numerical simulation of active structures beating in a viscous fluid we introduce, in Subsection 2.3.4, a saddle-point formulation of the problem, where the condition of equality of the fluid and structure velocities on the fluid-structure interface is treated by a Lagrangian multiplier. In particular, this enables the use of standard finite element methods and solvers. The numerical resolution process is detailed in Subsection 2.4.1. In Subsection 2.4.2 and in Subsection 2.4.3, we present some numerical results for one and two cilia with prescribed internal activity. The influences of the viscosity of the surrounding fluid, the phase shift between internal activities and the distance between cilia are investigated.

2.2 A continuum active structure model

The purpose of the present section is to develop a macroscopic model for the internal activity of cilia-like structures. The model we propose is inspired from the study of biological tissues, whose activity comes from embedded muscles. We start by giving a brief review of these models.

2.2.1 The active-stress method

For the study of biological tissues, two popular macroscopic approaches are used to model the muscles activity, namely the active-stress and active-strain methods (see [Ambrosi and Pezzuto, 2012] for a review). The former consists in adding an active component to the passive stress tensor usually derived from the strain energy law, while the later adopts a multiplicative decomposition of the tensor gradient of deformation in which the activation acts as a pre-strain. Both techniques have been extensively used in myocardium, arteries and even face muscles studies ([Smith, 2004, Panfilov et al., 2005, Bogen et al., 1980, Pezzuto et al., 2014]), but, to our knowledge, not in the context of microswimmers.

The use of one method or the other depends on whether we want to impose a stress or a strain on the structure. We remind that, physically, the stress expresses the internal forces that neighboring particles exert on each other, while the strain is a measure of the deformation. When the structural organization of the active components in the tissue is known, but rather complicated to model individually (as it is the case for cilia), the active-stress method appears to be a better suitable approach. Indeed, in this case, the internal stress can be approximated by averaging the geometric arrangement of the active elements at the micro scale, in order to exhibit a macroscopic fiber-like structure. Then, we suppose that the active behavior of the tissue is only due to elastic deformations in the direction of these fiber-like structures, which are called *active fibers*. More precisely, if e_a denotes a unit vector field in the direction of active fibers within the tissue, which depends on the material position and the time, the active stress tensor, which is denoted by Σ^* , writes

$$\Sigma^* = \Sigma_a e_a \otimes e_a,$$

where Σ_a is a scalar function, which also depends on the time and the material position, and \otimes denotes the tensor product. Thus, in the general case, the internal activity is given by a scalar function Σ_a , that we call the *activity scenario*, and by a unit vector field e_a which, at each material point, points in the direction of active fibers. For more information on models for contractile organs see [Payan and Ohayon, 2017, Chapter 2] and references therein.

2.2.2 The problem of active elasticity

Let Ω_s be a Lipschitz open connected bounded subset of \mathbb{R}^n , with $n \in \{2, 3\}$. Its boundary, $\partial\Omega_s$, is divided in two parts denoted Γ and Γ_s such that the boundaries satisfy $\partial\Omega_s = \Gamma \cup \Gamma_s$ and $\Gamma \cap \Gamma_s = \emptyset$. Moreover, we denote by n_s the exterior unit normal vector to Ω_s . We suppose that Ω_s is filled with an elastic active medium, subjected to a time dependent body force, denoted by f_s . The internal activity of the structure Σ^* is described using the active-stress method and is supposed to depend only on the time and the material position. Then, the quasi-static problem of active elasticity with homogeneous Dirichlet and Neumann boundary conditions, is to find the displacement of the structure d_s ,

solution for all time $t \geq 0$, of the following set of equations:

$$\begin{aligned} -\operatorname{div}((I + \nabla d_s(t))(\Sigma_s(d_s(t)) - \Sigma^*(t))) &= f_s(t), & \text{in } \Omega_s, \\ (I + \nabla d_s(t))(\Sigma_s(d_s(t)) - \Sigma^*(t))n_s &= 0, & \text{on } \Gamma, \\ d_s(t) &= 0, & \text{on } \Gamma_s. \end{aligned} \quad (2.1)$$

The matrix I is the identity matrix of \mathbb{R}^n and $\Sigma_s(d_s(t))$ is the so-called second Piola-Kirchhoff stress tensor at time t , which describes the passive elastic behavior of the structure. For simplicity, we will always assume that the elastic medium follows the Saint Venant-Kirchhoff law, i.e. that the second Piola-Kirchhoff stress tensor writes

$$\begin{aligned} \Sigma_s(d_s(t)) &= 2\mu_s E(d_s(t)) + \lambda_s \operatorname{tr}(E(d_s(t)))I, \\ E(d_s(t)) &= \frac{1}{2}(\nabla d_s(t) + \nabla d_s(t)^T + \nabla d_s(t)^T \nabla d_s(t)), \end{aligned} \quad (2.2)$$

where $\mu_s > 0$ and $\lambda_s > 0$ are Lamé's parameters and $E(d_s(t))$ is known as the Green-Lagrange strain tensor at time t . The elasticity parameters are usually given by mean of Young's modulus E_s , which represents the stiffness of the medium, and Poisson's ratio ν_s , which represents its compressibility, with the following formulas:

$$\mu_s = \frac{E_s}{2(1 + \nu_s)}, \quad \lambda_s = \frac{E_s \nu_s}{(1 + \nu_s)(1 - 2\nu_s)}.$$

Problem (2.1) differs from the classical elasticity equations by the presence of the stress tensor Σ^* , which acts in two different ways on the structure. First, it modifies the resulting forces that act on the structure by adding a body force which writes $\operatorname{div}(\Sigma^*(t))$ in Ω_s and a surface force which writes $\Sigma^*(t)n_s$ on Γ . Second, it modifies the elasticity operator by adding the term $\operatorname{div}(\nabla d_s(t)\Sigma^*(t))$ in the left-hand side of the continuity equation.

In particular, if the body force f_s is null, a displacement d^* which satisfies

$$\begin{aligned} \Sigma_s(d^*(t, x)) &= \Sigma^*(t, x), & \forall t \geq 0, \quad \forall x \in \Omega_s, \\ d^*(t, x) &= 0, & \forall t \geq 0, \quad \forall x \in \Gamma_s, \end{aligned}$$

is a solution of problem (2.1). This means that the internal activity acts as a constraint on the second Piola-Kirchhoff stress. At the infinitesimal scale, the second Piola-Kirchhoff stress describes the forces in the reference configuration that each particle of the elastic medium applies on its neighbors by unit area in the reference configuration. Thus, the active stress tensor Σ^* can be seen as a constraint on the internal forces that neighboring particles exert on each other.

Remark 2.1. The well-posedness of the problem of active elasticity in regular Sobolev spaces with pure Dirichlet boundary conditions is studied in Section 3.4, as a substep of the study of a quasi-static fluid-structure interaction problem.

2.2.3 Application to cilia-like structures

In the present study, a cilium-like structure is supposed to be an elastic active medium whose passive component satisfies the Saint Venant-Kirchhoff law and whose reference configuration, Ω_s , is a straight vertical cylinder of finite length. Moreover, the structure is supposed to be anchored at its bottom boundary, denoted Γ_s , and we denote by Γ the remaining of the boundary. In order to model the internal activity of the cilium-like structure, we will apply the active-stress method, based on the knowledge that we have of the biological structure of cilia. As we explained, the bending mechanics inside a

cilium come from the activation of several molecules which ends up in the sliding of the microtubules, the elongated rod-like structures located at the periphery of the cilium. At a more macroscopic scale, these dynamics can be seen as local elastic deformations in the direction of the microtubules which induce, because the cilium is anchored at the bottom, a bending deformation.

In consequence, we suppose that a cilium is embedded with vertical active fibers. Then, the unit vector field e_a is constant, in time and in space, and the active stress tensor Σ^* is given by

$$\Sigma^*(t, x) = \Sigma_a(t, x)e_a \otimes e_a, \quad t \geq 0, \quad x \in \Omega_s, \quad (2.3)$$

where the activity scenario Σ_a is a scalar field which only depends on the time and the material position in the reference configuration Ω_s . In particular, if the activity scenario is constant in time and in space, this will induce an elongation or a contraction of the whole structure in the direction given by e_a , depending on the sign of Σ_a . If Σ_a is positive the solid stretches, whereas if Σ_a is negative it shrinks. More generally, at a given time t and at a given point x , the sign of $\Sigma_a(t, x)$ indicates whether the structure expands or contracts locally. Thus, in the case of cilia-like bodies, we propose a model for active structures that only depends on the choice of an activity scenario Σ_a . In particular, this enables to easily reproduce biomimetic self-induced deformations of elongated elastic structures.

2.2.4 Examples of internal activity

In this subsection, we aim to imitate the characteristic flapping deformations of cilia and flagella. Since the structure is anchored at the bottom, the local expansion or shrinking of the medium will induce the bending of the whole structure, if the activity scenario is well-chosen.

Bending. The first scenario that we study is the case of the periodic (in time) bending of a two-dimensional structure. Let $L_c > 0$ be the length of the cilium-like structure, $r_c > 0$ be its radius and x_c be its mean position on the abscissa axis. Then, in two space dimensions, Ω_s is the rectangle defined by

$$\Omega_s = \{(x_1, x_2) \in \mathbb{R}^2; x_c - r_c \leq x_1 \leq x_c + r_c, 0 \leq x_2 \leq L_c\}. \quad (2.4)$$

Moreover, we suppose that the structure is anchored at $x_2 = 0$. We recall that in the case of a cilium-like structure, all active fibers are oriented in the direction of the vector $e_a = (0, 1)$. In order to make the structure bend, we consider a scenario which only depends on the time and on the first coordinate x_1 and which is proportional to the difference $x_c - x_1$. It writes

$$\Sigma_a(t, (x_1, x_2)) = \frac{C_a}{L_c r_c} \sin(2\pi f_a t)(x_c - x_1), \quad \forall t \geq 0, \quad \forall (x_1, x_2) \in \Omega_s, \quad (2.5)$$

where f_a is the *beating frequency* and $C_a > 0$ is the *intensity* of the internal activity. Actually, if the sign of $\sin(2\pi f_a t)$ is positive, the structure locally stretches in the half-domain defined by

$$\{(x_1, x_2); x_c - r_c \leq x_1 < x_c, 0 \leq x_2 \leq L_c\}$$

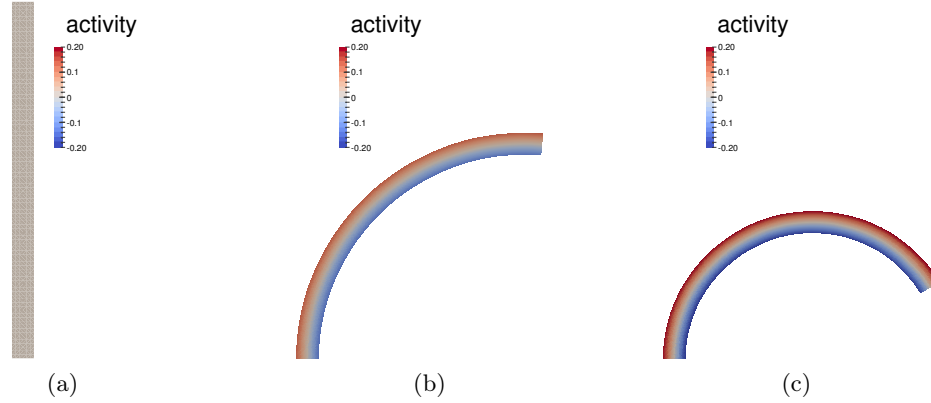
and locally shrinks in the half-domain defined by

$$\{(2x_c - x_1, x_2); x_c < x_1 \leq x_c + r_c, 0 \leq x_2 \leq L_c\}.$$

Thus, because the cilium is anchored at the bottom, it ends in the bending of the whole structure to the right. On the contrary, if the sign of $\sin(2\pi f_a t)$ is negative, the cilium bends to the left.

L_c (μm)	r_c (μm)	x_c (μm)	C_a ($\text{pN} \cdot \mu\text{m}^2$)	f_a (Hz)	E_s ($\text{pN} \cdot \mu\text{m}^{-2}$)	ν_s
6.5	0.2	0	1.3	10	10^6	0.49

Table 2.1 – Set of parameters for the bending scenario of activity.

Figure 2.1 – Bending of an elongated elastic structure with the internal activity given by (2.5) at different times: $t = 0\text{s}$ (a), $t = 0.012\text{s}$ (b), and $t = 0.025\text{s}$ (c). The activity scenario Σ_a is plotted, with the set of parameters be given in Table 2.1.

To illustrate this bending behavior, we numerically solve problem (2.1) with Σ_a defined by (2.5) and $e_a = (0, 1)$. To that aim we use the finite element method with P_1 elements and a Newton solver to handle the nonlinear elasticity operator. The resulting deformations of the structure are presented in Figure 2.1, with the set of parameters be given in Table 2.1. The elasticity parameters μ_s and λ_s are given by Young's modulus E_s and Poisson's ratio ν_s . The chosen value of Poisson's ratio means that the structure is nearly incompressible. For Young's modulus, this value comes from experimental studies ([Holwill and Satir, 1987]). The activity scenario is plotted on the mesh of the structure. A negative value of the activity corresponds to a shrinking behavior of the medium, whereas a positive value corresponds to stretching. For a time t between 0s and 0.025s , we observe in Figure 2.1 that the cilium bends to the right, since the sign of $\sin(2\pi f_a t)$ is positive. For greater values of t , the structure returns to its reference configuration while $\sin(2\pi f_a t)$ decreases and starts to bend to the left when the sign of $\sin(2\pi f_a t)$ becomes negative. At $t = 1$ the structure is back in its reference configuration and is about to bend to the right one more time.

Flapping. Now, we study the case of a two-dimensional flapping structure, by making the activity scenario depend also on the second coordinate x_2 . We still consider the domain Ω_s defined by (2.4), with L_c being the length of the cilium-like structure, r_c begin its radius and x_c its mean position on the abscissa axis. The cilium is still anchored at $x_2 = 0$ and the orientation of the active fibers is given by the vector $e_a = (0, 1)$. In order to make the structure flap, we consider an activity scenario representing a wave propagation along the length of the cilium, defined by

$$\Sigma_a(t, (x_1, x_2)) = \frac{C_a}{L_c r_c} \sin(2\pi f_a (x_2 - v_a t))(x_c - x_1), \quad \forall t \geq 0, \quad \forall (x_1, x_2) \in \Omega_s, \quad (2.6)$$

L_c (μm)	r_c (μm)	x_c (μm)	C_a ($\text{pN} \cdot \mu\text{m}^2$)
6.5	0.2	0	1.2
f_a (μm^{-1})	E_s ($\text{pN} \cdot \mu\text{m}^{-2}$)	ν_s	v_a ($\mu\text{m} \cdot \text{s}^{-1}$)
1	10^6	0.49	1

Table 2.2 – Set of parameters for the flapping scenario of activity.

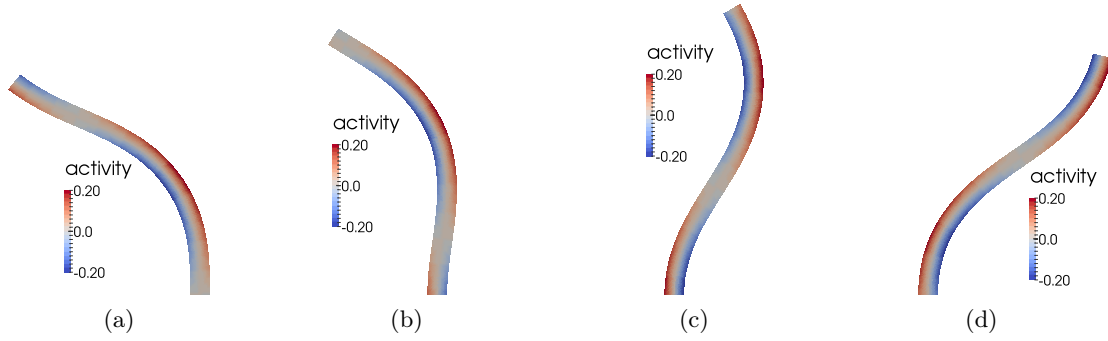


Figure 2.2 – Deformation of an elongated structure subjected to the internal activity defined by (2.6) at different times: $t = 0\text{s}$ (a), $t = 0.012\text{s}$ (b), $t = 0.025\text{s}$ (c) and $t = 0.037\text{s}$ (d). The activity scenario Σ_a is represented with the set of parameters be given in Table 2.2.

where f_a denotes the frequency of the wave, C_a still denotes the intensity of the internal activity and v_a is the *velocity* of propagation of the wave along the length of the cilium. In this situation, elongations and contractions of the medium are not constant along the length of the cilium and it results in undulations of the whole structure. As before, we numerically solve problem (2.1) with Σ_a defined by (2.6) and $e_a = (0, 1)$, using the finite element method and Newton's algorithm. The results are shown in Figure 2.2 with the set of parameters be given in Table 2.2. From Figure 2.2a to Figure 2.2d we observe that, while the wave propagates along the length of the cilium, the structure deforms itself with an oscillatory motion. For example, in Figure 2.2c, the sign of the activity scenario change along the direction of the active fibers and is zero at approximate mid-point of the length of the cilium. This results in a double curved deformation of the structure since two opposite contraction behaviors are induced by the internal activity: at the bottom of the cilium the medium stretches in the left and contracts in the right, whereas at the top it contracts in the left and stretches in the right.

A non symmetric scenario. In the study of the locomotion of microorganisms, it is well-known that in order to efficiently swim or propel the surrounding fluid, the movement of a cilium or a flagellum has to be non symmetric in time. This is the statement of Purcell's scallop Theorem [Purcell, 1977] and this is due to reversibility properties of viscous fluids at low Reynold's number (which is the case we are interested in). Thus, to be able to model non symmetric internal activities is of primary importance for the study of active structures in a viscous fluid. In particular, we propose in the present paragraph an activity scenario to mimic the deformations of cilia.

Again, we consider the domain Ω_s defined by (2.4), with L_c being the length of the cilium-like structure, r_c being its radius and x_c its mean position on the abscissa axis. The

L_c (μm)	r_c (μm)	x_c (μm)	C_a (pN \cdot μm)	f_a (Hz)	E_s (pN \cdot μm^{-2})	ν_s
6.5	0.2	0	3	10	10^6	0.49

Table 2.3 – Set of parameters for the non symmetric scenario of activity.

cilium is still anchored at $x_2 = 0$ and the orientation of the active fibers is given by the vector $e_a = (0, 1)$. The activity scenario that we propose is the following:

$$\Sigma_a(t, (x_1, x_2)) = \frac{C_a}{L_c r_c} (\sigma_{a,1}(t, x_2) + \sigma_{a,2}(t, x_2)) (x_c - x_1), \quad \forall t \geq 0, \quad \forall (x_1, x_2) \in \Omega_s, \quad (2.7)$$

where $\sigma_{a,1}(t, x_2)$ and $\sigma_{a,2}(t, x_2)$ are defined, for all $t \geq 0$ and for all x_2 in $[0, L_c]$ by

$$\sigma_{a,1}(t, x_2) = (x_2 - L_c)^2 \sin\left(2\pi f_a \left(t - \frac{T_a}{4}\right)\right),$$

and

$$\sigma_{a,2}(t, x_2) = \begin{cases} 0, & \text{if } t - \left\lfloor \frac{t}{T_a} \right\rfloor T_a < \frac{T_a}{2}, \\ x_2 \left(x_2 - \frac{L_c}{2}\right) \cos\left(2\pi f_a \left(t - \frac{T_a}{4}\right)\right), & \text{if } t - \left\lfloor \frac{t}{T_a} \right\rfloor T_a \geq \frac{T_a}{2}. \end{cases}$$

As before, f_a and C_a still denote the beating frequency and the intensity of the internal activity. The parameters T_a is the period of the beating, i.e. $T_a = \frac{1}{f_a}$. The results shown in Figure 2.3 correspond to set of parameters given in Table 2.3. They have been obtained by solving problem (2.1) with Σ_a defined by (2.7) and using the finite element method and Newton's algorithm. We can observe that the activity scenario (2.7) is divided in two phases. During the first phase (Figure 2.3a to Figure 2.3d), taking place during the first half period of the beat, the function $\sigma_{a,2}$ is null and the cilium starts from a deformed configuration represented in Figure 2.3a. Then a bending deformation occurs to the right with the intensity being the greater close to the bottom of the cilium because of the term $(x_2 - L_c)^2$. At the end of the first phase the cilium is in the configuration represented in Figure 2.3d. During the second phase (Figure 2.3h to Figure 2.3e), the function $\sigma_{a,2}$ becomes non null and the deformation of the cilium is induced by the sum of both contributions of $\sigma_{a,1}$ and $\sigma_{a,2}$. In this phase, the bending occurs to the left. In particular the term $x_2(x_2 - \frac{L_c}{2})$ induces a double curved deformation that we can observe in Figure 2.3f.

Remark 2.2. The activity scenario (2.7) is used in Section 2.4 to perform numerical simulations of active structures beating in a viscous fluid.

A scenario in three space dimensions. The framework developed in the present section is independent of the space dimension and can easily be adapted to model three-dimensional active structures. Let L_c , r_c and x_c still denote the length, the radius and the mean position on the x_1 -axis of the cilium-like structure. Moreover, we denote by y_c the mean position of the structure on the x_2 -axis. In three space dimensions, Ω_s is the cylinder in \mathbb{R}^3 defined by

$$\Omega_s = \{(x_1, x_2, x_3) \in \mathbb{R}^3; (x_c - x_1)^2 + (y_c - x_2)^2 \leq r_c^2, 0 \leq x_3 \leq L_c\}.$$

Then, we consider the following activity scenario defined for all time $t \geq 0$ and for all $x = (x_1, x_2, x_3)$ in Ω_s by

$$\Sigma_a(t, x) = \frac{C_a}{L_c \pi r_c^2} \sin(2\pi f_a (x_3 - v_a t)) (\cos(3\pi f_a t) (x_1 - x_c) + \sin(3\pi f_a t) (x_2 - y_c)), \quad (2.8)$$

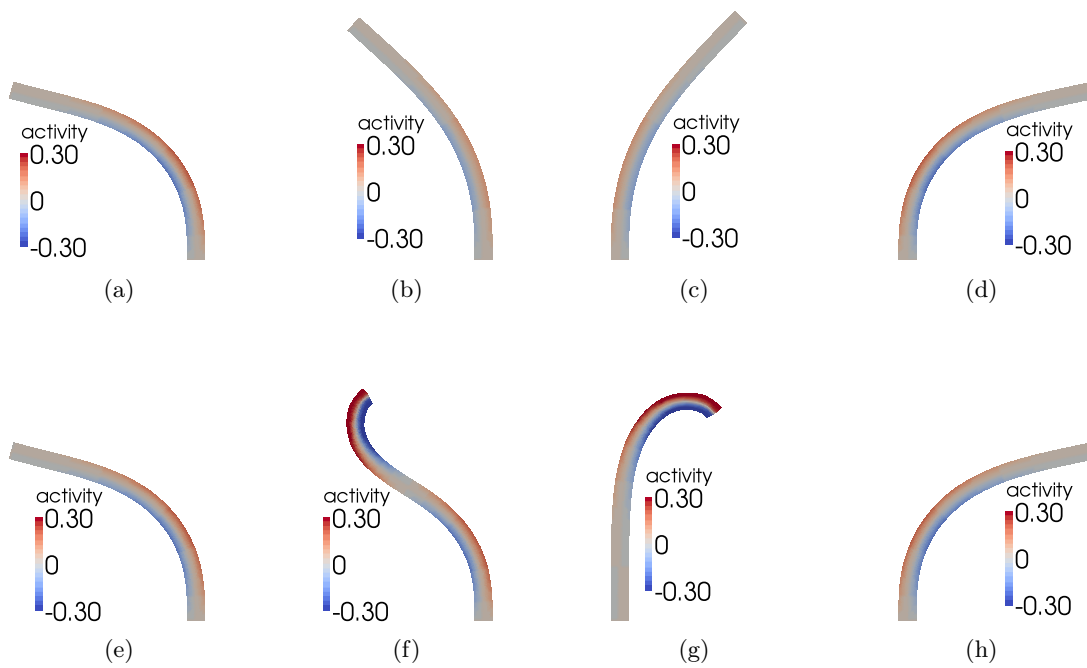
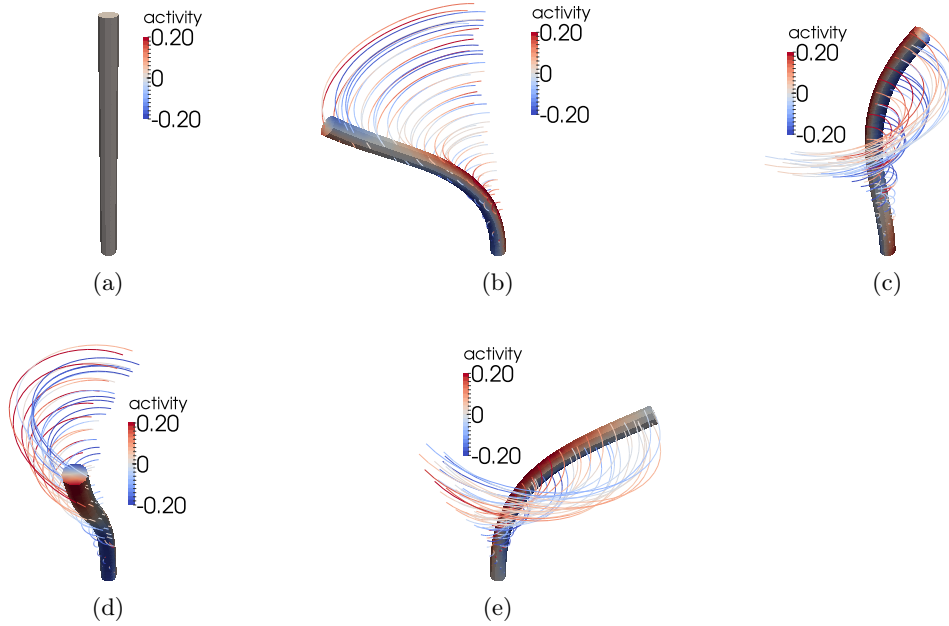


Figure 2.3 – Elongated structure subjected to the internal activity defined by (2.7) inducing cilia-like deformations at different time: $t = 0\text{s}$ (a), $t = 0.015\text{s}$ (b), $t = 0.035\text{s}$ (c), $t = 0.050\text{s}$ (d), $t = 0.050\text{s}$ (h), $t = 0.065\text{s}$ (g), $t = 0.085\text{s}$ (f), and $t = 0.1\text{s}$ (e). The activity scenario Σ_a is represented with the set of parameters be given in Table 2.3.

L_c (μm)	r_c (μm)	(x_c, y_c) (μm)	C_a ($\text{pN} \cdot \mu\text{m}^3$)
6.5	0.2	(0,0)	0.01
f_a (μm^{-1})	E_s ($\text{pN} \cdot \mu\text{m}^{-2}$)	ν_s	v_a ($\mu\text{m} \cdot \text{s}^{-1}$)
0.5	10^6	0.49	1

Table 2.4 – Set of parameters for the twirling scenario of activity in three space dimensions.

Figure 2.4 – Elongated three-dimensional structure subjected to the internal activity defined by (2.8) inducing twirling at different time: $t = 0\text{s}$ (a), $t = 0.052\text{s}$ (b), $t = 0.082\text{s}$ (c), $t = 0.107\text{s}$ (d), and $t = 0.128\text{s}$ (e). The activity scenario Σ_a is represented with the set of parameters be given in Table 2.4.

where, as before, f_a is the beating frequency, C_a is the intensity of the activity and v_a is the velocity of the wave that propagates along the length of the cilia. The deformations produced by the previous activity scenario are presented in Figure 2.4, with the set of parameters be given in Table 2.4. It results in a twirling movement of the structure.

2.3 A coupled fluid-structure interaction problem with cilia-like structures

In this section, we introduce a coupled fluid-structure interaction problem involving active structures, modeled by the active elasticity equations, and a Newtonian viscous incompressible homogeneous fluid, modeled by the Stokes equations. The choice of the Stokes equations is justified by the motivation of our study. Indeed, we recall that we aim at modeling the interaction between a biological fluid (essentially water) and microscopic ciliated organisms. Because of their microscopic size and their slow velocity, the Reynolds' number associated to this system is of the order of 10^{-6} . Thus, the inertial effects of the system can be neglected and we consider non-inertial equations for both the fluid and the

structures.

2.3.1 Description of the model

The problem presented in this section is intended to be used for numerical simulations. For that purpose we consider specific hypotheses on the domains to be meshed. Let Ω be a n -dimensional box ($n = 2$ or 3), i.e. the domain defined by $\Omega = \prod_{i=1}^n [0, L_i]$, where the $(L_i)_{i=1, \dots, n}$ are the dimensions of the box in every directions. The domain Ω is divided in two subsets, $\Omega = \Omega_s \cup \Omega_f$ such that $\Omega_f \cap \Omega_s = \emptyset$, where Ω_s is the solid domain, defined as the union of a finite number of cylindrical domains which represent cilia-like structures in their reference configuration, and Ω_f is the fluid domain in the reference configuration. The fluid-structure interface between Ω_s and Ω_f is denoted by Γ and we define the remaining boundaries of Ω_s by $\Gamma_s = \partial\Omega_s \setminus \Gamma$, where homogeneous Dirichlet boundary conditions are applied. The boundary of Ω_f is divided in four parts, where different boundary conditions are applied. The first one is the fluid-structure interface Γ . Then, on the bottom boundary $\Gamma_{f,D} = \{x = (x_1, \dots, x_n) \in \Omega; x_n = 0\}$ we consider homogeneous Dirichlet boundary conditions, while on the top boundary $\Gamma_{f,S} = \{x = (x_1, \dots, x_n) \in \Omega; x_n = L_n\}$ we consider slip boundary conditions. Finally, on the lateral boundaries $\Gamma_{f,N} = \partial\Omega_f \setminus (\Gamma \cup \Gamma_{f,D} \cup \Gamma_{f,S})$, homogeneous Neumann boundary conditions are applied. Moreover, we denote by Γ_f the union of $\Gamma_{f,D}$, $\Gamma_{f,S}$ and $\Gamma_{f,N}$:

$$\Gamma_f = \Gamma_{f,D} \cup \Gamma_{f,S} \cup \Gamma_{f,N}. \quad (2.9)$$

The domain Ω_s is filled with an active elastic medium which satisfies the Saint Venant-Kirchhoff law and whose activity is taken into account with the continuum mechanics framework developed in Section 2.2. Given a time dependent body force f_s and a time dependent internal activity Σ^* , the problem of elasticity we are considering is to find the displacement d_s of the solid medium such that, for all $t \geq 0$,

$$\begin{aligned} -\operatorname{div}((I + \nabla d_s(t))(\Sigma_s(d_s(t)) - \Sigma^*(t))) &= f_s(t), & \text{in } \Omega_s, \\ d_s(t) &= 0, & \text{on } \Gamma_s, \end{aligned} \quad (2.10)$$

where $\Sigma_s(d_s(t))$ is defined by (2.2).

The solid problem is always solved in the reference configuration of the structure Ω_s , i.e. in Lagrangian coordinates, whereas the fluid problem is usually set up in Eulerian coordinates, i.e. in the current (deformed) configuration. This deformed configuration at time $t \geq 0$ depends on the displacement of the solid medium on the interface Γ by means of a transformation denoted by $\Phi(d_s(t))$, which satisfies

$$\Phi(d_s(t)) = \mathcal{I} + d_s(t), \quad \text{on } \Gamma.$$

The mapping \mathcal{I} denotes the identity mapping in \mathbb{R}^n . Moreover, let γ_Γ be the trace operator from Ω_s onto Γ and \mathcal{R} be a lifting operator from Γ into Ω_f (in spaces made precise later on), then the transformation $\Phi(d_s(t))$ is defined in the whole domain Ω_f by

$$\Phi(d_s(t)) = \mathcal{I} + \mathcal{R}(\gamma_\Gamma(d_s(t))), \quad \text{in } \Omega_f,$$

such that $\mathcal{R}(\gamma_\Gamma(d_s(t)))$ is null on the exterior boundary Γ_f , defined by (2.9). Thus, the transformation $\Phi(d_s(t))$ maps the reference fluid domain Ω_f to the deformed fluid domain at time t , $\Phi(d_s(t))(\Omega_f)$. In practice, the construction of the lifting operator \mathcal{R} is done by solving an elliptic problem (typically a Laplace equation or the equations of linearized elasticity)

on Ω_f with homogeneous Dirichlet boundary conditions on Γ_f and applying $\gamma_\Gamma(d_s(t))$ on the interface Γ .

At time t , the domain $\Phi(d_s(t))(\Omega_f)$ is filled with a Newtonian viscous incompressible homogeneous fluid, whose viscosity, μ_f , is positive. Given a time dependent body force f_f , the velocity of the fluid u_f and the pressure of the fluid p_f satisfy, for all $t \geq 0$, the Stokes equations with mixed Dirichlet, Neumann and slip boundary conditions:

$$\begin{aligned} -\operatorname{div}(\sigma_f(u_f(t), p_f(t))) &= f_f(t), & \text{in } \Phi(d_s(t))(\Omega_f), \\ \operatorname{div}(u_f(t)) &= 0, & \text{in } \Phi(d_s(t))(\Omega_f), \\ u_f(t) &= 0, & \text{on } \Gamma_{f,D}, \\ u_f(t) \cdot n_f(t) &= 0, & \text{on } \Gamma_{f,S}, \\ (\sigma_f(u_f(t), p_f(t))n_f(t)) \cdot \tau_f(t) &= 0, & \text{on } \Gamma_{f,S}, \\ \sigma_f(u_f(t), p_f(t))n_f(t) &= 0, & \text{on } \Gamma_{f,N}. \end{aligned} \quad (2.11)$$

The tensor $\sigma_f(u_f(t), p_f(t))$ is the fluid stress tensor defined by

$$\sigma_f(u_f(t), p_f(t)) = 2\mu_f D(u_f(t)) - p_f(t)I,$$

where $D(u_f(t)) = \frac{1}{2}(\nabla u_f(t) + \nabla u_f(t)^T)$ is the symmetric gradient of $u_f(t)$ and I denotes the identity matrix of \mathbb{R}^n .

Equations (2.10) and (2.11) are completed by the usual fluid-structure coupling conditions on the interface Γ , namely the equality of the velocities and the continuity of the normal components of stress tensors. Because these conditions are written in the reference configuration, we introduce the velocity of the fluid written in the fluid reference configuration, w_f , and the pressure of the fluid written in the fluid reference configuration, q_f , defined by

$$w_f(t, \cdot) = u_f(t, \Phi(d_s(t, \cdot))) \quad \text{and} \quad q_f(t, \cdot) = p_f(t, \Phi(d_s(t, \cdot))), \quad \text{in } \Omega_f. \quad (2.12)$$

Moreover, the fluid stress tensor at time t written in the fluid reference configuration, denoted by $\Pi_f(w_f(t), q_f(t))$, is defined by

$$\begin{aligned} \Pi_f(w_f(t), q_f(t)) &= \mu_f (\nabla w_f(t)F(d_s(t)) + (\nabla(\Phi(d_s(t))))^{-T} \nabla w_f(t)^T G(d_s(t))) \\ &\quad - q_f(t)G(d_s(t)), \end{aligned}$$

where $F(d_s(t))$ and $G(d_s(t))$ are the following matrices:

$$\begin{aligned} F(d_s(t)) &= (\nabla(\Phi(d_s(t))))^{-1} \operatorname{cof}(\nabla(\Phi(d_s(t))))), \\ G(d_s(t)) &= \operatorname{cof}(\nabla(\Phi(d_s(t)))). \end{aligned} \quad (2.13)$$

Remark 2.3. The tensor Π_f is the Piola transform of the fluid stress tensor σ_f . For more information on how to transform the Stokes equations from the deformed configuration to the reference configuration, see Appendix B.

Then, for all $t \geq 0$, the coupling conditions on Γ write

$$\begin{aligned} \frac{\partial d_s(t)}{\partial t} &= w_f(t), & \text{on } \Gamma, \\ (I + \nabla d_s(t))(\Sigma_s(d_s(t)) - \Sigma^*(t))n_s &= \Pi_f(w_f(t), q_f(t))n_s, & \text{on } \Gamma. \end{aligned} \quad (2.14)$$

The condition on the continuity of the velocity through the interface Γ , considered in (2.14), requires an initial condition concerning the initial displacement of the structure on Γ . Then, we suppose that all cilia-like structures are in their reference configuration at time $t = 0$, i.e. that $d_s(0) = 0$ on Γ .

Remark 2.4. In problem (2.11), the current fluid domain $\Phi(d_s(t))(\Omega_f)$ is an unknown of the problem, since it depends on the displacement of the structure. In the present chapter, we discretize in time equations (2.10), (2.11) and (2.14), in order to make the configuration of the current fluid domain at a given time step entirely determined by the displacement of the structure at the previous time step. This is the purpose of the next subsection.

Remark 2.5. In definition (2.13), the matrix $F(d_s(t))$, that appears in the expression of the fluid stress tensor written in the fluid reference configuration, is well-defined if the mapping $\Phi(d_s(t))$ is, for example, a C^1 -diffeomorphism. This kind of regularity is not intended to be proved in the present chapter, but will be studied in Chapter 3. In the mean time, we can justify our approach by recalling that our purpose here is to compute numerical simulations based on the model constructed within the present section and that, in a context of numerical simulations, the deformation at a given time step is easily invertible. For this reason, we assume in the following that the deformations are sufficiently regular for what we write to make sense.

2.3.2 The discrete-in-time fluid-structure interaction problem

Let us introduce a discretization of \mathbb{R}^+ for the time variable t . Let $\delta t > 0$ be a constant time step. We construct a sequence $(t_k)_{k \in \mathbb{N}}$ such that

$$\begin{aligned} t_0 &= 0, \\ t_{k+1} &= t_k + \delta t, \forall k \geq 0, \end{aligned}$$

and, for all $k \geq 0$, we define the time-discretizations of the displacement of the structure d_s^k , the velocity of the fluid u_f^k and the pressure of the fluid p_f^k by

$$d_s^k = d_s(t_k), \quad u_f^k = u_f(t_k), \quad \text{and} \quad p_f^k = p_f(t_k).$$

Similarly, the time-discretization of the body forces f_f^k and f_s^k and the activity Σ_k^* are defined, for all $k \geq 0$ by

$$f_f^k = f_f(t_k), \quad f_s^k = f_s(t_k) \quad \text{and} \quad \Sigma_k^* = \Sigma^*(t_k)$$

Moreover, the first coupling condition in (2.14) is discretized using the implicit Euler scheme:

$$\begin{aligned} d_s^0 &= 0, \\ d_s^{k+1} &= d_s^k + \delta t w_f^{k+1}, \forall k \geq 0. \end{aligned}$$

For $k > 0$, the deformed fluid domain at time t_k , $\Phi(d_s(t_k))(\Omega_f)$, is denoted by Ω_f^k and depends on the displacement of the structure at the previous time step by

$$\Omega_f^k = \Phi(d_s^{k-1})(\Omega_f).$$

Similarly, the fluid-structure interface at time t_k writes

$$\Gamma^k = \Phi(d_s^{k-1})(\Gamma),$$

and the remaining fluid boundaries in the deformed configuration do not change, i.e.

$$\begin{aligned} \Gamma_{f,D}^k &= \Gamma_{f,D}, \\ \Gamma_{f,S}^k &= \Gamma_{f,S}, \\ \Gamma_{f,N}^k &= \Gamma_{f,N}. \end{aligned}$$

For $k = 0$, we suppose by convention that $d_s^{0-1} = 0$ on Γ , such that $\Omega_f^0 = \Omega_f$ and $\Gamma^0 = \Gamma$.

Then, the discrete-in-time fluid-structure interaction problem that we consider is to find, for all $k \geq 0$, the displacement of the structure d_s^k , the velocity of the fluid u_f^k and the pressure of the fluid p_f^k which satisfy

$$\begin{aligned} -\operatorname{div}((I + \nabla d_s^k)(\Sigma_s(d_s^k) - \Sigma_k^*)) &= f_s^k, & \text{in } \Omega_s, \\ d_s^k &= 0, & \text{on } \Gamma_s, \end{aligned} \quad (2.15)$$

$$\begin{aligned} -\operatorname{div}(\sigma_f(u_f^k, p_f^k)) &= f_f^k, & \text{in } \Omega_f^k, \\ \operatorname{div}(u_f^k) &= 0, & \text{in } \Omega_f^k, \\ u_f^k &= 0, & \text{on } \Gamma_{f,D}, \\ u_f^k \cdot n_f^k &= 0, & \text{on } \Gamma_{f,S}, \\ (\sigma_f(u_f^k, p_f^k)n_f^k) \cdot \tau_f^k &= 0, & \text{on } \Gamma_{f,S}, \\ \sigma_f(u_f^k, p_f^k)n_f^k &= 0, & \text{on } \Gamma_{f,N}, \end{aligned} \quad (2.16)$$

$$\begin{aligned} d_s^k &= d_s^{k-1} + \delta t w_f^k, & \text{on } \Gamma, \\ (I + \nabla d_s^k)(\Sigma_s(d_s^k) - \Sigma_k^*)n_s &= \Pi_f(w_f^k, q_f^k)n_s, & \text{on } \Gamma, \end{aligned} \quad (2.17)$$

where

$$w_f^k(\cdot) = u_f^k(\Phi(d_s^{k-1})(\cdot)) \quad \text{and} \quad q_f^k(\cdot) = p_f^k(\Phi(d_s^{k-1})(\cdot)), \quad \text{in } \Omega_f.$$

In Section 2.4 we will present the numerical method used for the simulation of active structures in a viscous fluid. The method is based on a saddle-point formulation for the discrete-in-time coupled system of equations (2.15), (2.16) and (2.17), that is well-suited for the numerical simulation with standard finite element techniques and solvers, and that will be introduced later on. To that aim, we first study the weak formulation of problem (2.15), (2.16) and (2.17) in Subsection 2.3.3, then, the constraint on the continuity of velocities is expressed with a Lagrange multiplier and the saddle-point problem is introduced in Subsection 2.3.4. For the sake of simplicity, the well-posedness of both problems is studied in the linearized case, i.e. the case where the active elasticity equations are linearized around the equilibrium. To that aim, we introduce the linearized active elasticity problem, which consists in finding the displacement of the structure d_s^k which satisfies

$$\begin{aligned} -\operatorname{div}(\sigma_s(d_s^k) - \nabla d_s^k \Sigma_k^*) &= f_s^k + \operatorname{div}(\Sigma^*), & \text{in } \Omega_s, \\ d_s^k &= 0, & \text{on } \Gamma_s, \end{aligned} \quad (2.18)$$

where $\sigma_s(d_s^k)$ is the linearized stress tensor of the structure around the equilibrium at time t_k which writes

$$\sigma_s(d_s^k) = 2\mu_f D(d_s^k) + \lambda_s \operatorname{div}(d_s^k)I. \quad (2.19)$$

Coupling conditions (2.17) are also linearized near the equilibrium and become

$$\begin{aligned} d_s^k &= d_s^{k-1} + \delta t w_f^k, & \text{on } \Gamma, \\ (\sigma_s(d_s^k) - \nabla d_s^k \Sigma_k^*)n_s &= \Pi_f(w_f^k, q_f^k)n_s + \Sigma^*n_s, & \text{on } \Gamma. \end{aligned} \quad (2.20)$$

Thus, the linearized coupled fluid-structure problem we are interested in and that will be studied in the next subsection is the system of equations (2.16), (2.18) and (2.20).

2.3.3 Existence and uniqueness of a weak solution to the linearized fluid-structure interaction problem

In this subsection, we define and study the weak formulation of the linearized fluid-structure problem (2.16), (2.18) and (2.20). First, let us introduce the following function spaces, for all $k \geq 0$:

$$\begin{aligned} V_f^k &= \left\{ v \in (H^1(\Omega_f^k))^n; \gamma_{\Gamma_{f,D}}(v) = 0, \gamma_{\Gamma_{f,S}}(v) \cdot n_f^k = 0 \right\}, \\ V_s &= \left\{ v \in (H^1(\Omega_s))^n; \gamma_{\Gamma_s}(v) = 0 \right\}. \\ W_u &= \left\{ (v_f, v_s) \in V_f^k \times V_s; \gamma_{\Gamma}(v_f \circ \Phi(d_s^{k-1})) = \gamma_{\Gamma}(v_s) \right\}, \\ W_d &= \left\{ (v_f, d_s) \in V_f^k \times V_s; \delta t \gamma_{\Gamma}(v_f \circ \Phi(d_s^{k-1})) + d_s^{k-1} = \gamma_{\Gamma}(d_s) \right\}. \end{aligned} \quad (2.21)$$

Then, the weak formulation of problem (2.16), (2.18) and (2.20) is given by the following lemma.

Lemma 2.1. *The weak formulation of problem (2.16), (2.18) and (2.20) is defined by*

$$\left\{ \begin{array}{l} \text{find } (u_f^k, d_s^k) \in W_d \text{ and } p_f^k \in L^2(\Omega_f^k) \text{ such that} \\ \int_{\Omega_f^k} \sigma_f(u_f^k, p_f^k) : \nabla v_f + \int_{\Omega_s} (\sigma_s(d_s^k) - \nabla d_s^k \Sigma_k^*) : \nabla v_s \\ \qquad \qquad \qquad = \int_{\Omega_f^k} f_f^k \cdot v_f + \int_{\Omega_s} f_s^k \cdot v_s - \int_{\Omega_s} \Sigma_k^* : \nabla v_s, \quad \forall (v_f, v_s) \in W_u, \\ \int_{\Omega_f^k} q_f \operatorname{div}(u_f^k) = 0, \quad \forall q_f \in L^2(\Omega_f^k). \end{array} \right. \quad (2.22)$$

Proof. Let (v_f, v_s) be a regular function in W_u and suppose that u_f^k , d_s^k and p_f^k are sufficiently regular. We can formally multiply the first equation in (2.16) by v_f and the first equation in (2.18) by v_s and integrate respectively over Ω_f^k and Ω_s . After an integration by part, we obtain

$$\int_{\Omega_f^k} \sigma_f(u_f^k, p_f^k) : \nabla v_f - \int_{\Gamma^k \cup \Gamma_{f,S}} (\sigma_f(u_f^k, p_f^k) n_f^k) \cdot v_f = \int_{\Omega_f^k} f_f^k \cdot v_f, \quad (2.23)$$

and

$$\begin{aligned} \int_{\Omega_s} (\sigma_s(d_s^k) - \nabla d_s^k \Sigma_k^*) : \nabla v_s - \int_{\Gamma} ((\sigma_s(d_s^k) - \nabla d_s^k \Sigma_k^*) n_s) \cdot v_s \\ = \int_{\Omega_s} f_s^k \cdot v_s - \int_{\Omega_s} \Sigma_k^* : \nabla v_s + \int_{\Gamma} (\Sigma_k^* n_s) \cdot v_s. \end{aligned} \quad (2.24)$$

Moreover, decomposing the normal stress $\sigma_f(u_f^k, p_f^k) n_f^k$ on $\Gamma_{f,S}$ in its normal and tangential components and using the slip boundary conditions on $\Gamma_{f,S}$ for the fluid problem, it follows that

$$\begin{aligned} \int_{\Gamma_{f,S}} (\sigma_f(u_f^k, p_f^k) n_f^k) \cdot v_f &= \int_{\Gamma_{f,S}} \left(((\sigma_f(u_f^k, p_f^k) n_f^k) \cdot n_f^k) n_f^k + ((\sigma_f(u_f^k, p_f^k) n_f^k) \cdot \tau_f^k) \tau_f^k \right) \cdot v_f, \\ &= 0. \end{aligned}$$

Then, after a change of variables and making use of the second coupling condition in (2.20), we have

$$\begin{aligned} \int_{\Gamma^k} (\sigma_f(u_f^k, p_f^k) n_f^k) \cdot v_f &= \int_{\Gamma} (\Pi_f(w_f^k, q_f^k) n_f) \cdot (v_f \circ \Phi(d_s^{k-1})), \\ &= \int_{\Gamma} ((\sigma_s(d_s^k) - \nabla d_s^k \Sigma_k^*) n_s) \cdot v_s - \int_{\Gamma} (\Sigma_k^* n_s) \cdot v_s. \end{aligned}$$

Now, summing equation (2.23) and equation (2.24) it comes

$$\begin{aligned} & \int_{\Omega_f^k} \sigma_f(u_f^k, p_f^k) : \nabla v_f + \int_{\Omega_s} (\sigma_s(d_s^k) - \nabla d_s^k \Sigma_k^*) : \nabla v_s \\ &= \int_{\Omega_f^k} f_f^k \cdot v_f + \int_{\Omega_s} f_s^k \cdot v_s - \int_{\Omega_s} \Sigma_k^* : \nabla v_s. \end{aligned}$$

Similarly, let q_f be in $L^2(\Omega_f^k)$. Formally, we multiply the second equation in (2.16) by q_f and integrate over Ω_f^k . We obtain

$$\int_{\Omega_f^k} q_f \operatorname{div}(u_f^k) = 0.$$

To prove that problem (2.22) is well-posed, we perform a change in variables in the displacement d_s^k in order to work on a velocity-velocity formulation of the fluid-structure problem (instead of a velocity-displacement formulation). Let us introduce the discrete-in-time velocity of the structure at time t_k , u_s^k , defined by

$$u_s^k = \frac{1}{\delta t} (d_s^k - d_s^{k-1}). \quad (2.25)$$

Thus, the previous weak problem is equivalent to the problem where d_s^k has been replaced by $\delta t u_s^k + d_s^{k-1}$:

$$\left\{ \begin{array}{l} \text{find } (u_f^k, u_s^k) \in W_u \text{ and } p_f^k \in L^2(\Omega_f^k) \text{ such that} \\ a^k((u_f^k, u_s^k), (v_f, v_s)) - \left(B(v_f, v_s), p_f^k \right)_{L^2(\Omega_f^k)} = L^k(v_f, v_s), \forall (v_f, v_s) \in W_u, \\ \left(B(u_f^k, u_s^k), q \right)_{L^2(\Omega_f^k)} = 0, \quad \forall q \in L^2(\Omega_f^k), \end{array} \right. \quad (2.26)$$

where $(\cdot, \cdot)_{L^2(\Omega_f^k)}$ denotes the scalar product in $L^2(\Omega_f^k)$ and a^k , L^k and B are defined by

$$\begin{aligned} a^k((u_f, u_s), (v_f, v_s)) &= 2\mu_f \int_{\Omega_f^k} D(u_f) : D(v_f) + \delta_t \int_{\Omega_s} \sigma_s(u_s) : \nabla v_s \\ &\quad - \delta_t \int_{\Omega_s} (\nabla u_s \Sigma_k^*) : \nabla v_s, \quad \forall (u_f, u_s), (v_f, v_s) \in V_f^k \times V_s, \\ L^k(v_f, v_s) &= \int_{\Omega_f^k} f_f^k \cdot v_f + \int_{\Omega_s} f_s^k \cdot v_s - \int_{\Omega_s} \Sigma_k^* : \nabla v_s \\ &\quad - \int_{\Omega_s} (\sigma_s(d_s^{k-1}) - \nabla d_s^{k-1} \Sigma_k^*) : \nabla v_s, \quad \forall (v_f, v_s) \in V_f^k \times V_s, \\ B(v_f, v_s) &= \operatorname{div}(v_f), \quad \forall (v_f, v_s) \in W_u. \end{aligned}$$

Theorem 2.1. *Let $k \geq 0$ and suppose that the force f_f^k belongs to $(L^2(\Omega_f^k))^n$, the force f_s^k belongs to $(L^2(\Omega_s))^n$, the displacement d_s^{k-1} belongs to V_s and the activity tensor Σ_k^* belongs to $(L^\infty(\Omega_s))^{n \times n}$. There exists a constant $C(n, \Omega_s)$ which only depends on the dimension n and on the domain Ω_s such that, if Σ_k^* satisfies*

$$\|\Sigma_k^*\|_{L^\infty(\Omega_s)} < C(\Omega_s) \mu_s, \quad (2.27)$$

then there exists a unique solution to problem (2.26).

Proof. Let us show that a is a continuous bilinear coercive form on $(V_f^k \times V_s)^2$, that L is a continuous linear form on $V_f^k \times V_s$ and that B is a continuous linear surjective operator from W_u to $L^2(\Omega_f^k)$.

Because Σ^* belongs to $(L^\infty(\Omega_s))^{n \times n}$, it is clear that a is a continuous bilinear form on $(V_f^k \times V_s)^2$ and that L is a continuous linear form on $V_f^k \times V_s$. In addition, the operator B is also continuous and linear from W_u to $L^2(\Omega_f^k)$.

Now, we show that a^k is coercive under condition (2.27). Using the L^∞ -regularity of Σ^* and Korn's inequality we have, for all (u_f, u_s) in $V_f^k \times V_s$,

$$\begin{aligned} a^k((u_f, u_s), (u_f, u_s)) &= 2\mu_f \|D(u_f)\|_{L^2(\Omega_f^k)}^2 + 2\mu_s \delta t \|D(u_s)\|_{L^2(\Omega_s)}^2 \\ &\quad + \lambda_s \delta t \|\operatorname{div}(u_s)\|_{L^2(\Omega_s)}^2 - \delta t \int_{\Omega_s} (\nabla u_s \Sigma_k^*) : \nabla u_s. \end{aligned}$$

Yet, the last integral writes

$$\begin{aligned} \int_{\Omega_s} (\nabla u_s \Sigma_k^*) : \nabla u_s &= \sum_{i,j=1}^n \int_{\Omega_s} (\nabla u_s \Sigma_k^*)_{ij} (\nabla u_s)_{ij}, \\ &= \sum_{i,j=1}^n \int_{\Omega_s} \left(\sum_{k=1}^n (\nabla u_s)_{ik} (\Sigma_k^*)_{kj} \right) (\nabla u_s)_{ij}, \end{aligned}$$

and using the L^∞ -regularity of Σ^* it follows that

$$\begin{aligned} \int_{\Omega_s} (\nabla u_s \Sigma_k^*) : \nabla u_s &\leq \|\Sigma_k^*\|_{L^\infty(\Omega_s)} \sum_{i,j=1}^n \int_{\Omega_s} \left(\sum_{k=1}^n (\nabla u_s)_{ik} \right) (\nabla u_s)_{ij}, \\ &\leq \|\Sigma_k^*\|_{L^\infty(\Omega_s)} \sum_{i=1}^n \int_{\Omega_s} \left(\sum_{j=1}^n (\nabla u_s)_{ij} \right)^2. \end{aligned}$$

Moreover, using Young's inequality, it comes

$$\begin{aligned} \int_{\Omega_s} (\nabla u_s \Sigma_k^*) : \nabla u_s &\leq \|\Sigma_k^*\|_{L^\infty(\Omega_s)} \sum_{i=1}^n \int_{\Omega_s} n \sum_{j=1}^n (\nabla u_s)_{ij}^2, \\ &\leq n \|\Sigma_k^*\|_{L^\infty(\Omega_s)} \|\nabla u_s\|_{L^2(\Omega_s)}^2. \end{aligned}$$

Now, using Poincaré and Korn inequalities, we have

$$\begin{aligned} a^k((u_f, u_s), (u_f, u_s)) &\geq 2\mu_f C_K(\Omega_f^k) \|u_f\|_{H^1(\Omega_f^k)}^2 + 2\mu_s \delta t C_K(\Omega_s) \|u_s\|_{H^1(\Omega_s)}^2 \\ &\quad - n \delta t C_P(\Omega_s) \|\Sigma^*\|_{L^\infty(\Omega_s)} \|u_s\|_{H^1(\Omega_s)}^2, \\ &\geq 2\mu_f C_K(\Omega_f^k) \|u_f\|_{H^1(\Omega_f^k)}^2 \\ &\quad + (2\mu_s C_K(\Omega_s) - n C_P(\Omega_s) \|\Sigma^*\|_{L^\infty(\Omega_s)}) \|u_s\|_{H^1(\Omega_s)}^2, \end{aligned}$$

where $C_K(\Omega_f^k)$, $C_K(\Omega_s)$ and $C_P(\Omega_s)$ are positive constants which only depend on the domains Ω_s^k and Ω_s . So, denoting

$$C(\Omega_s) = \frac{2C_K(\Omega_s)}{nC_P(\Omega_s)}$$

and under condition (2.27), the continuous bilinear form a^k is coercive on $V_f^k \times V_s$.

To conclude, it remains to show that the operator B is surjective from W_u to $L^2(\Omega_f^k)$. Indeed, let q be in $L^2(\Omega_f^k)$. We can extend the function q in the whole space $L^2_0(\Omega)$ considering the extension operator E_p , defined by

$$E_p q = \begin{cases} q & \text{in } \Omega_f^k, \\ \frac{-1}{|\Omega \setminus \Omega_f^k|} \int_{\Omega_f^k} q & \text{in } \Omega \setminus \Omega_f^k, \end{cases}$$

where $|\Omega \setminus \Omega_f^k|$ is the volume of the subset $\Omega \setminus \Omega_f^k$. Since $E_p q$ belongs to $L^2_0(\Omega)$, Bogovskii's result (see [Bogovski, 1979]) provides that there exists a function \tilde{u} in $(H^1_0(\Omega))^n$ such that $\operatorname{div}(\tilde{u}) = E_p q$. Then, we define $v_f = \tilde{u}|_{\Omega_f^k}$ and $v_s = \tilde{u}|_{\Omega_s^k}$ and it follows that the couple $(v_f, v_s \circ \Phi(d_s^{k-1}))$ belongs to W_u and satisfies

$$B(v_f, v_s \circ \Phi(d_s^{k-1})) = \operatorname{div}(v_f) = q.$$

This proves the surjectivity of the operator B .

Finally, according to [Brezzi, 1974], problem (2.26) admits a unique solution (u_f^k, u_s^k, p_f^k) . \square

Remark 2.6. Because problems (2.22) and (2.26) are equivalent, Theorem 2.1 also applies to problem (2.22).

2.3.4 A saddle-point formulation for the fluid-active structure interaction problem

Even though problems (2.22) and (2.26) are well-posed, they are rather complicated to solve in the context of numerical simulations with standard finite element techniques. The main reason is that the fluid equations (2.16) and the solid equations (2.18) are written in two different configurations, with transmission conditions on the fluid-structure interface. For the direct simulation using the finite element method, this means that one is supposed to construct a basis of finite element functions that approximates the whole space $W_u \times L^2(\Omega_f^k)$, which does not enable to use standard finite element solvers.

Another strategy is to use an iterative method and solve both problems separately. It has the advantage to make use of existing solvers for both problems, but it requires a particular method to treat the coupling conditions on the fluid-structure interface. In the present chapter, in the context of direct numerical simulations, we consider a fitted-mesh method based on a Lagrangian multiplier to impose the continuity of the velocity through the fluid-structure interface. Actually, This provides us with a precise and easy to implement method, as close as possible to the physical phenomenon of fluid-structure interaction.

For that purpose, the present subsection is dedicated to the introduction of a different formulation of problem (2.26), where the constraint of equality of the fluid and solid velocities on Γ , which appears in the function space W_u , is treated by duality and enforced with a Lagrangian multiplier.

Let us introduce the constraint operator K , defined by

$$K : \begin{aligned} V_f^k \times V_s &\rightarrow L^2(\Omega_f^k) \times \Upsilon \\ (v_f, v_s) &\mapsto (\operatorname{div}(v_f), \gamma_\Gamma(v_f \circ \Phi(d_s^{k-1})) - \gamma_\Gamma(v_s)), \end{aligned}$$

where the space Υ , defined by

$$\Upsilon = (H^{1/2}_0(\Gamma))^n,$$

denotes the image of V_s (resp. V_f) by the trace operator on Γ . In other words, Υ is the space of functions in $(H^{1/2}(\Gamma))^n$ whose extension by zero on Γ_s (resp. Γ_f) belongs to $(H^{1/2}(\partial\Omega_s))^n$ (resp. $(H^{1/2}(\partial\Omega_f))^n$). Then, we define and study the well-posedness of the following (non-constraint) saddle-point problem:

$$\left\{ \begin{array}{l} \text{find } (u_f^k, u_s^k) \in V_f^k \times V_s, p_f^k \in L^2(\Omega_f^k) \text{ and } \lambda^k \text{ in } \Upsilon \text{ such that} \\ a^k((u_f^k, u_s^k), (v_f, v_s)) - \left((p_f^k, \lambda^k), K(v_f, v_s) \right)_{L^2(\Omega_f^k) \times \Upsilon} \\ \qquad \qquad \qquad \qquad \qquad \qquad \qquad \qquad \qquad \qquad \qquad = L^k(v_f, v_s), \quad \forall (v_f, v_s) \in V_f^k \times V_s, \\ \left((q_f, \mu), K(u_f^k, u_s^k) \right)_{L^2(\Omega_f^k) \times \Upsilon} = 0, \quad \forall (q_f, \mu) \in L^2(\Omega_f^k) \times \Upsilon. \end{array} \right. \quad (2.28)$$

Theorem 2.2. *Let $k \geq 0$ and suppose that the force f_f^k belongs to $(L^2(\Omega_f^k))^n$, the force f_s^k belongs to $(L^2(\Omega_s))^n$, the displacement d_s^{k-1} belongs to V_s and the active tensor Σ_k^* belongs to $(L^\infty(\Omega_s))^{n \times n}$. If Σ_k^* satisfies condition (2.27), then there exists a unique solution to problem (2.28).*

Proof. As before, the well-posedness of problem (2.28) is proved using standard results on saddle-point problem (see [Brezzi, 1974]). It has already been argued in the proof of Theorem 2.1 that a^k is a continuous coercive bilinear form on $(V_f^k \times V_s)^2$ and that L^k is a continuous linear form on $V_f^k \times V_s$. Moreover, the operator K is clearly linear and continuous from $V_f^k \times V_s$ to $L^2(\Omega_f^k) \times \Upsilon$ due to the continuity of the divergence operator and the continuity of the trace operators from V_f to Γ and from V_s to Γ .

Let us show that K is surjective from $V_f^k \times V_s$ to $L^2(\Omega_f^k) \times \Upsilon$. Given a couple (q, μ) in $L^2(\Omega_f^k) \times \Upsilon$, we aim to find a couple (v_f, v_s) in $V_f^k \times V_s$ such that $K(v_f, v_s) = (q, \mu)$. First, suppose that v_s is known. Then, we construct \hat{v}_f in $(H_{\Gamma_f}^1(\Omega_f))^n$ such that the trace of \hat{v}_f on Γ satisfies

$$\gamma_\Gamma(\hat{v}_f) = \mu + \gamma_\Gamma(v_s). \quad (2.29)$$

This is due to the existence of a continuous linear lifting operator from Υ to $(H_{\Gamma_f}^1(\Omega_f))^n$, since Ω_f is a Lipschitz domain (see [Boyer and Fabrie, 2005, app. B]), and because $\mu + \gamma_\Gamma(v_s)$ belongs to Υ . Now, suppose that

$$\int_{\Omega_f^k} q - \operatorname{div}(\hat{v}_f \circ \Phi^{-1}(d_s^{k-1})) = 0. \quad (2.30)$$

Then, Bogovskii's result in [Bogovski, 1979] ensures that there exists a function \tilde{v}_f in the space $(H_0^1(\Omega_f^k))^n$ such that

$$\operatorname{div}(\tilde{v}_f) = q - \operatorname{div}(\hat{v}_f \circ \Phi^{-1}(d_s^{k-1})).$$

Defining $v_f = \hat{v}_f \circ \Phi^{-1}(d_s^{k-1}) + \tilde{v}_f$, then v_f belongs to $(H_{\Gamma_f}^1(\Omega_f^k))^n$ (a subspace of V_f^k) and one has $\operatorname{div}(v_f) = q$. It remains to construct v_s such that condition (2.30) holds true. In fact, using the Piola identity and equation (2.29), condition (2.30) becomes

$$\begin{aligned} \int_{\Omega_f^k} q &= \int_{\Omega_f^k} \operatorname{div}(\hat{v}_f \circ \Phi^{-1}(d_s^k)), \\ &= \int_{\Omega_f} \operatorname{div}(G(d_s^{k-1})^T \hat{v}_f), \\ &= \int_{\Gamma} (G(d_s^{k-1})^T \hat{v}_f) n_f, \\ &= \int_{\Gamma} (G(d_s^{k-1})^T (\mu + v_s)) n_f. \end{aligned}$$

Thus, we need to construct v_s in V_s such that

$$\int_{\Gamma} (G(d_s^{k-1})^T v_s) n_f = \int_{\Omega_f^k} q - \int_{\Gamma} (G(d_s^{k-1})^T \mu) n_f.$$

Taking any function \tilde{v}_s in V_s such that

$$\int_{\Gamma} (G(d_s^{k-1})^T \tilde{v}_s) n_f \neq 0,$$

we define

$$v_s = \frac{\int_{\Omega_f^k} q - \int_{\Gamma} (G(d_s^{k-1})^T \mu) n_f}{\int_{\Gamma} (G(d_s^{k-1})^T \tilde{v}_s) n_f} \tilde{v}_s.$$

Then v_s belongs to V_s and satisfies condition (2.30). As a consequence, the couple (v_f, v_s) belongs to $V_f^k \times V_s$ and satisfies $K(v_f, v_s) = (q, \mu)$.

Finally, the operator K is surjective from $V_f^k \times V_s$ to $L^2(\Omega_f^k) \times \Upsilon$ and problem (2.28) admits a unique solution $(u_f^k, u_s^k, p_f^k, \lambda^k)$. \square

The main difference between problem (2.26) and problem (2.28) is that the function spaces involved in problem (2.28) are free of constraints, whereas the function space W_u involved in problem (2.26) is not. In particular, recalling that u_s^k is defined by (2.25), problem (2.28) is equivalent to the following problem:

$$\left\{ \begin{array}{l} \text{find } u_f^k \in V_f^k, p_f^k \in L^2(\Omega_f^k), d_s^k \in V_s \text{ and } \lambda^k \text{ in } \Upsilon \text{ such that} \\ 2\mu_f \int_{\Omega_f^k} D(u_f^k): D(v_f) - \int_{\Omega_f^k} p_f^k \operatorname{div}(v_f) \\ \quad = \int_{\Omega_f^k} f_f^k \cdot v_f + \left(\lambda^k, v_f \circ \Phi(d_s^{k-1}) \right)_{\Upsilon}, \quad \forall v_f \in V_f^k, \\ \int_{\Omega_f^k} q_f \operatorname{div}(u_f^k) = 0, \quad \forall q_f \in L^2(\Omega_f^k), \\ \int_{\Omega_s} \sigma_s(d_s^k): \nabla v_s - \int_{\Omega_s} (\nabla d_s \Sigma_k^*): \nabla v_s = \int_{\Omega_s} f_s^k \cdot v_s - \left(\lambda^k, v_s \right)_{\Upsilon}, \quad \forall v_s \in V_s, \\ \left(\mu, \gamma_{\Gamma}(u_f^k \circ \Phi(d_s^{k-1})) - \frac{1}{\delta t} (\gamma_{\Gamma}(d_s^k) - \gamma_{\Gamma}(d_s^{k-1})) \right)_{\Upsilon} = 0, \quad \forall \mu \in \Upsilon. \end{array} \right. \quad (2.31)$$

For the direct simulation of fluid-structure problems, the unconstrained problem (2.31) is particularly interesting since the resolution of the fluid and structure problems are independent if the Lagrange multiplier λ^k is known. Especially, this suggests the use of an iterative method, such as Uzawa's algorithm, to numerically approximate the solution of such a saddle-point problem. This is the purpose of the next section.

2.4 Numerical simulations of active structures in a viscous fluid

2.4.1 Description of the method

Now, we come back to our initial problem, where the structure satisfies the (nonlinear) equations of elasticity, and we define for all $k \geq 0$, by analogy with problem (2.31), the

saddle-point formulation of equations (2.15), (2.16) and (2.17) by

$$\left\{ \begin{array}{l} \text{find } u_f^k \in V_f^k, p_f^k \in L^2(\Omega_f^k), d_s^k \in V_s \text{ and } \lambda^k \text{ in } \Upsilon \text{ such that} \\ 2\mu_f \int_{\Omega_f^k} D(u_f^k) : D(v_f) - \int_{\Omega_f^k} p_f^k \operatorname{div}(v_f) \\ \qquad \qquad \qquad = \int_{\Omega_f^k} f_f^k \cdot v_f + \left(\lambda^k, v_f \circ \Phi(d_s^{k-1}) \right)_{\Upsilon}, \quad \forall v_f \in V_f^k, \\ \int_{\Omega_f^k} q_f \operatorname{div}(u_f^k) = 0, \quad \forall q_f \in L^2(\Omega_f^k), \\ \int_{\Omega_s} (I + \nabla d_s^k)(\Sigma_s(d_s^k) - \Sigma_s^*) : \nabla v_s = \int_{\Omega_s} f_s^k \cdot v_s - \left(\lambda^k, v_s \right)_{\Upsilon}, \quad \forall v_s \in V_s, \\ \left(\mu, \gamma_{\Gamma}(u_f^k \circ \Phi(d_s^{k-1})) - \frac{1}{\delta t}(\gamma_{\Gamma}(d_s^k) - \gamma_{\Gamma}(d_s^{k-1})) \right)_{\Upsilon} = 0, \quad \forall \mu \in \Upsilon. \end{array} \right. \quad (2.32)$$

Problem (2.32) is solved at each time t_k using Uzawa's algorithm. It consists in constructing a sequence $(\lambda^{k,j})_{j \in \mathbb{N}}$ in the space Υ which converges, under assumption, to the Lagrange multiplier solution of problem (2.32). At each iteration j of Uzawa's algorithm, the Lagrange multiplier $\lambda^{k,j}$ is known. Thus, the resolution of problem (2.32) reduces to the resolution of a Stokes problem and an elasticity problem, where $\lambda^{k,j}$ is seen as a Neumann boundary condition on the fluid-structure interface. In practice, solutions of both problems are approximated with the finite element method on conformal meshes and standard finite element solvers are used, since both variational problems are classical. In two space dimensions, the Stokes problem is solved in mixed formulation with a direct solver and using Mini elements. The nonlinear equations of elasticity are solved with a Newton solver and using P_1 Lagrange elements. With these choices, the elements are compatible on the fluid-structure interface, since the meshes are conformal.

Uzawa's algorithm is summarized in Algorithm 2.1. At time t_k , given a parameter $\rho > 0$ and a initial guess for the Lagrange multiplier $\lambda^{k,0}$, we construct for all $j \geq 0$ a new function $\lambda^{k,j+1}$ by *i*) solving the Stokes problem appearing in problem (2.32) with $\lambda^k = \lambda^{k,j}$ as Neumann boundary condition on the fluid-structure interface, *ii*) solving the elasticity problem with $\lambda^k = \lambda^{k,j}$ as Neumann boundary condition on Γ and *iii*) updating the Lagrange multiplier using the fourth equation in (2.32):

$$\lambda^{k,j+1} = \lambda^{k,j} + \rho(\delta t \gamma_{\Gamma}(u_f^{k,j} \circ \Phi(d_s^{k-1})) - \gamma_{\Gamma}(d_s^{k,j}) + \gamma_{\Gamma}(d_s^{k-1})), \text{ on } \Gamma.$$

In practice, the function $\lambda^{k,j}$ is approximated by a P_1 function in the whole domain Ω_s , but only its values on the boundary Γ are used in the resolution of both the Stokes and elasticity problems. This algorithm is known to converge in the sense that, if the parameter ρ is chosen small enough, the sequences $(u_f^{k,j})_{j \in \mathbb{N}}$, $(p_f^{k,j})_{j \in \mathbb{N}}$, $(d_s^{k,j})_{j \in \mathbb{N}}$ and $(\lambda^{k,j})_{j \in \mathbb{N}}$ converges to u_f^k , p_f^k , d_s^k and λ^k , for all $k \geq 0$.

Once Uzawa's algorithm has converged, we recover the velocity of the fluid at time t_k , u_f^k , and the pressure of the fluid at time t_k , p_f^k , both defined in the deformed domain Ω_f^k . We also obtain the displacement of the structure at time t_k , d_s^k , expressed in the reference solid configuration Ω_s . The Lagrange multiplier at time t_k , λ^k , is also obtained in Ω_s and is used at the next time step as an initialization for Uzawa's algorithm. Besides, to go the next time step, we move the fluid and structure meshes using the displacement of the structure. The solid mesh at time t_{k+1} is directly obtained by moving the mesh representing the domain Ω_s with the displacement of the structure at time t_k . For the fluid domain, we can not use directly the fluid displacement since fluid recirculations may occur and it could lead to poor quality meshes. Then, we construct the deformation $\Phi(d_s^k)$ which maps the reference fluid

Algorithm 2.1 Uzawa's algorithm for the resolution of problem (2.32) at time t_k .

Choose a parameter ρ and an initial guess $\lambda^{k,0}$ for the Lagrange multiplier.

$j = 0$.

tant que convergence criteria are not satisfied **faire**

Compute the solution of the fluid problem $(u_f^{k,j}, p_f^{k,j})$, with $\lambda^k = \lambda^{k,j}$.

Compute the solution of the structure problem $d_s^{k,j}$ with $\lambda^k = \lambda^{k,j}$.

Update the Lagrange multiplier:

$$\lambda^{k,j+1} = \lambda^{k,j} + \rho(\delta t \gamma_\Gamma(u_f^{k,j} \circ \Phi(d_s^{k-1})) - \gamma_\Gamma(d_s^{k,j}) + \gamma_\Gamma(d_s^{k-1})), \text{ on } \Gamma.$$

Update the number of iterations $j = j + 1$.

fin tant que

domain Ω_f to the deformed fluid domain at time t_{k+1} , Ω_f^{k+1} . For that purpose, we solve a problem of linearized elasticity in the domain Ω_f^k with Dirichlet boundary conditions on the deformed fluid-structure interface Γ^k given by the displacement of the structure d_s^k :

$$\left\{ \begin{array}{ll} \text{find } d_f^k : \Omega_f^k \rightarrow \mathbb{R}^n \text{ such that} & \\ -\text{div}(\sigma_s(d_f^k)) = 0, & \text{in } \Omega_f^k, \\ d_f^k = d_s^k \circ \Phi^{-1}(d_s^{k-1}), & \text{on } \Gamma^k, \\ d_f^k = 0, & \text{on } \Gamma_f^k, \end{array} \right. \quad (2.33)$$

where $\sigma_s(d_f^k)$ is the linearized elasticity stress tensor defined by (2.19). Thus, the deformation of the fluid domain is given by

$$\Phi(d_s^k) = \Phi(d_s^{k-1}) + d_f^k, \text{ in } \Omega_f.$$

The displacement of the fluid domain, d_f^k , obtained through this process is smoother than the real displacement of the fluid, since the operator of linearized elasticity extend the displacement of the structure from the interface Γ^k to the whole domain Ω_f^k with a diffusion process, characteristic of elliptic operators. However, this regularization process is not enough when the displacement of the structure is large, in which case the fluid domain has to be remeshed. More particularly, the interior of the deformed fluid domain is remeshed but we never touch the boundary, since we want the fluid mesh and the solid mesh to be conformal at the interface Γ . The whole algorithm is summarized in Algorithm 2.2.

The results shown in the remaining of the present section have been obtained using the finite element softwares *FEniCS* ([Logg et al., 2012]) and *FreeFem++* ([Hecht, 2012]). The remeshing of the fluid domain is done with the *Mmg* platform ([Dapogny et al., 2014]).

2.4.2 Influence of the fluid viscosity

We start our numerical investigations with the study of the influence of the fluid viscosity on the fluid-structure system. In particular, we examine its effects on the deformations of the structure and on the displacements of the fluid. We consider the case of one cilium beating in a viscous fluid of viscosity μ_f with the activity scenario be given by (2.7). The computational domain is a two-dimensional box of dimensions $L_1 = 20\mu\text{m}$ and $L_2 = 10\mu\text{m}$. Initially, the cilium is represented as a vertical thin cylinder of length $L_c = 6.5\mu\text{m}$ and radius $r_c = 0.2\mu\text{m}$, anchored at the bottom and centered at position $(1, 0)$. For the elasticity parameters of the structure we take $E_s = 10^6 \text{pN} \cdot \mu\text{m}^{-2}$ and $\nu_s = 0.49$.

Algorithm 2.2 Algorithm for the resolution of the fluid-structure problem.

Choose a maximal number of iterations N .

Choose an initial guess λ^{-1} for the Lagrange multiplier at $t = 0$.

Set $k = 0$.

tant que $k < N$ **faire**

Initialize Uzawa's algorithm with $\lambda^{k,0} = \lambda^{k-1}$.

Solve fluid-structure problem (2.32) with Uzawa's algorithm (Algorithme 2.1) and obtain

$$(u_f^k, p_f^k, d_s^k, \lambda^k).$$

Find the displacement of the fluid domain d_f^k by solving problem (2.33).

Move the solid and fluid meshes.

Remesh the fluid domain if necessary.

Update the number of iterations $k = k + 1$.

fin tant que

In Figure 2.5, we show the result of the resolution of the fluid-structure problem with a fluid viscosity $\mu_f = 0.01\text{pN} \cdot \mu\text{m}^{-2} \cdot \text{s}$ (ten times more viscous than water) at different times. Even though the internal activity of the cilium is imposed, the emerging beating pattern results from both the elasticity properties of the solid and the strong coupling with the surrounding fluid. The fluid velocity is represented as streamlines and glyphs while, in the deformed solid domain, we plot at each point of the mesh the Frobenius norm of the Green-Lagrange strain tensor, defined in the reference configuration by

$$\sqrt{E(d_s(x)) : E(d_s(x))}, \forall x \in \Omega_s.$$

The Green-Lagrange strain tensor $E(d_s)$ physically is a measure of the deformations of the solid material. It can also be seen as the variations of the deformations of the structure compared to rigid deformations. In the present context, the Frobenius norm of the Green-Lagrange tensor gives us a general scalar criterion to observe the action of the fluid viscosity on the deformations of the structure.

In Figure 2.6, we compare the solutions of the fluid-structure problem for different values of the fluid viscosity at different times, when the cilium beats with the same activity scenario. As the viscosity of the fluid increases, we remark that the displacements of the cilium are less important because the surrounding fluid acts like a damper on the structure. In particular, this result enlightens the particularity of our model, which considers active structures with a finite internal energy and whose displacements result from a strong interaction between the surrounding fluid and the (elastic and internal) properties of the cilium. In comparison, models considered in [Lacouture, 2016] and [Chateau et al., 2017] for the cilia does not take the effects of the fluid into account, thus the beating of the cilia does not change when the viscosity of the fluid is modified. To quantify this phenomenon, we study the evolution of the mean of the Frobenius norm of the gradient of the displacement in Ω_s , defined at time t_k by

$$\frac{1}{|\Omega_s|} \int_{\Omega_s} \sqrt{\nabla d_s^k : \nabla d_s^k}.$$

Actually, this quantity is a measure of the deformation of the structure and gives information on the damping effects of the fluid. In Figure 2.7, we plot the solid deformations as a function of the time and observe the increase of the damping effect of the fluid on the structure with the increase of the viscosity. Indeed, the more important the viscosity is,

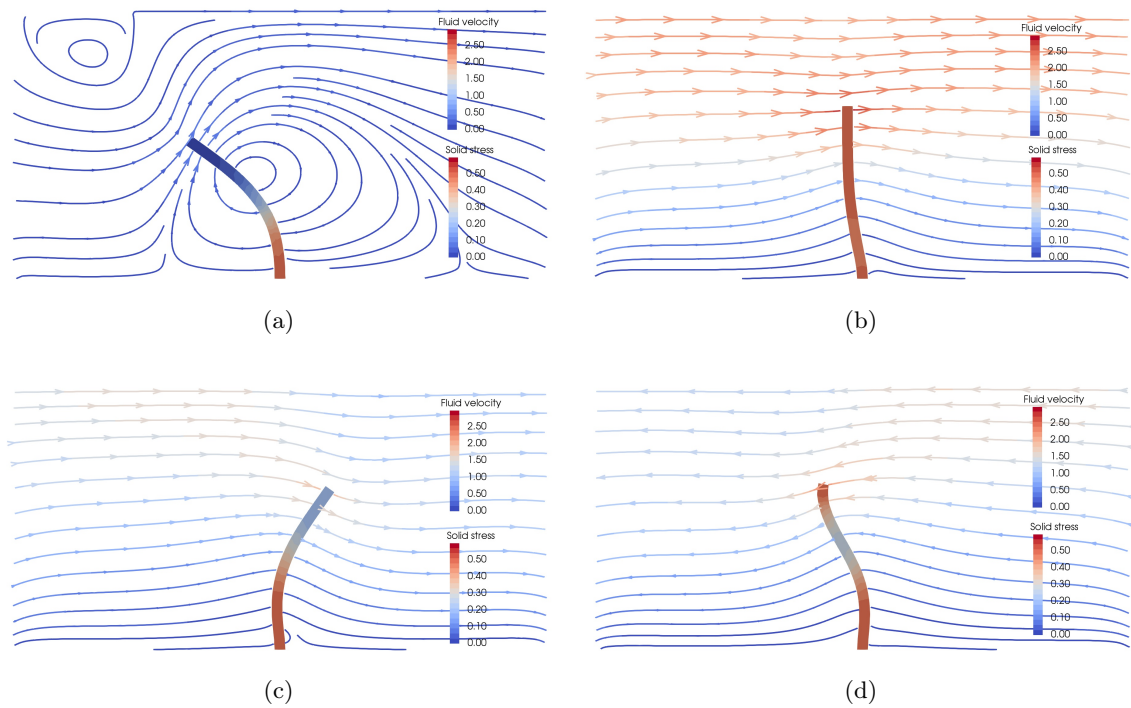


Figure 2.5 – One cilium beating in a viscous fluid of viscosity $\mu_f = 0.01\text{pN} \cdot \mu\text{m} \cdot \text{s}$ at different times: $t = 0.091\text{s}$ (a), $t = 0.110\text{s}$ (b), $t = 0.120\text{s}$ (c), and $t = 0.166\text{s}$ (d). The activity scenario of the structure is given by (2.7).

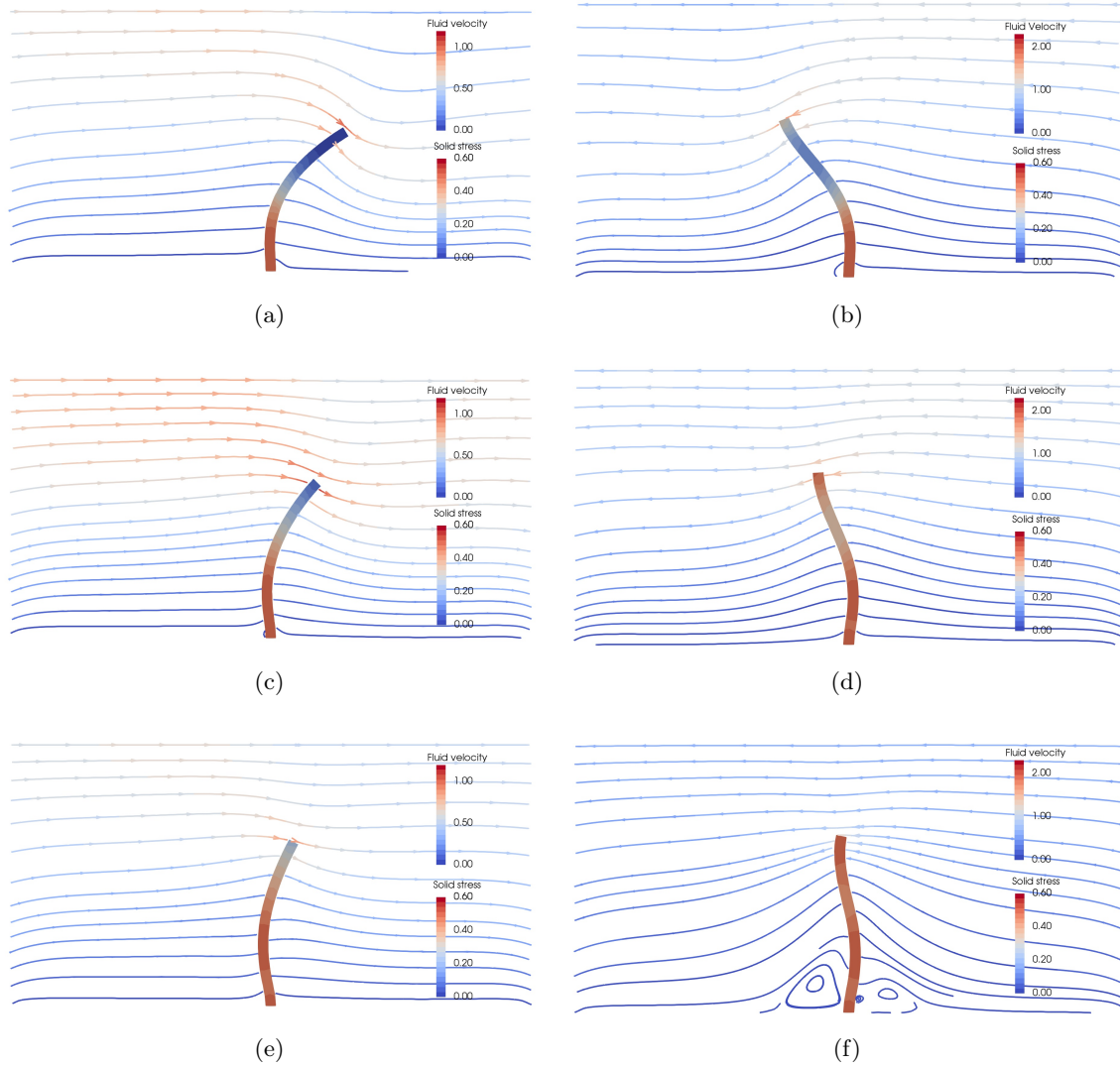


Figure 2.6 – One cilium beating in a viscous fluid at time $t = 0.128$ s (left) and at time $t = 0.171$ s (right) for different values of the fluid viscosity: $\mu_f = 0.01$ pN \cdot μm^{-1} \cdot s (a, b), $\mu_f = 0.02$ pN \cdot μm^{-1} \cdot s (c, d) and $\mu_f = 0.04$ pN \cdot μm^{-1} \cdot s (e, f). The activity scenario of the structure is given by (2.7).

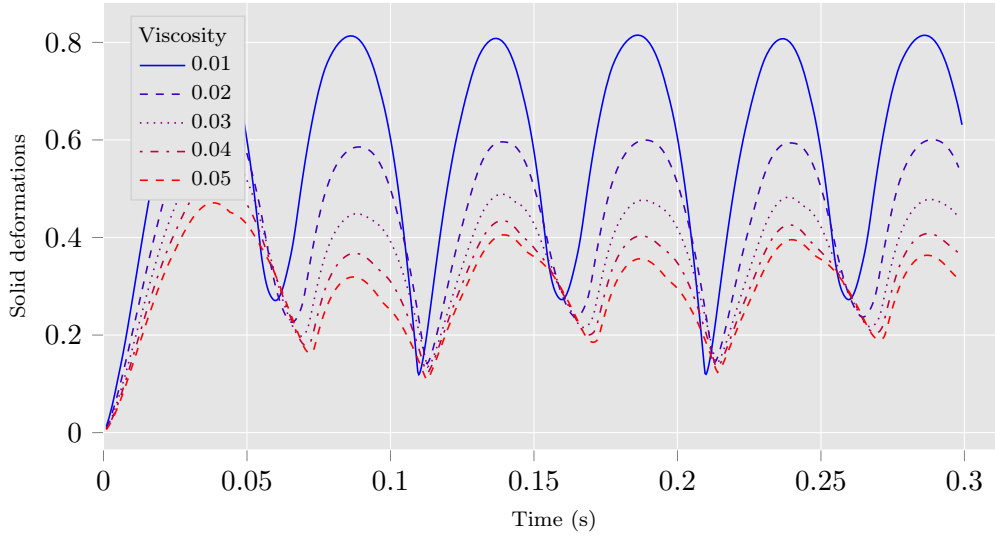


Figure 2.7 – Mean deformation of the solid as a function of the time for different values of the fluid viscosity (in $\text{pN} \cdot \mu\text{m}^{-2} \cdot \text{s}$).

the smaller are the deformations of the structure. To go further, we represent in Figure 2.8a the time average of the deformation with respect to the viscosity of the fluid, defined for a number of iterations $N > 0$ by

$$\frac{1}{t_N |\Omega_s|} \sum_{k=1}^N (t_k - t_{k-1}) \int_{\Omega_s} \sqrt{\nabla d_s^k : \nabla d_s^k}.$$

In particular, the deformations of the cilium decrease by half when the viscosity increases from 0.01 to $0.05 \text{pN} \cdot \mu\text{m}^{-2} \cdot \text{s}$. Moreover, it suggests that if the fluid is too viscous, the cilium will not be able to deform at all. In Figure 2.7, we also remark that the increase in the fluid viscosity induces a time shift in the beating of the cilium. This time shift is represented in Figure 2.8b, with respect to the viscosity of the fluid.

Another important criterion for the study of this fluid-structure system, is the capacity of the cilium to propel the surrounding fluid. To study this phenomenon we plot in Figure 2.9 the evolution of the average horizontal fluid velocity in Ω_f^k with respect to the time, defined at time t_k by

$$\int_{\Omega_f^k} u_f^k \cdot e_1,$$

where e_1 is the first vector of the canonical basis of \mathbb{R}^2 . The increase in the fluid viscosity induces a diminution of the instantaneous velocity of the fluid and we also observe the same time shift as in 2.8b. Moreover, the order of $100 \mu\text{m} \cdot \text{s}^{-1}$ that we find for the fluid velocity, is consistent with the typical velocity of micro-swimmer at low-Reynolds number. To quantify the transport of fluid by the cilium, we represent in Figure 2.10a the mean horizontal fluid velocity in time with respect to the viscosity, defined for a number of iterations $N > 0$ by

$$\frac{1}{t_N} \sum_{k=1}^N (t_k - t_{k-1}) \int_{\Omega_f^k} u_f^k \cdot e_1. \quad (2.34)$$

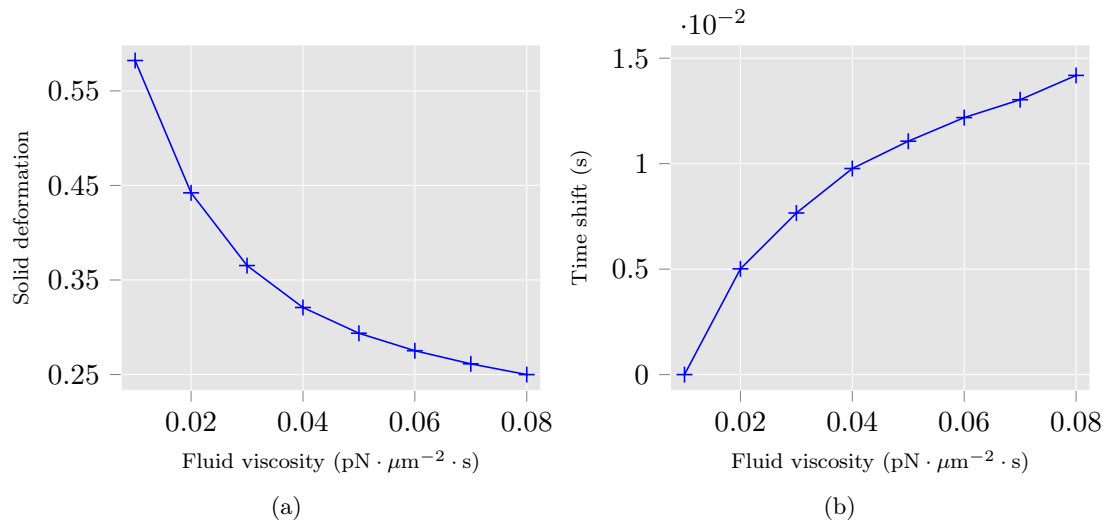


Figure 2.8 – Time average of the solid deformation as a function of the viscosity of the fluid.

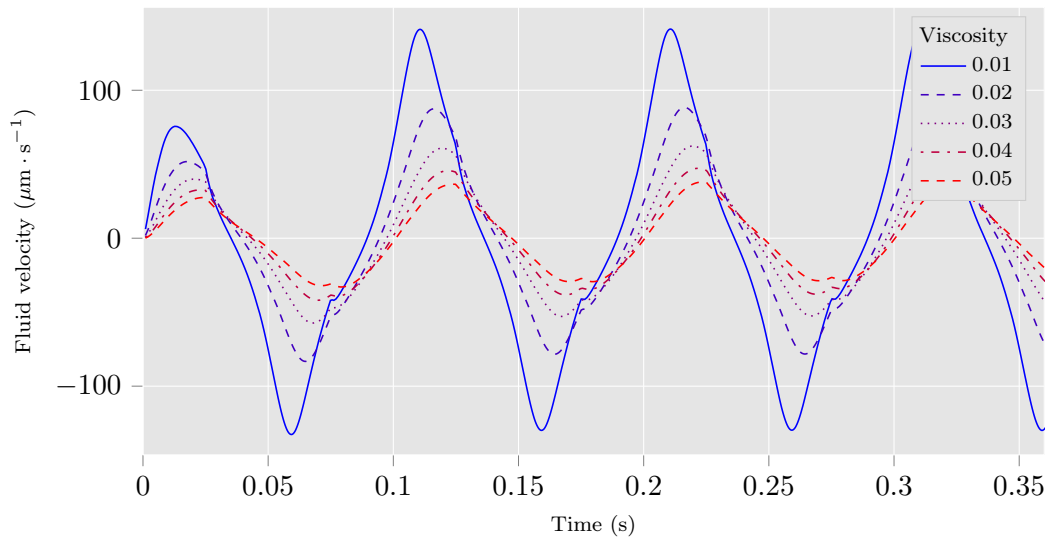


Figure 2.9 – Mean horizontal velocity of the fluid in function of the time for different values of the fluid viscosity (in $\text{pN} \cdot \mu\text{m}^{-2} \cdot \text{s}$).

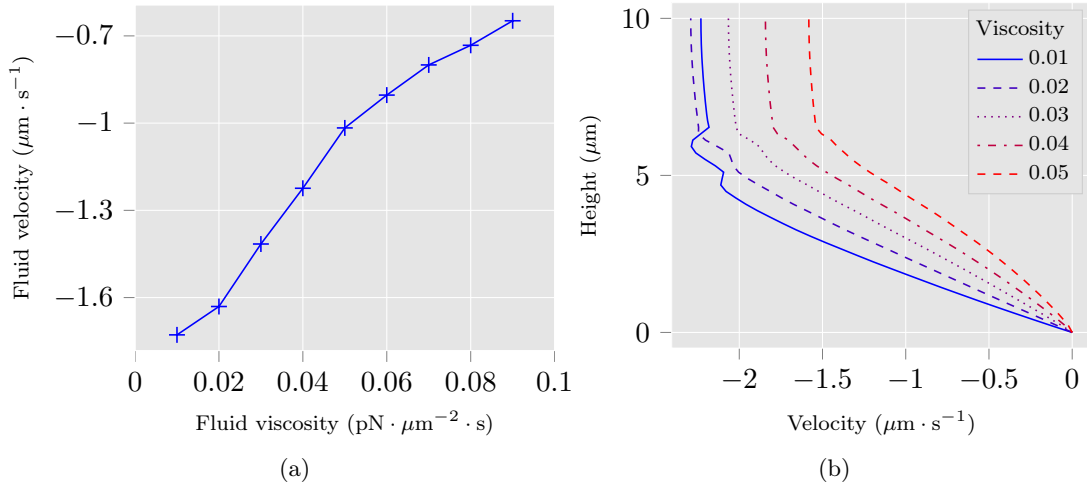


Figure 2.10 – Time average of the horizontal fluid velocity in function of the viscosity of the fluid (a) and horizontal velocity of the fluid as a function of the height for different values of the viscosity (b).

With the chosen activity scenario for the cilium, the mean horizontal fluid velocity is negative, which means that the fluid goes to the left on average. Furthermore, the velocity tends to zero as the viscosity increases, which is coherent with what is found for the deformation of the structure: when the viscosity increases the damping effects of the fluid tend to immobilize the whole system. In particular, this behavior illustrates well the decrease of the mucociliary clearance efficiency in the lungs when the viscosity of the mucus increases, which is for example the case in diseases such as cystic fibrosis. In Figure 2.10b, we plot the mean horizontal velocity of the fluid as a function of the height for different values of the viscosity. Recalling that the length of the cilium is $6.5\mu\text{m}$, it appears that the velocity of the fluid grows linearly with the height close to the cilium and is almost constant far from the bottom of the domain. When the viscosity of the fluid increases, the damping effects make the fluid go slower. However, it is interesting to remark that the velocity of the fluid at the top of the domain is more important for a viscosity of $0.02\text{pN} \cdot \mu\text{m}^{-2} \cdot \text{s}$ than for $\mu_f = 0.01$, which may suggest the existence of an optimal value of the viscosity for the transport of the fluid far from the bottom. These velocity profiles are very similar to those found in [Lacouture, 2016] and in [Smith et al., 2008], only considering the bottom layer of their bi-fluid models for the mucociliary clearance process.

2.4.3 Interaction of two cilia in a viscous fluid

A cilium rarely beats alone in a fluid but is often in interaction with other cilia. Thus, the study of the interaction of two cilia beating in a viscous fluid is of particular interest if we aim to study a more complex system. The numerical simulations that we present in this subsection correspond to two cylindrical cilia of length $L_c = 6.5\mu\text{m}$ and radius $r_c = 0.2\mu\text{m}$ anchored at positions $(x_{c_1}, 0)$ and $(x_{c_2}, 0)$. The whole domain of simulation is the same as the one described in the previous subsection, i.e. a two-dimensional box of dimensions $L_1 = 20\mu\text{m}$ and $L_2 = 10\mu\text{m}$. The activity scenario for both cilia is the one defined by (2.7), but we add a phase shift between cilia whose effects on the fluid-structure system is studied. In addition to the phase shift, the effects of the distance between cilia on the fluid-structure

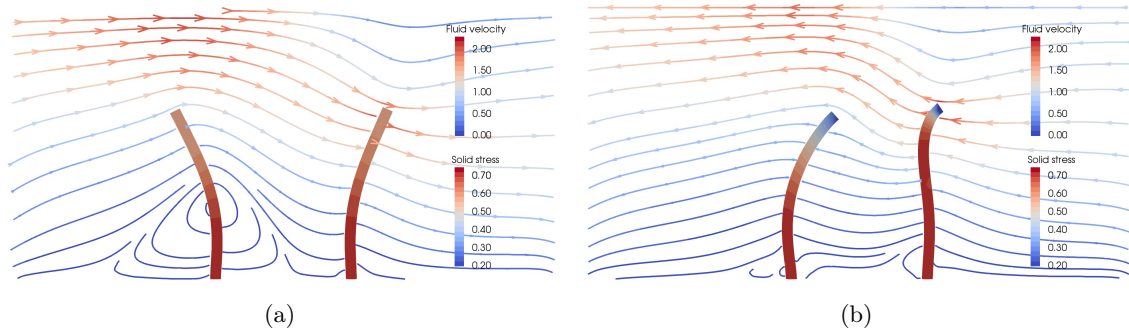


Figure 2.11 – Two cilia beating in a viscous fluid with $\mu_f = 0.01\text{pN} \cdot \mu\text{m}^{-2} \cdot \text{s}$ at $t = 0.788\text{s}$ (a) and $t = 0.83\text{s}$ (b). The cilia are anchored at $x_{c_1} = 7.5$ and $x_{c_2} = 12.5$. The phase shift between the two cilia is $\delta\phi = 0.075\text{s}$.

system is also investigated. In Figure 2.11, we represent the two cilia beating in the fluid at two different times. In this simulation, the cilia are anchored at positions $x_{c_1} = 7.5$ and $x_{c_2} = 12.5$. The elasticity parameters of the structure are $E_s = 10^6\text{pN} \cdot \mu\text{m}^{-2}$ and $\nu_s = 0.49$ and the viscosity of the fluid is $\mu_f = 0.01\text{pN} \cdot \mu\text{m}^{-2} \cdot \text{s}$. The beating frequency of both cilia is $f_a = 10\text{Hz}$ and the intensity of the activity is $C_a = 3\text{pN} \cdot \mu\text{m}$. Moreover, we consider a phase shift $\delta\phi = 0.075\text{s}$ between the activity scenarios of the cilia, i.e. the second cilia (at position x_{c_2}) starts to beat at $t = 0.075\text{s}$. The emerging beating pattern for both cilia is more complicated than what we observed in the previous subsection, since each cilium is now subjected to the fluid flow generated not only by its own activity but also by the one of the other cilium. Actually, this behavior can be seen in Figure 2.12, where we plot the trajectories of the cilia summits during one beating period, for two different values of the phase shift: $\delta\phi = 0.025\text{s}$ in Figure 2.12a and $\delta\phi = 0.075\text{s}$ in Figure 2.12b. In each simulation the two cilia have completely different beating patterns, which are also different from one simulation to the other. Thus, both cilia act on each other by means of hydrodynamic interactions, which depend on several parameters: the viscosity of the fluid, the elastic parameters of the structures, the parameters of the activity scenario and the geometrical parameters.

In this subsection, we assume that the two cilia are identical, except for the presence of a phase shift between their activity scenario, and that the viscosity of the fluid is fixed at $\mu_f = 0.01\text{pN} \cdot \mu\text{m}^{-2} \cdot \text{s}$. Thus, it only remains two parameters of interest to study, namely the phase shift between the activity scenarios of the cilia, denoted by $\delta\phi$, and the distance between their anchorage points, denoted by δx_c .

We start with the study of the influence of the phase shift. For that matter, we solve the fluid-structure problem during six beating periods and consider different values for the phase shift from $\delta\phi = 0\text{s}$ to $\delta\phi = 0.1\text{s}$. In these simulations, all other parameters are fixed. In particular, the distance between the two cilia is $\delta x_c = 5\mu\text{m}$ and the activity scenario is given by (2.7). In Figure 2.13a, we plot the mean horizontal fluid velocity as a function of the height for different values of the phase shift. Depending on the phase shift, it appears that the behavior of the system is totally different. Actually, for $\delta\phi = 0.025\text{s}$ the mean velocity of the fluid is negative, such that the fluid goes to the left (this is what we observed with one cilium), whereas for $\delta\phi = 0.075\text{s}$ the fluid goes to the right on average. This phenomenon is confirmed in Figure 2.13a, which represents the average fluid velocity with

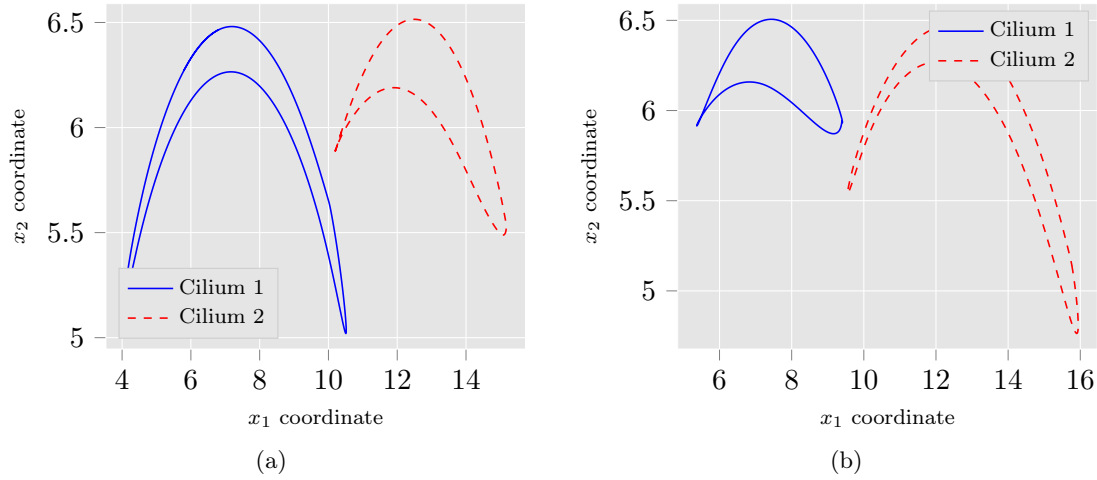


Figure 2.12 – Trajectories of the two cilia summits for different values of the phase shift between their activity scenario: $\delta\phi = 0.025$ (a) and $\delta\phi = 0.075$ (b).

respect to the phase shift. For a phase shift from 0 to approximately 0.05, the fluid moves to the left on average, since its velocity is negative, and from 0.05 to 0.1, the fluid moves to the right. Thus, for the internal activity scenario considered in these simulations, the transport of the fluid by the active structures strongly depends on the phase shift between their activity.

Similarly, we study the influence of the distance between the two cilia on the fluid-structure system. To that aim several simulations are realised by considering different values for the distance between them, from $\delta x_c = 2\mu\text{m}$ to $\delta x_c = 6.5\mu\text{m}$. The other parameters remain constant and, in particular, we consider a phase shift $\delta\phi = 0.075\text{s}$ between the activity scenarios of the two cilia. The velocity profiles presented in Figure 2.14a are similar, which suggest that the distance between the two cilia is less determinant than the phase shift. Here, the profile with $\delta x_c = 5\mu\text{m}$ correspond to the profile with $\delta\phi = 0.075\text{s}$ in Figure 2.13a. In Figure 2.14b, the average of horizontal fluid velocity is represented with respect to the distance between the two cilia. For all values of the distance, the fluid moves to the right on average. However, the fluid velocity does not seem to be linear with respect to this distance. In particular, a maximum of the transport efficiency is reached at approximately $\delta x_c = 3\mu\text{m}$.

2.4.4 Discussion

The continuum model for active structures that we have presented enables to fully take into account the fluid-structure interactions between the cilia and the surrounding fluid, including the hydrodynamic forces due to the deformations of neighboring cilia. For a given activity scenario of the cilia, we were able to study the influence on the fluid-structure system of the viscosity of the fluid, when one cilium is considered, as well as the influence of the phase shift and the distance between cilia, when two cilia are involved. As a conclusion we showed that, even with an imposed internal activity scenario for the active structures, hydrodynamic forces really are the principal ingredient that controls the beating patterns of cilia, since completely different deformations of the structures are observed depending of the different physical and geometrical parameters.

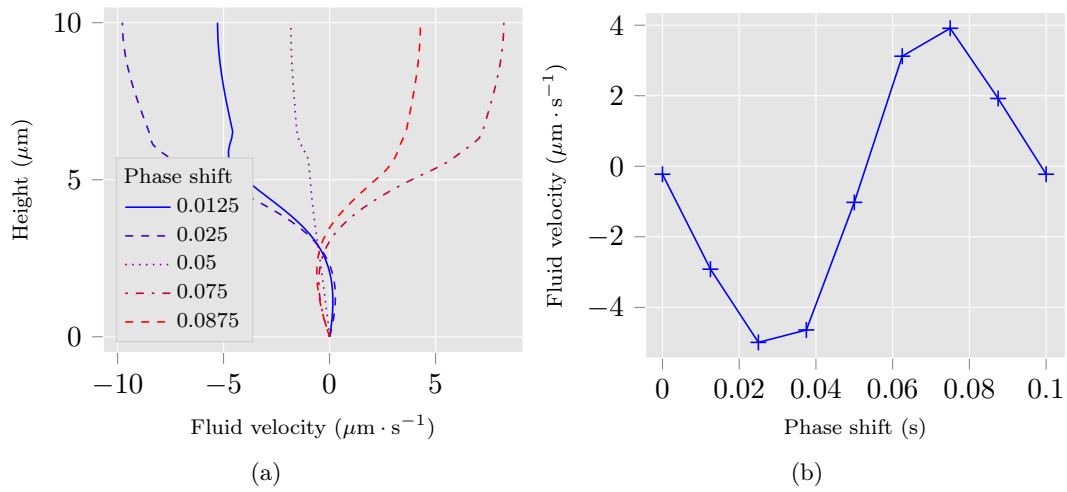


Figure 2.13 – Horizontal velocity of the fluid as a function of the height for different values of the phase shift (a) and time average of the horizontal fluid velocity in function of the phase shift (b).

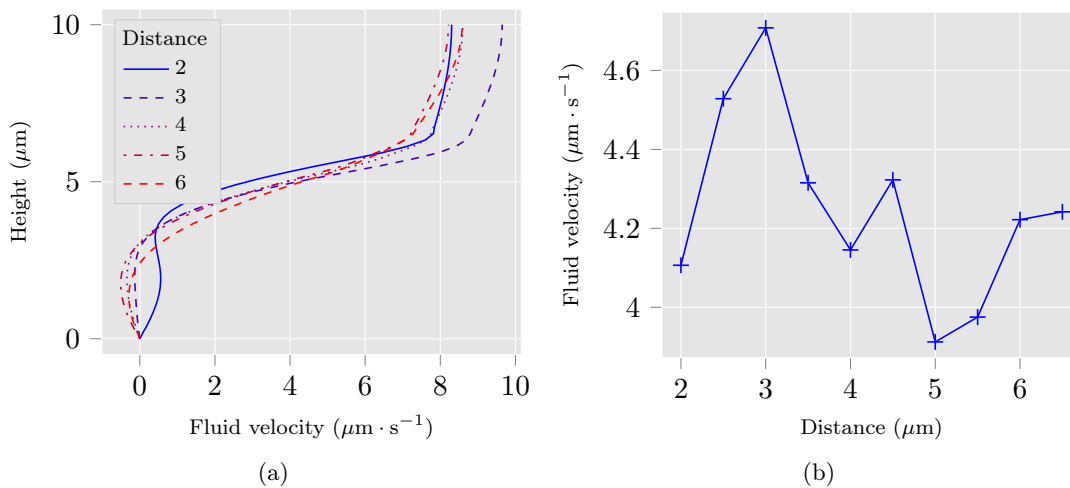


Figure 2.14 – Horizontal velocity of the fluid as a function of the height for different values of the distance between the two cilia (a) and time average of the horizontal fluid velocity in function of the distance (b).

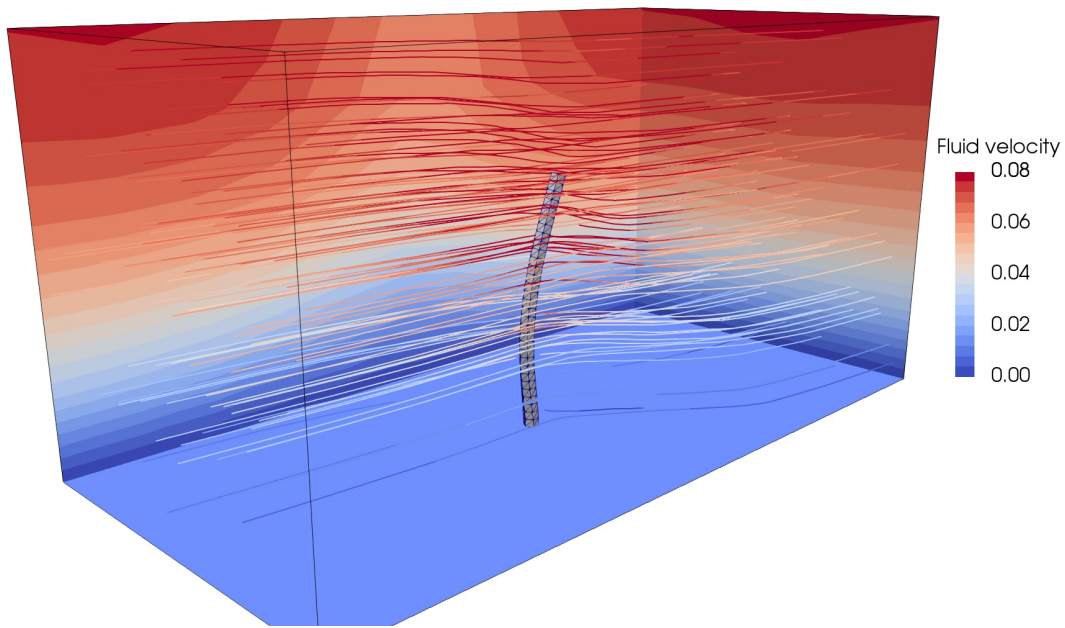


Figure 2.15 – Three-dimensional simulation of a cilium-like structure in a viscous fluid.

Even though two-dimensional simulations are a good start for the study of such a complex system, it is not quite representative of the real fluid-structure interactions for microorganisms. Actually, in two space dimensions the system is much more constrained than in three space dimensions, since the fluid can not circumvent a cilium. It results that hydrodynamic interactions are less important in three space dimensions and their effects on the emergence of the beating patterns of cilia should be further investigated.

The model as well as the numerical method that we proposed are both compatible with three-dimensional simulations. As an example, we plot in Figure 2.15 the result of the simulation of an active elastic elongated structure beating in a fluid modeled by the Stokes equations in three space dimensions. The activity scenario is the same as the one used for two-dimensional simulations, but we can remark that most of the fluid goes around the cilium instead of above, which leads to slower fluid velocities.

In this three space dimensions simulation, the computational cost of the method is much more important and necessitates the development of more sophisticated numerical tools. With Uzawa's algorithm, one should consider the use of preconditioners and parallel finite element solvers to really improve the performance of the method. A different approach would be to consider some methods on non conformal and fixed meshes, which then could be implemented with the use of fast solvers (e.g. solvers using the discrete fast Fourier transform). Such a method is developed in Chapter 4 in the general case of transmission problems.

Chapter 3

Existence and uniqueness for a quasi-static interaction problem between a viscous fluid and an active structure

In collaboration with Céline Grandmont.

3.1 Introduction

Many living beings move, breathe and reproduce themselves by means of thin active structures that interact with fluids. Cilia and flagella are examples of such soft materials that deform themselves using internal biological motors and thus, induce a flow within the surrounding fluid. Understanding the underlying mechanisms of the coupling of such a fluid-structure system is of great interest for biological, medical and even engineering applications. The problem we are interested in is the interaction between an elastic medium, subjected to an internal time depending stress, and a viscous fluid, whose domain depends on the displacement of the elastic medium. In this chapter, we prove the existence and the uniqueness (locally in time) of a regular solution to a quasi-static interaction problem involving an elastic structure subjected to an internal stress and a Newtonian viscous incompressible homogeneous fluid, modeled by the Stokes equations, under smallness assumptions on the data.

The following results of related works focuses on the mathematical analysis for the well-posedness of interaction problems between a viscous incompressible homogeneous fluid and elastic media. First, we concentrate on problems involving *passive* elastic structures, then we survey studies involving *active* structures.

Concerning interaction problems involving a viscous incompressible homogeneous fluid and a passive solid medium, several models have been studied. In [Desjardins et al., 2001], the Navier-Stokes equations are coupled to a finite-dimensional approximation of the equations of linearized elasticity, where the displacement is written as a linear combination of a finite number of eigenmodes associated to the linearized elasticity equations. The existence of weak solutions is proven locally in time (up to a contact). A similar approach is considered for the same system in [Boulakia et al., 2012], where an approximation of Galerkin type of the equations of linearized elasticity is constructed and the existence and the uniqueness of strong solutions are proven. Both articles illustrate the use of a

finite-dimensional approximation of the equation of linearized elasticity in order to avoid the loss of regularity inherent to this fluid-structure system. Another strategy for the same problem, adopted in [Boulakia, 2003], in two space dimensions, and in [Boulakia, 2007], in three space dimensions, is to add a regularizing term in the equations of linearized elasticity. In both articles, the existence of weak solutions is proven until no contact occurs.

The interaction problem between an incompressible viscous fluid and an elastic structure have been studied in fewer cases. In [Du et al., 2003], the coupled problem involving the linearized Navier-Stokes equations (sometimes called the unstationary Stokes equations) and the equations of linearized elasticity have been studied, in the situation where the displacements of the structure are infinitesimal but the velocities are important (thus the fluid-structure interface is stationary). The authors prove results of existence and uniqueness of weak and strong solutions. For systems coupling the incompressible Navier-Stokes equations with the equations of linearized elasticity, results have been successively obtained in [Coutand and Shkoller, 2005], [Kukavica and Tuffaha, 2012], [Raymond and Vanninathan, 2014] and more recently in [Boulakia et al., 2018], for the existence and uniqueness of strong solutions locally in time.

Finally, when the structure is modeled with the Saint Venant-Kirchhoff law, very few results on the well-posedness of the fluid-structure system are known. In [Coutand and Shkoller, 2006], the Navier-Stokes equations coupled to the equations of elastodynamics, are considered and the existence and uniqueness of strong solutions are proven locally in time, under compatibility conditions on the initial data. In [Grandmont, 2002], a result of existence of strong solutions is proven in the steady-state situation, considering either the Stokes or the Navier-Stokes equations, if the data are sufficiently small.

Concerning the well-posedness of fluid-structure problems involving active structures and viscous incompressible homogeneous fluid, few results are available. In [Galdi, 1999], the steady self-propelled motion of a constant shape solid in a non-inertial fluid, modeled by either the Stokes or the non-inertial Navier-Stokes equations, is studied. The velocity of the solid on its boundary is divided in two parts: the first one is imposed and represents the self-propelled velocity of the solid, whereas the other one is due to the interaction with the surrounding fluid. The existence of solutions is proven and conditions under which a distribution of the self-propelled velocity on the boundary of the structure is able to propel the solid is investigated. In [San Martín et al., 2008], an initial and boundary value problem for the swimming of a fish-like deformable structure is treated. In this model the movement of the structure is divided in two: the rigid part of the displacement results from the interaction of the fluid and the solid, whereas the deformation part of the displacement is imposed. The resulting coupled system between the Navier-Stokes equations for the fluid and Newton's laws for the structure is proven to be well-posed. For the same problem, the existence and uniqueness of weak solutions is studied in [Nečasová et al., 2011]. The same system is studied in [Court, 2017] in three space dimensions and limiting the regularity of the imposed displacement of the structure (still a datum of the problem). The author proves local existence in time for any data and global existence in time under smallness assumptions on the data.

In all these works the strategy is the same: decompose the movements of the structures in two parts. The first part is imposed and describes the internal activity of the structure, while the second part is a rigid movement which satisfies Newton's law and results from the interaction with the fluid. The originality of the present work lies in the fact that the activity of the structure is modeled by a given internal active stress, such that the whole movement of the structure results from the interaction with the surrounding fluid.

Let us now introduce the fluid-structure problem we are interested in. Let n be the

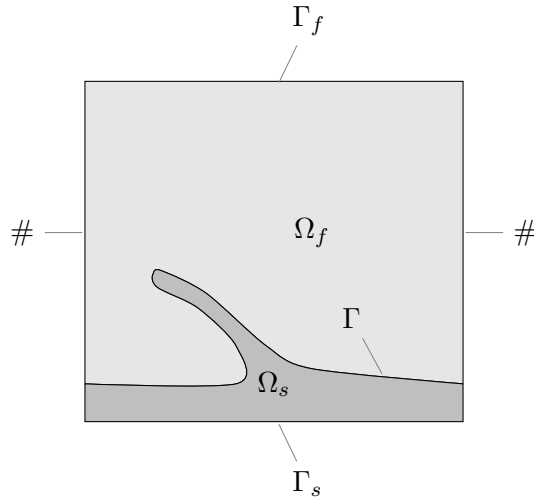


Figure 3.1 – Two-dimensional example of the geometry of the fluid-structure problem.

space dimension (2 or 3) and Ω be a regular toroidal open connected bounded subset of \mathbb{R}^n , whose definition will be made clear by hypotheses (\mathbf{H}_1) - (\mathbf{H}_4) . The domain Ω is supposed to be the union of two domains: $\Omega = \Omega_s \cup \Omega_f$, with $\Omega_s \cap \Omega_f = \emptyset$, such as Ω_s and Ω_f are also toroidal subsets of \mathbb{R}^n . The interface between Ω_s and Ω_f is denoted by Γ and we define the remaining frontiers of Ω_s and Ω_f by $\Gamma_s = \partial\Omega_s \setminus \Gamma$ and $\Gamma_f = \partial\Omega_f \setminus \Gamma$ (see Figure 3.1).

The domain Ω_s is filled with an active elastic medium. At time t , the behavior of the structure is modeled by the non-inertial equations of elasticity, set in the reference configuration Ω_s . Denoting by d_s the displacement of the structure, these equations write

$$\begin{aligned} -\operatorname{div}(\Pi_s(d_s(t), t)) &= f_s(t), & \text{in } \Omega_s, \\ d_s(t) &= 0, & \text{on } \Gamma_s, \end{aligned} \quad (3.1)$$

where f_s denotes the exterior body forces applied on the structure. The tensor Π_s represents the first Piola-Kirchhoff stress tensor of the structure which, in the present study, includes the active component, which will now be defined. In the framework of continuum mechanics, two popular approaches are used to model contractility in solid materials, namely the active-stress and active-strain methods (see [Ambrosi and Pezzuto, 2012]). The former consists in adding an active component to the passive stress tensor, while in the later, the activation is considered as a pre-strain in a multiplicative decomposition of the tensor gradient of deformation. Both techniques have been extensively studied for biological structures and particularly in a context of myocardium and arteries studies. For more information on models for active organs, we refer to [Payan and Ohayon, 2017, Chapter 2]. In this work, we choose the active-stress formalism to model internal motors and denote by Σ^* this active stress tensor which is added to the passive component. Moreover, we do not suppose Σ^* to have any particular shape, but we consider the most general case where this tensor depends on both the time t and the material position x . If we consider the Saint Venant-Kirchhoff behavior law for the passive component of the elastic medium, its constitutive equations at time t become

$$\begin{aligned} \Pi_s(d_s(t), t) &= (I + \nabla d_s(t))(\Sigma_s(d_s(t)) - \Sigma^*(t)), \\ \Sigma_s(d_s) &= 2\mu_s E(d_s(t)) + \lambda_s \operatorname{tr}(E(d_s(t)))I, \\ E(d_s) &= \frac{1}{2}(\nabla d_s(t) + \nabla d_s(t)^T + \nabla d_s(t)^T \cdot \nabla d_s(t)), \end{aligned} \quad (3.2)$$

where μ_s and λ_s are Lamé's parameters ($\lambda_s > 0$, $\mu_s > 0$) and I stands for the identity matrix of \mathbb{R}^n . Thus, with the present elasticity model, the activity of the structure is completely internal and enables to fully take into account the fluid-structure interaction, whereas imposing a part of the velocity or the deformation as in [Galdi, 1999] or [San Martín et al., 2008] does not.

At time t , the structure moves under the influence of its internal activity and the action of the surrounding fluid on its boundary. Then, the deformation of the fluid domain at time t , denoted by $\Phi(d_s(t))$, depends on the displacement of the structure on the interface Γ and satisfies

$$\Phi(d_s(t)) = \mathcal{I} + d_s(t), \quad \text{on } \Gamma,$$

where \mathcal{I} is the identity mapping in \mathbb{R}^n . Moreover, let γ_Γ be the trace operator from Ω_s onto Γ and \mathcal{R} be a continuous linear lifting from Γ to Ω_f (in spaces made precise later on). Then, we define the fluid domain deformation $\Phi(d_s(t))$ in the whole domain Ω_f as follows:

$$\Phi(d_s(t)) = \mathcal{I} + \mathcal{R}(\gamma_\Gamma(d_s(t))), \quad \text{in } \Omega_f,$$

such that the deformation is equal to zero on the fluid boundary Γ_f . Thus the mapping $\Phi(d_s(t))$, maps the reference fluid domain Ω_f with the deformed fluid domain at time t , denoted by $\Phi(d_s(t))(\Omega_f)$.

The domain Ω_f is filled with a Newtonian viscous fluid whose viscosity is denoted by μ_f . The velocity u_f and the pressure p_f of the fluid satisfy, at each time t , the Stokes equations in the deformed configuration $\Phi(d_s(t))(\Omega_f)$, which write

$$\begin{aligned} -\operatorname{div}(\sigma_f(u_f(t), p_f(t))) &= 0, & \text{in } \Phi(d_s(t))(\Omega_f), \\ \operatorname{div}(u_f(t)) &= 0, & \text{in } \Phi(d_s(t))(\Omega_f), \\ u_f(t) &= 0, & \text{on } \Phi(d_s(t))(\Gamma_f), \end{aligned}$$

where

$$\sigma_f(u_f(t), p_f(t)) = \mu_f \nabla u_f(t) - p_f(t)I,$$

is the fluid stress tensor written in the deformed configuration $\Phi(d_s(t))(\Omega_f)$. Moreover, we suppose that no external force is applied to the fluid. Let us precise that, in the definition of the fluid stress tensor, we consider the gradient of u_f and not its symmetric part, which should be the physical quantity to consider. This choice is justified here because all mathematical difficulties of the problem already appear without considering the symmetric part of the gradient of u_f . Furthermore, all computations that will be made at a later stage are then slightly less tedious.

In the previous Stokes equations, the domain $\Phi(d_s(t))(\Omega_f)$ is an unknown of the problem. A usual approach to deal with this issue is to work in a fixed domain by transforming the fluid equations and writing them in the reference configuration of the fluid. To that aim, we introduce the mapping F and G defined (in Sobolev spaces that will be defined later on) by

$$\begin{aligned} F(d_s(t)) &= (\nabla(\Phi(d_s(t))))^{-1} \operatorname{cof}(\nabla(\Phi(d_s(t)))), \\ G(d_s(t)) &= \operatorname{cof}(\nabla(\Phi(d_s(t)))). \end{aligned} \tag{3.3}$$

The matrix $F(d_s(t))$ is well defined whenever $\Phi(d_s(t))$ is, for instance, a C^1 -diffeomorphism, which will be the case for small enough displacements in well chosen spaces. Then, using the definitions of the mappings F and G , it follows from a change of variables that the Stokes equations written in the reference configuration of the fluid is

$$\begin{aligned} -\mu_f \operatorname{div}((F(d_s(t))\nabla)w_f(t)) + G(d_s(t))\nabla q_f(t) &= 0, & \text{in } \Omega_f, \\ \operatorname{div}(G(d_s(t))^t w_f(t)) &= 0, & \text{in } \Omega_f, \\ w_f(t) &= 0, & \text{on } \Gamma_f, \end{aligned} \tag{3.4}$$

where the velocity w_f and the pressure q_f in the reference configuration are defined at time t by

$$w_f(t, \cdot) = u_f(t, \Phi(d_s(t)(\cdot))) \text{ and } q_f(t, \cdot) = p_f(t, \Phi(d_s(t)(\cdot))), \text{ in } \Omega_f .$$

Moreover, the fluid stress tensor written in the reference configuration at time t is defined by

$$\Pi_f(w_f(t), q_f(t)) = \mu_f(F(d_s(t))\nabla)w_f(t) - q_f(t)G(d_s(t)). \quad (3.5)$$

Remark 3.1. The tensor Π_f is the Piola transform of the fluid stress tensor σ_f . For more information on how to transform the Stokes equations from the deformed configuration to the reference configuration, see Appendix B.

To complete the set of equations (3.1), (3.2) and (3.4), we add the usual coupling conditions on the fluid-structure interface Γ , namely the continuity conditions on the velocities and on the normal component of the solid stress tensor:

$$\frac{\partial d_s}{\partial t}(t) = w_f(t), \quad \text{on } \Gamma, \quad (3.6)$$

$$\Pi_f(w_f(t), q_f(t))n_f = \Pi_s(d_s(t), t)n_f, \quad \text{on } \Gamma, \quad (3.7)$$

where n_f is the exterior unit normal vector of $\partial\Omega_f$.

Even though the interaction problem we consider in the present study is non-inertial, it requires an initial condition for the displacement of the structure on the interface Γ at time $t = 0$, because of the condition on the continuity of the velocities in (3.6). For the sake of simplicity, as in [Boulakia et al., 2018] and [Raymond and Vanninathan, 2014] for instance, we suppose that the structure is in its reference configuration initially, i.e. that

$$d_s(0) = 0, \text{ on } \Gamma, \quad (3.8)$$

so that the kinematic boundary condition (3.6) writes

$$d_s(t) = \int_0^t w_f(s)ds, \text{ on } \Gamma. \quad (3.9)$$

Conditions (3.6) and (3.9) differ in the sense that condition (3.6) can be seen as a Dirichlet boundary condition for the fluid problem whereas the condition (3.9) is a Dirichlet boundary condition for the structure problem.

Moreover, we will suppose at first that the structure is at rest initially, i.e. that we have $f_s(0) = \text{div}(\Sigma^*(0))$ which, combined with the initial condition (3.8), implies that $d_s(0) = 0$ in Ω_s . The more general case where $f_s(0) \neq \text{div}(\Sigma^*(0))$ is discussed in Section 3.7.

We now briefly outline the content of the present chapter. In Section 3.2 we introduce some notations and prove some preliminary results. In particular, we show that, for sufficiently small displacements of the structure, the mapping F , defined by (3.3), is well-defined, such that the fluid problem in the reference configuration (3.4) is also well-defined. In Section 3.3, we state our main result, namely the existence and the uniqueness (locally in time) of a regular strong solution to the problem (3.1)-(3.2)-(3.4)-(3.6)-(3.7), if the data are sufficiently small and if the structure is at rest initially. The proof is done thanks to Banach's fixed point Theorem, constructing a mapping that iterates between the resolution of the structure problem and the fluid problem. The particularity of the present quasi-static problem compared to steady problems relies on the kinematic condition (3.6) on the

interface Γ , which is an unsteady condition. So that, in order to prove the convergence of the iterative process we have to split the fluid-structure problem by solving the structure problem with the Dirichlet boundary condition (3.9) and the fluid problem with the Neumann boundary condition (3.7). By doing so we ensure compactness in time, whereas if one solve the structure problem with the Neumann boundary condition (3.7) and the fluid problem with the Dirichlet boundary condition (3.6), then we loose time regularity in the iterative process. To that aim, we study in Section 3.4 and in Section 3.5, the structure and fluid problems independently. In Section 3.6, the actual fixed point procedure is conducted, showing that the aforementioned mapping goes from a ball into itself and is a contraction. Finally, in Section 3.7, we extend our result to the case where the structure is not at rest initially, i.e. $f_s(0) \neq \text{div}(\Sigma^*(0))$.

3.2 Notations and preliminaries

3.2.1 Technical lemma

In this subsection, Ω denotes an open connected bounded subset of \mathbb{R}^n of class $C^{k-1,1}$, for $k \geq 1$. For $r \geq 0$, the space $H^r(\Omega)$ denotes a standard Sobolev space associated to the L^2 -norm. Moreover, the same notation is used whenever it is a space of real-valued functions or vector-valued functions.

If Γ is a part of the boundary of Ω , we say that Γ is a disjoint part of $\partial\Omega$ if Γ is non empty and $\overline{\Gamma} \cap (\overline{\partial\Omega} \setminus \overline{\Gamma}) = \emptyset$. Then, if Γ is a disjoint part of $\partial\Omega$, we denote by γ_Γ the trace operator on Γ , which is continuous and surjective from $H^r(\Omega)$ onto $H^{r-1/2}(\Gamma)$ for all r such that $\frac{1}{2} < r \leq k$ (see [Boyer and Fabrie, 2012, sec. 2.5.3]). In particular, there exists a continuous lifting operator from $H^{r-1/2}(\Gamma)$ into $H^r(\Omega)$. Using this notations, we denote by $H_\Gamma^1(\Omega)$ the space defined by

$$H_\Gamma^1(\Omega) = \{u \in H^1(\Omega); \gamma_\Gamma(u) = 0\}.$$

For $s \geq 0$, the space $H^s(0, T; H^r(\Omega))$ denotes the space of Sobolev-valued functions in the time interval $(0, T)$, with $T > 0$. For $s = 0$ we should denote this space by $L^2(0, T; H^r(\Omega))$.

The constant C that appears through the text always denotes a positive constant that can change from line to line. However, its dependencies on domains, variables or parameters would be made clear.

We start by giving a technical lemma.

Lemma 3.1. *Let Ω be a Lipschitz open connected bounded subset of \mathbb{R}^n , with $n \geq 1$, and consider Γ , a disconnected part of its boundary.*

i) Let $r > \frac{n}{2}$. If u and v belong to $H^r(\Omega)$, then the product uv belongs to $H^r(\Omega)$ and there exists a constant $C(\Omega)$ which depends on the domain Ω such that,

$$\|uv\|_{H^r(\Omega)} \leq C(\Omega) \|u\|_{H^r(\Omega)} \|v\|_{H^r(\Omega)}.$$

ii) Let $r \geq 0$ and $s > \max(\frac{n}{2}, r)$. If u belongs to $H^s(\Omega)$ and v belongs to $H^r(\Omega)$, then the product uv belongs to $H^r(\Omega)$ and there exists a constant $C(\Omega)$ which depends on the domain Ω such that,

$$\|uv\|_{H^r(\Omega)} \leq C(\Omega) \|u\|_{H^s(\Omega)} \|v\|_{H^r(\Omega)}.$$

Moreover, we shall say that $H^s(\Omega)$ is a multiplier space of $H^r(\Omega)$.

iii) Let $r > \frac{1}{2}$ and $T > 0$. Moreover, suppose that Ω is of class $C^{r-1,1}$. If w belongs to $L^2(0, T; H^r(\Omega))$, then the function δ defined by

$$\delta(t) = \int_0^t \gamma_\Gamma(w(s)) ds, \quad \forall t \in [0, T],$$

belongs to $H^1(0, T; H^{r-1/2}(\Gamma))$, and there exists a constant $C(\Omega)$ which depends on the domain Ω such that,

$$\|\delta\|_{L^\infty(0, T; H^{r-1/2}(\Gamma))} \leq C(\Omega) T^{1/2} \|w\|_{L^2(0, T; H^r(\Omega))}.$$

Proof. The proof of point *i*) relies on Sobolev injections and we refer to [Adams and Fournier, 2003] for detailed information. The essential point here is that the space $H^r(\Omega)$ is a Banach algebra, because $2r$ is greater than the dimension n .

Point *ii*) is a consequence of [Behzadan and Holst, 2015, Theorem 7.5] and also relies on embedding theorems for Sobolev spaces.

For the point *iii*), a straightforward computation gives us that, for all $t \in [0, T]$,

$$\|\delta(t)\|_{H^{r-1/2}(\Gamma)} = \left\| \int_0^t \gamma_\Gamma(w(s)) ds \right\|_{H^{r-1/2}(\Gamma)} \leq C(\Omega) t^{1/2} \|w\|_{L^2(0, T; H^r(\Omega))},$$

where $C(\Omega)$ is a constant coming from the continuity of the trace operator from $H^r(\Omega)$ onto $H^{r-1/2}(\Gamma)$. It follows that

$$\|\delta\|_{L^\infty(0, T; H^{r-1/2}(\Gamma))} \leq C(\Omega) T^{1/2} \|w\|_{L^2(0, T; H^r(\Omega))}.$$

Moreover, because $\frac{\partial \delta}{\partial t} = \gamma_\Gamma(w)$ belongs to $L^2(0, T; H^{r-1/2}(\Gamma))$, we can conclude that δ belongs to $H^1(0, T; H^{r-1/2}(\Gamma))$. □

3.2.2 Assumptions and preliminary results

In all that follows, we assume that the following assumptions hold true.

- (H₁) Domain Ω is an open connected bounded subset of \mathbb{R}^n ($n \in \{2, 3\}$) divided in two open connected bounded sets Ω_f and Ω_s by an interface Γ .
- (H₂) The interface Γ is of class $C^{3,1}$, is non empty and does not encounter the boundary of Ω , i.e. $\bar{\Gamma} \cap \bar{\partial\Omega} = \emptyset$.
- (H₃) The remaining boundaries are denoted $\Gamma_f = \partial\Omega_f \setminus \Gamma$ and $\Gamma_s = \partial\Omega_s \setminus \Gamma$ and are of class $C^{2,1}$.
- (H₄) The boundary Γ_f is such that $|\Gamma_f| \neq 0$, whereas the boundary Γ_s could be such that $|\Gamma_s| = 0$.

Remark 3.2. Note that at many steps one could only assume a $C^{2,1}$ regularity of the domains, yet the required $C^{3,1}$ regularity on Γ is used to prove the elliptic regularity of the solution of the fluid problem with mixed Dirichlet and Neumann boundary conditions, which requires more regularity than when considering only a Dirichlet boundary condition (see [Boyer and Fabrie, 2012]).

Remark 3.3. Under assumptions (\mathbf{H}_1) - (\mathbf{H}_4) , we see that the boundaries Γ , Γ_f and Γ_s are all disjoint parts of $\partial\Omega_f$ and $\partial\Omega_s$. An example of such a domain is given in Figure 3.1.

Let $T > 0$. The fluid problem written in the reference configuration, defined by (3.4), is well-defined if, for almost every t in $(0, T)$, the displacement of the structure at time t , $d_s(t)$, is sufficiently regular and if the deformation $\Phi(d_s(t))$ is a C^1 -diffeomorphism that maps Ω_f into $\Phi(d_s(t))(\Omega_f)$. In the next lemma, we show that this is true if the displacement of the structure at time t belongs to the ball $\mathcal{B}_{\mathcal{M}_0}^S$ of $H^3(\Omega_s)$, defined by

$$\mathcal{B}_{\mathcal{M}_0}^S = \{b \in H^3(\Omega_s); \|b\|_{H^3(\Omega_s)} \leq \mathcal{M}_0\}, \quad (3.10)$$

if the constant \mathcal{M}_0 is sufficiently small.

Let \mathcal{R} be a linear lifting operator from $H^{5/2}(\Gamma)$ to $H^3(\Omega_f) \cap H_{\Gamma_f}^1(\Omega_f)$ and we recall that γ_Γ is the trace operator on the interface Γ . Since the domains are of class $C^{3,1}$, they are both continuous operators (at this step, domains of class $C^{2,1}$ would, in fact, have been enough). We have the following result adapted from [Grandmont, 2002]:

Lemma 3.2. *There exists a constant $\mathcal{M}_0 > 0$ such that for all b in $\mathcal{B}_{\mathcal{M}_0}^S$, we have*

- i) $\nabla(\mathcal{I} + \mathcal{R}(\gamma_\Gamma(b))) = I + \nabla(\mathcal{R}(\gamma_\Gamma(b)))$ is an invertible matrix in $H^2(\Omega_f)$,*
- ii) $\Phi(b) = \mathcal{I} + \mathcal{R}(\gamma_\Gamma(b))$ is one to one on $\bar{\Omega}_f$,*
- iii) $\Phi(b)$ is a C^1 -diffeomorphism from Ω_f onto $\Phi(b)(\Omega_f)$,*

Proof. It is clear that $\Phi(b) = \mathcal{I} + \mathcal{R}(\gamma_\Gamma(b))$ belongs to $H^3(\Omega_f)$ for all b in $H^3(\Omega_s)$. From Lemma 3.1, we know that $H^2(\Omega_f)$ is a Banach algebra. Thus, if \mathcal{M}_0 is chosen such that

$$\|b\|_{H^3(\Omega_s)} \leq \mathcal{M}_0 \implies \|\nabla(\mathcal{R}(\gamma_\Gamma(b)))\|_{H^2(\Omega_f)} < \frac{1}{C(\Omega_f)},$$

where $C(\Omega_f)$ is defined in Lemma 3.1, then $I + \nabla(\mathcal{R}(\gamma_\Gamma(b)))$ is an invertible matrix in $H^2(\Omega_f)$ and *i)* is proven.

Let us prove *ii)*. From [Ciarlet, 1988, Theorem 5.5-1], there exists a constant $C > 0$ such that for all ϕ in $C^1(\bar{\Omega}_f)$,

$$\|\nabla\phi\|_{C^0(\bar{\Omega}_f)} \leq C \implies \begin{cases} \det(\nabla(\mathcal{I} + \phi))(x) > 0, \forall x \in \bar{\Omega}_f, \\ \mathcal{I} + \phi \text{ is injective on } \bar{\Omega}_f. \end{cases}$$

Then, because of the continuous embedding of $H^3(\Omega_f)$ into $C^1(\bar{\Omega}_f)$ (see [Adams and Fournier, 2003, Theorem 6.3, part III]), and if \mathcal{M}_0 is chosen small enough, this result can be applied to $\mathcal{R}(\gamma_\Gamma(b))$ and we obtain *ii)*. Finally, using the continuous embedding of $H^3(\Omega_f)$ into $C^1(\bar{\Omega}_f)$, the fact that $\det(\nabla\Phi(b))(x) > 0, \forall x \in \bar{\Omega}_f$ and *ii)*, we can apply the implicit function theorem and get *iii)*. \square

With the previous lemma, we know that F , defined by (3.3), is well-defined in $H^2(\Omega_f)$ for all d_s in $\mathcal{B}_{\mathcal{M}_0}^S$. Now we state another lemma adapted from [Grandmont, 2002], dealing with the mappings F and G defined by (3.3).

Lemma 3.3. *The mapping G defined from $H^3(\Omega_s)$ into $H^2(\Omega_f)$ is of class C^∞ . The mapping F is defined from $\mathcal{B}_{\mathcal{M}_0}^S$ into $H^2(\Omega_f)$ and is infinitely differentiable everywhere in $\mathcal{B}_{\mathcal{M}_0}^S$.*

Proof. Let b be in $\mathcal{B}_{\mathcal{M}_0}^S$, then $G(b)$ belongs to $H^2(\Omega_f)$ because $H^2(\Omega_f)$ is a Banach algebra according to Lemma 3.1. The fact that $F(b)$ belong to $H^2(\Omega_f)$ is also due to the fact that $H^2(\Omega_f)$ is a Banach algebra, along with the invertible property of $\nabla\Phi(b)$ in $H^2(\Omega_f)$.

The mapping G is of class C^∞ by composition of C^∞ mappings (such as γ , \mathcal{R} , ∇ , \det , cof). For the regularity of the mapping F , it is sufficient to use the fact that the mapping

$$\begin{aligned} H^2(\Omega_f) &\rightarrow H^2(\Omega_f) \\ M &\mapsto M^{-1} \end{aligned}$$

is infinitely differentiable for all invertible matrix in $H^2(\Omega_f)$ (see [Cartan, 1967, chap. I]). \square

Corollary 3.1. *For all b_1 and b_2 in $\mathcal{B}_{\mathcal{M}_0}^S$, we have the following estimates,*

$$\begin{aligned} \|F(b_1) - F(b_2)\|_{H^2(\Omega_f)} &\leq C(\mathcal{M}_0) \|b_1 - b_2\|_{H^3(\Omega_s)}, \\ \|G(b_1) - G(b_2)\|_{H^2(\Omega_f)} &\leq C(\mathcal{M}_0) \|b_1 - b_2\|_{H^3(\Omega_s)}. \end{aligned}$$

where $C(\mathcal{M}_0)$ are positive constants which depend on \mathcal{M}_0 .

Proof. This result is a straightforward application of Lemma 3.3 and the mean value inequality (see [Cartan, 1967, Thm. 3.3.2]). The constants appearing in these inequalities are in fact given by

$$\sup_{b \in \mathcal{B}_{\mathcal{M}_0}^S} \|DF(b)\|_{\mathcal{L}(H^3(\Omega_s), H^2(\Omega_f))} \quad \text{and} \quad \sup_{b \in \mathcal{B}_{\mathcal{M}_0}^S} \|DG(b)\|_{\mathcal{L}(H^3(\Omega_s), H^2(\Omega_f))}.$$

For the sake of simplicity in the upcoming computations, we denote them all by $C(\mathcal{M}_0)$. \square

3.3 Main result

In this section, we state the existence of a local (in time) solution for the fluid-structure interaction system with an active stress term, for small enough applied forces and a small enough internal activity of the structure.

Theorem 3.1. *Let Ω_f , Ω_s , Γ_f , Γ_s and Γ be defined by (\mathbf{H}_1) - (\mathbf{H}_4) and let $T > 0$. Consider a force f_s in $L^\infty(0, T; H^1(\Omega_s))$ and an internal activity Σ^* in $L^\infty(0, T; H^2(\Omega_s))$, the data of the problem, such that $f_s(0) = \text{div}(\Sigma^*(0))$. Let us introduce the solution of a Stokes problem, denoted by (w_f^0, q_f^0) , which satisfies the equations,*

$$\begin{aligned} -\mu_f \Delta w_f^0 + \nabla q_f^0 &= 0, & \text{in } \Omega_f, \\ \text{div}(w_f^0) &= 0, & \text{in } \Omega_f, \\ w_f^0 &= 0, & \text{on } \Gamma_f, \\ \sigma_f(w_f^0, q_f^0) \cdot n_f &= -\Sigma^*(0) \cdot n_f, & \text{on } \Gamma. \end{aligned} \tag{3.11}$$

Let $\mathcal{M}_1 > 0$ and consider the ball $\mathcal{B}_{\mathcal{M}_1}^F$ defined by

$$\mathcal{B}_{\mathcal{M}_1}^F = \left\{ (\omega, \pi) \in L^2(0, T; H^3(\Omega_f) \cap H_{\Gamma_f}^1(\Omega_f)) \times L^2(0, T; H^2(\Omega_f)) \ ; \right. \\ \left. \|\omega - w_f^0\|_{L^2(0, T, H^3(\Omega_f))} + \|\pi - q_f^0\|_{L^2(0, T, H^2(\Omega_f))} \leq \mathcal{M}_1 \right\}. \tag{3.12}$$

There exist positive constants R_0 , R_1 , \mathcal{M}_0 , C_s^1 , C_s^2 , C_f , C_1 , C_2 and C_3 , which only depend on the domains Ω_f and Ω_s , the viscosity of the fluid μ_f and the elasticity parameters μ_s and λ_s of the structure such that, if the data f_s and Σ^* , the time T and the constant \mathcal{M}_1 satisfy the following conditions:

$$\|f_s - \text{div}(\Sigma^*)\|_{L^\infty(0, T, H^1(\Omega_s))} + R_0 \|\Sigma^*\|_{L^\infty(0, T, H^2(\Omega_s))} + C_1 \mathcal{M}_1 T^{1/2} \leq R_1, \tag{3.13}$$

$$C_s^1 \|\Sigma^*\|_{L^\infty(0,T,H^2(\Omega_s))} < 1, \quad (3.14)$$

$$\|f_s - \operatorname{div}(\Sigma^*)\|_{L^\infty(0,T,H^1(\Omega_s))} + (R_0 + C_1 C_f T) \|\Sigma^*\|_{L^\infty(0,T,H^2(\Omega_s))} + C_1 \mathcal{M}_1 T^{1/2} \leq \frac{\mathcal{M}_0}{C_s^2}, \quad (3.15)$$

$$\begin{aligned} & C_2 (T^{1/2} (1 + \|\Sigma^*\|_{L^\infty(0,T,H^2(\Omega_s))}) + \mathcal{M}_1) \\ & \times \left(\|f_s - \operatorname{div}(\Sigma^*)\|_{L^\infty(0,T,H^1(\Omega_s))} + (1+T) \|\Sigma^*\|_{L^\infty(0,T,H^2(\Omega_s))} + T^{1/2} \mathcal{M}_1 \right) \\ & + C_2 T^{1/2} \|\Sigma^*\|_{L^\infty(0,T,H^2(\Omega_s))} \leq \mathcal{M}_1, \end{aligned} \quad (3.16)$$

$$\begin{aligned} C_3 \left(\frac{T (1 + \|\Sigma^*\|_{L^\infty(0,T,H^2(\Omega_s))}) + T^{1/2} \mathcal{M}_1}{1 - C_s^1 \|\Sigma^*\|_{L^\infty(0,T,H^2(\Omega_s))}} + \|f_s - \operatorname{div}(\Sigma^*)\|_{L^\infty(0,T,H^1(\Omega_s))} \right. \\ \left. + (1+T) \|\Sigma^*\|_{L^\infty(0,T,H^2(\Omega_s))} + T^{1/2} \mathcal{M}_1 \right) < 1, \end{aligned} \quad (3.17)$$

then, there exists a unique solution (w_f, q_f, d_s) of (3.1), (3.2), (3.4), (3.6) and (3.7), with the couple (w_f, q_f) which belongs to $\mathcal{B}_{\mathcal{M}_1}^F$ and d_s in the space $L^\infty(0, T; \mathcal{B}_{\mathcal{M}_0}^S \cap H_{\Gamma_s}^1(\Omega_s))$.

The proof of Theorem 3.1 is based on Banach's fixed point theorem (see [Brezis, 1999, Theorem V.7]). In this scope, we construct a mapping \mathcal{S} defined from $\mathcal{B}_{\mathcal{M}_1}$, the ball defined by equation (3.12), into $L^2(0, T; H^3(\Omega_f)) \times L^2(0, T; H^2(\Omega_f))$. This mapping is defined through a composition of mappings that takes a couple (ω, π) in $\mathcal{B}_{\mathcal{M}_1}$, constructs a boundary condition δ in $H^1(0, T; H^{5/2}(\Gamma))$, solves an elasticity problem with Dirichlet boundary conditions and associated to the data (f_s, Σ^*, δ) and, finally, solves a fluid problem with mixed Dirichlet and Neumann boundary conditions. In fact, \mathcal{S} can be represented as the following composition of mappings:

$$\mathcal{S} = \mathcal{O}_3 \circ \mathcal{O}_2 \circ \mathcal{O}_1, \quad (3.18)$$

where each mapping writes

$$\begin{aligned} \mathcal{O}_1 & : \quad \mathcal{B}_{\mathcal{M}_1} \rightarrow H^1(0, T; H^{5/2}(\Gamma)) \\ & \quad (\omega, \pi) \mapsto \delta, \\ \mathcal{O}_2 & : \quad H^1(0, T; H^{5/2}(\Gamma)) \rightarrow L^\infty(0, T; H^3(\Omega_s)) \\ & \quad \delta \mapsto d_s, \\ \mathcal{O}_3 & : \quad L^\infty(0, T; H^3(\Omega_s)) \rightarrow L^2(0, T; H^3(\Omega_f)) \times L^2(0, T; H^2(\Omega_f)) \\ & \quad d_s \mapsto (w_f, q_f), \end{aligned}$$

and will now be defined.

Given a couple (ω, π) in $\mathcal{B}_{\mathcal{M}_1}$, the boundary condition δ is constructed, for all $t \in [0, T]$, by

$$\delta(t) = \int_0^t \gamma_\Gamma(\omega(s)) ds,$$

which, according to Lemma 3.1, belongs to $H^1(0, T; H^{5/2}(\Gamma))$. This defines the mapping \mathcal{O}_1 .

Then, with this boundary condition, we consider the following problem, to obtain a structure displacement d_s such that, for almost every t in $(0, T)$,

$$\begin{cases} -\operatorname{div}(\Pi_s(d_s(t), t)) = f_s(t) & \text{in } \Omega_s, \\ d_s(t) = \delta(t) & \text{on } \Gamma, \\ d_s(t) = 0 & \text{on } \Gamma_s. \end{cases} \quad (3.19)$$

This elasticity problem with internal activity is studied in Section 3.4. As we will see, it admits a unique solution if the data (f_s, Σ^*, δ) are small enough, namely if conditions (3.13) and (3.14) are satisfied. This step defines the mapping \mathcal{O}_2 .

Next, to define the mapping \mathcal{O}_3 , we consider a fluid problem, obtained from fluid equations written in the reference configuration (3.4) through a perturbation argument, which writes: find (w_f, q_f) such that, for almost every t in $(0, T)$,

$$\left\{ \begin{array}{ll} -\mu_f \Delta w_f(t) + \nabla q_f(t) = -\mu_f \operatorname{div}(((I - F(d_s(t))) \nabla) \omega(t) \\ \quad + ((I - G(d_s(t))) \nabla) \pi(t)) & \text{in } \Omega_f, \\ \operatorname{div}(w_f(t)) = -\operatorname{div}((I - G(d_s(t)))^t \omega(t)) & \text{in } \Omega_f, \\ w_f(t) = 0 & \text{on } \Gamma_f, \\ \sigma_f(w_f(t), q_f(t)) n_f = \Pi_s(d_s(t), t) n_f \\ \quad + \mu_f (((I - F(d_s(t))) \nabla) \omega(t)) n_f \\ \quad - (\pi(t) (I - G(d_s(t)))) n_f & \text{on } \Gamma. \end{array} \right. \quad (3.20)$$

This is a Stokes problem with mixed Dirichlet and Neumann boundary conditions, which is studied in Section 3.5. Moreover, condition (3.15) ensures that, for almost all t in $(0, T)$, the displacement $d_s(t)$ belongs to the ball $\mathcal{B}_{\mathcal{M}_0}$ (defined by (3.10)), such that problem (3.20) is well-defined.

Finally, under condition (3.16) the image by \mathcal{S} of the ball $\mathcal{B}_{\mathcal{M}_1}$ is included in $\mathcal{B}_{\mathcal{M}_1}$ (i.e. that $\mathcal{S}(\mathcal{B}_{\mathcal{M}_1}) \subset \mathcal{B}_{\mathcal{M}_1}$) and under condition (3.17), \mathcal{S} is a contraction mapping such that we can apply Banach's fixed point theorem.

Each fixed point of \mathcal{S} in $\mathcal{B}_{\mathcal{M}_1}$ is a solution of equations (3.1), (3.2), (3.4), (3.6) and (3.7). Indeed, suppose that there exists a couple (\bar{w}_f, \bar{q}_f) in $\mathcal{B}_{\mathcal{M}_1}$ such that $\mathcal{S}(\bar{w}_f, \bar{q}_f) = (\bar{w}_f, \bar{q}_f)$. The solution of the structure problem, defined during the process is denoted by \bar{d}_s . Then, the triplet $(\bar{w}_f, \bar{q}_f, \bar{d}_s)$ satisfies, for almost every t in $(0, T)$,

$$\begin{aligned} -\operatorname{div}(\Pi_s(\bar{d}_s(t), t)) &= f_s(t) & \text{in } \Omega_s, \\ \bar{d}_s(t) &= 0 & \text{on } \Gamma_s, \\ -\mu_f \Delta \bar{w}_f(t) + \nabla \bar{q}_f(t) &= -\mu_f \operatorname{div}(((I - F(\bar{d}_s(t))) \nabla) \bar{w}_f(t) \\ &\quad + ((I - G(\bar{d}_s(t))) \nabla) \bar{q}_f(t)) & \text{in } \Omega_f, \\ \operatorname{div}(\bar{w}_f(t)) &= -\operatorname{div}((I - G(\bar{d}_s(t)))^t \bar{w}_f(t)) & \text{in } \Omega_f, \\ \bar{w}_f(t) &= 0 & \text{on } \Gamma_f, \\ \frac{\partial \bar{d}_s}{\partial t}(t) &= \bar{w}_f(t) & \text{on } \Gamma, \\ \sigma_f(\bar{w}_f(t), \bar{q}_f(t)) \cdot n_f &= \Pi_s(\bar{d}_s(t), t) \cdot n_f \\ &\quad - \mu_f (((I - F(\bar{d}_s(t))) \nabla) \bar{w}_f(t)) \cdot n_f \\ &\quad + (\bar{q}_f(t) (I - G(\bar{d}_s(t)))) \cdot n_f & \text{on } \Gamma. \end{aligned}$$

Reorganizing the terms in the right-hand sides, these equations exactly match equations (3.1), (3.4), (3.6) and (3.7). Then the fixed point of \mathcal{S} is a solution of this coupled nonlinear fluid-structure problem.

Remark 3.4. In the stationary case, the fixed point procedure has been done in [Grandmont, 2002] by solving the fluid problem in a given geometry with Dirichlet boundary conditions and the solid problem with Neumann boundary conditions and performing the fixed point on the geometry. However, in the present study, where we consider a quasi-static time dependent model, the fixed point is conducted on the velocity and the pressure of the fluid by solving the structure with Dirichlet boundary conditions and the fluid problem with Neumann boundary conditions. Our choice on boundary conditions is due to the fact that we need time regularity on the solution. Indeed, because of the equality of the fluid and solid velocities on the interface Γ , we instantly lose time regularity in the decoupling process, if the Dirichlet boundary conditions are applied to the fluid.

Remark 3.5. The condition $f_s(0) = \operatorname{div}(\Sigma^*(0))$ appearing in Theorem 3.1 ensures that the structure is at rest initially. Along with the hypothesis that the trace of the displacement of the structure is null at $t = 0$, it implies that $d_s(0) = 0$. If it is not the case, the linearization of the fluid problem in reference configuration (3.4), that we considered in problem (3.20), has to be done around the initial geometrical configuration given by $d_s(0)$, instead of the reference one.

The remaining of this chapter is the following. In Section 3.4, we consider system (3.19) and prove its well-posedness and the regularity of its solution. In Section 3.5, we study equations (3.20) and prove existence, uniqueness and regularity results. In Section 3.6, the proof of Theorem 3.1 is done using a fixed point procedure on the mapping \mathcal{S} . Finally, in Section 3.7, an extension of Theorem 3.1 with more general data is given.

3.4 Structure equations

In this section we study the two or three-dimensional elasticity equations with non-homogeneous Dirichlet boundary conditions, where the solid is described by the nonlinear Saint Venant-Kirchhoff law, and with an additional activity term. The domain Ω_s satisfies (\mathbf{H}_1) - (\mathbf{H}_4) . For a given body force f_s , a given Dirichlet boundary condition δ on Γ and a given active stress tensor Σ^* , the considered structure problem writes:

$$\begin{cases} -\operatorname{div}((I + \nabla d)(\Sigma_s(E(d)) - \Sigma^*)) = f_s & \text{in } \Omega_s, \\ d = \delta & \text{on } \Gamma, \\ d = 0 & \text{on } \Gamma_s, \end{cases} \quad (3.21)$$

with the passive stress tensor Σ_s defined by (3.2). Then, the following lemma states that problem (3.21) admits a unique solution d in $H^3(\Omega_s)$, for small enough data.

Lemma 3.4. *Let Ω_s , Γ_s and Γ be defined by (\mathbf{H}_1) - (\mathbf{H}_4) and suppose that the force f_s belongs to $H^1(\Omega_s)$, the displacement δ belongs to $H^{5/2}(\Gamma)$ and the internal activity Σ^* belongs to $H^2(\Omega_s)$. There exist three real positive constants R_0 , R_1 and C_s^1 , that only depend on the domain Ω_s and the elasticity parameters μ_s and λ_s such that, if the data satisfy the conditions*

$$\|f_s - \operatorname{div}(\Sigma^*)\|_{H^1(\Omega_s)} + R_0\|\Sigma^*\|_{H^2(\Omega_s)} + \|\delta\|_{H^{5/2}(\Gamma)} \leq R_1, \quad (3.22)$$

$$C_s^1\|\Sigma^*\|_{H^2(\Omega_s)} < 1, \quad (3.23)$$

then there exists a unique solution d of (3.21) in a neighborhood of 0 in $H^3(\Omega_s) \cap H_{\Gamma_s}^1(\Omega_s)$. Moreover, there exists a positive constant C_s^2 that only depends on Ω_s , μ_s and λ_s such that the solution can be estimated with respect to the data:

$$\|d\|_{H^3(\Omega_s)} \leq C_s^2(\|f_s - \operatorname{div}(\Sigma^*)\|_{H^1(\Omega_s)} + R_0\|\Sigma^*\|_{H^2(\Omega_s)} + \|\delta\|_{H^{5/2}(\Gamma)}). \quad (3.24)$$

Proof. The proof is based on Banach's fixed point Theorem. We construct a mapping \mathcal{T} defined from $H^3(\Omega_s) \cap H_{\Gamma_s}^1(\Omega_s)$ into itself which, to all u in $H^3(\Omega_s) \cap H_{\Gamma_s}^1(\Omega_s)$, associates the solution of the following passive elasticity problem: find a structure displacement d such that

$$\begin{cases} -\operatorname{div}((I + \nabla d)\Sigma_s(E(d))) = f_s - \operatorname{div}(\Sigma^*) - \operatorname{div}(\nabla u \Sigma^*) & \text{in } \Omega_s, \\ d = \delta & \text{on } \Gamma, \\ d = 0 & \text{on } \Gamma_s. \end{cases} \quad (3.25)$$

More precisely, \mathcal{T} is the following mapping:

$$\begin{aligned} \mathcal{T} : H^3(\Omega_s) \cap H_{\Gamma_s}^1(\Omega_s) &\rightarrow H^3(\Omega_s) \cap H_{\Gamma_s}^1(\Omega_s) \\ u &\mapsto d. \end{aligned}$$

The objective is to show that the mapping \mathcal{T} has a fixed point d in $H^3(\Omega_s) \cap H_{\Gamma_s}^1(\Omega_s)$, which in turns solves problem (3.21).

The rest of the proof is divided in three parts. Firstly, we prove that, under condition (3.22) on the data, the mapping \mathcal{T} is well-defined, i.e. that problem (3.25) admits a unique solution in $H^3(\Omega_s) \cap H_{\Gamma_s}^1(\Omega_s)$. Secondly, we show that, under condition (3.23) on the data, the mapping \mathcal{T} is a contraction from a ball in $H^3(\Omega_s) \cap H_{\Gamma_s}^1(\Omega_s)$ into itself. Finally, we apply Banach's fixed point Theorem and obtain the desired estimate.

Let us show that (3.25) admits a unique solution in a neighborhood of 0 in the space $H^3(\Omega_s) \cap H_{\Gamma_s}^1(\Omega_s)$ if the data are sufficiently small. A study of elasticity problems similar to problem (3.25) has been conducted in [Ciarlet, 1988] in Sobolev spaces $W^{2,p}$ with $p > n$ and considering homogeneous Dirichlet boundary conditions; our proof essentially uses the same arguments. We introduce the following nonlinear operator of passive elasticity:

$$\begin{aligned} A : H^3(\Omega_s) \cap H_{\Gamma_s}^1(\Omega_s) &\rightarrow H^1(\Omega_s) \times H^{5/2}(\Gamma), \\ d &\mapsto (-\operatorname{div}((I + \nabla d)\Sigma_s(E(d))), \gamma_{\Gamma}(d)), \end{aligned}$$

where we recall that γ_{Γ} is the trace operator on Γ . The mapping A is defined since $H^2(\Omega_s)$ is an algebra in two or three space dimensions (see Lemma 3.1) and is infinitely differentiable since it is a sum of continuous multilinear mappings. As a consequence, problem (3.25) can be written in term of operator: find d such that

$$A(d) = (\tilde{f}_s, \delta),$$

where

$$\tilde{f}_s := f_s - \operatorname{div}(\Sigma^*) - \operatorname{div}(\nabla u \Sigma^*).$$

We can observe that $d = 0$ is a particular solution corresponding to $(\tilde{f}_s, \delta) = (0, 0)$. Thus, a natural idea consists in showing that the mapping A is locally invertible in a neighborhood of this particular solution. In order to prove it, we need to check that the differential of A at 0 is an isomorphism between $H^3(\Omega_s) \cap H_{\Gamma_s}^1(\Omega_s)$ and $H^1(\Omega_s) \times H^{5/2}(\Gamma)$, to be able to use the Implicit Function Theorem. This differential at point 0 is given by

$$\mathcal{D}A(0) \cdot d = (-\operatorname{div}(2\mu_s D(d) + \lambda_s \operatorname{div}(d)I), \gamma_{\Gamma}(d)),$$

where $D(d) = \frac{1}{2}(\nabla d + \nabla d^T)$ is the symmetric gradient of d . The operator $\mathcal{D}A(0)$ is the linearized elasticity operator and is an isomorphism if for all \tilde{f}_s in $H^1(\Omega_s)$ and for all δ in

the space $H^{5/2}(\Gamma)$, there exists a unique solution d in $H^3(\Omega_s) \cap H_{\Gamma_s}^1(\Omega_s)$ to the problem: find d such that

$$\begin{cases} -\operatorname{div}(2\mu_s D(d) + \lambda_s \operatorname{div}(d)I), & = \tilde{f}_s & \text{in } \Omega_s, \\ d & = \delta, & \text{on } \Gamma, \\ d & = 0, & \text{on } \Gamma_s. \end{cases} \quad (3.26)$$

Because δ belongs to $H^{5/2}(\Gamma)$ and Ω_s is of class $C^{2,1}$, there exists a lifting of δ in the space $H^3(\Omega_s) \cap H_{\Gamma_s}^1(\Omega_s)$, denoted by $\tilde{\delta}$, such that $\gamma_\Gamma(\tilde{\delta}) = \delta$. Then, the function $\tilde{d} = d - \tilde{\delta}$ is solution of the linearized elasticity problem with homogeneous Dirichlet boundary conditions: find \tilde{d} such that,

$$\begin{cases} -\operatorname{div}(2\mu_s D(\tilde{d}) + \lambda_s \operatorname{div}(\tilde{d})I) & = \tilde{f}_s + 2\mu_s \Delta \tilde{\delta} + \lambda_s \operatorname{div}(\operatorname{div}(\tilde{\delta})I) & \text{in } \Omega_s, \\ d & = 0 & \text{on } \partial\Omega_s. \end{cases} \quad (3.27)$$

Problem (3.27) is known as the *linearized pure displacement problem* and has been studied for instance in [Ciarlet, 1988, Theorem 6.3-6]. Because the boundary of Ω_s is of class $C^{2,1}$ and the right-hand side in the first equation of (3.27) belongs to $H^1(\Omega_s)$, it follows that problem (3.27) admits a unique solution in $H^3(\Omega_s) \cap H_0^1(\Omega_s)$ (see [Grisvard, 2011, Theorem 2.5.1.1]). Furthermore, problem (3.26) admits $\tilde{d} + \tilde{\delta}$ as unique solution. Hence, the linear continuous operator

$$\mathcal{D}A(0) : H^3(\Omega_s) \cap H_{\Gamma_s}^1(\Omega_s) \rightarrow H^1(\Omega_s) \times H^{5/2}(\Gamma)$$

is bijective and its inverse is also continuous, by the closed graph Theorem. Thus, we can apply the implicit function Theorem. Consequently, there exists \mathcal{V}_0 a neighborhood of 0 in $H^3(\Omega_s) \cap H_{\Gamma_s}^1(\Omega_s)$ and \mathcal{V}_1 a neighborhood of $(0, 0)$ in $H^1(\Omega_s) \times H^{5/2}(\Gamma)$ such that the mapping A is a C^1 -diffeomorphism from \mathcal{V}_0 to \mathcal{V}_1 . In particular, there exist two positive constants R_0 and R_1 such that the ball

$$\mathcal{B}_{R_0}^S = \{u \in H^3(\Omega_s) \cap H_{\Gamma_s}^1(\Omega_s); \|u\|_{H^3(\Omega_s)} \leq R_0\},$$

satisfies

$$A^{-1} \left(\left\{ (f, \delta) \in H^1(\Omega_s) \times H^{3/2}(\Gamma); \|f\|_{H^1(\Omega_s)} + \|\delta\|_{H^{5/2}(\Gamma)} \leq R_1 \right\} \right) \subset \mathcal{B}_{R_0}^S.$$

Going back to the nonlinear problem (3.25), for all u in $\mathcal{B}_{R_0}^S$, if the couple (\tilde{f}_s, δ) belongs to the space

$$\left\{ (f, \delta) \in H^1(\Omega_s) \times H^{3/2}(\Gamma); \|f\|_{H^1(\Omega_s)} + \|\delta\|_{H^{5/2}(\Gamma)} \leq R_1 \right\},$$

i.e. if the inequality (3.22) is satisfied, there exists a unique solution d in $\mathcal{B}_{R_0}^S$ of problem (3.25). Moreover, this solution can be estimated with respect to the data:

$$\|d\|_{H^3(\Omega_s)} \leq C_s^2 \left(\|f_s - \operatorname{div}((I + \nabla u)\Sigma^*)\|_{H^1(\Omega_s)} + \|\delta\|_{H^{5/2}(\Gamma)} \right), \quad (3.28)$$

where the constant C_s^2 is defined by

$$C_s^2 = \sup_{\|(f, \delta)\| \leq R_1} \|\mathcal{D}A^{-1}(f, \delta)\|_{\mathcal{L}(H^1(\Omega_s) \times H^{5/2}(\Gamma), H^3(\Omega_s))}.$$

Thus, we just proved that the mapping \mathcal{T} is well-defined from $\mathcal{B}_{R_0}^S$ into itself, if the data satisfy condition (3.22).

Now, let us show that, under condition (3.23), \mathcal{T} is a contraction from $\mathcal{B}_{R_0}^S$ into itself. Under condition (3.22) on the data, we have that, for all u_1 and u_2 in $\mathcal{B}_{R_0}^S$,

$$\begin{aligned}\mathcal{T}(u_1) &= A^{-1}(f_s - \operatorname{div}((I + \nabla u_1)\Sigma^*), \delta), \\ \mathcal{T}(u_2) &= A^{-1}(f_s - \operatorname{div}((I + \nabla u_2)\Sigma^*), \delta).\end{aligned}$$

Since the mapping A^{-1} is a C^1 -diffeomorphism from \mathcal{V}_1 to \mathcal{V}_0 , the mean value inequality can be applied. From the mean value inequality and Lemma 3.1, we obtain

$$\begin{aligned}\|\mathcal{T}(u_1) - \mathcal{T}(u_2)\|_{H^3(\Omega_s)} &\leq C_s^2 \|(\operatorname{div}((\nabla u_1 - \nabla u_2)\Sigma^*), 0)\|_{H^1(\Omega_s) \times H^{5/2}(\Gamma)}, \\ &\leq C_s^1 \|\Sigma^*\|_{H^2(\Omega_s)} \|u_1 - u_2\|_{H^3(\Omega_s)},\end{aligned}$$

where $C_s^1 = C_s^2 C(\Omega_s)$. It follows that \mathcal{T} is a contraction from $\mathcal{B}_{R_0}^S$ into itself if the active stress Σ^* satisfies inequality (3.23).

So, under conditions (3.22) and (3.23) on the data, the mapping \mathcal{T} is a contraction from $\mathcal{B}_{R_0}^S$ into itself. Thus, Banach's fixed point theorem implies that \mathcal{T} has a unique fixed point d in $\mathcal{B}_{R_0}^S$, which proves that there exists a unique solution $d \in H^3(\Omega_s) \cap H_{\Gamma_s}^1(\Omega_s)$ of (3.21), under smallness assumptions on the data. Moreover, replacing the fixed point d in (3.28) and using the fact that d belongs to $\mathcal{B}_{R_0}^S$ we obtain the estimate

$$\|d\|_{H^3(\Omega_s)} \leq C_s^2 (\|f_s - \operatorname{div}(\Sigma^*)\|_{H^1(\Omega_s)} + R_0 \|\Sigma^*\|_{H^2(\Omega_s)} + \|\delta\|_{H^{5/2}(\Gamma)}).$$

□

Remark 3.6. In the particular where $f_s = \operatorname{div}(\Sigma^*)$ and $\delta = 0$, if Σ^* satisfies conditions (3.22) and (3.23), then Lemma 3.4 implies that $d_s = 0$ is the unique solution of problem (3.21).

Using the notation introduced in the proof of Lemma 3.4, we also state the following corollary, which gives a continuity estimate of the solutions of (3.21) with respect to the data.

Corollary 3.2. *Let f_s be in $H^1(\Omega_s)$, Σ^* be in $H^2(\Omega_s)$, and δ_1 and δ_2 be in $H^{5/2}(\Gamma)$. Moreover, suppose that these data satisfy the following conditions:*

$$\begin{aligned}\|f_s - \operatorname{div}(\Sigma^*)\|_{H^1(\Omega_s)} + R_0 \|\Sigma^*\|_{H^2(\Omega_s)} + \|\delta_1\|_{H^{5/2}(\Gamma)} &\leq R_1, \\ \|f_s - \operatorname{div}(\Sigma^*)\|_{H^1(\Omega_s)} + R_0 \|\Sigma^*\|_{H^2(\Omega_s)} + \|\delta_2\|_{H^{5/2}(\Gamma)} &\leq R_1, \\ C_s^1 \|\Sigma^*\|_{H^2(\Omega_s)} &< 1,\end{aligned}$$

where R_0 , R_1 and C_s^1 have been defined in Lemma 3.4. Then there exists a unique solution d_1 of (3.21) in a neighborhood of 0 in $H^3(\Omega_s) \cap H_{\Gamma_s}^1(\Omega_s)$, associated to the data $(f_s, \Sigma^*, \delta_1)$ and there exists a unique solution d_2 to the same problem associated to the data $(f_s, \Sigma^*, \delta_2)$. Furthermore, we have the following estimate:

$$(1 - C_s^1 \|\Sigma^*\|_{H^2(\Omega_s)}) \|d_1 - d_2\|_{H^3(\Omega_s)} \leq C_s^2 \|\delta_1 - \delta_2\|_{H^{5/2}(\Gamma)},$$

where C_s^2 has been defined in Lemma 3.4.

Proof. The existence and uniqueness of d_1 and d_2 is a direct consequence of Lemma 3.4. Moreover, using the fact that the mapping A^{-1} is everywhere differentiable in \mathcal{V}_1 and Lemma 3.1, we have that

$$\begin{aligned}&\|d_1 - d_2\|_{H^3(\Omega_s)} \\ &= \|A^{-1}(f - \operatorname{div}(\Sigma^*) - \operatorname{div}(\nabla d_1 \Sigma^*), \delta_1) - A^{-1}(f - \operatorname{div}(\Sigma^*) - \operatorname{div}(\nabla d_2 \Sigma^*), \delta_2)\|_{H^3(\Omega_s)}, \\ &\quad \leq C_s^2 \|(\operatorname{div}((\nabla d_1 - \nabla d_2)\Sigma^*), \delta_1 - \delta_2)\|_{H^1(\Omega_s) \times H^{5/2}(\Gamma)}, \\ &\quad \leq C_s^1 \|\Sigma^*\|_{H^2(\Omega_s)} \|d_1 - d_2\|_{H^3(\Omega_s)} + C_s^2 \|\delta_1 - \delta_2\|_{H^{5/2}(\Gamma)}.\end{aligned}$$

Then, condition (3.23) enables us to obtain the estimate

$$(1 - C_s^1 \|\Sigma^*\|_{H^2(\Omega_s)}) \|d_1 - d_2\|_{H^3(\Omega_s)} \leq C_s^2 \|\delta_1 - \delta_2\|_{H^{5/2}(\Gamma)}.$$

□

3.5 Fluid equations

In this section, we study the two or three-dimensional Stokes equations with mixed non-homogeneous Dirichlet and Neumann boundary conditions, where the domain Ω_f is defined by (\mathbf{H}_1) - (\mathbf{H}_4) . The cases of pure Dirichlet or Neumann boundary conditions have been, for example, treated in [Boyer and Fabrie, 2012], where existence, uniqueness and regularity have been obtained for the solution of the Stokes problem, depending on the regularity of the domain and the data.

Let f be a given body force, g be a given divergence constraint and h be a given Neumann boundary condition. We consider the Stokes problem: find (u, p) such that

$$\begin{cases} -\operatorname{div}(\sigma_f(u, p)) = f & \text{in } \Omega_f, \\ \operatorname{div}(u) = g & \text{in } \Omega_f, \\ u = 0 & \text{on } \Gamma_f, \\ \sigma_f(u, p)n_f = h & \text{on } \Gamma, \end{cases} \quad (3.29)$$

where $\sigma_f(u, p)$ is the fluid stress tensor defined by

$$\sigma_f(u, p) = \mu_f \nabla u - pI.$$

In the following lemma, we state an existence, uniqueness and regularity result for the solution of problem (3.29). The key argument here is the fact that the boundary Γ_f , where the homogeneous Dirichlet boundary condition is applied, and the boundary Γ , where the Neumann boundary condition is applied, are such that $\overline{\Gamma_f} \cap \overline{\Gamma} = \emptyset$. Actually, this assumption on the domain Ω_f enables us to easily obtain the regularity of the solution, using existing regularity results on the solution of the pure Dirichlet boundary problem and the pure Neumann boundary problem, that can be found in [Boyer and Fabrie, 2012].

Lemma 3.5. *Let Ω_f , Γ_f and Γ be defined by (\mathbf{H}_1) - (\mathbf{H}_4) and suppose that f belongs to $H^1(\Omega_f)$, g belongs to $H^2(\Omega_f)$ and h belongs to $H^{3/2}(\Gamma)$. Then, the Stokes problem (3.29) admits a unique solution in $(H^3(\Omega_f) \cap H_{\Gamma_f}^1(\Omega_f)) \times H^2(\Omega_f)$. Moreover, there exists a positive constant C_f depending only on Ω_f and μ_f such that*

$$\|u\|_{H^3(\Omega_f)} + \|p\|_{H^2(\Omega_f)} \leq C_f (\|f\|_{H^1(\Omega_f)} + \|g\|_{H^2(\Omega_f)} + \|h\|_{H^{3/2}(\Gamma)}).$$

To prove this lemma, we start by giving a preliminary result concerning the divergence operator, which is based on Bogovskii's result in [Bogovski, 1979].

Lemma 3.6. *Let Ω_f and Γ_f be defined by (\mathbf{H}_1) - (\mathbf{H}_4) and suppose that g is a function in $L^2(\Omega_f)$. Then, there exists a function u in $H_{\Gamma_f}^1(\Omega_f)$ such that $\operatorname{div}(u) = g$. Moreover, there exists a constant $C(\Omega_f)$ which depends on Ω_f such that,*

$$\|u\|_{H^1(\Omega_f)} \leq C(\Omega_f) \|g\|_{L^2(\Omega_f)}.$$

Proof. We consider an extension of Ω_f , denoted by Ω^* , which strictly contains Ω_f and whose part of its boundary coincides with Γ_f . We define the function g^* by

$$g^*(x) = \begin{cases} g(x) & \text{for } x \in \Omega_f \\ \frac{|\Omega_f|}{|\Omega^* \setminus \Omega_f|} \int_{\Omega_f} g & \text{for } x \in \Omega^* \setminus \Omega_f \end{cases},$$

where $|\Omega_f|$ (resp. $|\Omega^* \setminus \Omega_f|$) is the volume of the domain Ω_f (resp. $\Omega^* \setminus \Omega_f$). Then, g^* is in $L^2_0(\Omega^*)$ and we can apply Bogovskii's result [Bogovski, 1979], which states that there exists a function u^* in $H^1_0(\Omega^*)$ such that $\operatorname{div}(u^*) = g^*$. Moreover, there exists a constant that depends on the domain Ω^* , then on Ω_f , such that

$$\|u^*\|_{H^1(\Omega^*)} \leq C(\Omega_f) \|g^*\|_{L^2(\Omega^*)}.$$

Now, defining u as the restriction of u^* over Ω_f , we obtain that $\operatorname{div}(u) = g$ in Ω_f . Moreover, we have the following estimate:

$$\|u\|_{H^1(\Omega_f)} \leq C(\Omega_f) \|g\|_{L^2(\Omega_f)}.$$

□

We are now able to prove Lemma 3.5.

Proof of Lemma 3.5. We define the saddle-point formulation of problem (3.29) to be the following problem:

$$\begin{cases} \text{find } (u, p) \text{ in } H^1_{\Gamma_f}(\Omega_f) \times L^2(\Omega_f) \text{ such that,} \\ a(u, v) + (p, Bv)_{L^2(\Omega_f)} = l(v) \quad \forall v \in H^1_{\Gamma_f}(\Omega_f), \\ (q, Bu)_{L^2(\Omega_f)} = \int_{\Omega_f} gq \quad \forall q \in L^2(\Omega_f), \end{cases} \quad (3.30)$$

where (\cdot, \cdot) denotes the scalar product in $L^2(\Omega_f)$. The bilinear and linear forms a and l are defined by

$$\begin{aligned} a(u, v) &= \mu_f \int_{\Omega_f} \nabla u : \nabla v, \\ l(v) &= \int_{\Omega_f} f \cdot v + \int_{\Gamma} h \cdot v. \end{aligned}$$

Moreover, B is the divergence operator defined by

$$\begin{aligned} B : H^1_{\Gamma_f}(\Omega_f) &\rightarrow L^2(\Omega_f) \\ u &\mapsto \operatorname{div}(u). \end{aligned}$$

It is easy to check that a is a symmetric coercive continuous bilinear form on the product space $H^1_{\Gamma_f}(\Omega_f) \times H^1_{\Gamma_f}(\Omega_f)$ and that l is a continuous linear form on $H^1_{\Gamma_f}(\Omega_f)$. Moreover, the operator B is a linear continuous operator from $H^1_{\Gamma_f}(\Omega_f)$ into $L^2(\Omega_f)$ and Lemma 3.6 ensures that B is surjective. Thus, according to Brezzi's result on saddle-point problems (see [Brezzi, 1974]), there exists a unique solution (u, p) of problem (3.30). Moreover, there exists a constant which depends on Ω_f such that

$$\|u\|_{H^1(\Omega_f)} + \|p\|_{L^2(\Omega_f)} \leq C(\Omega_f) (\|f\|_{H^1(\Omega_f)} + \|g\|_{H^2(\Omega_f)} + \|h\|_{H^{3/2}(\Gamma)}).$$

Hence, since the boundaries Γ_f and Γ are disjoint and because Γ_f is of class $C^{2,1}$ and Γ is of class $C^{3,1}$, the rest of the proof, i.e. the regularity of the solution, follows from the method of translations. For local (interior) regularity we refer to Theorem IV.6.1 in [Boyer and Fabrie, 2012]. For tangential regularity on the boundary Γ_f , we refer to the proof of Theorem IV.5.8 in [Boyer and Fabrie, 2012]. For the tangential regularity on the boundary Γ , we refer to the proof of Theorem IV.7.1 in [Boyer and Fabrie, 2012]. Then, we use the tangential and normal coordinates in a tubular neighborhood of $\partial\Omega_f$ in Ω_f , to deduce the regularity up to the boundary of the solution from the tangential regularity. The desired estimate follows from these results. \square

Remark 3.7. On one hand, in [Boyer and Fabrie, 2012], no assumption on the regularity of the domain is necessary to apply the result on the interior regularity of the solution, stated in Theorem IV.6.1, which is also independent of the chosen boundary conditions. On the other hand, Theorem IV.5.8, dealing with pure Dirichlet boundary conditions, and Theorem IV.7.1, dealing with pure Neumann boundary conditions, require hypotheses on the regularity of the domain and compatibility conditions on the data due to the particular choice of boundary conditions. Yet, these compatibility conditions only appear in the case of pure Dirichlet or pure Neumann boundary conditions, which is not the case here. Nevertheless, the proofs for the regularity of the solution apply in the same way, since the boundaries where Dirichlet and Neumann boundary conditions are applied are disjoint.

3.6 Fixed point procedure. Proof of Theorem 3.1

In this section, we go back to the coupled fluid-structure problem and apply the results of sections 4 and 5 to prove Theorem 3.1.

We recall that we consider $T > 0$, a positive constant \mathcal{M}_1 , a force f_s in $L^\infty(0, T; H^1(\Omega_s))$ and an internal activity of the structure Σ^* in $L^\infty(0, T; H^2(\Omega_s))$, that satisfy conditions (3.13), (3.14), (3.15), (3.16) and (3.17). Moreover, the structure is supposed to be at equilibrium initially, i.e. we suppose that $f_s(0) = \operatorname{div}(\Sigma^*(0))$ and that $d_0 = 0$, which implies that $d_s(0) = 0$ (see Remark 3.6). However, because the active stress tensor Σ^* is not necessarily zero at $t = 0$, neither are the velocity and pressure of the fluid. That is why we introduce the initial solution of the fluid problem (3.20), denoted by (w_f^0, q_f^0) , which satisfies equations (3.11), that we recall:

$$\begin{cases} -\mu_f \Delta w_f^0 + \nabla q_f^0 = 0, & \text{in } \Omega_f, \\ \operatorname{div}(w_f^0) = 0, & \text{in } \Omega_f, \\ w_f^0 = 0, & \text{on } \Gamma_f, \\ \sigma_f(w_f^0, q_f^0)n_f = -\Sigma^*(0)n_f, & \text{on } \Gamma. \end{cases}$$

This Stokes problem is similar to the one studied in Lemma 3.5. Then, because the domain Ω_f is of class $C^{3,1}$ and $\Sigma^*(0) \cdot n_f$ is in $H^{3/2}(\Gamma)$, it follows that equations (3.11) admit a unique solution (w_f^0, q_f^0) in $(H^3(\Omega_f) \cap H_{\Gamma_f}^1(\Omega_f)) \times H^2(\Omega_f)$, which verifies the following inequality:

$$\|w_f^0\|_{H^3(\Omega_f)} + \|q_f^0\|_{H^2(\Omega_f)} \leq C_f \|\Sigma^*(0)\|_{H^2(\Omega_s)}.$$

Furthermore, by taking the L^2 -norm in time we obtain:

$$\|w_f^0\|_{L^2(0, T; H^3(\Omega_f))} + \|q_f^0\|_{L^2(0, T; H^2(\Omega_f))} \leq C_f T^{1/2} \|\Sigma^*\|_{L^\infty(0, T; H^2(\Omega_s))}. \quad (3.31)$$

As explained in Section 3.3, the fixed-point procedure will be done on the fluid velocity and pressure, in a neighborhood of the initial fluid state (w_f^0, q_f^0) . That is why we introduced the ball $\mathcal{B}_{\mathcal{M}_1}^F$, defined in (3.12), for which we recall the definition:

$$\mathcal{B}_{\mathcal{M}_1}^F = \{(\omega, \pi) \in L^2(0, T; H^3(\Omega_f)) \cap H_{\Gamma_f}^1(\Omega_f) \times L^2(0, T; H^2(\Omega_f)); \\ \|\omega - w_f^0\|_{L^2(0, T; H^3(\Omega_f))} + \|\pi - q_f^0\|_{L^2([0, T]; H^2(\Omega_f))} \leq \mathcal{M}_1\}.$$

Remark 3.8. From (3.31), we deduce that a given couple (ω, π) in $\mathcal{B}_{\mathcal{M}_1}^F$ can be estimated with respect to \mathcal{M}_1 and the norm of Σ^* :

$$\|\omega\|_{L^2(0, T; H^3(\Omega_f))} + \|\pi\|_{L^2(0, T; H^2(\Omega_f))} \leq \mathcal{M}_1 + C_f T^{1/2} \|\Sigma^*\|_{L^\infty(0, T; H^2(\Omega_s))}. \quad (3.32)$$

The remaining of the proof is divided in three steps. First, we show that the mapping \mathcal{S} is well-defined from $\mathcal{B}_{\mathcal{M}_1}^F$ into itself under condition (3.16). Then, we prove that \mathcal{S} is a contraction mapping if the data satisfy condition (3.17). Finally, we conclude using Banach's fixed point theorem.

Step 1. Let us show that the mapping \mathcal{S} is well-defined from $\mathcal{B}_{\mathcal{M}_1}^F$ into itself under conditions (3.16). We consider a couple (ω, π) in $\mathcal{B}_{\mathcal{M}_1}^F$. We construct, for all $t \in [0, T]$,

$$\delta(t) = \int_0^t \gamma_\Gamma(\omega(s)) ds.$$

According to Lemma 3.1, δ belongs to $H^1(0, T; H^{5/2}(\Gamma))$, with the following estimate,

$$\|\delta\|_{L^\infty(0, T; H^{5/2}(\Gamma))} \leq C_1 T^{1/2} \|\omega\|_{L^2(0, T; H^3(\Omega_f))}, \quad (3.33)$$

where $C_1 = C(\Omega_f)$.

Now, we consider the elasticity problem (3.19) associated to δ , that writes: find d_s such that, for almost every $t \in (0, T)$,

$$\begin{cases} -\operatorname{div}(\Pi_s(d_s(t), t)) = f_s(t) & \text{in } \Omega_s, \\ d_s(t) = \delta(t) & \text{on } \Gamma, \\ d_s(t) = 0 & \text{on } \Gamma_s. \end{cases}$$

Conditions (3.13) and (3.14) guarantee that f_s , Σ^* and δ satisfy conditions (3.22) and (3.23) for almost every t in $(0, T)$:

$$\|f_s(t) - \operatorname{div}(\Sigma^*(t))\|_{H^1(\Omega_s)} + R_0 \|\Sigma^*(t)\|_{H^2(\Omega_s)} + \|\delta(t)\|_{H^{5/2}(\Gamma)} \leq R_1, \\ C_s^1 \|\Sigma^*(t)\|_{H^2(\Omega_s)} < 1,$$

where R_0 , R_1 and C_s^1 have been introduced in Lemma 3.4. Then, for almost every t in $(0, T)$, Lemma 3.4 ensures the existence of a unique solution d_s in $\mathcal{B}_{R_0}^S$ of problem (3.19). Moreover, it can be estimated with respect to the data:

$$\|d_s(t)\|_{H^3(\Omega_s)} \leq C_s^2 \left(\|f_s(t) - \operatorname{div}(\Sigma^*(t))\|_{H^1(\Omega_s)} + R_0 \|\Sigma^*(t)\|_{H^2(\Omega_s)} + \|\delta(t)\|_{H^{5/2}(\Gamma)} \right),$$

where C_s^2 has been introduced in Lemma 3.4. It follows, using (3.33) and (3.32), that

$$\|d_s\|_{L^\infty(0, T; H^3(\Omega_s))} \leq C_s^2 \left(\|f_s - \operatorname{div}(\Sigma^*)\|_{L^\infty(0, T; H^1(\Omega_s))} \right. \\ \left. + R_0 \|\Sigma^*\|_{L^\infty(0, T; H^2(\Omega_s))} \right. \\ \left. + C_1 T^{1/2} \|\omega\|_{L^2(0, T; H^3(\Omega_f))} \right), \\ \|d_s\|_{L^\infty(0, T; H^3(\Omega_s))} \leq C_s^2 \left(\|f_s - \operatorname{div}(\Sigma^*)\|_{L^\infty(0, T; H^1(\Omega_s))} \right. \\ \left. + (R_0 + C_1 C_f T) \|\Sigma^*\|_{L^\infty(0, T; H^2(\Omega_s))} \right. \\ \left. + C_1 T^{1/2} \mathcal{M}_1 \right). \quad (3.34)$$

The next step is the study of the fluid problem (3.20), that we recall:

$$\left\{ \begin{array}{ll} -\mu_f \Delta w_f(t) + \nabla q_f(t) & = -\mu_f \operatorname{div}(((I - F(d_s(t)))\nabla)\omega(t)) \\ & \quad + ((I - G(d_s(t)))\nabla)\pi(t) & \text{in } \Omega_f, \\ \operatorname{div}(w_f(t)) & = -\operatorname{div}((I - G(d_s(t)))^t)\omega(t) & \text{in } \Omega_f, \\ w_f(t) & = 0 & \text{on } \Gamma_f, \\ \sigma_f(w_f(t), q_f(t))n_f & = \Pi_s(d_s(t), t)n_f \\ & \quad + \mu_f(((I - F(d_s(t)))\nabla)\omega(t))n_f \\ & \quad - (\pi(t)(I - G(d_s(t))))n_f & \text{on } \Gamma. \end{array} \right.$$

Problem (3.20) is well-defined if $d_s(t)$ belongs to the ball $\mathcal{B}_{\mathcal{M}_0}^S$ (defined by (3.10)) for almost every t . Indeed, the matrix $F(d_s(t))$ is well-defined under this condition (see Lemma 3.3). From estimate (3.34), we see that condition (3.15) ensures that $d_s(t)$ belongs to $\mathcal{B}_{\mathcal{M}_0}^S$, hence that problem (3.20) is well-defined. Moreover, in order to apply Lemma 3.5, we must show that every term in the right-hand side of problem (3.20) is regular enough. The term

$$f = -\mu_f \operatorname{div}(((I - F(d_s(t)))\nabla)\omega(t)) + ((I - G(d_s(t)))\nabla)\pi(t),$$

belongs to $H^1(\Omega_f)$, because of the $H^2(\Omega_f)$ regularity of $F(d_s(t))$ and $G(d_s(t))$ and because $H^2(\Omega_f)$ is a Banach algebra and a multiplier space of $H^1(\Omega_f)$ (see Lemma 3.1). For the same reasons and because of the $H^2(\Omega_f)$ regularity of $\Sigma^*(t)$, the term

$$h = \Pi_s(d_s(t), t)n_f + \mu_f(((I - F(d_s(t)))\nabla)\omega(t))n_f - (\pi(t)(I - G(d_s(t))))n_f$$

belongs to $H^{3/2}(\Gamma)$. In addition, thanks to the fact that $G(d_s(t)) = \operatorname{cof}(\nabla\Phi(d_s(t)))$, the Piola identity (see [Ciarlet, 1988, Chapter I, p 39]) implies that the term

$$g = -\operatorname{div}((I - G(d_s(t)))^t)\omega(t) = (I - G(d_s(t)))^t : \nabla\omega(t)$$

belongs to $H^2(\Omega_f)$. Moreover, the domain Ω_f satisfies assumptions (\mathbf{H}_1) - (\mathbf{H}_4) . As a consequence, using Lemma 3.5, problem (3.20) admits a unique solution $(w_f(t), q_f(t))$ in $(H^3(\Omega_f) \cap H_{\Gamma_f}^1(\Omega_f)) \times H^2(\Omega_f)$ for almost every t in $(0, T)$. Therefore, due to the linearity of the Stokes equations (3.20), the couple $(w_f(t) - w_f^0, q_f(t) - q_f^0)$, is also solution of a Stokes problem. Using one more time Lemma 3.5, we have the following estimate for almost every t in $(0, T)$:

$$\begin{aligned} & \|w_f(t) - w_f^0\|_{H^3(\Omega_f)} + \|q_f(t) - q_f^0\|_{H^2(\Omega_f)} \\ & \leq C_f (\|\mu_f \operatorname{div}(((I - F(d_s(t)))\nabla)\omega(t))\|_{H^1(\Omega_f)} \\ & \quad + \|((I - G(d_s(t)))\nabla)\pi(t)\|_{H^1(\Omega_f)} \\ & \quad + \|\operatorname{div}((I - G(d_s(t)))^t)\omega(t)\|_{H^2(\Omega_f)} \\ & \quad + \|(\Pi_s(d_s(t), t) + \Sigma^*(0))n_f\|_{H^{3/2}(\Gamma)} \\ & \quad + \|\mu_f(((I - F(d_s(t)))\nabla)\omega(t))n_f\|_{H^{3/2}(\Gamma)} \\ & \quad + \|(\pi(t)(I - G(d_s(t))))n_f\|_{H^{3/2}(\Gamma)}). \end{aligned} \tag{3.35}$$

Now, we estimate each term appearing in the right-hand side of the previous inequality. For the first three terms of the right-hand side of estimate (3.35), using Lemma 3.1 and Corollary 3.1, since $d_s(t)$ belongs to $\mathcal{B}_{\mathcal{M}_0}^S$, we have

$$\begin{aligned} \|\mu_f \operatorname{div}(((I - F(d_s(t)))\nabla)\omega(t))\|_{H^1(\Omega_f)} & \leq \mu_f C(\Omega_f) \|I - F(d_s(t))\|_{H^2(\Omega_f)} \|\nabla\omega(t)\|_{H^2(\Omega_f)}, \\ & \leq \mu_f C(\Omega_f, \mathcal{M}_0) \|d_s(t)\|_{H^3(\Omega_s)} \|\omega(t)\|_{H^3(\Omega_f)}, \end{aligned}$$

$$\begin{aligned}
\|((I - G(d_s(t)))\nabla)\pi(t)\|_{H^1(\Omega_f)} &\leq C(\Omega_f)\|I - G(d_s(t))\|_{H^2(\Omega_f)}\|\nabla\pi(t)\|_{H^1(\Omega_f)}, \\
&\leq C(\Omega_f, \mathcal{M}_0)\|d_s(t)\|_{H^3(\Omega_s)}\|\pi(t)\|_{H^2(\Omega_f)}, \\
\|\operatorname{div}((I - G(d_s(t)))^t)\omega(t)\|_{H^2(\Omega_f)} &\leq \|(I - G(d_s(t)))^t : \nabla\omega(t)\|_{H^2(\Omega_f)}, \\
&\leq C(\Omega_f)\|I - G(d_s(t))\|_{H^2(\Omega_f)}\|\nabla\omega(t)\|_{H^2(\Omega_f)}, \\
&\leq C(\Omega_f, \mathcal{M}_0)\|d_s(t)\|_{H^3(\Omega_s)}\|\omega(t)\|_{H^3(\Omega_f)}.
\end{aligned}$$

For the fourth term of the right-hand side of estimate (3.35), we use the continuity of the trace operator from $H^2(\Omega_s)$ to $H^{3/2}(\Gamma)$, Lemma 3.1 and the facts that $d_s(t)$ belongs to $\mathcal{B}_{R_0}^S$ and that the elasticity operator A , defined in the proof of Lemma 3.4, is multilinear. We obtain:

$$\begin{aligned}
&\|(\Pi_s(d_s(t), t) + \Sigma^*(0))n_f\|_{H^{3/2}(\Gamma)} \\
&\leq C(\Omega_s)\|\Pi_s(d_s(t), t) + \Sigma^*(0)\|_{H^2(\Omega_s)}, \\
&\leq C(\Omega_s)\left(\|(I + \nabla d_s(t))\Sigma_s(d_s(t))\|_{H^2(\Omega_s)} + \|\nabla d_s(t)\Sigma^*(t)\|_{H^2(\Omega_s)}\right. \\
&\quad \left. + \|\Sigma^*(t) - \Sigma^*(0)\|_{H^2(\Omega_s)}\right), \\
&\leq C(\Omega_s, R_0)\|d_s(t)\|_{H^3(\Omega_s)} + C(\Omega_s)\|\nabla d_s(t)\|_{H^2(\Omega_s)}\|\Sigma^*(t)\|_{H^2(\Omega_s)} \\
&\quad + C(\Omega_s)\|\Sigma^*\|_{L^\infty(0, T; H^2(\Omega_s))}, \\
&\leq C(\Omega_s, R_0)\|d_s(t)\|_{H^3(\Omega_s)} + C(\Omega_s)\|\Sigma^*\|_{L^\infty(0, T; H^2(\Omega_s))}\|d_s(t)\|_{H^3(\Omega_s)} \\
&\quad + C(\Omega_s)\|\Sigma^*\|_{L^\infty(0, T; H^2(\Omega_s))},
\end{aligned}$$

Finally, for the fifth and sixth terms of the right-hand side of estimate (3.35), we use the continuity of the trace operator from $H^2(\Omega_f)$ to $H^{3/2}(\Gamma)$, Lemma 3.1 and Corollary 3.1 (since $d_s(t)$ belongs to $\mathcal{B}_{\mathcal{M}_0}^S$). It follows that

$$\begin{aligned}
\|\mu_f(((I - F(d_s(t)))\nabla)\omega(t))n_f\|_{H^{3/2}(\Gamma)} &\leq \mu_f C(\Omega_f)\|(I - F(d_s(t)))\nabla\omega(t)\|_{H^2(\Omega_f)}, \\
&\leq \mu_f C(\Omega_f)\|I - F(d_s(t))\|_{H^2(\Omega_f)}\|\nabla\omega(t)\|_{H^2(\Omega_f)}, \\
&\leq \mu_f C(\Omega_f, \mathcal{M}_0)\|d_s(t)\|_{H^3(\Omega_s)}\|\omega(t)\|_{H^3(\Omega_f)}, \\
\|(\pi(t)(I - G(d_s(t))))n_f\|_{H^{3/2}(\Gamma)} &\leq C(\Omega_f)\|\pi(t)(I - G(d_s(t)))\|_{H^2(\Omega_f)}, \\
&\leq C(\Omega_f)\|\pi(t)\|_{H^2(\Omega_f)}\|I - G(d_s(t))\|_{H^2(\Omega_f)}, \\
&\leq C(\Omega_f, \mathcal{M}_0)\|d_s(t)\|_{H^3(\Omega_s)}\|\pi(t)\|_{H^2(\Omega_f)}.
\end{aligned}$$

Replacing each term in (3.35), yields

$$\begin{aligned}
&\|w_f(t) - w_f^0\|_{H^3(\Omega_f)} + \|q_f(t) - q_f^0\|_{H^2(\Omega_f)} \\
&\leq C(\Omega_f, \mathcal{M}_0)\|d_s(t)\|_{H^3(\Omega_s)}\left(\|\omega(t)\|_{H^3(\Omega_f)} + \|\pi(t)\|_{H^2(\Omega_f)}\right) \\
&\quad + C(\Omega_s, R_0)\|d_s(t)\|_{H^3(\Omega_s)} + C(\Omega_s)\|\Sigma^*\|_{L^\infty(0, T; H^2(\Omega_s))}\|d_s(t)\|_{H^3(\Omega_s)} \\
&\quad + C(\Omega_s)\|\Sigma^*\|_{L^\infty(0, T; H^2(\Omega_s))}, \\
&\leq C\left(1 + \|\Sigma^*\|_{L^\infty(0, T; H^2(\Omega_s))} + \|\omega(t)\|_{H^3(\Omega_f)} + \|\pi(t)\|_{H^2(\Omega_f)}\right)\|d_s(t)\|_{H^3(\Omega_s)} \\
&\quad + C(\Omega_s)\|\Sigma^*\|_{L^\infty(0, T; H^2(\Omega_s))},
\end{aligned}$$

where $C = C(\Omega_f, \Omega_s, R_0, \mathcal{M}_0)$. Then, taking the L^2 -norm in time, leads to

$$\begin{aligned}
&\|w_f - w_f^0\|_{L^2(0, T; H^3(\Omega_f))} + \|q_f - q_f^0\|_{L^2(0, T; H^2(\Omega_f))} \\
&\leq C\left(T^{1/2}(1 + \|\Sigma^*\|_{L^\infty(0, T; H^2(\Omega_s))})\right. \\
&\quad \left. + \|\omega(t)\|_{L^2(0, T; H^3(\Omega_f))} + \|\pi(t)\|_{L^2(0, T; H^2(\Omega_f))}\right)\|d_s(t)\|_{L^\infty(0, T; H^3(\Omega_s))} \\
&\quad + C(\Omega_s)T^{1/2}\|\Sigma^*\|_{L^\infty(0, T; H^2(\Omega_s))},
\end{aligned}$$

Moreover, using estimates (3.34) and (3.32), we obtain

$$\begin{aligned}
& \|w_f - w_f^0\|_{L^2(0,T;H^3(\Omega_f))} + \|q_f - q_f^0\|_{L^2(0,T;H^2(\Omega_f))} \\
& \leq C \left(T^{1/2} \left(1 + (1 + C_f) \|\Sigma^*\|_{L^\infty(0,T;H^2(\Omega_s))} \right) + \mathcal{M}_1 \right) \\
& \quad \times C_s^2 \left(\|f_s - \operatorname{div}(\Sigma^*)\|_{L^\infty(0,T;H^1(\Omega_s))} + (R_0 + C_1 C_f T) \|\Sigma^*\|_{L^\infty(0,T;H^2(\Omega_s))} \right. \\
& \quad \left. + C_1 T^{1/2} \mathcal{M}_1 \right) \\
& \quad + C(\Omega_s) T^{1/2} \|\Sigma^*\|_{L^\infty(0,T;H^2(\Omega_s))}, \\
& \leq C_2 \left(T^{1/2} \left(1 + \|\Sigma^*\|_{L^\infty(0,T;H^2(\Omega_s))} \right) + \mathcal{M}_1 \right) \\
& \quad \times \left(\|f_s - \operatorname{div}(\Sigma^*)\|_{L^\infty(0,T;H^1(\Omega_s))} + (1 + T) \|\Sigma^*\|_{L^\infty(0,T;H^2(\Omega_s))} + T^{1/2} \mathcal{M}_1 \right) \\
& \quad + C_2 T^{1/2} \|\Sigma^*\|_{L^\infty(0,T;H^2(\Omega_s))},
\end{aligned}$$

where $C_2 = C(\Omega_f, \Omega_s, R_0, \mathcal{M}_0)$. Therefore, condition (3.16) guarantees that the solution of the fluid problem (w_f, q_f) belongs to $\mathcal{B}_{\mathcal{M}_1}^F$. Hence, the mapping \mathcal{S} is well-defined from $\mathcal{B}_{\mathcal{M}_1}^F$ into $\mathcal{B}_{\mathcal{M}_1}^F$ if the data f_s and Σ^* , the time T and the constant \mathcal{M}_1 satisfy condition (3.16).

Step 2. Now, let us show that \mathcal{S} is a contraction mapping. Let (ω_1, π_1) and (ω_2, π_2) be given in $\mathcal{B}_{\mathcal{M}_1}^F$. We built δ_1 and δ_2 such that, for all $t \in [0, T]$,

$$\begin{aligned}
\delta_1(t) &= \int_0^t \gamma_\Gamma(\omega_1(s)) ds, \\
\delta_2(t) &= \int_0^t \gamma_\Gamma(\omega_2(s)) ds.
\end{aligned}$$

Applying Lemma 3.1 to the difference $\delta_1 - \delta_2$, it comes

$$\|\delta_1 - \delta_2\|_{L^\infty(0,T;H^{5/2}(\Gamma))} \leq C_1 T^{1/2} \|\omega_1 - \omega_2\|_{L^2(0,T;H^3(\Omega_f))}, \quad (3.36)$$

where C_1 has been introduced in (3.33) and depends on the domain Ω_f .

As before, conditions (3.13) and (3.14) ensure that the data $(f_s, \Sigma^*, \delta_1)$ and $(f_s, \Sigma^*, \delta_2)$ are sufficiently small to apply Lemma 3.4. Thus, there exists a unique solution $d_{s,1}(t)$ to problem (3.19) associated to the data $(f_s, \Sigma^*, \delta_1)$ and a unique solution $d_{s,2}(t)$ to problem (3.19) associated to the data $(f_s, \Sigma^*, \delta_2)$. Moreover, according to Corollary 3.2 and using (3.36), we also have the estimate:

$$\|d_{s,1} - d_{s,2}\|_{L^\infty([0,T],H^3(\Omega_s))} \leq \frac{C_s^2 C_1 T^{1/2}}{1 - C_s^1 \|\Sigma^*\|_{L^\infty(0,T;H^2(\Omega_s))}} \|\omega_1 - \omega_2\|_{L^2(0,T;H^3(\Omega_f))}. \quad (3.37)$$

Furthermore, condition (3.15) ensures that $d_{s,1}(t)$ and $d_{s,2}(t)$ belong to $\mathcal{B}_{\mathcal{M}_0}^S$ for almost every t in $(0, T)$ and, as before, the two fluid problems of type (3.20), associated with the data $(d_{s,1}, \omega_1, \pi_1)$ and $(d_{s,2}, \omega_2, \pi_2)$ are well-defined for almost every t in $(0, T)$. According to Lemma 3.5, it follows that they both admit a unique solution in the product space that is $(H^3(\Omega_f) \cap H_{\Gamma_f}^1(\Omega_f)) \times H^2(\Omega_f)$, respectively denoted by the couples $(w_{f,1}(t), q_{f,1}(t))$ and $(w_{f,2}(t), q_{f,2}(t))$. By linearity of the Stokes problem (3.20) the difference of these two solutions, i.e. the couple $(w_{f,1}(t) - w_{f,2}(t), q_{f,1}(t) - q_{f,2}(t))$, is also solution of a Stokes problem, which writes

$$\begin{aligned}
-\mu_f \Delta(w_{f,1}(t) - w_{f,2}(t)) + \nabla(q_{f,1}(t) - q_{f,2}(t)) &= \bar{f}(t) & \text{in } \Omega_f, \\
\operatorname{div}(w_{f,1}(t) - w_{f,2}(t)) &= \bar{g}(t) & \text{in } \Omega_f, \\
w_{f,1}(t) - w_{f,2}(t) &= 0 & \text{on } \Gamma_f, \\
\sigma_f(w_{f,1}(t) - w_{f,2}(t), q_{f,1}(t) - q_{f,2}(t)) \cdot n_f &= \bar{h}(t) & \text{on } \Gamma,
\end{aligned} \quad (3.38)$$

where, \bar{f} , \bar{g} and \bar{h} are defined, for almost all t in $(0, T)$ by

$$\begin{aligned}\bar{f}(t) &= -\mu_f \operatorname{div}(((I - F(d_{s,1}(t)))\nabla)(\omega_1(t) - \omega_2(t))) \\ &\quad + \mu_f \operatorname{div}(((F(d_{s,1}(t)) - F(d_{s,2}(t)))\nabla)\omega_2(t)) \\ &\quad + ((I - G(d_{s,1}(t)))\nabla)(\pi_1(t) - \pi_2(t)) \\ &\quad - ((G(d_{s,1}(t)) - G(d_{s,2}(t)))\nabla)\pi_2(t),\end{aligned}$$

$$\begin{aligned}\bar{g}(t) &= -\operatorname{div}((I - G(d_{s,1}(t)))^t(\omega_1(t) - \omega_2(t))) \\ &\quad + \operatorname{div}((G(d_{s,1}(t)))^t - G(d_{s,2}(t)))^t\omega_2(t)),\end{aligned}$$

$$\begin{aligned}\bar{h}(t) &= (\Pi_s(d_{s,1}(t)) - \Pi_s(d_{s,2}(t))) \cdot n_f \\ &\quad + \mu_f ((I - F(d_{s,1}(t)))\nabla)(\omega_1(t) - \omega_2(t)) \cdot n_f \\ &\quad - \mu_f ((F(d_{s,1}(t)) - F(d_{s,2}(t)))\nabla)\omega_2(t) \cdot n_f \\ &\quad - ((\pi_1(t) - \pi_2(t))(I - G(d_{s,1}(t)))) \cdot n_f \\ &\quad + (\pi_2(t)(G(d_{s,1}(t)) - G(d_{s,2}(t)))) \cdot n_f.\end{aligned}$$

Once again, using the H^2 -regularity of the matrices $F(d_{s,1}(t))$, $F(d_{s,2}(t))$, $G(d_{s,1}(t))$ and $G(d_{s,2}(t))$ and the fact that $H^2(\Omega_f)$ is a Banach algebra and a multiplier space of $H^1(\Omega_f)$, we can show that $\bar{f}(t)$ belongs to $H^1(\Omega_f)$, $\bar{g}(t)$ belongs to $H^2(\Omega_f)$ and $\bar{h}(t)$ belongs to $H^{5/2}(\Gamma)$. Thus, applying Lemma 3.5, the solution of problem (3.38) satisfies the estimate

$$\begin{aligned}\|w_{f,1}(t) - w_{f,2}(t)\|_{H^3(\Omega_f)} + \|q_{f,1}(t) - q_{f,2}(t)\|_{H^2(\Omega_f)} \\ \leq C_f (\|\bar{f}(t)\|_{H^1(\Omega_f)} + \|\bar{g}(t)\|_{H^2(\Omega_f)} + \|\bar{h}(t)\|_{H^{3/2}(\Gamma)}).\end{aligned}\tag{3.39}$$

Let us estimate each term in the right-hand side of (3.39). Using Lemma 3.1 and Corollary 3.1 the first two terms become

$$\begin{aligned}\|\bar{f}(t)\|_{H^1(\Omega_f)} &\leq \\ C(\Omega_f, \mathcal{M}_0) &\left(\|d_{s,1}(t)\|_{H^3(\Omega_s)} \left(\|\omega_1(t) - \omega_2(t)\|_{H^3(\Omega_f)} + \|\pi_1(t) - \pi_2(t)\|_{H^2(\Omega_f)} \right) \right. \\ &\quad \left. + \|d_{s,1}(t) - d_{s,2}(t)\|_{H^3(\Omega_s)} \left(\|\omega_2(t)\|_{H^3(\Omega_f)} + \|\pi_2(t)\|_{H^2(\Omega_f)} \right) \right),\end{aligned}$$

$$\begin{aligned}\|\bar{g}(t)\|_{H^2(\Omega_f)} &\leq C(\Omega_f, \mathcal{M}_0) \left(\|d_{s,1}(t)\|_{H^3(\Omega_s)} \|\omega_1(t) - \omega_2(t)\|_{H^3(\Omega_f)} \right. \\ &\quad \left. + \|d_{s,1}(t) - d_{s,2}(t)\|_{H^3(\Omega_s)} \|\omega_2(t)\|_{H^3(\Omega_f)} \right).\end{aligned}$$

Then, using the continuity of the trace operator from $H^2(\Omega_f)$ to $H^{3/2}(\Gamma)$ and from $H^2(\Omega_s)$ into $H^{3/2}(\Gamma)$, Lemma 3.1, Corollary 3.1 and the facts that $d_{s,1}(t)$ and $d_{s,2}(t)$ belong to $\mathcal{B}_{R_0}^S$ and that the elasticity operator A defined in the proof of Lemma 3.4 is multilinear, the third term writes

$$\begin{aligned}\|\bar{h}(t)\|_{H^{3/2}(\Gamma)} &\leq C(\Omega_s, R_0) (1 + \|\Sigma^*\|_{L^\infty(0,T;H^2(\Omega_s))}) \|d_{s,1}(t) - d_{s,2}(t)\|_{H^3(\Omega_s)} \\ &\quad + C(\Omega_f, \mathcal{M}_0) \left(\left(\|\omega_1(t) - \omega_2(t)\|_{H^3(\Omega_f)} + \|\pi_1(t) - \pi_2(t)\|_{H^2(\Omega_f)} \right) \|d_{s,1}(t)\|_{H^3(\Omega_s)} \right. \\ &\quad \left. + \left(\|\omega_2(t)\|_{H^3(\Omega_f)} + \|\pi_2(t)\|_{H^2(\Omega_f)} \right) \|d_{s,1}(t) - d_{s,2}(t)\|_{H^3(\Omega_s)} \right).\end{aligned}$$

Replacing them in inequality (3.39), yields

$$\begin{aligned}
& \|w_{f,1}(t) - w_{f,2}(t)\|_{H^3(\Omega_f)} + \|q_{f,1}(t) - q_{f,2}(t)\|_{H^2(\Omega_f)} \\
& \leq C(\Omega_s, R_0) \left(1 + \|\Sigma^*\|_{L^\infty(0,T;H^2(\Omega_s))}\right) \|d_{s,1}(t) - d_{s,2}(t)\|_{H^3(\Omega_s)} \\
& \quad + C(\Omega_f, \mathcal{M}_0) \left(\left(\|\omega_2(t)\|_{H^3(\Omega_f)} + \|\pi_2(t)\|_{H^2(\Omega_f)}\right) \|d_{s,1}(t) - d_{s,2}(t)\|_{H^3(\Omega_s)} \right. \\
& \quad \left. + \left(\|\omega_1(t) - \omega_2(t)\|_{H^3(\Omega_f)} + \|\pi_1(t) - \pi_2(t)\|_{H^2(\Omega_f)}\right) \|d_{s,1}(t)\|_{H^3(\Omega_s)} \right), \\
& \leq C \left(\left(1 + \|\Sigma^*\|_{L^\infty(0,T;H^2(\Omega_s))} + \|\omega_2(t)\|_{H^3(\Omega_f)} + \|\pi_2(t)\|_{H^2(\Omega_f)}\right) \|d_{s,1}(t) - d_{s,2}(t)\|_{H^3(\Omega_s)} \right. \\
& \quad \left. + \left(\|\omega_1(t) - \omega_2(t)\|_{H^3(\Omega_f)} + \|\pi_1(t) - \pi_2(t)\|_{H^2(\Omega_f)}\right) \|d_{s,1}(t)\|_{H^3(\Omega_s)} \right),
\end{aligned}$$

where $C = C(\Omega_f, \Omega_s, \mathcal{M}_0, R_0)$. Then, taking the L^2 -norm in time and using (3.32), it follows that

$$\begin{aligned}
& \|w_{f,1} - w_{f,2}\|_{L^2(0,T;H^3(\Omega_f))} + \|q_{f,1} - q_{f,2}\|_{L^2(0,T;H^2(\Omega_f))} \\
& \leq C \left((T^{1/2} (1 + (1 + C_f)\|\Sigma^*\|_{L^\infty(0,T;H^2(\Omega_s))}) + \mathcal{M}_1) \|d_{s,1} - d_{s,2}\|_{L^\infty(0,T;H^3(\Omega_s))} \right. \\
& \quad \left. + \left(\|\omega_1 - \omega_2\|_{L^2(0,T;H^3(\Omega_f))} + \|\pi_1 - \pi_2\|_{L^2(0,T;H^2(\Omega_f))}\right) \|d_{s,1}\|_{L^\infty(0,T;H^3(\Omega_s))} \right),
\end{aligned}$$

Finally, with the use of (3.34) and (3.37), we obtain

$$\begin{aligned}
& \|w_{f,1} - w_{f,2}\|_{L^2(0,T;H^3(\Omega_f))} + \|q_{f,1} - q_{f,2}\|_{L^2(0,T;H^2(\Omega_f))} \\
& \leq C \left((T^{1/2} (1 + (1 + C_f)\|\Sigma^*\|_{L^\infty(0,T;H^2(\Omega_s))}) + \mathcal{M}_1) \right. \\
& \quad \times \frac{C_s^2 C_1 T^{1/2}}{1 - C_s^1 \|\Sigma^*\|_{L^\infty(0,T;H^2(\Omega_s))}} \|\omega_1 - \omega_2\|_{L^2(0,T;H^3(\Omega_f))} \\
& \quad \left. + \left(\|\omega_1 - \omega_2\|_{L^2(0,T;H^3(\Omega_f))} + \|\pi_1 - \pi_2\|_{L^2(0,T;H^2(\Omega_f))}\right) \right. \\
& \quad \left. \times C_s^2 \left(\|f_s - \operatorname{div}(\Sigma^*)\|_{L^\infty(0,T;H^1(\Omega_s))} + (R_0 + C_1 C_f T)\|\Sigma^*\|_{L^\infty(0,T;H^2(\Omega_s))} + C_1 T^{1/2} \mathcal{M}_1\right) \right), \\
& \leq C_3 \left(\frac{T (1 + \|\Sigma^*\|_{L^\infty(0,T;H^2(\Omega_s))}) + T^{1/2} \mathcal{M}_1}{1 - C_s^1 \|\Sigma^*\|_{L^\infty(0,T;H^2(\Omega_s))}} \right. \\
& \quad \left. + \|f_s - \operatorname{div}(\Sigma^*)\|_{L^\infty(0,T;H^1(\Omega_s))} + (1 + T)\|\Sigma^*\|_{L^\infty(0,T;H^2(\Omega_s))} + T^{1/2} \mathcal{M}_1 \right) \\
& \quad \times \left(\|\omega_1 - \omega_2\|_{L^2(0,T;H^3(\Omega_f))} + \|\pi_1 - \pi_2\|_{L^2(0,T;H^2(\Omega_f))} \right)
\end{aligned}$$

where $C_3 = C(\Omega_f, \Omega_s, R_0, \mathcal{M}_0)$. Therefore, we see that condition (3.17) guarantees that the mapping \mathcal{S} is a contraction.

Step 3. To conclude, we have proved that, *i*) under conditions (3.13), (3.14) and (3.15), the mapping \mathcal{S} is well-defined from $\mathcal{B}_{\mathcal{M}_1}^F$ into $L^2(0, T; H^3(\Omega_f)) \times L^2(0, T; H^2(\Omega_f))$, *ii*) under condition (3.16), the image of $\mathcal{B}_{\mathcal{M}_1}^F$ by \mathcal{S} is included in $\mathcal{B}_{\mathcal{M}_1}^F$ and *iii*) under condition (3.17), \mathcal{S} is a contraction mapping. Moreover, $\mathcal{B}_{\mathcal{M}_1}^F$ is a bounded closed subset of a Banach space. Consequently, we apply Banach's fixed point theorem and conclude that the mapping \mathcal{S} has a unique fixed point in $\mathcal{B}_{\mathcal{M}_1}^F$. Furthermore, this also proves the existence and the uniqueness, for small enough forces and a small enough time, of a regular solution to the fluid-structure interaction system (3.1), (3.2), (3.4), (3.6) and (3.7). \square

Remark 3.9. Note that here we have both smallness conditions on the time and on the amplitude of the applied forces. It is due to the quasi-static nature of the problem we consider with elliptic problems coupled through a kinematic condition at the interface.

3.7 More general conditions on the data

In this section, let us relax the assumption on the initial configuration of the system, i.e. that $f_s(0) = \text{div}(\Sigma^*(0))$. This means that the structure is not at rest initially, even if it starts from its reference configuration. Then, we show that the result stated in Theorem 3.1 is still true, i.e. that, under some smallness conditions on the data, the time T and the constant \mathcal{M}_1 , there exists a unique solution (w_f, q_f, d_s) to the coupled fluid-structure system (3.1), (3.2), (3.4), (3.6) and (3.7).

Theorem 3.2. *Let Ω_f , Ω_s , Γ_f , Γ_s and Γ be defined by (\mathbf{H}_1) - (\mathbf{H}_4) and let $T > 0$ and $0 < \varepsilon < T$. Consider f_s in $L^\infty(0, T; H^1(\Omega_s))$ and Σ^* in $L^\infty(0, T; H^2(\Omega_s))$, the data of the problem. Let $\mathcal{M}_1 > 0$ and consider the ball $\mathcal{B}_{\mathcal{M}_1}^\varepsilon$ defined by*

$$\mathcal{B}_{\mathcal{M}_1}^{F, \varepsilon} = \left\{ (\omega, \pi) \in L^2(0, T - \varepsilon; H^3(\Omega_f) \cap H_{\Gamma_f}^1(\Omega_f)) \times L^2(0, T - \varepsilon; H^2(\Omega_f)) \ ; \right. \\ \left. \|\omega - w_f^0\|_{L^2(0, T - \varepsilon; H^3(\Omega_f))} + \|\pi - q_f^0\|_{L^2(0, T - \varepsilon; H^2(\Omega_f))} \leq \mathcal{M}_1 \right\},$$

where (w_f^0, q_f^0) is the initial state of the fluid, solution of (3.11).

There exists positive constants R_0 , R_1 , \mathcal{M}_0 , C_s^1 , C_s^2 , C_f , C_1 , C_2 and C_3 , which only depend on the domains Ω_f and Ω_s , the viscosity of the fluid μ_f and the elasticity parameters μ_s and λ_s of the structure such that, if the data f_s and Σ^* , the time T and the constant \mathcal{M}_1 satisfy conditions (3.13), (3.14), (3.15), (3.16) and (3.17), then, there exists a unique solution (w_f, q_f, d_s) of (3.1), (3.2), (3.4), (3.6) and (3.7), with (w_f, q_f) in $\mathcal{B}_{\mathcal{M}_1}^{F, \varepsilon}$ and d_s in $L^\infty(0, T - \varepsilon; \mathcal{B}_{\mathcal{M}_0} \cap H_{\Gamma_s}^1(\Omega_s))$.

The idea of the proof of Theorem 3.2 is inspired by the *incremental method*, usually used for the numerical resolution of elasticity problems involving large deformations. In [Ciarlet, 1988, sec. 6.10], Ciarlet describes it as a method which consists in “letting the forces vary by small increments from zero to the given ones and to compute corresponding approximate solutions by successive linearization”. Actually, in the context of numerical simulation, it enables to compute the displacement of a structure whose equilibrium position is “far” from its reference position, and which could not be obtained directly. Here, this trick is used to apply Theorem 3.1 on a slightly different problem whose data, f_s^ε and Σ_ε^* , satisfy the condition $f_s^\varepsilon(0) = \text{div}(\Sigma_\varepsilon^*(0))$. Then, we recover the solution associated with the true data, f_s and Σ^* .

Proof. Let us introduce a body force f_s^ε and an internal activity Σ_ε^* , defined by

$$f_s^\varepsilon(t) = \begin{cases} \frac{1}{\varepsilon} f_s(0)t & \text{if } t \leq \varepsilon, \\ f_s(t - \varepsilon) & \text{for almost every } t \text{ in } (\varepsilon, T), \end{cases} \\ \Sigma_\varepsilon^*(t) = \begin{cases} \frac{1}{\varepsilon} \Sigma^*(0)t & \text{if } t \leq \varepsilon, \\ \Sigma^*(t - \varepsilon) & \text{for almost every } t \text{ in } (\varepsilon, T). \end{cases}$$

With these definitions, f_s^ε belongs to $L^\infty(0, T; H^1(\Omega_s))$, Σ_ε^* belongs to $L^\infty(0, T; H^2(\Omega_s))$ and the condition $f_s^\varepsilon(0) = \text{div}(\Sigma_\varepsilon^*(0)) = 0$ is satisfied. Moreover,

$$\|f_s^\varepsilon - \text{div}(\Sigma_\varepsilon^*)\|_{L^\infty(0, T; H^1(\Omega_s))} \leq \|f_s - \text{div}(\Sigma^*)\|_{L^\infty(0, T; H^1(\Omega_s))}, \\ \|\Sigma_\varepsilon^*\|_{L^\infty(0, T; H^2(\Omega_s))} \leq \|\Sigma^*\|_{L^\infty(0, T; H^2(\Omega_s))},$$

then the data f_s^ε and Σ_ε^* , the time T and the constant \mathcal{M}_1 also satisfy the conditions (3.13), (3.14), (3.16) and (3.17) of Theorem 3.1. Thus, we can apply Theorem 3.1 to the

fluid-structure system (3.1), (3.2), (3.4), (3.6) and (3.7) associated to the data f_s^ε and Σ_ε^* . Consequently, there exists a unique solution $(w_f^\varepsilon, q_f^\varepsilon, d_s^\varepsilon)$, with $(w_f^\varepsilon, q_f^\varepsilon)$ in $\mathcal{B}_{\mathcal{M}_1}$ and d_s^ε in $L^\infty(0, T; \mathcal{B}_{\mathcal{M}_0} \cap H_{\Gamma_s}^1(\Omega_s))$. Furthermore, if we choose $\varepsilon < T$, the triplet (w_f, q_f, d_s) defined almost everywhere in $(0, T - \varepsilon)$ by,

$$\begin{aligned} w_f(t) &= w_f^\varepsilon(t + \varepsilon), \\ q_f(t) &= q_f^\varepsilon(t + \varepsilon), \\ d_s(t) &= d_s^\varepsilon(t + \varepsilon), \end{aligned}$$

is solution to the fluid-structure system (3.1), (3.2), (3.4), (3.6) and (3.7), associated to the data f_s and Σ^* , but only almost everywhere in $(0, T - \varepsilon)$:

$$(w_f, q_f) \in \mathcal{B}_{\mathcal{M}_1}^\varepsilon \quad \text{and} \quad d_s \in L^\infty(0, T - \varepsilon; \mathcal{B}_{\mathcal{M}_0} \cap H_{\Gamma_s}^1(\Omega_s)).$$

□

Chapter 4

A smooth extension method for transmission problems

4.1 Introduction

The numerical simulation of transmission problems (also known as interface problems or problems with discontinuous coefficients) is of major importance for the mathematical study of many physical and living systems. As examples, we can mention the study of composite materials (see [Oevermann and Klein, 2006]), the flow of multiphase fluids or the swimming of bacteria in a viscous fluid (see [Decoene et al., 2018]). There exists a wide variety of numerical methods for this type of problems, which can be categorized in two classes: fitted and unfitted mesh techniques.

Fitted mesh methods are successful when dealing with stationary problems or problems with domains undergoing moderate displacements. In the latter, the mesh is moved using a regular extension of the displacement of the interface, which is only possible in practice if this displacement is small enough. For example, in the case of fluid-structure interaction problems it can be done using an arbitrary Lagrangian-Eulerian (ALE) description of the fluid (see [dos Santos, 2007]). The main advantage of fitted mesh techniques is their optimal convergence rate in space. However, when transmission problems involve large deformations, a much more appropriate method is the use of unfitted meshes, in which the interface deforms independently of a background fixed mesh.

Unfitted mesh techniques use a non-conformal mesh, i.e. a mesh that does not fit the interface. Among these methods we can reference the immersed boundary method (see [Peskin, 2002]), fictitious domain methods with Lagrange multipliers (see [Baaijens, 2001], [Yu, 2005]) or penalization terms (see [Janela et al., 2005]), the extended-finite element method (XFEM, see [Moës and Belytschko, 2002], [Fournié and Lozinski, 2014] and [Fournié and Lozinski, 2017]), the Nitsche-XFEM method (see [Alauzet et al., 2016]) and the fat boundary method (FBM, see [Bertoluzza et al., 2011]). The first two techniques do not converge with optimal orders in space (see [Girault and Glowinski, 1995], [Girault et al., 2001], [Tomas, 1997], [Maury, 2009]), because of the discrete treatment of transmission conditions. The XFEM and the Nitsche-XFEM overcome this issue, but they come with a cost: the XFEM is known to lack robustness; the Nitsche-XFEM method circumvents these difficulties but, still, all cut-FEM based methods require a specific evaluation of the interface intersections, which can be difficult, especially in three space dimensions (see [Boilevin-Kayl et al., 2019]). An interesting fictitious domain method is also presented in [Lozinski, 2016], where the optimal rates of convergence are obtained for the Poisson problem with Dirichlet boundary conditions on a mesh that does not fit the boundary of the

domain. The originality of this work consists in avoiding integration over the elements cut by the boundary of the problem domain, while preserving the optimal rates of convergence. The FBM is a fictitious domain method designed to recover the optimal convergence at any order. It is well suited for elliptic stationary problems or problems involving rigid domains, but it is not straightforward to adapt it to deformable moving materials. An other class of unfitted mesh techniques is the control based approach presented in [Atamian et al., 1991], initially developed to solve boundary value problems in complex geometries and which is based on an optimal control formulation. In [Atamian et al., 1991], the authors consider the Poisson problem for the Laplace operator with an included obstacle on which Dirichlet and Neumann boundary conditions are applied. The idea of the method is to extend the problem inside the obstacle and use the right-hand side of the equations as a control to impose the boundary conditions on the frontier of the obstacle. This method has also been used to treat boundary conditions in a fictitious domain approach for the Helmholtz equations in [Atamian et al., 1991], [Atamian and Joly, 1993] and [Perret, 1998]. In [Fabrèges, 2012] and [Fabrèges et al., 2013], the authors present the *smooth extension method*, an extension of the control based method to the resolution of fluid-structure interaction problems involving rigid particles and a viscous fluid. This method has the advantages to recover optimal convergence in space and to be rather simple to implement (it does not necessitate any mesh adaptation or local enrichment of the function spaces).

Here, we aim to generalize this smooth extension method to transmission problems, i.e. to a class of problems where the behavior of the obstacle is also described by partial differential equations with transmission conditions on the interface. Then, the smooth extension method presented in this chapter is a finite element method based on a control approach to solve elliptic transmission problems with unfitted meshes and which recovers the optimal convergence rates. This method is designed to be suitable for transmission problems involving several small materials included in a bigger material, such bubbles in a fluid, rigid and deformable particles in a fluid or problems of conductivity and elasticity of non-homogeneous materials. Because it is an unfitted mesh technique, it enables to precisely mesh the small materials without necessarily considering a thin mesh on the whole domain and thus, speed up the numerical resolutions of such problems. It also enables to use a Cartesian mesh on the bigger domain, which permits the utilization of fast solvers (e.g. FFT solvers).

The remaining of the chapter is organized as follows. In Section 4.2, we state the smooth extension method for the Laplace transmission problem. Section 4.3 is devoted to the presentation of numerical experiments using the methodology described in Section 4.2. In Section 3.7, we extend the method to other transmission problems: the Stokes transmission problem and a fluid-structure interaction problem involving a linear elastic structure and a viscous fluid.

4.2 Presentation of the method

The smooth extension method presented here is devoted to the numerical simulation of transmission problems. It is a fictitious domain method which enables to recover the optimal order of convergence in space by smoothly extending a part of the exact solution to the whole domain. In this section we focus on a toy model, the Laplace transmission problem, in order to properly explain the main steps of the method. This section is divided in four parts. In Subsection 4.2.1, we state the smooth extension formulation of the problem as a control problem and explain how to recover the exact solution from it. Then, in Subsection 4.2.2 we rewrite this control problem as a minimization problem and prove the

equivalence of the two formulations. In Subsection 4.2.3 we discuss the advantage of this method compared to the classical finite element method. Finally, in Subsection 4.2.4, we extend the method to the particular case of strictly included domains.

4.2.1 The smooth extension formulation

Let $n > 0$ and Ω be a domain of \mathbb{R}^n that satisfies the following set of hypotheses:

- i) Domain Ω is a bounded connected Lipschitz domain of \mathbb{R}^n .
- ii) Domain Ω is divided in two subdomains, Ω_1 and Ω_2 , which have Lipschitz boundaries. (H₁)
- iii) The interface $\Gamma = \partial\Omega_1 \cap \partial\Omega_2$ is not empty.
- iv) The remaining boundaries $\Gamma_1 = \partial\Omega_1 \setminus \Gamma$ and $\Gamma_2 = \partial\Omega_2 \setminus \Gamma$ are not empty.

The problem we are interested in, for now, is the coupled Laplace problem with homogeneous Dirichlet boundary conditions, also called Laplace transmission problem or Laplace problem with discontinuous coefficients. It is the simplest coupled system of partial differential equations that we can think of and, given two positive real constants μ_1 and μ_2 such that $\mu_1 \neq \mu_2$ and two source terms $f_1 \in L^2(\Omega_1)$ and $f_2 \in L^2(\Omega_2)$, it writes:

$$\left\{ \begin{array}{l} \text{find } u_1: \Omega_1 \rightarrow \mathbb{R} \text{ and } u_2: \Omega_2 \rightarrow \mathbb{R} \text{ such that} \\ \begin{array}{ll} -\mu_1 \Delta u_1 = f_1, & \text{in } \Omega_1, \\ u_1 = 0, & \text{on } \Gamma_1, \end{array} & (4.1a) \\ \begin{array}{ll} -\mu_2 \Delta u_2 = f_2, & \text{in } \Omega_2, \\ u_2 = 0, & \text{on } \Gamma_2, \end{array} & (4.1b) \\ \begin{array}{ll} u_1 = u_2, & \text{on } \Gamma, \\ \mu_1 \nabla u_1 \cdot n_1 = -\mu_2 \nabla u_2 \cdot n_2, & \text{on } \Gamma. \end{array} & (4.1c) \end{array} \right.$$

This problem is completely equivalent to the more classical formulation of the Laplace problem, written in the whole domain Ω ,

$$\left\{ \begin{array}{l} \text{find } u: \Omega \rightarrow \mathbb{R} \text{ such that} \\ -\text{div}(\mu \nabla u) = f \quad \text{in } \Omega, \\ u = 0 \quad \text{on } \partial\Omega, \end{array} \right.$$

where μ and f are defined by

$$\mu = \begin{cases} \mu_1 & \text{in } \Omega_1, \\ \mu_2 & \text{in } \Omega_2, \end{cases} \quad f = \begin{cases} f_1 & \text{in } \Omega_1, \\ f_2 & \text{in } \Omega_2. \end{cases}$$

However, the formulation (4.1) has the advantage of making the coupling between the two subproblems (4.1a) and (4.1b) clear. The so-called coupling conditions are detailed in equations (4.1c) and physically represent the continuity of the field and the continuity of the normal constraint through the interface Γ . Moreover, n_1 (resp. n_2) is the unit exterior normal vector of Ω_1 (resp. Ω_2). The solution of problem (4.1) will be searched in $V_1 \times V_2$, where these two functional spaces are defined by

$$\begin{aligned} V_1 &= \{v_1 \in H^1(\Omega_1); v_1|_{\Gamma_1} = 0\}, \\ V_2 &= \{v_2 \in H^1(\Omega_2); v_2|_{\Gamma_2} = 0\}. \end{aligned}$$

In addition, the dual spaces of V_1 and V_2 will be denoted by V_1' and V_2' .

Let v be a distribution in $\mathcal{D}(\Omega)$ and suppose that u_1 and u_2 are sufficiently regular. We can formally multiply the first equation in (4.1a) by $v|_{\Omega_1}$ and the first equation in (4.1b) by $v|_{\Omega_2}$ and integrate respectively over Ω_1 and Ω_2 . After an integration by part, we obtain

$$\begin{aligned} \mu_1 \int_{\Omega_1} \nabla u_1 \cdot \nabla v|_{\Omega_1} - \int_{\Gamma} (\mu_1 \nabla u_1 \cdot n_1) v + \mu_2 \int_{\Omega_2} \nabla u_2 \cdot \nabla v|_{\Omega_2} - \int_{\Gamma} (\mu_2 \nabla u_2 \cdot n_2) v \\ = \int_{\Omega_1} f_1 v|_{\Omega_1} + \int_{\Omega_2} f_2 v|_{\Omega_2}, \quad \forall v \in \mathcal{D}(\Omega). \end{aligned}$$

Using the second transmission condition in (4.1c) i.e., that $\mu_1 \nabla u_1 \cdot n_1 = -\mu_2 \nabla u_2 \cdot n_2$ on Γ , it follows that

$$\mu_1 \int_{\Omega_1} \nabla u_1 \cdot \nabla v|_{\Omega_1} + \mu_2 \int_{\Omega_2} \nabla u_2 \cdot \nabla v|_{\Omega_2} = \int_{\Omega_1} f_1 v|_{\Omega_1} + \int_{\Omega_2} f_2 v|_{\Omega_2}, \quad \forall v \in \mathcal{D}(\Omega).$$

Then, introducing the space

$$\mathcal{V} = \{(v_1, v_2) \in V_1 \times V_2; v_1|_{\Gamma} = v_2|_{\Gamma}\},$$

we can define the weak formulation of problem (4.1):

$$\begin{cases} \text{find } (u_1, u_2) \text{ in } \mathcal{V} \text{ such that,} \\ \mu_1 \int_{\Omega_1} \nabla u_1 \cdot \nabla v_1 + \mu_2 \int_{\Omega_2} \nabla u_2 \cdot \nabla v_2 = \int_{\Omega_1} f_1 v_1 + \int_{\Omega_2} f_2 v_2, \quad \forall (v_1, v_2) \in \mathcal{V}. \end{cases} \quad (4.2)$$

Problem (4.2) is well-posed, since $f_1 \in L^2(\Omega_1)$ and $f_2 \in L^2(\Omega_2)$, according to the Lax-Milgram theorem. Furthermore, the unique solution of problem (4.2) will be denoted by (\bar{u}_1, \bar{u}_2) .

At this point, we can precise in what sense the solution of (4.2) is also solution of the initial problem (4.1). Taking test functions v_1 in $\mathcal{D}(\Omega_1)$ and v_2 in $\mathcal{D}(\Omega_2)$ in (4.2) gives that

$$-\mu_1 \Delta \bar{u}_1 = f_1 \text{ and } -\mu_2 \Delta \bar{u}_2 = f_2 \text{ in } L^2.$$

It also implies that $\nabla \bar{u}_1$ belongs to $H_{\text{div}}(\Omega_1)$ and that $\nabla \bar{u}_2$ belongs to $H_{\text{div}}(\Omega_2)$, where the spaces $H_{\text{div}}(\Omega_1)$ and $H_{\text{div}}(\Omega_2)$ are defined by

$$H_{\text{div}}(X) = \{\sigma \in (L^2(X))^n; \text{div}(\sigma) \in L^2(X)\},$$

and where X stands for either Ω_1 or Ω_2 . In particular, we are able to give a weak sense to the normal derivatives of \bar{u}_1 and \bar{u}_2 . Let X stand for either Ω_1 or Ω_2 and let η be the unit exterior normal vector of X . Let $\Lambda = H_{00}^{1/2}(\Gamma)$ be the image of $H_{\partial X \setminus \Gamma}^1(X)$ by the trace operator on the interface Γ , i.e. the space of functions in $H^{1/2}(\Gamma)$ whose extension by zero on $\partial X \setminus \Gamma$ belongs to $H^{1/2}(\partial X)$. Then, For all σ in $H_{\text{div}}(X)$, we have the following Stokes formula:

$$\int_X \sigma \cdot \nabla v + \int_X \text{div}(\sigma) v = \langle \gamma_{\eta}(\sigma), v \rangle_{\Lambda', \Lambda}, \quad \forall v \in H_{\partial X \setminus \Gamma}^1(X). \quad (4.3)$$

where $\Lambda' = (H_{00}^{1/2}(\Gamma))'$ is the dual space of Λ and γ_{η} denotes the normal trace operator on Γ . Then, \bar{u}_1 verifies $-\mu_1 \Delta \bar{u}_1 = f_1$ a.e. in Ω_1 , \bar{u}_2 verifies $-\mu_2 \Delta \bar{u}_2 = f_2$ a.e. in Ω_2 , the first transmission condition, $\bar{u}_1 = \bar{u}_2$ on Γ , is included in the functional space \mathcal{V} and the second one is verified in a weak sense:

$$\langle \mu_1 \gamma_{n_1}(\nabla \bar{u}_1), v \rangle_{\Lambda', \Lambda} = -\langle \mu_2 \gamma_{n_2}(\nabla \bar{u}_2), v \rangle_{\Lambda', \Lambda}, \quad \forall v \in \Lambda. \quad (4.4)$$

Now, we present the smooth extension method applied to problem (4.1). This method consists in *i*) extending the problem in Ω_1 into a problem defined in the whole domain Ω , *ii*) relaxing the condition of equality in the functional space \mathcal{V} and *iii*) finding a control term in Ω_2 to enforce the condition of equality on Γ . We denote by g this control term, which should belong to V_2' , and we define \bar{g}^Ω , the extension of g in the whole domain Ω such that

$$\langle \bar{g}^\Omega, v \rangle_{H^{-1}(\Omega), H_0^1(\Omega)} := \langle g, v|_{\Omega_2} \rangle_{V_2', V_2}, \forall v \in H_0^1(\Omega).$$

In a similar way, as f_1 belongs to $L^2(\Omega_1)$, \bar{f}_1^Ω denotes the extension of f_1 by 0 over the whole space Ω .

Formally, we define the smooth extension problem associated to problem (4.1) as the problem of finding a suitable control g in V_2' , such that the solution of the following problem,

$$\left\{ \begin{array}{ll} \text{find } u_1: \Omega \rightarrow \mathbb{R} \text{ and } u_2: \Omega_2 \rightarrow \mathbb{R} \text{ such that} \\ -\mu_1 \Delta u_1 = \bar{f}_1^\Omega + \bar{g}^\Omega, & \text{in } \Omega, \\ u_1 = 0, & \text{on } \partial\Omega, \\ -\mu_2 \Delta u_2 = f_2, & \text{in } \Omega_2, \\ u_2 = 0, & \text{on } \Gamma_2, \\ \mu_2 \nabla u_2 \cdot n_2 = -\mu_1 \nabla u_1 \cdot n_1, & \text{on } \Gamma, \end{array} \right. \quad (4.5a)$$

$$\left\{ \begin{array}{ll} -\mu_2 \Delta u_2 = f_2, & \text{in } \Omega_2, \\ u_2 = 0, & \text{on } \Gamma_2, \\ \mu_2 \nabla u_2 \cdot n_2 = -\mu_1 \nabla u_1 \cdot n_1, & \text{on } \Gamma, \end{array} \right. \quad (4.5b)$$

satisfies the equality

$$(u_1|_{\Omega_1}, u_2) = (\bar{u}_1, \bar{u}_2),$$

where (\bar{u}_1, \bar{u}_2) is the solution of the initial problem (4.1). Again, let v be in $\mathcal{D}(\Omega)$ and suppose that u_1 and u_2 are sufficiently regular. Moreover, we assume for the moment that g belongs to $L^2(\Omega_2)$ in order to do formal computations. We multiply equation (4.5a) by v and equation (4.5b) by $v|_{\Omega_2}$ and integrate respectively over Ω and Ω_2 . After an integration by part and using the Neumann condition on Γ , we find

$$\begin{aligned} \mu_1 \int_{\Omega} \nabla u_1 \cdot \nabla v &= \int_{\Omega_1} f_1 v|_{\Omega_1} + \int_{\Omega_2} g v|_{\Omega_2}, \\ \mu_2 \int_{\Omega_2} \nabla u_2 \cdot \nabla v|_{\Omega_2} &= \int_{\Omega_2} f_2 v|_{\Omega_2} - \int_{\Gamma} (\mu_1 \nabla u_1 \cdot n_1) v. \end{aligned}$$

Furthermore, we remark that

$$\begin{aligned} - \int_{\Gamma} (\mu_1 \nabla u_1 \cdot n_1) v &= \int_{\Gamma} (\mu_1 \nabla u_1 \cdot n_2) v, \\ &= \mu_1 \int_{\Omega_2} \Delta u_1|_{\Omega_2} v|_{\Omega_2} + \mu_1 \int_{\Omega_2} \nabla u_1|_{\Omega_2} \cdot \nabla v|_{\Omega_2}, \\ &= - \int_{\Omega_2} g v|_{\Omega_2} + \mu_1 \int_{\Omega_2} \nabla u_1|_{\Omega_2} \cdot \nabla v|_{\Omega_2}. \end{aligned}$$

Thus, we define the weak formulation of the smooth extension problem associated to problem (4.2), that makes sense for g in V_2' , as the problem of finding a suitable control g

in V_2' , such that the solution of the following problem,

$$\left\{ \begin{array}{l} \text{find } (u_1, u_2) \text{ in } H_0^1(\Omega) \times V_2 \text{ such that} \\ \mu_1 \int_{\Omega} \nabla u_1 \cdot \nabla v_1 = \int_{\Omega_1} f_1 v_1|_{\Omega_1} + \langle g, v_1|_{\Omega_2} \rangle_{V_2', V_2}, \quad \forall v_1 \in H_0^1(\Omega), \\ \mu_2 \int_{\Omega_2} \nabla u_2 \cdot \nabla v_2 = \int_{\Omega_2} f_2 v_2 - \langle g, v_2 \rangle_{V_2', V_2} \\ \quad + \mu_1 \int_{\Omega_2} \nabla u_1|_{\Omega_2} \cdot \nabla v_2, \quad \forall v_2 \in V_2. \end{array} \right. \quad (4.6)$$

satisfies the equality

$$(u_1|_{\Omega_1}, u_2) = (\bar{u}_1, \bar{u}_2), \quad (4.7)$$

where (\bar{u}_1, \bar{u}_2) is the solution of the initial weak problem (4.2). By standard arguments and considering the regularity of f_1 and f_2 , it is straightforward to prove that problem (4.6) is well-posed for every g in V_2' , using the Lax-Milgram theorem. Consequently, we denote by (u_1^g, u_2^g) its unique solution. Problem (4.6) is weakly coupled, in the sense that, given g in V_2' , u_1^g is obtained independently of u_2^g and u_2^g is obtained afterwards from g and u_1^g . We remark that finding such a control g enables to directly obtain the solution of the initial coupled problem (4.2). Then, in what follows, we will prove the existence of at least one control g and detail the process of finding it.

With these notations we state the following theorem, showing the existence of a control g for which the couple (u_1^g, u_2^g) , the unique solution of (4.6), verifies the condition (4.7).

Theorem 4.1. *Let Ω be a domain that satisfies Assumption (H_1) . Consider f_1 in $L^2(\Omega_1)$, f_2 in $L^2(\Omega_2)$ and let (\bar{u}_1, \bar{u}_2) be the unique solution of problem (4.2). Then, there exists a function g in V_2' such that the solution (u_1^g, u_2^g) of problem (4.6) verifies (4.7).*

Proof. We can construct an extension operator E that extend \bar{u}_1 into the whole space $H_0^1(\Omega)$. Indeed, consider the operator defined by

$$E\bar{u}_1 = \begin{cases} \bar{u}_1 & \text{in } \Omega_1 \\ \bar{u}_2 & \text{in } \Omega_2 \end{cases}.$$

Since \bar{u}_1 belongs to V_1 , \bar{u}_2 belongs to V_2 and $\bar{u}_1 = \bar{u}_2$ on the interface Γ , then $E\bar{u}_1$ is an extension of \bar{u}_1 which belongs to $H_0^1(\Omega)$. Furthermore, $\Delta(E\bar{u}_1)$ belongs to $L^2(\Omega)$.

Then, we construct g in V_2' such that

$$\begin{aligned} \langle g, v \rangle_{V_2', V_2} &= \mu_1 \int_{\Omega_2} \nabla(E\bar{u}_1)|_{\Omega_2} \cdot \nabla v + \langle \mu_1 \gamma_{n_1}(\nabla E\bar{u}_1), v \rangle_{\Lambda', \Lambda}, \\ &= -\mu_1 \int_{\Omega_2} \Delta(E\bar{u}_1)|_{\Omega_2} v + \langle \mu_1 \gamma_{n_2}(\nabla E\bar{u}_1), v \rangle_{\Lambda', \Lambda} \\ &\quad + \langle \mu_1 \gamma_{n_1}(\nabla E\bar{u}_1), v \rangle_{\Lambda', \Lambda}, \quad \forall v \in V_2. \end{aligned} \quad (4.8)$$

Using the Stokes formula (4.3), it follows that the extension $E\bar{u}_1$ in $H_0^1(\Omega)$ verifies

$$\begin{aligned} \mu_1 \int_{\Omega} \nabla(E\bar{u}_1) \cdot \nabla v_1 &= \mu_1 \int_{\Omega_1} \nabla \bar{u}_1 \cdot \nabla v_1|_{\Omega_1} + \mu_1 \int_{\Omega_2} \nabla(E\bar{u}_1)|_{\Omega_2} \cdot \nabla v_1|_{\Omega_2}, \\ &= -\mu_1 \int_{\Omega_1} \Delta \bar{u}_1 v_1|_{\Omega_1} + \langle \mu_1 \gamma_{n_1}(\nabla E\bar{u}_1), v_1|_{\Omega_2} \rangle_{\Lambda', \Lambda} \\ &\quad + \mu_1 \int_{\Omega_2} \nabla(E\bar{u}_1)|_{\Omega_2} \cdot \nabla v_1|_{\Omega_2}, \\ &= \int_{\Omega_1} f_1 v_1|_{\Omega_1} + \langle g, v_1|_{\Omega_2} \rangle_{V_2', V_2}, \quad \forall v_1 \in H_0^1(\Omega). \end{aligned}$$

Similarly, the function \bar{u}_2 in V_2 verifies, using (4.3) and (4.4),

$$\begin{aligned} \mu_2 \int_{\Omega_2} \nabla \bar{u}_2 \cdot \nabla v_2 &= -\mu_2 \int_{\Omega_2} \Delta \bar{u}_2 v_2 + \langle \mu_2 \gamma_{n_2}(\nabla \bar{u}_2), v_2 \rangle_{\Lambda', \Lambda} \\ &= \langle f_2, v_2 \rangle_{V_2', V_2} - \langle \mu_1 \gamma_{n_1}(\nabla \bar{u}_1), v_2 \rangle_{\Lambda', \Lambda}, \\ &= \int_{\Omega_2} f_2 v_2 + \mu_1 \int_{\Omega_2} \nabla(E\bar{u}_1)|_{\Omega_2} \cdot \nabla v_2 - \langle g, v_2 \rangle_{V_2', V_2}, \quad \forall v_2 \in V_2. \end{aligned}$$

Finally, we can conclude that the couple $(E\bar{u}_1, \bar{u}_2)$ is the solution of problem (4.6). Thus

$$(u_1^g, u_2^g) = (E\bar{u}_1, \bar{u}_2)$$

and by construction of the operator E , the condition (4.7) is verified since

$$(u_{1|\Omega_1}^g, u_2^g) = (\bar{u}_1, \bar{u}_2).$$

□

Remark 4.1. The control g is not unique. In fact, the extension operator E constructed in the preceding proof can be defined in different ways, leading to the construction of a different control g from an other extension of \bar{u}_1 .

Remark 4.2. If \bar{u}_1 is of regularity $H^2(\Omega_1)$ and if $E\bar{u}_1$ is an extension which preserves this regularity on the whole domain Ω , then the following weak transmission condition holds:

$$\langle \mu_1 \gamma_{n_2}(\nabla E\bar{u}_1), v \rangle_{\Lambda', \Lambda} = - \langle \mu_1 \gamma_{n_1}(\nabla E\bar{u}_1), v \rangle_{\Lambda', \Lambda}.$$

Thus, because $\Delta(E\bar{u}_1)|_{\Omega_2}$ belongs to $L^2(\Omega_2)$, we see from the definition of the control g in (4.8) that g belongs to $L^2(\Omega_2)$ and can be identified to $-\mu_1 \Delta(E\bar{u}_1)|_{\Omega_2}$. This justifies the use of the smooth extension method because the numerical approximation of the solution of the smooth extension problem (4.6) will converge in space with optimal rates of convergence, using $P1$ finite elements, whereas the numerical approximation of the solution of the transmission problem (4.2) will not in the general case. We refer to Subsection 4.2.3 for details. Moreover, in what follows, we will explicit some cases where such a regular extension can be constructed (in Subsection 4.2.3 and Subsection 4.2.4).

Remark 4.3. For the presentation of the smooth extension method, we considered the Laplace transmission problem with homogeneous Dirichlet boundary conditions. However, the extension of our results to the non-homogeneous case is straight forward and amounts to study a problem with homogeneous Dirichlet boundary conditions, where only the external forces are modified.

Remark 4.4. The hypothesis that Γ_1 and Γ_2 should not be empty could also be weakened. For example, the case where Ω_2 is strictly included in Ω_1 could be particularly interesting to study. In this situation u_2^g is not unique in V_2 but can be searched such that it has a zero mean value. This is the subject of Subsection 4.2.4.

4.2.2 Formulation as an optimization problem

We saw in the previous subsection that a suitable control g can be obtained by extending u_1 in the whole domain. In practice, the control g can not be constructed in such a

direct manner, since the solution (\bar{u}_1, \bar{u}_2) of the initial problem (4.2) is unknown. To that matter, we introduce the following cost function, defined from V_2' to \mathbb{R}^+ ,

$$J(g) = \frac{1}{2} \int_{\Gamma} |u_1^g - u_2^g|^2, \quad (4.9)$$

where (u_1^g, u_2^g) is the unique solution of problem (4.6). The main idea to overcome this issue is to write the problem of finding a function g such that the solution (u_1^g, u_2^g) of the problem (4.6) verifies the equation (4.7), as a minimization problem on the function J . A first link between the minimization of J and the research of a good control g is given by the following theorem.

Theorem 4.2. *Let g be in V_2' be such that the solution (u_1^g, u_2^g) of (4.6) satisfies condition (4.7). Then, g is a minimizer of J .*

Proof. Let g be such a control, which exists according to Theorem 4.1. We know that the couple $(u_{1|\Omega_1}^g, u_2^g)$ is the unique solution of the weak initial problem (4.2). In particular, this couple satisfies the constraint of continuity through the interface Γ , which writes $u_{1|\Gamma}^g = u_{2|\Gamma}^g$ and implies that $J(g) = 0$, so that g is in fact a minimizer of J . \square

Remark 4.5. Theorem 4.2, along with Theorem 4.1, proves the existence of several minimizers of J . Actually, every control g such that the solution (u_1^g, u_2^g) of (4.6) verifies (4.7) is a suitable minimizer. At the end of this section, we will prove the reciprocal statement of Theorem 4.2, i.e. that for every minimizer g of J , (u_1^g, u_2^g) verifies the condition (4.7). In other words, finding a minimizer of J would enable us to obtain the solution of the transmission problem (4.1).

The problem we face now is the minimization of the cost function J . To do that, classical methods such as gradient methods or quasi-Newton methods require the computation of the gradient of the cost function with respect to the control g . For that purpose, we will use the adjoint approach (see [Chavent, 2010]), a suitable method to compute the gradient of a cost function which depends on the solution of a system of differential equations. The idea is the following: knowing that, for any g in V_2' , $J(g)$ is obtained by solving problem (4.6) and computing the explicit formula $\frac{1}{2} \int_{\Gamma} |u_1^g - u_2^g|^2$, we will prove that we can compute the gradient $\nabla J(g)$ by solving a system of linear partial differential equations, called *the adjoint equations*, and evaluating $\nabla J(g)$ with an explicit formula. The key here is to remark that the minimization of $J(g)$ can be seen as the minimization of the real-valued function

$$\begin{aligned} H_0^1(\Omega) \times V_2 &\rightarrow \mathbb{R}^+ \\ (v_1, v_2) &\mapsto \frac{1}{2} \int_{\Gamma} |v_{1|\Gamma} - v_{2|\Gamma}|^2, \end{aligned}$$

under the constraint that (v_1, v_2) is solution of (4.6). Thus, it is indicated to introduce the Lagrangian function associated to this constrained optimization problem, defined from

$$V_2' \times (H_0^1(\Omega) \times V_2) \times (H_0^1(\Omega) \times V_2)$$

to \mathbb{R} by

$$\begin{aligned} \mathcal{L}(g, (v_s, v_2), (\lambda_1, \lambda_2)) &= \frac{1}{2} \|v_1 - v_2\|_{L^2(\Gamma)}^2 + \mu_1 \int_{\Omega} \nabla v_1 \cdot \nabla \lambda_1 - \mu_1 \int_{\Omega_2} \nabla v_{1|\Omega_2} \cdot \nabla \lambda_2 \\ &+ \mu_2 \int_{\Omega_2} \nabla v_2 \cdot \nabla \lambda_2 - \int_{\Omega_1} f_1 \lambda_1 - \int_{\Omega_2} f_2 \lambda_2 - \langle g, \lambda_{1|\Omega_2} \rangle_{V_2', V_2} \\ &+ \langle g, \lambda_2 \rangle_{V_2', V_2}, \end{aligned} \quad (4.10)$$

where the Lagrangian multipliers λ_1 and λ_2 are called the *adjoint variables* of v_1 and v_2 , associated to the state equations (4.5a)-(4.5b). We also introduce the so-called *adjoint equations*, defined for all g in V_2' by

$$\begin{aligned} \left\langle \frac{\partial \mathcal{L}}{\partial v_1}(g, (u_1^g, u_2^g), (\lambda_1, \lambda_2)), \delta v_1 \right\rangle_{H^{-1}(\Omega), H_0^1(\Omega)} &= 0, \quad \forall \delta v_1 \in H_0^1(\Omega), \\ \left\langle \frac{\partial \mathcal{L}}{\partial v_2}(g, (u_1^g, u_2^g), (\lambda_1, \lambda_2)), \delta v_2 \right\rangle_{V_2', V_2} &= 0, \quad \forall \delta v_2 \in V_2, \end{aligned} \quad (4.11)$$

where (u_1^g, u_2^g) is the solution of the smooth extension problem (4.6). The computation of the differential forms $\frac{\partial \mathcal{L}}{\partial v_1}$ and $\frac{\partial \mathcal{L}}{\partial v_2}$ will be detailed later on.

Remark 4.6. The Lagrangian \mathcal{L} is differentiable with respect to v_1 and v_2 because all its terms are quadratic or linear with respect to each of them. Thus, equations (4.11) are well defined.

With all these notations, we state the following theorem adapted from [Chavent, 2010], where the use of the Lagrangian function \mathcal{L} is made clear in providing a convenient way to compute the gradient of J .

Theorem 4.3. *The mapping $g \in V_2' \mapsto J(g) \in \mathbb{R}$ is differentiable and its gradient $\nabla J(g)$, which belongs to V_2'' , is given by*

$$\langle \nabla J(g), \delta g \rangle_{V_2'', V_2'} = \left\langle \delta g, \lambda_2^g - \lambda_{1|\Omega_2}^g \right\rangle_{V_2', V_2}, \quad \forall \delta g \in V_2', \quad (4.12)$$

where $(\lambda_1^g, \lambda_2^g)$ verifies the adjoint equations (4.11).

To prove this theorem, we first need to prove the following result.

Lemma 4.1. *There exists a unique $(\lambda_1^g, \lambda_2^g)$ in $H_0^1(\Omega) \times V_2$, solution of the adjoint equations (4.11).*

Proof. We start by computing the partial derivatives of \mathcal{L} with respect to v_1 and v_2 . Let $\varepsilon > 0$. For all $g \in V_2'$, and for all (v_1, v_2) , $(\delta v_1, \delta v_2)$ and (λ_1, λ_2) in $H_0^1(\Omega) \times V_2$,

$$\begin{aligned} &\mathcal{L}(g, (v_1 + \varepsilon \delta v_1, v_2), (\lambda_1, \lambda_2)) \\ &= \frac{1}{2} \|v_1 - v_2 + \varepsilon \delta v_1\|_{L^2(\Gamma)}^2 + \mu_1 \int_{\Omega} \nabla(v_1 + \varepsilon \delta v_1) \cdot \nabla \lambda_1 + \mu_2 \int_{\Omega_2} \nabla v_2 \cdot \nabla \lambda_2 \\ &\quad - \mu_1 \int_{\Omega_2} \nabla(v_1|_{\Omega_2} + \varepsilon \delta v_1) \cdot \nabla \lambda_2 - \int_{\Omega_1} f_1 \lambda_1|_{\Omega_1} - \int_{\Omega_2} f_2 \lambda_2 - \left\langle g, \lambda_1|_{\Omega_2} \right\rangle_{V_2', V_2} \\ &\quad + \langle g, \lambda_2 \rangle_{V_2', V_2}, \\ &= \mathcal{L}(g, (v_1, v_2), (\lambda_1, \lambda_2)) + \varepsilon \mu_1 \int_{\Omega} \nabla(\delta v_1) \cdot \nabla \lambda_1 - \varepsilon \mu_1 \int_{\Omega_2} \nabla(\delta v_1|_{\Omega_2}) \cdot \nabla \lambda_2 \\ &\quad + \varepsilon \int_{\Gamma} (v_1 - v_2) \delta v_1 + \frac{\varepsilon^2}{2} \|\delta v_1\|_{L^2(\Gamma)}^2. \end{aligned}$$

It leads to define $\frac{\partial \mathcal{L}}{\partial v_1}(g, (v_1, v_2), (\lambda_1, \lambda_2)) \in H^{-1}(\Omega)$ as:

$$\begin{aligned} &\left\langle \frac{\partial \mathcal{L}}{\partial v_1}(g, (v_1, v_2), (\lambda_1, \lambda_2)), \delta v_1 \right\rangle_{H^{-1}(\Omega), H_0^1(\Omega)} \\ &= \mu_1 \int_{\Omega} \nabla(\delta v_1) \cdot \nabla \lambda_1 - \mu_1 \int_{\Omega_2} \nabla(\delta v_1|_{\Omega_2}) \cdot \nabla \lambda_2 + \int_{\Gamma} (v_1 - v_2) \delta v_1, \quad \forall \delta v_1 \in H_0^1(\Omega). \end{aligned}$$

Similarly, we define the derivative of the Lagrangian function \mathcal{L} with respect to v_2 evaluated at point δv_2 , $\frac{\partial \mathcal{L}}{\partial v_2}(g, (v_1, v_2), (\lambda_1, \lambda_2)) \in V_2'$ as:

$$\begin{aligned} & \left\langle \frac{\partial \mathcal{L}}{\partial v_2}(g, (v_1, v_2), (\lambda_1, \lambda_2)), \delta v_2 \right\rangle_{V_2', V_2} \\ &= \mu_2 \int_{\Omega_2} \nabla(\delta v_2) \cdot \nabla \lambda_2 - \int_{\Gamma} (v_1 - v_2) \delta v_2, \quad \forall \delta v_2 \in V_2. \end{aligned}$$

Then, we can deduce the *adjoint problem*:

$$\left\{ \begin{array}{l} \text{find } (\lambda_1, \lambda_2) \text{ in } H_0^1(\Omega) \times V_2 \text{ such that,} \\ \mu_1 \int_{\Omega} \nabla \lambda_1 \cdot \nabla v_1 = \mu_1 \int_{\Omega_2} \nabla \lambda_2 \cdot \nabla v_1|_{\Omega_2} - \int_{\Gamma} (u_1^g - u_2^g) v_1, \quad \forall v_1 \in H_0^1(\Omega), \\ \mu_2 \int_{\Omega_2} \nabla \lambda_2 \cdot \nabla v_2 = \int_{\Gamma} (u_1^g - u_2^g) v_2, \quad \forall v_2 \in V_2. \end{array} \right. \quad (4.13)$$

Again, we can use the Lax-Milgram Theorem to show that problem (4.13) admits a unique solution $(\lambda_1^g, \lambda_2^g)$. \square

We now have all the tools we need to prove Theorem 4.3.

Proof of Theorem 4.3. The solution (u_1^g, u_2^g) of problem (4.6) is unique for every control g in V_2' . Thus, we can define the so called *direct mapping*

$$\begin{aligned} \phi: V_2' &\rightarrow H_0^1(\Omega) \times V_2, \\ g &\mapsto (\phi_1(g), \phi_2(g)) = (u_1^g, u_2^g). \end{aligned} \quad (4.14)$$

Because of the linearity of the equations in (4.6), the mapping ϕ is linear, thus differentiable on V_2' . Similarly, the mapping which for every (u_1, u_2) in $H_0^1(\Omega) \times V_2$ associates the quadratic functional $\int_{\Gamma} |u_1 - u_2|^2$ is differentiable. By composition, it follows that the mapping $g \mapsto J(g)$ is differentiable on V_2' .

Taking $(v_1, v_2) = (u_1^g, u_2^g)$ the Lagrangian (4.10) reduces to

$$\mathcal{L}(g, (u_1^g, u_2^g), (\lambda_1, \lambda_2)) = J(g), \quad \forall g \in V_2', \quad \forall (\lambda_1, \lambda_2) \in H_0^1(\Omega) \times V_2.$$

Then, we differentiate this previous equality with respect to g for a fixed couple (λ_1, λ_2) and we obtain, using the chain rule, the following equation:

$$\begin{aligned} \langle \nabla J(g), \delta g \rangle_{V_2'', V_2'} &= \left\langle \frac{\partial \mathcal{L}}{\partial g}(g, (u_1^g, u_2^g), (\lambda_1, \lambda_2)), \delta g \right\rangle_{V_2'', V_2} \\ &+ \left\langle \frac{\partial \mathcal{L}}{\partial v_1}(g, (u_1^g, u_2^g), (\lambda_1, \lambda_2)), \frac{\partial \phi_1}{\partial g}(g) \cdot \delta g \right\rangle_{H^{-1}(\Omega) H_0^1(\Omega)} \\ &+ \left\langle \frac{\partial \mathcal{L}}{\partial v_2}(g, (u_1^g, u_2^g), (\lambda_1, \lambda_2)), \frac{\partial \phi_2}{\partial g}(g) \cdot \delta g \right\rangle_{V_2', V_2}, \end{aligned}$$

for all $\delta g \in V_2'$. Considering $(\lambda_1, \lambda_2) = (\lambda_1^g, \lambda_2^g)$, the solution of the adjoint equations (4.13) (see Lemma 4.1), this reduces to

$$\langle \nabla J(g), \delta g \rangle_{V_2'', V_2'} = \left\langle \frac{\partial \mathcal{L}}{\partial g}(g, (u_1^g, u_2^g), (\lambda_1^g, \lambda_2^g)), \delta g \right\rangle_{V_2'', V_2'}, \quad \forall \delta g \in V_2'.$$

It remains to compute the derivative of \mathcal{L} with respect to g at point δg : let $\varepsilon > 0$, for all g and δg in V_2' , and for all (v_1, v_2) and (λ_1, λ_2) in $H_0^1(\Omega) \times V_2$,

$$\begin{aligned} \mathcal{L}(g + \varepsilon \delta g, (v_1, v_2), (\lambda_1, \lambda_2)) &= \mathcal{L}(g, (v_1, v_2), (\lambda_1, \lambda_2)) - \varepsilon \left\langle \delta g, \lambda_{1|\Omega_2} \right\rangle_{V_2', V_2} \\ &\quad + \varepsilon \left\langle \delta g, \lambda_2 \right\rangle_{V_2', V_2}, \end{aligned}$$

which leads to the definition of $\frac{\partial \mathcal{L}}{\partial g}(g, (v_1, v_2), (\lambda_1, \lambda_2)) \in V_2''$ as:

$$\left\langle \frac{\partial \mathcal{L}}{\partial g}(g, (v_1, v_2), (\lambda_1, \lambda_2)), \delta g \right\rangle_{V_2'', V_2'} = \left\langle \delta g, \lambda_2 - \lambda_{1|\Omega_2} \right\rangle_{V_2', V_2}, \quad \forall \delta g \in V_2'.$$

Finally, we obtain an explicit expression for the gradient of J , which writes

$$\langle \nabla J(g), \delta g \rangle_{V_2'', V_2'} = \left\langle \delta g, \lambda_2^g - \lambda_{1|\Omega_2}^g \right\rangle_{V_2', V_2}, \quad \forall \delta g \in V_2'.$$

□

Now that we have an explicit expression for ∇J , we can prove the reciprocal statement of Theorem 4.2.

Theorem 4.4. *Let g be a minimizer of J in V_2' . Then, the solution (u_1^g, u_2^g) of (4.6) satisfies condition (4.7).*

Proof. As a minimizer of J , g verifies the equality $\langle \nabla J(g), \delta g \rangle_{V_2'', V_2'} = 0$, for all δg in V_2' . According to Theorem 4.3, it follows that the couple $(\lambda_1^g, \lambda_2^g)$ verifies

$$\left\langle \delta g, \lambda_2^g - \lambda_{1|\Omega_2}^g \right\rangle_{V_2', V_2} = 0, \quad \forall \delta g \in V_2'.$$

It comes that $\lambda_{1|\Omega_2}^g = \lambda_2^g$ in V_2 and the couple $(\lambda_{1|\Omega_1}^g, \lambda_2^g)$ belongs to the space \mathcal{V} . Yet, the couple $(\lambda_1^g, \lambda_2^g)$ is solution of problem (4.13). In particular, for all (v_1, v_2) in the space $\tilde{\mathcal{V}}$ defined by

$$\tilde{\mathcal{V}} = \{(v_1, v_2) \in H_0^1(\Omega) \times V_2; v_{1|\Omega_1} = v_2\},$$

the two equations in (4.13) write

$$\begin{aligned} \mu_1 \int_{\Omega} \nabla \lambda_1^g \cdot \nabla v_1 &= \mu_1 \int_{\Omega_2} \nabla \lambda_2^g \cdot \nabla v_{1|\Omega_2} - \int_{\Gamma} (u_1^g - u_2^g) v_1, \\ \mu_2 \int_{\Omega_2} \nabla \lambda_2^g \cdot \nabla v_2 &= \int_{\Gamma} (u_1^g - u_2^g) v_1. \end{aligned} \tag{4.15}$$

Summing the two equations in (4.15) and using the fact that $\lambda_{1|\Omega_2}^g = \lambda_2^g$, we find that

$$\mu_1 \int_{\Omega_1} \nabla \lambda_{1|\Omega_1}^g \cdot \nabla v_{1|\Omega_1} + \mu_2 \int_{\Omega_2} \nabla \lambda_2^g \cdot \nabla v_2 = 0, \quad \forall (v_1, v_2) \in \tilde{\mathcal{V}}.$$

Moreover, let (v_1, v_2) be in \mathcal{V} . We can construct an extension of v_1 in the whole space $H_0^1(\Omega)$ using v_2 , as in the proof of Theorem 4.1 and we still denote Ev_1 this extension. Then, the couple (Ev_1, v_2) belongs to $\tilde{\mathcal{V}}$ and it follows that the couple $(\lambda_{1|\Omega_1}^g, \lambda_2^g)$ verifies the equation

$$\mu_1 \int_{\Omega_1} \nabla \lambda_{1|\Omega_1}^g \cdot \nabla v_1 + \mu_2 \int_{\Omega_2} \nabla \lambda_2^g \cdot \nabla v_2 = 0, \quad \forall (v_1, v_2) \in \mathcal{V}.$$

We conclude that the couple $(\lambda_{1|\Omega_1}^g, \lambda_2^g)$ is solution of a weak problem similar to (4.2) but with no external force and, thus, is the zero of \mathcal{V} . Especially, this implies that $\lambda_2^g = 0$ and, according to the second equation of (4.15), that

$$\int_{\Gamma} (u_1^g - u_2^g)v_2 = 0, \quad \forall v_2 \in V_2.$$

Because $u_{1|\Gamma}^g$ and $u_{2|\Gamma}^g$ belong to $H^{1/2}(\Gamma)$ the previous equality implies that $u_{1|\Gamma}^g = u_{2|\Gamma}^g$ in $H^{1/2}(\Gamma)$, so that the couple $(u_{1|\Omega_1}^g, u_2^g)$ belongs to the space \mathcal{V} . As the unique solution of problem (4.6), the pair (u_1^g, u_2^g) verifies, in particular, for all (v_1, v_2) in $\tilde{\mathcal{V}}$,

$$\begin{aligned} \mu_1 \int_{\Omega} \nabla u_1^g \cdot \nabla v_1 &= \int_{\Omega_1} f_1 v_{1|\Omega_1} + \langle g, v_2 \rangle_{V_2', V_2}, \\ \mu_2 \int_{\Omega_2} \nabla u_2^g \cdot \nabla v_2 &= \int_{\Omega_2} f_2 v_2 - \langle g, v_2 \rangle_{V_2', V_2} + \mu_1 \int_{\Omega_2} \nabla u_1^g \cdot \nabla v_{1|\Omega_2}. \end{aligned} \quad (4.16)$$

Summing the two equations in (4.16) it follows that the pair $(u_{1|\Omega_1}^g, u_2^g)$, which belongs to \mathcal{V} , verifies the equation

$$\mu_1 \int_{\Omega_1} \nabla u_{1|\Omega_1}^g \cdot \nabla v_{1|\Omega_1} + \mu_2 \int_{\Omega_2} \nabla u_2^g \cdot \nabla v_2 = \int_{\Omega_1} f_1 v_{1|\Omega_1} + \int_{\Omega_2} f_2 v_2, \quad \forall (v_1, v_2) \in \tilde{\mathcal{V}}.$$

As before, for all (v_1, v_2) in \mathcal{V} , the couple (Ev_1, v_2) belongs to $\tilde{\mathcal{V}}$ and, finally, the couple $(u_{1|\Omega_1}^g, u_2^g)$ verifies the equation

$$\mu_1 \int_{\Omega_1} \nabla u_{1|\Omega_1}^g \cdot \nabla v_1 + \mu_2 \int_{\Omega_2} \nabla u_2^g \cdot \nabla v_2 = \int_{\Omega_1} f_1 v_1 + \int_{\Omega_2} f_2 v_2, \quad \forall (v_1, v_2) \in \mathcal{V}.$$

Thus, $(u_{1|\Omega_1}^g, u_2^g)$ is the unique solution to the initial coupled problem (4.2) and verifies, *a fortiori*, condition (4.7). \square

So, the minimization of the function J in V_2' is equivalent to the resolution of the problem of finding a suitable control g such that the solution (u_1^g, u_2^g) verifies (4.7) and thus, to the resolution of the initial coupled problem (4.2). As we will explain it in the next section, this minimization formulation offers, for the purpose of the numerical resolution of problem (4.2), the advantage of conserving the optimal rates of convergence, even with non-conformal meshes.

Remark 4.7. Theorem 4.4 also shows that all extrema of J correspond to global minimizers. Actually, in Theorem 4.4, it is enough to assume that g verifies $\langle \nabla J(g), \delta g \rangle_{V_2', V_2} = 0$ i.e., that $J(g)$ is a local extremum of J , to conclude that the solution (u_1^g, u_2^g) of (4.6) verifies the condition (4.7). According to Theorem 4.2, this implies that g is a global minimizer of J .

4.2.3 On convergence rates for the numerical method

The main difficulty with the numerical simulation of the Laplace transmission problem, that we will also find in other transmission problems, is to recover the optimal rate of convergence when the solution is more regular. Actually, even if f_1 belongs to $L^2(\Omega_1)$, f_2 to $L^2(\Omega_2)$ and the boundaries of Ω_1 and Ω_2 are smooth, the solution of problem (4.2) is not of regularity H^2 in the whole domain Ω , because of the jump in its gradient across the

interface Γ . As a consequence, the standard finite element method with $P1$ elements does not enable to recover the optimal rates of convergence in L^2 and H^1 -norms, unless we use a conformal mesh that fully represents the interface Γ (see Figure 4.5).

Nevertheless, with such a regularity on the data and the boundaries, one can show that the solution of problem (4.2) is *partially of regularity H^2* , in the following sense: \bar{u}_1 belongs to $H^2(\Omega_1) \cap V_1$ and \bar{u}_2 to $H^2(\Omega_2) \cap V_2$ (see [Costabel et al., 2010, Theorem 5.2.1]). Thus, if we can extend \bar{u}_1 in the whole domain Ω with regularity H^2 , we know how to construct a suitable control g in $L^2(\Omega_2)$ such that the solution of the smooth extension problem (4.6) is also of regularity H^2 : u_1^g belongs to $H^2(\Omega) \cap H_0^1(\Omega)$ and u_2^g belongs to $H^2(\Omega_2) \cap V_2$.

The advantage to consider the smooth extension problem (4.6), instead of problem (4.2), is now clear: the approximations of the two functions u_1^g and u_2^g are defined on two independent meshes and the two subproblems in (4.6) can be solved consecutively using standard finite element function spaces. These make the smooth extension method a fictitious domain method with optimal rates of convergence, even with non-conformal meshes.

To precise more the possibility to actually extend a function u_1 which belongs to $H^2(\Omega_1)$ into the whole space Ω with the same regularity, we state the following theorem, which requires some (rather weak) assumptions on the domains.

Theorem 4.5. *Let $\Omega \in \mathbb{R}^n$, with $n \in \{2, 3\}$, be a bounded open set with Lipschitz boundary $\partial\Omega$, and let Γ be an interface that divides Ω into two bounded open connected subdomains Ω_1 and Ω_2 with Lipschitz boundaries. Consider a function u_1 in $H^2(\Omega_1) \cap V_1$. Moreover, if $n = 3$, we assume that $\Gamma \cap \partial\Omega$ is a curve of regularity C^2 . If Γ and $\partial\Omega$ have at least C^2 -regularity in a neighborhood of each element of $\Gamma \cap \partial\Omega$ (a curve in three space dimensions and a point in two space dimensions), there exists a regular extension $u \in H^2(\Omega) \cap H_0^1(\Omega)$ such that $u = u_1$ in Ω_1 .*

Remark 4.8. The case where $\partial\Omega_2 = \Gamma$ is particularly easy to study and is the subject of Subsection 4.2.4. Thus we will only consider the case where $\partial\Omega_1 \cap \partial\Omega$ and $\partial\Omega_2 \cap \partial\Omega$ are both non empty in the following proof.

Proof. Suppose that $\partial\Omega_1 \cap \partial\Omega$ and $\partial\Omega_2 \cap \partial\Omega$ are both non empty. For the sake of simplicity, we consider the two-dimensional case, i.e. $\Omega \subset \mathbb{R}^2$, but the extension to the three-dimensional case can be performed in a similar manner. In two space dimension, the interface Γ intersects the boundary $\partial\Omega$ in two points that we denote by x_1 and x_2 , i.e. $\Gamma \cap \partial\Omega = \{x_1, x_2\}$.

For $i \in \{1, 2\}$, let us denote by $B_i = B(x_i, \varepsilon_i)$ the open ball of radius ε_i and center x_i . Moreover, we consider two open balls $B_i^+ = B(x_i, \varepsilon_i + \varepsilon_i/4)$ and $B_i^- = B(x_i, \varepsilon_i - \varepsilon_i/4)$, such that $B_i^- \subset B_i \subset B_i^+$. Furthermore, we should ensure that, for $i \in \{1, 2\}$, ε_i is small enough such that $\Gamma \cap B_i^+$ and $\partial\Omega \cap B_i^+$ are included in the neighborhood of x_i where both frontiers Γ and $\partial\Omega$ have C^2 -regularity. A quite general example of such a configuration is illustrated in Figure 4.1.

Let $\varphi \in C^\infty(\mathbb{R}^+)$ be a real-valued function satisfying

$$\varphi(x) = \begin{cases} 1 & \text{if } x < 3/4, \\ 0 & \text{if } x > 1. \end{cases}$$

Then we can define, for $i \in \{1, 2\}$, the functions

$$\begin{aligned} \varphi_i & : \Omega_1 \rightarrow [0, 1] \\ x & \mapsto \varphi\left(\frac{|x - x_i|}{\varepsilon}\right), \end{aligned}$$

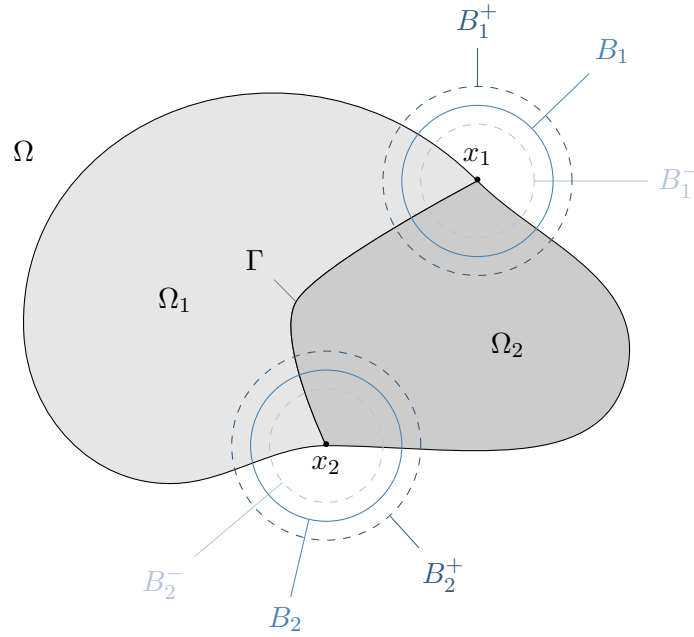


Figure 4.1 – Two-dimensional example of a geometry considered for the proof of the smooth extension.

whose regularity is $C^\infty(\Omega_1)$, and the functions

$$\begin{aligned} \xi_i &: \Omega_1 \rightarrow \mathbb{R} \\ x &\mapsto u_1(x)\varphi_i(x). \end{aligned}$$

Thus, we can write the following decomposition for the function u_1 on Ω_1 :

$$u_1 = u_1\varphi_1 + u_1\varphi_2 + u_1(1 - \varphi_1 - \varphi_2) = \xi_1 + \xi_2 + \xi_0,$$

where $\xi_0 = u_1(1 - \varphi_1 - \varphi_2)$. The problem to construct a regular extension for u_1 is equivalent to extend the three functions ξ_0 , ξ_1 and ξ_2 to the whole domain Ω .¹ Moreover, let us remark that we have

$$\begin{aligned} \xi_i(x) &= u_1(x), & \forall x \in B_i^- \cap \Omega_1, & \forall i \in \{0, 1\}, \\ \xi_i(x) &= 0, & \forall x \in \Omega_1 \setminus (B_i \cap \Omega_1), & \forall i \in \{0, 1\}, \end{aligned}$$

and

$$\begin{aligned} \xi_0(x) &= 0, & \forall x \in B_i^- \cap \Omega_1, & \forall i \in \{0, 1\}, \\ \xi_0(x) &= u_1(x), & \forall x \in \Omega_1 \setminus (B_i \cap \Omega_1), & \forall i \in \{0, 1\}. \end{aligned}$$

We begin with the function ξ_0 . For that matter, we make use of Stein's theorem ([Adams and Fournier, 2003, Theorem 5.24]), which states that, for any bounded Lipschitz domain $\mathcal{O} \subset \mathbb{R}^n$, there exists a total extension operator, i.e. an extension operator from $H^m(\mathcal{O})$ into the whole space $H^m(\mathbb{R}^n)$, for all $m \geq 0$. Then, Ω_1 being a bounded Lipschitz domain, there exists an extension operator from $H^2(\Omega_1)$ into the whole space $H^2(\mathbb{R}^2)$. We denote by $E\xi_0$ the restriction to Ω of such a regular extension of ξ_0 to \mathbb{R}^2 . This extension is regular enough but it is not zero on the boundary $\partial\Omega \cap \partial\Omega_2$. Therefore, we introduce a compact set \mathfrak{V} such that $(\partial\Omega \cap \partial\Omega_2) \subset \mathfrak{V}$ and $\mathfrak{V} \cap \Omega_1 = \emptyset$, and an open neighborhood

1. I thank K. Pankrashkin for his helpfull on this particular idea.

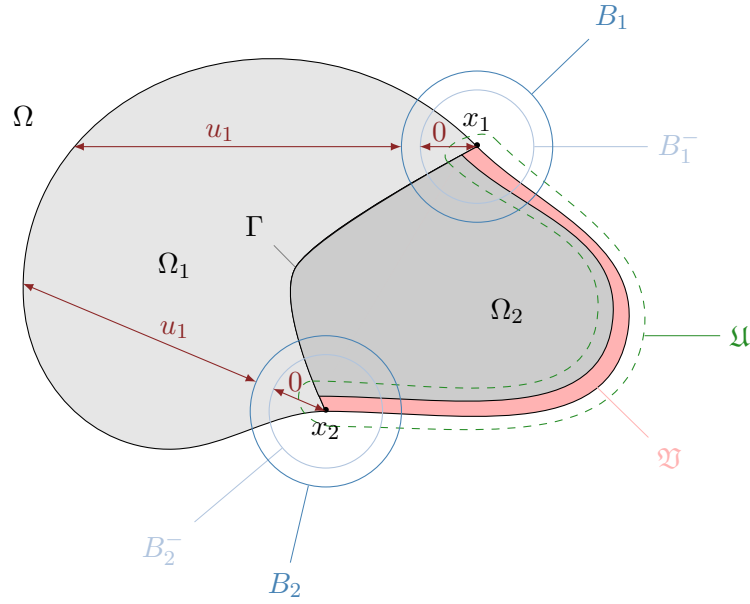


Figure 4.2 – Construction of the function ξ_0 and its regular extension, $\tilde{\xi}_0$.

of \mathfrak{A} , denoted by \mathfrak{U} , such that $(\mathfrak{U} \cap \Omega_1) \subset (B_1^- \cup B_2^-)$. We also define a smooth cut-off function $\psi : x \in \Omega \rightarrow \psi(x)$ such that $\psi(x) = 0$ in \mathfrak{A} , and $\psi(x) = 1$ in $\Omega \setminus \mathfrak{U}$. Then, the function $\tilde{\xi}_0 = \psi E \xi_0$ is an extension of ξ_0 to the whole domain Ω of regularity H^2 , which satisfies $\tilde{\xi}_0 = 0$ on $\partial\Omega$. The construction of $\tilde{\xi}_0$ is represented in Figure 4.2.

Let us now proceed with the construction of a smooth extension of ξ_i , for $i \in \{1, 2\}$. First, since $\xi_i = 0$ in $\Omega_1 \setminus (B_i \cap \Omega_1)$, we can extend it by 0 in $\Omega_2 \setminus (B_i^+ \cap \Omega_2)$. Then, it remains to construct the extension in $B_i^+ \cap \Omega_2$. Due to the C^2 -regularity of the interface Γ and the boundary $\partial\Omega$ inside the balls B_1^+ and B_2^+ (if ε_1 and ε_2 are chosen small enough), there exist two C^2 -diffeomorphisms χ_1 and χ_2 that map B_1^+ and B_2^+ respectively into the open unit square Q , and such that

$$\begin{aligned} \chi_i(x_i) &= 0, & \forall i \in \{1, 2\}, \\ \chi_i(\Gamma \cap B_i^+) &= \{0\} \times]0, \frac{1}{2}[, & \forall i \in \{1, 2\}, \\ \chi_i(\partial\Omega \cap B_i^+) &=]-\frac{1}{2}, \frac{1}{2}[\times \{0\}, & \forall i \in \{1, 2\}. \end{aligned}$$

For $i \in \{1, 2\}$, we define $\hat{\xi}_i = \xi_i \circ \chi_i^{-1}$ in

$$\chi_i(B_i^+ \cap \Omega_1) =]-\frac{1}{2}, 0[\times]0, \frac{1}{2}[,$$

which belongs to $H^2(\chi_i(B_i^+ \cap \Omega_1))$ (see [Adams and Fournier, 2003, Theorem 3.41]) and, recalling that $\xi_i = 0$ in $(B_i^+ \setminus B_i) \cap \Omega_1$, it follows that $\hat{\xi}_i = 0$ in $\chi_i((B_i^+ \setminus B_i) \cap \Omega_1)$. Then, a regular extension of $\hat{\xi}_i$ to the whole square Q can be obtained using Babič's extension (see [Babič, 1953] or [Adams and Fournier, 2003, Theorem 5.19]), defined for $i \in \{1, 2\}$ by

$$E\hat{\xi}_i(x, y) = \begin{cases} \hat{\xi}_i(x, y), & \text{if } x \leq 0, \\ -3\hat{\xi}_i(-x, y) + 4\hat{\xi}_i(-\frac{x}{2}, y), & \text{if } x > 0, \end{cases} \quad \forall (x, y) \in]-\frac{1}{2}, \frac{1}{2}[\times]0, \frac{1}{2}[.$$

Clearly, for $i \in \{1, 2\}$, the extension $E\hat{\xi}_i$ and its first derivative are continuous through the interface $\{0\} \times]0, \frac{1}{2}[$, such that $E\hat{\xi}_i$ well defines an extension of $\hat{\xi}_i$ in $H^2(\chi_i(B_i^+ \cap \Omega))$. However, the extension $E\hat{\xi}_i$ is not zero on the exterior frontier $\frac{1}{2} \times]0, \frac{1}{2}[$, thus we multiply it by a smooth cut-off function that is zero for $x > 1/2 - \varepsilon$ and equal to 1 for $x < 1/2 - 2\varepsilon$, for some $\varepsilon < 1/4$. Let us denote by $\bar{\xi}_i$ the product of $E\hat{\xi}_i$ by this cut-off function, which belongs to $H^2(\chi_i(B_i^+ \cap \Omega))$ and is zero on $\chi_i(\partial\Omega \cap B_i^+)$. Mapping this extension into B_i^+ we obtain $\bar{\xi}_i \circ \chi_i$, which then is an extension of ξ_i in $B_i^+ \cap \Omega$ of regularity H^2 . Now, we can construct the smooth extension of ξ_i to the whole domain Ω , denoted $\tilde{\xi}_i$ and defined by

$$\begin{aligned} \tilde{\xi}_i &= \xi_i, & \text{in } \Omega_1, \\ \tilde{\xi}_i &= 0, & \text{in } \Omega_2 \setminus (B_i^+ \cap \Omega_2), \\ \tilde{\xi}_i &= \bar{\xi}_i \circ \chi_i, & \text{in } B_i^+ \cap \Omega. \end{aligned}$$

Thus, for $i \in \{1, 2\}$, $\tilde{\xi}_i$ is an extension of ξ_i which belongs to $H^2(\Omega)$ and is zero on $\partial\Omega$.

Finally, we define

$$\tilde{u} = \tilde{\xi}_0 + \tilde{\xi}_1 + \tilde{\xi}_2, \text{ in } \Omega$$

and it follows that \tilde{u} belongs to $H^2(\Omega) \cap H_0^1(\Omega)$ and $\tilde{u} = u_1$ in Ω_1 . \square

Remark 4.9. The proof of Theorem 4.5 in three dimensions of space follows the same path. We start by considering three tubular neighborhoods of the intersection $\Gamma \cap \partial\Omega$ with circular cross sections and decompose the function u_1 in two regular functions ξ_0 and ξ_1 . The function ξ_0 is zero inside the smallest neighborhood and is equal to u_1 far from the intersection $\Gamma \cap \partial\Omega$, while the function ξ_1 is equal to u_1 inside the smallest neighborhood and is zero far from $\Gamma \cap \partial\Omega$. On one hand, the extension of the function ξ_0 is done using Stein's extension theorem. On the other hand, the extension of the function ξ_1 is conducted by transforming the largest tubular neighborhood into the unit torus with square cross section with a C^2 -diffeomorphism. Then, Babič's extension theorem is used in the unit torus and the resulting extension is brought back to the initial domain. In both cases, the extensions are multiplied by cut-off functions to ensure that they are zero on the exterior frontier $\partial\Omega$.

To conclude, the smooth extension formulation of transmission problems is possible as soon as the domains have Lipschitz regularities. Moreover, if their frontiers are more regular, such that the hypotheses of Theorem 4.5 are satisfied, then the smooth extension method applied to the numerical resolution of transmission problems has optimal rates of convergence.

A well-suited situation where the domains only have Lipschitz regularities is presented in the next subsection.

4.2.4 Particular case for strictly included domains

We explained in the previous subsection that the smooth extension method preserves the optimal order of convergence if there exists a H^2 -extension of the solution of the Laplace transmission problem from Ω_1 into the whole space $H_0^1(\Omega)$. However, this may not always be possible, depending on the geometry of the problem. A most suitable case is, for example, the one where Ω_2 is strictly included in Ω_1 . Indeed, we will show that the construction of such a regular extension is always possible in this case, so that the smooth extension method could always converge with optimal rates. Then, in this subsection we relax the

hypothesis *iv*) in Assumption (H_1) , i.e. we suppose that Ω_2 is strictly included in Ω_1 and that $\Gamma_1 = \partial\Omega$. Then, the set of hypotheses in this subsection is the following:

- i*) Domain Ω is a bounded connected Lipschitz domain of \mathbb{R}^n .
- ii*) Domain Ω is divided in two subdomains, Ω_1 and Ω_2 , which have Lipschitz boundaries. (H₂)
- iii*) The interface is $\Gamma = \partial\Omega_2$.
- iv*) The remaining boundary of Ω_1 is $\Gamma_1 = \partial\Omega$.

Again, we are able to define a smooth extension formulation for the Laplace transmission problem.

We still consider the Laplace problem presented in Subsection 4.2.1:

$$\begin{cases} \text{find } u: \Omega \rightarrow \mathbb{R} \text{ such that} \\ -\operatorname{div}(\mu \nabla u) = f & \text{in } \Omega, \\ u = 0 & \text{on } \partial\Omega, \end{cases} \quad (4.17)$$

where μ and f are defined by

$$\begin{aligned} \mu &= \begin{cases} \mu_1 & \text{in } \Omega_1, \\ \mu_2 & \text{in } \Omega_2, \end{cases} \\ f &= \begin{cases} f_1 & \text{in } \Omega_1, \\ f_2 & \text{in } \Omega_2. \end{cases} \end{aligned}$$

For the same reasons, problem (4.17) admits a unique solution \bar{u} in $H_0^1(\Omega)$.

Let us define the following subspace of $H^1(\Omega_2)'$:

$$V = \left\{ v \in H^1(\Omega_2)', \langle v, 1 \rangle_{H^1(\Omega_2)', H^1(\Omega_2)} = \int_{\Omega_2} f_2 \right\}.$$

The smooth extension problem associated to problem (4.17) is the problem of finding a suitable control g in V , such that the solution of the following weak problem,

$$\begin{cases} \text{find } u_1 \in H_0^1(\Omega) \text{ and } u_2 \in H^1(\Omega_2) \cap L_0^2(\Omega_2) \text{ such that} \\ \mu_1 \int_{\Omega} \nabla u_1 \cdot \nabla v_1 = \int_{\Omega_1} f_1 v_1|_{\Omega_1} + \langle g, v_1|_{\Omega_2} \rangle_{H^1(\Omega_2)', H^1(\Omega_2)}, & \forall v_1 \in H_0^1(\Omega), \\ \mu_2 \int_{\Omega_2} \nabla u_2 \cdot \nabla v_2 = \int_{\Omega_2} f_2 v_2 - \langle g, v \rangle_{H^1(\Omega_2)', H^1(\Omega_2)} \\ \quad + \int_{\Omega_2} \nabla u_1 \cdot \nabla v_2, & \forall v_2 \in H^1(\Omega_2), \end{cases} \quad (4.18)$$

enables to recover the solution \bar{u} of the initial Laplace problem (4.17).

Theorem 4.6. *Let Ω be a domain that satisfies Assumption (H_2) . For every $f_1 \in L^2(\Omega_1)$, every $f_2 \in L^2(\Omega_2)$ and every $g \in V$, problem (4.18) admits a unique solution (u_1^g, u_2^g) in $H_0^1(\Omega) \times (H^1(\Omega_2) \cap L_0^2(\Omega_2))$. Moreover, there exists a control g such that (u_1^g, u_2^g) satisfies the following equality:*

$$u_1^g - \frac{1}{|\Gamma|} \int_{\Gamma} u_1^g = u_2^g - \frac{1}{|\Gamma|} \int_{\Gamma} u_2^g, \quad \text{on } \Gamma \quad (4.19)$$

and we can recover the solution of the initial Laplace problem (4.17):

$$\begin{aligned} \bar{u}|_{\Omega_1} &= u_1^g|_{\Omega_1}, \\ \bar{u}|_{\Omega_2} &= u_2^g + \frac{1}{|\Gamma|} \left(\int_{\Gamma} (u_1^g - u_2^g) \right). \end{aligned} \quad (4.20)$$

Proof. Problem (4.18) is well-posed under the compatibility condition

$$\int_{\Omega_2} f_2 = \langle g, 1 \rangle_{H^{-1/2}(\Gamma), H^{1/2}(\Gamma)},$$

which is satisfied if the control g belongs to the space V .

Now, we prove the existence of a suitable control g in V such that the equality (4.19) holds. We define

$$\begin{aligned} \bar{u}_1 &= \bar{u}|_{\Omega_1}, \\ \bar{u}_2 &= \bar{u}|_{\Omega_2}, \end{aligned}$$

and construct an extension of \bar{u}_1 in the whole space $H_0^1(\Omega)$. This is possible according to the Stein extension theorem (see [Adams and Fournier, 2003, Theorem 5.24]) which states that, for any bounded Lipschitz domain \mathcal{O} of \mathbb{R}^n , there exists a total extension operator, i.e. an extension operator from $H^m(\mathcal{O})$ into the whole space $H^m(\mathbb{R}^n)$, for all $m \geq 0$. We apply this theorem to \bar{u}_1 and we denote by $E\bar{u}_1$ the restriction to Ω of its total extension. Thus, if \bar{u}_1 belongs to $H^m(\Omega_1) \cap V_1$ for $m \geq 1$, the extension $E\bar{u}_1$ belongs to $H^m(\Omega) \cap H_0^1(\Omega)$. In particular, if \bar{u}_1 belongs to $H^2(\Omega_1) \cap V_1$, $E\bar{u}_1$ belongs to $H^2(\Omega) \cap H_0^1(\Omega)$. Then, we construct g in $H^1(\Omega_2)'$ such that

$$\begin{aligned} \langle g, v_2 \rangle_{H^1(\Omega_2)', H^1(\Omega_2)} &= \mu_1 \int_{\Omega_2} \nabla(E\bar{u}_1) \cdot \nabla v_2 \\ &\quad + \mu_1 \langle \gamma_{n_1}(\nabla E\bar{u}_1), v_2 \rangle_{H^{-1/2}(\Gamma), H^{1/2}(\Gamma)}, \quad \forall v_2 \in H^1(\Omega_2). \end{aligned} \quad (4.21)$$

Moreover, using equality (4.4), it follows that, for all v in $H^1(\Omega_2)$,

$$\begin{aligned} \langle g, v_2 \rangle_{H^1(\Omega_2)', H^1(\Omega_2)} &= \mu_1 \int_{\Omega_2} \nabla(E\bar{u}_1) \cdot \nabla v_2 - \langle \mu_2 \gamma_{n_2}(\nabla \bar{u}_2), v_2 \rangle_{H^{-1/2}(\Gamma), H^{1/2}(\Gamma)}, \\ &= \mu_1 \int_{\Omega_2} \nabla(E\bar{u}_1) \cdot \nabla v_2 - \mu_2 \int_{\Omega_2} \Delta \bar{u}_2 v_2 - \mu_2 \int_{\Omega_2} \nabla \bar{u}_2 \cdot \nabla v_2, \\ &= \mu_1 \int_{\Omega_2} \nabla(E\bar{u}_1) \cdot \nabla v_2 + \int_{\Omega_2} f_2 v_2 - \mu_2 \int_{\Omega_2} \nabla \bar{u}_2 \cdot \nabla v_2. \end{aligned}$$

In particular, taking $v = 1$ in $H^1(\Omega_2)$, it proves that the control g belongs to the space V .

Now, using the Stokes formula (4.3), the extension $E\bar{u}_1$ satisfies, for all v_1 in $H_0^1(\Omega)$,

$$\begin{aligned} \mu_1 \int_{\Omega} \nabla(E\bar{u}_1) \cdot \nabla v_1 &= \mu_1 \int_{\Omega_1} \nabla(E\bar{u}_1) \cdot \nabla v_1 + \mu_1 \int_{\Omega_2} \nabla(E\bar{u}_1) \cdot \nabla v_1, \\ &= \int_{\Omega_1} f_1 v_1 + \mu_1 \langle \gamma_{n_1}(\nabla E\bar{u}_1), v_1 \rangle_{H^{-1/2}(\Gamma), H^{1/2}(\Gamma)} \\ &\quad + \mu_1 \int_{\Omega_2} \nabla(E\bar{u}_1) \cdot \nabla v_1, \\ &= \int_{\Omega_1} f_1 v_1 + \langle g, v_1 \rangle_{V_2', V_2}. \end{aligned}$$

Similarly, the function $\tilde{u}_2 = \bar{u}_2 - \frac{1}{|\Omega_2|} \int_{\Omega_2} \bar{u}_2$ belongs to $H^1(\Omega_2) \cap L_0^2(\Omega_2)$ and satisfies, for all $v_2 \in H^1(\Omega_2)$,

$$\begin{aligned} \mu_2 \int_{\Omega_2} \nabla \tilde{u}_2 \cdot \nabla v_2 &= \mu_2 \int_{\Omega_2} \nabla \bar{u}_2 \cdot \nabla v_2, \\ &= \int_{\Omega_2} f_2 v_2 + \mu_1 \langle \gamma_{n_1}(\nabla E\bar{u}_1), v_2 \rangle_{H^{-1/2}(\Gamma), H^{1/2}(\Gamma)} \end{aligned}$$

It follows that $(E\bar{u}_1, \tilde{u}_2)$ is the solution of (4.18), i.e.

$$(u_1^g, u_2^g) = (E\bar{u}_1, \tilde{u}_2).$$

Moreover, on Γ we have

$$\begin{aligned} u_1^g - \frac{1}{|\Gamma|} \int_{\Gamma} u_1^g &= \bar{u}_2 - \frac{1}{|\Gamma|} \int_{\Gamma} \bar{u}_2, \\ &= u_2^g + \frac{1}{|\Omega_2|} \int_{\Omega_2} \bar{u}_2 - \frac{1}{|\Gamma|} \int_{\Gamma} (u_2^g + \frac{1}{|\Omega_2|} \int_{\Omega_2} \bar{u}_2), \\ &= u_2^g - \frac{1}{|\Gamma|} \int_{\Gamma} u_2^g, \end{aligned}$$

which proves equality (4.19).

Finally, the solution (\bar{u}_1, \bar{u}_2) of the Laplace problem (4.17) can be recovered from the couple (u_1^g, u_2^g) :

$$\begin{aligned} \bar{u}_1 &= u_{1|\Omega_1}^g, \\ \bar{u}_2 &= u_2^g + C, \end{aligned}$$

where the constant C can be determined by integrating the difference $\bar{u}_2 - u_2^g$ on Γ :

$$\int_{\Gamma} C = \int_{\Gamma} (\bar{u}_2 - u_2^g) = \int_{\Gamma} (u_1^g - u_2^g),$$

which leads to

$$C = \frac{1}{|\Gamma|} \int_{\Gamma} (u_1^g - u_2^g).$$

□

Theorem 4.6 implies that, if we can construct a suitable control g , then we are able to recover the solution of the Laplace transmission problem (4.17) from the resolution of the smooth extension problem (4.18). To obtain such a control, we can solve the following optimization problem:

$$\min_{g \in V} J(g) = \frac{1}{2} \int_{\Gamma} \left| u_1^g - u_1^g + \frac{1}{|\Gamma|} \int_{\Gamma} (u_2^g - u_1^g) \right|^2. \quad (4.22)$$

Problem (4.22) admits at least one solution, according to Theorem 4.6, which corresponds to a zero of the cost function J . As before, one can show that if g is a minimizer of J , the solution (u_1^g, u_2^g) of problem (4.18) can be used to recover the solution of the Laplace transmission problem, with formulas (4.20). The proof is similar to what we have done in Subsection 4.2.2 and is left to the reader.

4.3 Validation of the method

In Subsection 4.2.2 we have proved the equivalence between the initial coupled problem and the smooth extension formulation stated as a minimization problem. Based on this result, we detail the numerical procedure used to solve the smooth extension formulation of the Laplace transmission problem presented above. In particular, in Subsection 4.3.1, we explain how to minimize the function J defined in (4.9) using its gradient. Thereafter, we present in Subsection 4.3.2, Subsection 4.3.3 and Subsection 4.3.4 some numerical experiments obtained through this process.

4.3.1 Numerical procedure for the smooth extension method

To solve the smooth extension formulation of problem (4.2), we consider an optimization problem whose solution allows to directly recover the solution of the initial transmission problem. In the case of the Laplace transmission problem, it gives the right control term g for which the solution u_1^g of problem (4.6) is a smooth extension of \bar{u}_1 in the whole domain Ω . Then, instead of directly finding \bar{u}_1 and \bar{u}_2 by solving a Laplace problem with discontinuous coefficients, one solves a minimization problem on the control g . As already explained, this formulation is advantageous for the numerical resolution because it allows the use of non-conformal meshes on Ω . Thus, the smooth extension method is a fictitious domain method in the sense that the various problems appearing in the numerical resolution process are solved on two meshes, one for Ω and an other for Ω_2 which are not conformal.

An explicit formula is provided for the computation of the gradient of the cost function to minimize (see Theorem 4.3), which enables to treat the minimization problem with a classical descent method. The general algorithm that we use is the following: we choose an initial guess g_0 for the control term. For each iteration k of the gradient algorithm, we first solve problem (4.6) with $g = g_k$ and obtain the couple $(u_1^{g_k}, u_2^{g_k})$. Then, we solve the adjoint problem (4.13) with $g = g_k$ to get the adjoint variables $(\lambda_1^{g_k}, \lambda_2^{g_k})$. The gradient $\nabla J(g_k)$ is computed using the explicit formula given by Theorem 4.3. Finally, the control is updated using the chosen optimization algorithm. The general formula for the update can be written

$$g_{k+1} = g_k - \rho_k \nabla J(g_k),$$

where ρ_k is either a real positive parameter or a matrix, depending on the chosen optimization algorithm. This process is summarized in the Algorithm 4.1.

Algorithm 4.1 Implementation of the smooth extension method

Choose an initial guess g_0 for the control term.

$k = 0$.

tant que exit criteria are not satisfied **faire**

 Compute the solution $(u_1^{g_k}, u_2^{g_k})$ of problem (4.6) with $g = g_k$.

 Compute the solution $(\lambda_1^{g_k}, \lambda_2^{g_k})$ of the adjoint problem (4.13) with $g = g_k$.

 Compute the gradient $\nabla J(g_k) = \lambda_2^{g_k} - \lambda_1^{g_k}|_{\Omega_2}$.

 Update the control $g_{k+1} = g_k - \rho_k \nabla J(g_k)$, with ρ_k depending on the chosen gradient method.

 Update the number of iterations $k = k + 1$.

fin tant que

In practice, the exit criteria for a descent method usually concern the norm of the difference between two successive solutions $\|g_{k+1} - g_k\|$ divided by the update coefficient ρ_k . The choice of the initial guess g_0 is of minor importance for the convergence of the algorithm since, as we explained in Remark 4.7, every extremum of the cost function J corresponds to one of its minimizers.

4.3.2 Test case 1: the transmission Laplace problem in the unit square

Let Ω be the unit square of \mathbb{R}^2 , divided in two pieces by a vertical segment which represents the interface Γ (see Figure 4.3). We denote by x_Γ the position of this interface on the x -axis. We aim to apply the smooth extension method to the Laplace transmission problem (4.1) with homogeneous Dirichlet boundary conditions, studied in Subsection 4.2.1. Because the interface Γ meets the boundary $\partial\Omega$ with a right-angled corner and because f_1

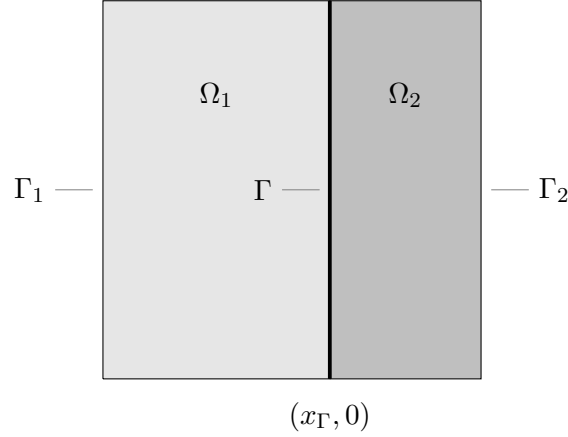


Figure 4.3 – Two dimensional representation of the geometry for the Laplace transmission problems (4.1).

and f_2 are constants, the solution of (4.1), denoted by \bar{u} , is partially of regularity H^2 , i.e. $\bar{u}|_{\Omega_1}$ belongs to $H^2(\Omega_1)$ and $\bar{u}|_{\Omega_2}$ belongs to $H^2(\Omega_2)$. Moreover, because Γ is a straight line, we can construct a H^2 -extension of $\bar{u}|_{\Omega_1}$ in the whole space $H^2(\Omega) \cap H_0^1(\Omega)$. This is done using the Babič extension (see [Babič, 1953] or [Adams and Fournier, 2003, Theorem 5.19]), defined for all $0 < x_\Gamma < 1$ and for all $0 \leq x, y \leq 1$ by

$$E\bar{u}|_{\Omega_1}(x, y) = \begin{cases} \bar{u}(x, y), & \text{if } x \leq x_\Gamma, \\ \frac{x_\Gamma - 2}{x_\Gamma} \bar{u}\left(\frac{x_\Gamma(x-1)}{x_\Gamma-1}, y\right) + \frac{2}{x_\Gamma} \bar{u}\left(\frac{1}{2} \frac{x_\Gamma(x-1)}{x_\Gamma-1}, y\right), & \text{if } x > x_\Gamma. \end{cases}$$

It is straightforward to see that $E\bar{u}|_{\Omega_1}$ and its first order partial derivatives are continuous through Γ , then $E\bar{u}|_{\Omega_1}$ well defines an extension of $\bar{u}|_{\Omega_1}$ in $H^2(\Omega)$. Furthermore, we can see that

$$E\bar{u}|_{\Omega_1}(x, 0) = E\bar{u}|_{\Omega_1}(x, 1) = 0.$$

Then, it remains to multiply this extension by a cut function such that it is zero on $\partial\Omega$. To do that we consider two real values α and β in $]0, 1[$ such that $\alpha < \beta$ and we define the following cut function:

$$\chi(x) = \begin{cases} 1, & \text{if } x_\Gamma \leq x \leq x_\alpha, \\ \frac{(2x^3 - 3(x_\alpha + x_\beta)x^2 + 6x_\alpha x_\beta x + x_\beta^2(x_\beta - 3x_\alpha))}{(x_\beta - x_\alpha)^3}, & \text{if } x_\alpha < x \leq x_\beta, \\ 0, & \text{if } x_\beta < x \leq 1, \end{cases}$$

where

$$x_\alpha = x_\Gamma + \alpha(1 - x_\Gamma), \quad x_\beta = x_\Gamma + \beta(1 - x_\Gamma).$$

Because χ is regular enough, it follows that $E\bar{u}|_{\Omega_1}\chi$ belongs to $H^2(\Omega) \cap H_0^1(\Omega)$. Thus, all conditions are satisfied so that the smooth extension method applied to this problem converges with optimal rates.

The numerical values of all parameters are $\mu_1 = 1$, $\mu_2 = 10$, $f_1 = 1$, $f_2 = 1$ and $x_\Gamma = 0.57$. An approximation of the solution \bar{u} of (4.1), obtained with the classical finite element method, is represented in Figure 4.4. Because of the jump of its gradient through Γ , the

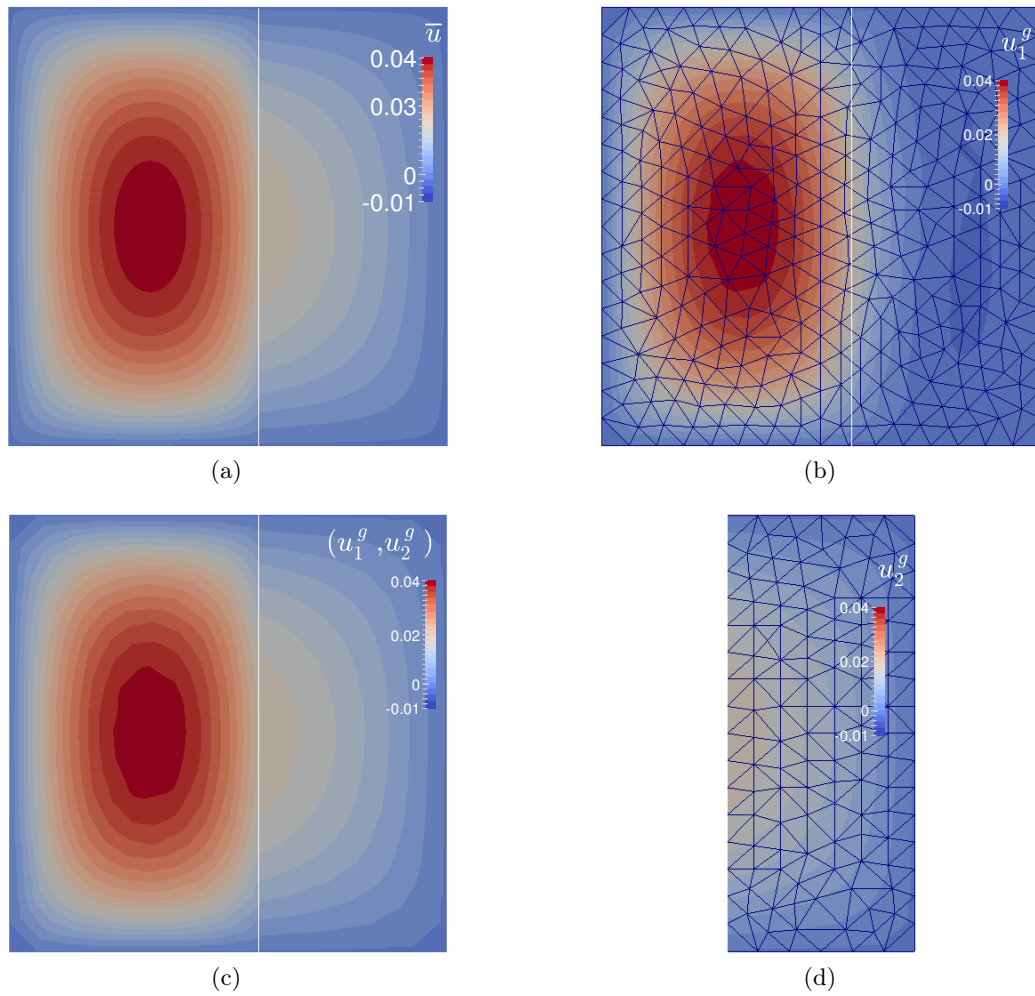


Figure 4.4 – Numerical solution for the Laplace problem (4.1) with $\mu_1 = 1$, $\mu_2 = 10$, $f_1 = 1$, $f_2 = 1$ and $x_\Gamma = 0.57$. We compare the reference solution \bar{u} obtained with the standard finite element method on a fine mesh (a) to the one obtained through the smooth extension method (c). The fields u_1^g (b) and u_2^g (d) are superposed (c) to show the continuity through the interface Γ despite the use of non-conformal meshes. For the SEM, the mesh is 16×16 .

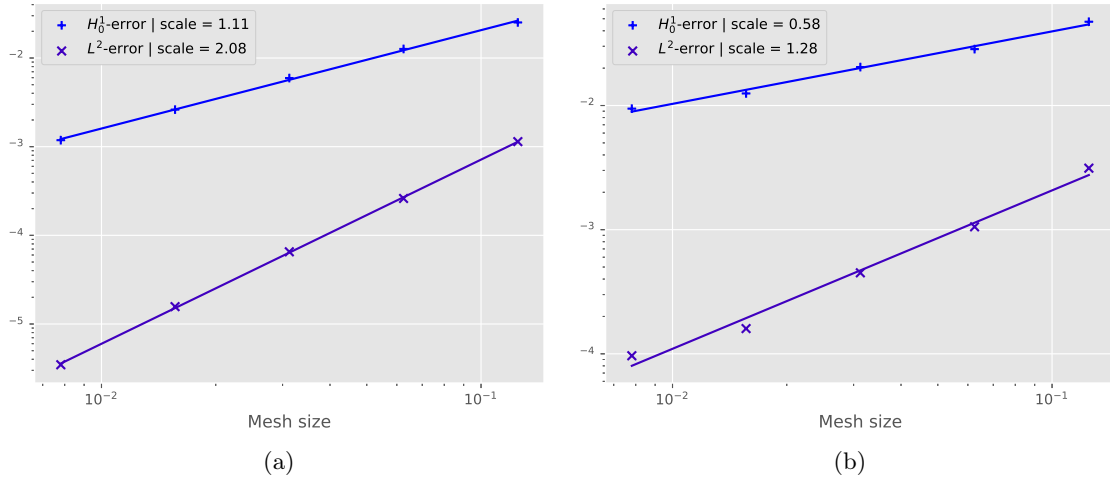


Figure 4.5 – Rates of convergence in space for the finite element method ($P1$ elements) applied to the resolution of the Laplace problem (4.1) with $\mu_1 = 1$, $\mu_2 = 10$, $f_1 = 1$, $f_2 = 1$ and $x_\Gamma = 0.57$. The solution with a conformal mesh (a) is compared to the one with a non-conformal mesh (b)

entire field \bar{u} does not belong to $H^2(\Omega)$. As a consequence, the use of the classical finite element method to approach the solution of (4.1) leads to different rates of convergence when refining the space discretization, whether the mesh of the domain fits the interface Γ or not. Indeed, in Figure 4.5 we can observe that if the mesh fits the interface Γ , the rates of convergence are of order 2 for the L^2 -norm and of order 1 for the H_0^1 -norm, using $P1$ elements. These are the classical rates of convergence with $P1$ elements for a H^2 solution of a Laplace problem, which is not the case here. Then, this result is only due to the fact that the interface Γ is well represented by the mesh. On the other hand, if the mesh does not fit the interface, we recover degraded rates of convergence: here we find a rate of order 1 in L^2 -norm and 0.5 in H_0^1 -norm.

For the numerical resolution with the smooth extension method, we follow Algorithm 4.1. In particular, we choose the initial guess g_0 to be zero and use a classical gradient descent with constant parameter ρ to minimize J . The value of ρ is chosen such that the gradient method converges and can be different depending on the mesh size. We use unstructured meshes for both Ω and Ω_2 , such that the interface Γ is not represented by the mesh on Ω . At each iteration of the method, we solve 4 second-order boundary problems (the direct and adjoint equations) using $P1$ elements, whose solutions enable us to compute the gradient $\nabla J(g_k)$. Then, we update the control such that,

$$g_{k+1} = g_k - \rho \nabla J(g_k).$$

We also compute the residual error,

$$\frac{\|g_{k+1} - g_k\|}{\rho}, \quad (4.23)$$

and stop the algorithm if it is smaller than a given tolerance ε . This method shows to easily converge to an optimal control.

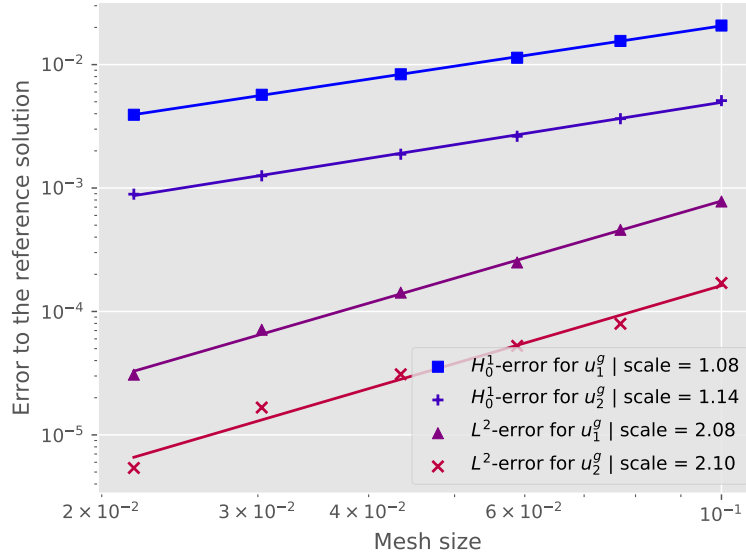


Figure 4.6 – Rates of convergence in space for the smooth extension method applied to the resolution of the Laplace transmission problem with homogeneous boundary conditions (4.1), with $\mu_1 = 1$, $\mu_2 = 10$, $f_1 = 1$, $f_2 = 2$ and $x_\Gamma = 0.67$.

The solution of (4.1) obtained through the minimization of the function J is represented in Figure 4.4. It is clear that $u_1^g|_{\Omega_1}$ and u_2^g are approximations of $\bar{u}|_{\Omega_1}$ and $\bar{u}|_{\Omega_2}$. Moreover, superposing these two solutions, we can observe that the condition on the equality of u_1^g and u_2^g on Γ is fulfilled. Refining the mesh, we compute the L^2 and H_0^1 -errors between the couple (u_1^g, u_2^g) and the reference solution obtained with the classical Finite Element method and using a fine conformal mesh. We obtain the convergence graph presented in Figure 4.6 where we observe that optimal rates of convergence are conserved by the smooth extension method in this case.

4.3.3 Test case 2: the transmission Laplace problem with a spherical inclusion

Let Ω be the unit square of \mathbb{R}^2 and let Ω_2 be the disk of center (x_c, y_c) and radius r_c , strictly included in Ω (see Figure 4.7). We aim to apply the smooth extension method to the Laplace transmission problem (4.17) with a strictly included domain Ω_2 in Ω , studied in Subsection 4.2.4. Because the interface Γ is smooth and Ω is convex, the solution of (4.17), denoted \bar{u} , is partially of regularity H^2 . Moreover, we have seen in Subsection 4.2.4 that it is possible to construct an extension of $\bar{u}|_{\Omega_1}$ in the whole space $H^2(\Omega) \cap H_0^1(\Omega)$. Then, this test case is particularly adapted to the use of the smooth extension method, which enables to recover the optimal rates of convergence in space with non-conformal meshes, whereas the classical finite element method does not.

Choosing the set of parameters, $\mu_1 = 1$, $\mu_2 = 10$, $f_1 = 1$, $f_2 = 2$, $(x_c, y_c) = (0.62, 0.43)$ and $r_c = 0.2$, we apply the smooth extension method to this transmission problem and obtain the convergence graph presented in Figure 4.8, where we observe, one more time, that optimal rates of convergence are preserved by the smooth extension method.

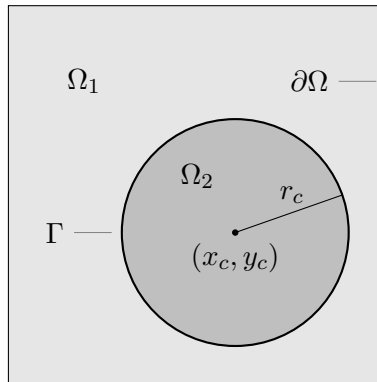


Figure 4.7 – Two dimensional representation of the geometry for the Laplace transmission problem (4.17).

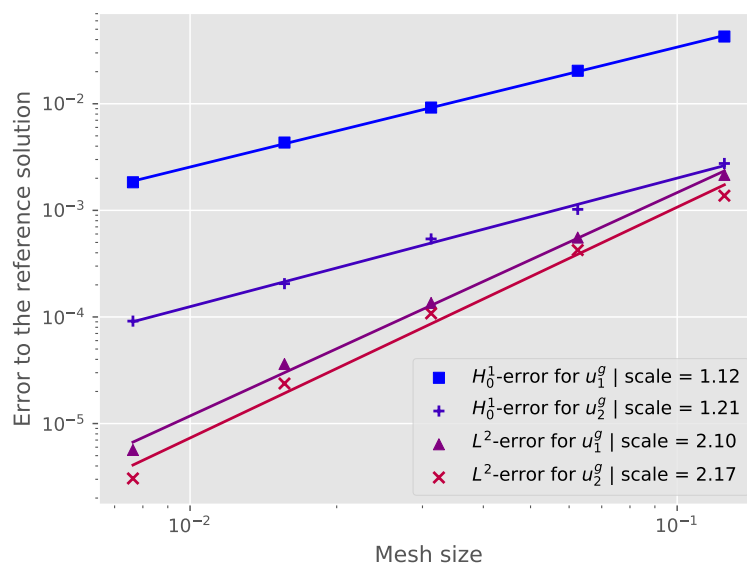


Figure 4.8 – Rates of convergence in space for the smooth extension method applied to the resolution of the Laplace transmission problem with a strictly included subdomain Ω_2 (4.17), for $\mu_1 = 1$, $\mu_2 = 10$, $f_1 = 1$, $f_2 = 2$, $(x_c, y_c) = (0.62, 0.43)$ and $r_c = 0.2$.

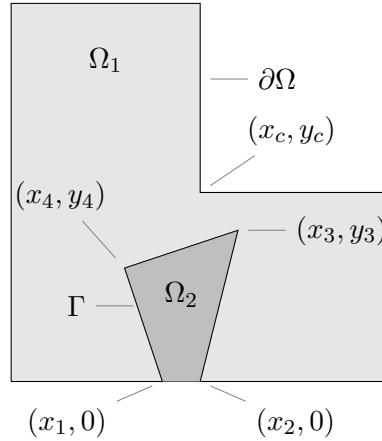


Figure 4.9 – Two dimensional representation of the geometry for the Laplace transmission problem (4.1) in a L-shape domain.

4.3.4 Test case 3: the transmission Laplace problem in a L-shape domain

Let Ω be a L-shape domain of \mathbb{R}^2 and let Ω_2 be a quadrilateral included in Ω (see Figure 4.9). As before, we apply the smooth extension method to the Laplace transmission problem with homogeneous Dirichlet boundary condition (4.1). Because of the geometry of the problem and especially the presence of a reentrant corner, the solution is not regular and only belongs to $H_0^1(\Omega)$. Thus, there do not exist a H^2 -extension from Ω_1 to the whole domain and the method will not converge with optimal order. However, the smooth extension method can also be applied in this case and we will see that it is still better than the Finite Element method with non-conformal mesh (see Table 4.1). Considering the set of parameters $\mu_1 = 1$, $\mu_2 = 10$, $f_1 = 1$, $f_2 = 1$, $(x_c, y_c) = (0.62, 0.7)$, $x_1 = 0.43$, $x_2 = 0.58$, $(x_3, y_3) = (0.36, 0.38)$ and $(x_4, y_4) = (0.64, 0.49)$, we obtain the convergence graph represented in Figure 4.9.

To summarise the results obtained for all test cases that we have studied, the convergence rates are presented in Table 4.1. As a result, the Smooth Extension method applied to the Laplace transmission problem, converges with optimal rates even with non-conformal meshes when the solution of the Laplace transmission problem is partially of regularity H^2 . When the solution is less regular (because of the geometry of the domain or the regularity of the right-hand sides) the Smooth Extension method can also be applied and showed to converge with the same rates than the Finite Element method with conformal mesh. In the next section we will show that this method can be extended to other kind of coupled problems and enables to treat the numerical resolution of more general transmission problems with non-conformal meshes.

4.4 Extension to other coupled problems

In this section we extend the smooth extension method to two other coupled problems: the Stokes transmission problem in Subsection 4.4.1 and a fluid-structure interaction problem in Subsection 4.4.2.

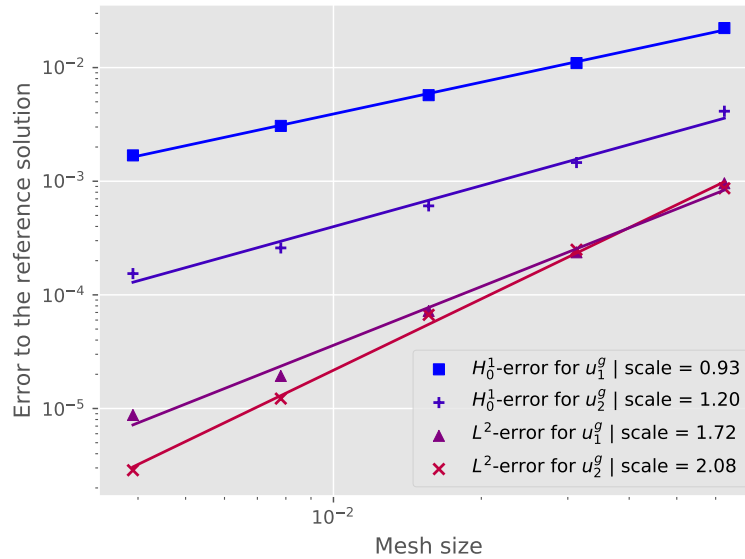


Figure 4.10 – Rates of convergence in space for the smooth extension method applied to the resolution of the Laplace transmission problem (4.1) in a L-shape domain.

Test case	Method	Mesh conformity	conv. rate in H_0^1 -norm	conv. rate in L^2 -norm
1	FEM	Conformal	1.11	2.08
1	FEM	Non-conformal	0.58	1.28
1	SEM	Non-conformal	1.08 (in Ω_1) / 1.14 (in Ω_2)	2.08 (in Ω_1) / 2.1 (in Ω_2)
2	FEM	Conformal	1.06	2.13
2	FEM	Non-conformal	0.58	1.04
2	SEM	Non-conformal	1.12 (in Ω_1) / 1.21 (in Ω_2)	2.1 (in Ω_1) / 2.17 (in Ω_2)
3	FEM	Conformal	0.96	1.7
3	FEM	Non-conformal	0.76	1.43
3	SEM	Non-conformal	0.93 (in Ω_1) / 1.2 (in Ω_2)	1.72 (in Ω_1) / 2.08 (in Ω_2)

Table 4.1 – Comparison of the rates of convergence between the finite element method (FEM) with a conformal mesh, the FEM with a non-conformal mesh and the smooth extension method (SEM) with a non-conformal mesh for different test cases.

4.4.1 The Stokes transmission problem

Let $n > 0$ and Ω be a domain of \mathbb{R}^n that satisfies the following set of hypotheses:

- i) Domain Ω is a bounded connected Lipschitz domain of \mathbb{R}^n .
 - ii) Domain Ω is divided into two connected Lipschitz subdomains, Ω_1 and Ω_2 .
 - iii) The interface $\Gamma = \partial\Omega_1 \cap \partial\Omega_2$ is not empty.
 - iv) The remaining boundaries $\Gamma_1 = \partial\Omega_1 \setminus \Gamma$ and $\Gamma_2 = \partial\Omega_2 \setminus \Gamma$ are not empty.
- (H₃)

Consider two real coefficients, μ_1 and μ_2 , and two external forces, f_1 in $(L^2(\Omega_1))^n$ and f_2 in $(L^2(\Omega_2))^n$. Then, the Stokes transmission problem writes:

$$\left\{ \begin{array}{ll} \text{find } u_1: \Omega_1 \rightarrow \mathbb{R}^n, p_1: \Omega_1 \rightarrow \mathbb{R}, u_2: \Omega_2 \rightarrow \mathbb{R}^n \text{ and } p_2: \Omega_2 \rightarrow \mathbb{R} \text{ such that} \\ \quad -\mu_1 \Delta u_1 + \nabla p_1 = f_1, & \text{in } \Omega_1, \\ \quad \operatorname{div}(u_1) = 0, & \text{in } \Omega_1, \\ \quad u_1 = 0, & \text{on } \Gamma_1, \\ \quad -\mu_2 \Delta u_2 + \nabla p_2 = f_2, & \text{in } \Omega_2, \\ \quad \operatorname{div}(u_2) = 0, & \text{in } \Omega_2, \\ \quad u_2 = 0, & \text{on } \Gamma_2, \\ \quad u_1 = u_2, & \text{on } \Gamma, \\ (\mu_1 \nabla u_1 - p_1 I) \cdot n_1 = -(\mu_2 \nabla u_2 - p_2 I) \cdot n_2, & \text{on } \Gamma. \end{array} \right. \quad (4.24a)$$

Equations (4.24a) and (4.24b) are two sets of Stokes equations coupled at the interface Γ with the coupling conditions (4.24c). These conditions represent the continuity of the fluid velocity and the continuity of the constraints applied by the fluid on Γ . The vectors n_1 and n_2 still denote the unit exterior normal vector of Ω_1 and Ω_2 . Of course, problem (4.24) is equivalent to the Stokes problem with discontinuous viscosity and external force,

$$\left\{ \begin{array}{ll} \text{find } u: \Omega \rightarrow \mathbb{R}^n \text{ and } p: \Omega \rightarrow \mathbb{R} \text{ such that} \\ \quad -\operatorname{div}(\mu \nabla u - p I) = f & \text{in } \Omega, \\ \quad \operatorname{div}(u) = 0 & \text{in } \Omega, \\ \quad u = 0 & \text{on } \partial\Omega, \end{array} \right. \quad (4.25)$$

where μ and f are defined by

$$\mu = \begin{cases} \mu_1 & \text{in } \Omega_1 \\ \mu_2 & \text{in } \Omega_2 \end{cases}, \quad f = \begin{cases} f_1 & \text{in } \Omega_1 \\ f_2 & \text{in } \Omega_2 \end{cases}.$$

We can define a weak formulation of problem (4.24). Let us introduce the functional spaces

$$\begin{aligned} W_1 &= \{v_1 \in (H^1(\Omega_1))^n; v_1|_{\Gamma_1} = 0\}, \\ W_2 &= \{v_2 \in (H^1(\Omega_2))^n; v_2|_{\Gamma_2} = 0\}, \\ \mathcal{W} &= \{(v_1, v_2) \in W_1 \times W_2; v_1|_{\Gamma} = v_2|_{\Gamma}\}, \\ Q &= \left\{ (p_1, p_2) \in L^2(\Omega_1) \times L^2(\Omega_2); \frac{1}{|\Omega|} \left(\int_{\Omega_1} p_1 + \int_{\Omega_2} p_2 \right) = 0 \right\}, \\ (H_{\operatorname{div}}(X))^n &= \{\sigma \in (L^2(X))^{n \times n}; \operatorname{div}(\sigma) \in (L^2(X))^n\}, \end{aligned}$$

Let v be in $(\mathcal{D}(\Omega))^n$ and suppose that u_1 , p_1 , u_2 and p_2 are sufficiently regular. Moreover, we assume for the moment that g belongs to $(L^2(\Omega_2))^n$ in order to do formal computations. Formally, we multiply equation (4.29a) by v and equation (4.29b) by $v|_{\Omega_2}$ and integrate respectively over Ω and Ω_2 . After an integration by part and using the Neumann condition on Γ , we find

$$\begin{aligned} \mu_1 \int_{\Omega} \nabla u_1 : \nabla v - \int_{\Omega} p_1 \operatorname{div}(v) &= \int_{\Omega_1} f_1 \cdot v|_{\Omega_1} + \int_{\Omega_2} g \cdot v|_{\Omega_2}, \\ \mu_2 \int_{\Omega_2} \nabla u_2 : \nabla v|_{\Omega_2} - \int_{\Omega_2} p_2 \operatorname{div}(v|_{\Omega_2}) &= \int_{\Omega_2} f_2 \cdot v|_{\Omega_2} + \int_{\Gamma} ((\mu_1 \nabla u_1 - p_1 I)n_2) \cdot v. \end{aligned}$$

Moreover, we remark that

$$\begin{aligned} \int_{\Gamma} ((\mu_1 \nabla u_1 - p_1 I)n_2) \cdot v &= \int_{\Omega_2} (\mu_1 \Delta u_1 - \nabla p_1) \cdot v|_{\Omega_2} + \mu_1 \int_{\Omega_2} \nabla u_1 : \nabla v|_{\Omega_2} \\ &\quad - \int_{\Omega_2} p_1 \operatorname{div}(v|_{\Omega_2}), \\ &= - \int_{\Omega_2} g \cdot v|_{\Omega_2} + \mu_1 \int_{\Omega_2} \nabla u_1 : \nabla v|_{\Omega_2} \\ &\quad - \int_{\Omega_2} p_1 \operatorname{div}(v|_{\Omega_2}). \end{aligned}$$

Thus, we define the weak formulation of the smooth extension problem associated to problem (4.29), which makes sense for $g \in W_2'$, as the problem of finding a suitable control g in W_2' , such that the solution of the following problem,

$$\left\{ \begin{array}{l} \text{find } (u_1, p_1) \in (H_0^1(\Omega))^n \times L_0^2(\Omega) \text{ and } (u_2, p_2) \in W_2 \times L^2(\Omega_2) \text{ such that} \\ \mu_1 \int_{\Omega} \nabla u_1 : \nabla v_1 - \int_{\Omega} p_1 \operatorname{div}(v_1) \\ \qquad \qquad \qquad = \int_{\Omega_1} f_1 \cdot v_1|_{\Omega_1} + \langle g, v_1|_{\Omega_2} \rangle_{W_2', W_2}, \quad \forall v_1 \in (H_0^1(\Omega))^n, \\ \int_{\Omega} q_1 \operatorname{div}(u_1) = 0, \quad \forall q_1 \in L_0^2(\Omega), \\ \mu_2 \int_{\Omega_2} \nabla u_2 : \nabla v_2 - \int_{\Omega_2} p_2 \operatorname{div}(v_2) \\ \qquad \qquad \qquad = \int_{\Omega_2} f_2 \cdot v_2 - \langle g, v_2 \rangle_{W_2', W_2} \\ \qquad \qquad \qquad + \mu_1 \int_{\Omega_2} \nabla u_1 : \nabla v_2 - \int_{\Omega_2} p_1 \operatorname{div}(v_2), \quad \forall v_2 \in W_2, \\ \int_{\Omega_2} q_2 \operatorname{div}(u_2) = 0, \quad \forall q_2 \in L^2(\Omega_2), \end{array} \right. \quad (4.30)$$

satisfies the equality

$$u_1 = u_2, \quad \text{on } \Gamma. \quad (4.31)$$

For every f_1 in $(L^2(\Omega_1))^n$, every f_2 in $(L^2(\Omega_2))^n$ and every g in W_2' , the two subproblems in problem (4.30) admit a unique solution. They are denoted by (w_1^g, p_1^g) and (w_2^g, p_2^g) . These are well-known results on Stokes equations; we refer to [Boyer and Fabrie, 2012] for details. In the following theorem, we state the existence of a control g such that the solution of (4.30) satisfies the condition (4.31) and explain how to recover the solution of the initial Stokes transmission problem (4.26).

Theorem 4.7. *Let Ω be a domain that satisfies Assumption (H_3) . Consider f_1 in $(L^2(\Omega_1))^n$ and f_2 in $(L^2(\Omega_2))^n$. Then, there exists a function g in W'_2 such that the solution $((w_1^g, p_1^g), (w_2^g, p_2^g))$ of (4.30) satisfies (4.31). Moreover, we can recover the solution of the Stokes transmission problem (4.26):*

$$\begin{aligned}(\bar{w}_1, \bar{w}_2) &= (w_{1|\Omega_1}^g, w_2^g), \\(\bar{p}_1, \bar{p}_2) &= (p_{1|\Omega_1}^g - C, p_2^g - C),\end{aligned}$$

where

$$C = \frac{1}{|\Omega|} \left(\int_{\Omega_1} p_{1|\Omega_1}^g + \int_{\Omega_2} p_2^g \right).$$

The proof of Theorem 4.7 is similar to the proof of Theorem 4.1. It relies on the construction of extensions for the velocity \bar{w}_1 and the pressure \bar{p}_1 in the whole domain Ω . Details are given in Section A.1.

As before, the problem of finding a suitable control g such that the solution of problem (4.30) satisfies (4.31), can be formulated as an optimization problem. In practice, it is this minimization problem which is solved in order to obtain a suitable control and recover the solution of the transmission problem (4.24). The cost function to consider, that we denote by \tilde{J} , is now defined from W'_2 to \mathbb{R}^+ with the formula

$$\tilde{J}(g) = \frac{1}{2} \int_{\Gamma} |w_1^g - w_2^g|^2, \quad (4.32)$$

where w_1^g and w_2^g are the velocities of the fluid, solutions of problem (4.30). Yet, the minimization of this cost function is equivalent to the minimization of the real-valued function

$$\begin{aligned}(H_0^1(\Omega))^n \times W_2 &\rightarrow \mathbb{R}^+ \\(v_1, v_2) &\mapsto \frac{1}{2} \int_{\Gamma} |v_{1|\Gamma} - v_{2|\Gamma}|^2,\end{aligned}$$

under the constraint that v_1 and v_2 are the velocities that solve the problem (4.30). Then, to this constrained optimization problem we associate the following Lagrangian function defined from

$$W'_2 \times [((H_0^1(\Omega))^n \times L_0^2(\Omega)) \times (W_2 \times L^2(\Omega_2))] \times [((H_0^1(\Omega))^n \times L_0^2(\Omega)) \times (W_2 \times L^2(\Omega_2))]$$

to \mathbb{R} by

$$\begin{aligned}\tilde{\mathcal{L}}(g, ((u_1, p_1), (u_2, p_2)), ((\lambda_1, \pi_1), (\lambda_2, \pi_2))) &= \\&\frac{1}{2} \int_{\Gamma} |u_1 - u_2|^2 + \mu_1 \int_{\Omega} \nabla u_1 : \nabla \lambda_1 - \mu_1 \int_{\Omega_2} \nabla u_1 : \nabla \lambda_2 + \mu_2 \int_{\Omega_2} \nabla u_2 : \nabla \lambda_2 \\&- \int_{\Omega} p_1 \operatorname{div}(\lambda_1) - \int_{\Omega} \pi_1 \operatorname{div}(u_1) - \int_{\Omega_2} p_2 \operatorname{div}(\lambda_2) - \int_{\Omega_2} \pi_2 \operatorname{div}(u_2) + \int_{\Omega_2} p_1 \operatorname{div}(\lambda_2) \\&- \int_{\Omega_1} f_1 \cdot \lambda_{1|\Omega_1} - \langle g, \lambda_{1|\Omega_2} \rangle_{W'_2, W_2} - \int_{\Omega_2} f_2 \cdot \lambda_2 + \langle g, \lambda_2 \rangle_{W'_2, W_2}\end{aligned} \quad (4.33)$$

Again, this Lagrangian function enables to compute the gradient of \tilde{J} and it is possible to show the equivalence between the minimization of \tilde{J} and the research of a suitable control such that the solution of (4.30) satisfies the condition (4.31). For that matter, we introduce

we apply this method to the numerical simulation of a two-layer Stokes fluid in the unit square of \mathbb{R}^2 . The geometric settings are represented in Figure 4.11: Ω_1 and Ω_2 are separated by a smooth curve which encounters the boundary $\partial\Omega$ at two points, $(1, \alpha_\Gamma)$ and $(\beta_\Gamma, 1)$, where α_Γ and β_Γ are two positive constants. The interface Γ is defined such that a point (x, y) in $[\beta_\Gamma, 1] \times [\alpha_\Gamma, 1]$ belongs to Γ if and only if

$$1 - x \leq \beta_\Gamma \sqrt{\frac{y - \alpha_\Gamma}{y}}.$$

We consider homogeneous Dirichlet boundary conditions on the left and right boundaries and a pressure drop of 1 between the top and the bottom boundaries. No external force are considered and constant viscosities $\mu_1 = 1$ and $\mu_2 = 10$ are chosen. For the interface Γ , we choose $\alpha_\Gamma = 0.25$ and $\beta_\Gamma = 0.5$.

The solution given by the smooth extension method is obtained following Algorithm 4.1 and using the gradient method with fixed parameter ρ . This parameter is chosen such that the gradient method converges and the stopping criteria is defined in (4.23). The resolution of the four different Stokes problems appearing in the minimization process is done using Mini elements. To compare the smooth extension method to the classical finite element method, we use meshes that have about the same numbers of cells: 26×26 .

Results are shown in Figure 4.12, where both the velocity and the pressure of the fluid are plotted. We compare the solution obtained through the standard finite element method with a mesh which is actually conform with the interface Γ , to the one produced by the smooth extension method with unstructured meshes. We observe that both solutions are similar at the difference that the Smooth Extension method well represents the physical jump in pressure through the interface Γ , while the finite element method with Mini elements does not. Moreover, the former also has the advantage to be computed with a non-conformal mesh.

4.4.2 A fluid-structure interaction problem

Now, we are interested in the resolution of a fluid-structure problem where the fluid is modeled by the Stokes equations and the structure by the stationary equations of linear elasticity. The unknowns for these two systems of equations are the fluid velocity and pressure as well as the displacement of the structure from its reference configuration. The fluid problem will be set in Eulerian coordinates, i.e. in the current configuration, whereas the elastic equations will be written in Lagrangian coordinates, i.e. in the reference configuration. This amounts to consider two configurations for both problems, supposing that, at each time, there exists a smooth enough mapping between the two configurations to ensure that all boundaries in the current configuration are sufficiently regular.

Let $n > 0$ and Ω be a domain of \mathbb{R}^n that satisfies the following set of hypotheses:

- i)* Domain Ω is a bounded connected Lipschitz domain of \mathbb{R}^n .
- ii)* Domain Ω is divided in two connected Lipschitz subdomains, Ω_f the fluid subdomain and Ω_s the solid subdomain. (H₄)
- iii)* The interface $\Gamma = \partial\Omega_f \cap \partial\Omega_s$ is not empty.
- iv)* The remaining boundaries $\Gamma_f = \partial\Omega_f \setminus \Gamma$ and $\Gamma_s = \partial\Omega_s \setminus \Gamma$ are not empty.

We assume that, at each time $t \geq 0$, there exists a deformation Φ_t , i.e. a smooth enough injective and orientation-preserving mapping, defined from Ω to \mathbb{R}^n , such that the current fluid configuration $\Phi_t(\Omega_f)$ and the current solid configuration $\Phi_t(\Omega_s)$ also are Lipschitz subdomains of Ω . Moreover, $\Phi_t(\Omega_f)$ and $\Phi_t(\Omega_s)$ should be connected. We should precise

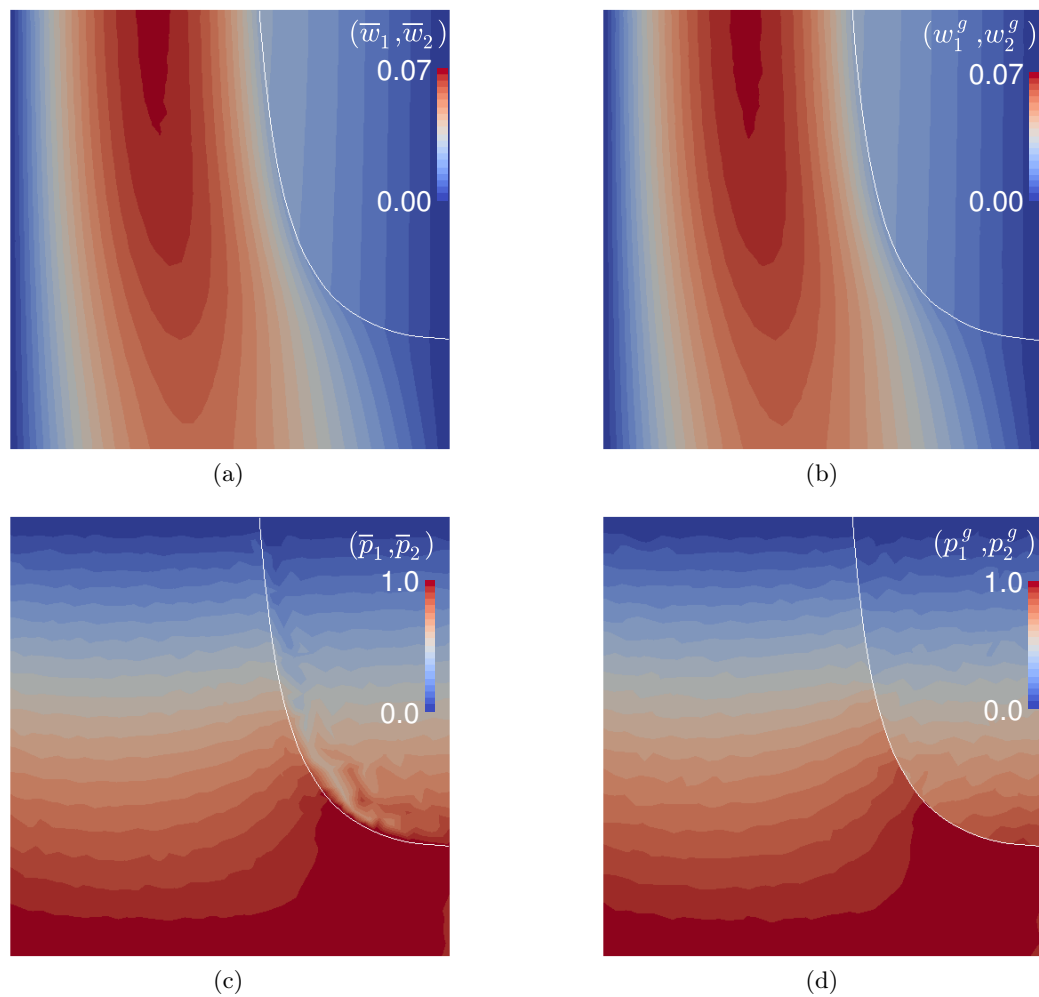


Figure 4.12 – Representation of the solution for the Stokes transmission problem (4.24) with $\mu_1 = 1$, $\mu_2 = 10$, $f_1 = (1, 0)$, $f_2 = (1, 0)$, $\alpha_\Gamma = 0.25$ and $\beta_\Gamma = 0.5$. On the top, we compare the magnitude of the fluid velocity obtained with a standard finite element method (a) and with the smooth extension method (b). On the bottom, we compare the pressure of the fluid computed with the classical finite element method (c) and the smooth extension method (d). The interface Γ is highlighted with a white curve.

here that the mapping Φ_t directly depends on the displacement of the structure at time t . For all x in Ω_s , this mapping writes

$$\Phi_t(x) = x + d_s(t)(x),$$

and we can easily extend Φ_t in the whole domain Ω . The existence of a smooth transformation Φ_t is rather complicated to prove and is out of the scope of this study. However, for the numerical resolution of this fluid-structure interaction problem, it is possible to construct Φ_t if the deformation of the structure is reasonable, i.e. if the structure does not enter in contact with itself or the boundary $\partial\Omega \setminus \Gamma_s$ and if the mesh which represents the domain Ω_s is admissible (no overlapping cell).

Then, at each time $t \geq 0$, the subdomain $\Phi_t(\Omega_f)$ is filled with an incompressible Newtonian fluid whose velocity $u_f(t) : \Phi_t(\Omega_f) \rightarrow \mathbb{R}^n$ and pressure $p_f(t) : \Phi_t(\Omega_f) \rightarrow \mathbb{R}$ satisfy the Stokes equations in conservative form

$$\begin{aligned} -\operatorname{div}(\sigma_f(u_f(t), p_f(t))) &= f_f(t) && \text{in } \Phi_t(\Omega_f), \\ \operatorname{div}(u_f(t)) &= 0 && \text{in } \Phi_t(\Omega_f), \\ u_f(t) &= 0 && \text{on } \Phi_t(\Gamma_f), \end{aligned}$$

where σ_f is the fluid tensor defined for all $u : \mathbb{R}^n \rightarrow \mathbb{R}^n$ and all $p : \mathbb{R} \rightarrow \mathbb{R}$ by

$$\begin{aligned} \sigma_f(u, p) &= 2\mu_f D(u) - pI, \\ D(u) &= \frac{1}{2}(\nabla u + \nabla u^T), \end{aligned}$$

the constant μ_f is the viscosity of the fluid and $f_f(t) : \Phi_t(\Omega_f) \rightarrow \mathbb{R}^n$ is the external force applied to the fluid at time t . Inside the fluid lies an elastic medium, whose displacement at time t , $d_s(t) : \Omega_s \rightarrow \mathbb{R}^n$, verifies the following equations of linear elasticity written in the reference solid configuration Ω_s

$$\begin{aligned} -\operatorname{div}(\sigma_s(d_s(t))) &= f_s(t) && \text{in } \Omega_s, \\ d_s(t) &= 0 && \text{on } \Gamma_s, \end{aligned}$$

where σ_s is the solid tensor defined for all $u : \mathbb{R}^n \rightarrow \mathbb{R}^n$ by

$$\sigma_s(u) = 2\mu_s D(u) + \lambda_s \operatorname{div}(u)I,$$

the two positive constants μ_s and λ_s are the Lamé coefficients and $f_s(t) : \Omega_s \rightarrow \mathbb{R}^n$ is the external force applied to the structure at time t . To complete this system of equations, we consider at each time t the coupling conditions that correspond to the continuity of the velocities and the normal constraints through the fluid-structure interface in the reference configuration Γ . For that matter, we introduce the fluid velocity and pressure written in the reference fluid configuration, denoted by w_f and q_f , and defined at time t by

$$w_f(t) = u_f(t) \circ \Phi_t, \quad \text{and } q_f(t) = p_f(t) \circ \Phi_t.$$

Moreover, we introduce the fluid stress tensor written in the fluid reference configuration, denoted by Π_f , and defined at time t by

$$\begin{aligned} \Pi_f(w_f(t), q_f(t)) &= \begin{aligned} &\mu_f(\nabla w_f(t)F(d_s(t)) + (\nabla(\Phi(d_s(t))))^{-T}\nabla w_f(t)^T G(d_s(t))) \\ &-q_f(t)G(d_s(t)), \end{aligned} && \text{in } \Omega_f, \end{aligned}$$

where $F(d_s(t))$ and $G(d_s(t))$ are the following matrices:

$$\begin{aligned} F(d_s(t)) &= (\nabla(\Phi(d_s(t))))^{-1} \operatorname{cof}(\nabla(\Phi(d_s(t))))), \\ G(d_s(t)) &= \operatorname{cof}(\nabla(\Phi(d_s(t)))). \end{aligned} \tag{4.36}$$

Remark 4.10. The tensor Π_f is the Piola transform of the fluid stress tensor σ_f . For more information on how to transform the Stokes equations from the deformed configuration to the reference configuration, see Appendix B.

Thus the transmission conditions write

$$\begin{aligned} \frac{\partial d_s}{\partial t}(t) &= u_f(t) \circ \Phi_t && \text{on } \Gamma, \\ \sigma_s(d_s(t))n_s &= \Pi_f(w_f(t), q_f(t))n_s && \text{on } \Gamma, \end{aligned} \quad (4.37)$$

where the vector n_s denotes the exterior unit normal vector to $\partial\Omega_s$. Similarly we denote n_d the exterior unit normal vector to $\partial\Omega_f$. Furthermore, we suppose that the structure is at rest initially, i.e. that $d_s(0) = 0$.

For the purpose of the numerical resolution we consider a discretization of \mathbb{R}^+ for the time variable. Let $\delta t > 0$ be the step size. We construct a sequence $(t_k)_{k \in \mathbb{R}^+}$ such that $t_0 = 0$ and $t_{k+1} = t_k + \delta t$ for $k > 0$. Thus, we define the time discretizations of u_f , p_f and d_s such that, for all $k \geq 0$,

$$\begin{aligned} u_f^k &= u_f(t_k), \\ p_f^k &= p_f(t_k), \\ d_s^k &= d_s(t_k). \end{aligned}$$

In addition, we also define $f_f^k = f_f(t_k)$ and $f_s^k = f_s(t_k)$ for all $k \geq 0$. The discretization of the first coupling condition (4.37) is obtained using the implicit Euler scheme:

$$\begin{aligned} d_s^{k+1} &= d_s^k + \delta t u_f^{k+1}, \quad \forall k \geq 0, \\ d_s^0 &= \delta t u_f^0. \end{aligned}$$

At time t_k the current solid domain is given by $\Phi_{t_k}(\Omega_s) = (id + d_s^{k-1})(\Omega_s)$ and the current fluid domain $\Phi_{t_k}(\Omega_f)$ is obtained by extending the mapping Φ_{t_k} in the whole domain Ω . Moreover, because of the homogeneous Dirichlet boundary conditions on the external frontier $\partial\Omega$, it is clear that for all $k \geq 0$, $\Phi_{t_k}(\Omega) = \Omega$. Furthermore, the matrices F_{t_k} and G_{t_k} only depend on the displacement of the structure at time t_{k-1} .

Hence, for all $k \geq 0$, the triplet (u_f^k, p_f^k, d_s^k) is solution of the following problem,

$$\left\{ \begin{array}{l} \text{find } u: \Phi_{t_k}(\Omega_f) \rightarrow \mathbb{R}^n, p: \Phi_{t_k}(\Omega_f) \rightarrow \mathbb{R} \text{ and } d: \Omega_s \rightarrow \mathbb{R}^n \text{ such that} \\ \quad -\text{div}(\sigma_f(u, p)) = f_f^k, \quad \text{in } \Phi_{t_k}(\Omega_f), \\ \quad \text{div}(u) = 0, \quad \text{in } \Phi_{t_k}(\Omega_f), \\ \quad u = 0, \quad \text{in } \Phi_{t_k}(\Gamma_f), \\ \\ \quad -\text{div}(\sigma_s(d)) = f_s^k, \quad \text{in } \Omega_s, \\ \quad d = 0, \quad \text{on } \Gamma_s, \\ \\ \quad d = d_s^{k-1} + \delta t u \circ \Phi_{t_k}, \quad \text{on } \Gamma, \\ \quad \sigma_s(d)n_s = \Pi_f(u \circ \Phi_{t_k}, p \circ \Phi_{t_k})n_s, \quad \text{on } \Gamma, \end{array} \right. \quad (4.38a)$$

$$\quad \quad \quad (4.38b)$$

$$\quad \quad \quad (4.38c)$$

where by convention $d_s^{-1} = 0$ for $k = 0$. We can define a weak formulation of problem (4.38). Let X stand for either Ω_f , Ω_s , $\Phi_{t_k}(\Omega_f)$ or $\Phi_{t_k}(\Omega_s)$. We introduce the following

functional spaces:

$$\begin{aligned}
V_f^k &= \{v \in (H^1(\Phi_{t_k}(\Omega_f)))^n ; v|_{\Phi_{t_k}(\Gamma_f)} = 0\}, \\
V_s^k &= \{v \in (H^1(\Phi_{t_k}(\Omega_s)))^n ; v|_{\Phi_{t_k}(\Gamma_s)} = 0\}, \\
V_s &= \{v \in (H^1(\Omega_s))^n ; v|_{\Gamma_s} = 0\}, \\
W_u &= \{(v_f, v_s) \in V_f^k \times V_s ; (v_f \circ \Phi_{t_k})|_{\Gamma} = v_s|_{\Gamma}\}, \\
W_d &= \{(v_f, d_s) \in V_f^k \times V_s ; \delta_t(v_f \circ \Phi_{t_k})|_{\Gamma} + d_s^{k-1} = d_s|_{\Gamma}\}, \\
(H_{\text{div}}(X))^n &= \{\sigma \in (L^2(X))^{n \times n} ; \text{div}(\sigma) \in (L^2(X))^n\}.
\end{aligned}$$

The weak formulation of problem (4.38) writes:

$$\left\{ \begin{array}{l} \text{find } (u, d) \in W_d \text{ and } p \in L^2(\Phi_{t_k}(\Omega_f)) \text{ such that} \\ \int_{\Phi_{t_k}(\Omega_f)} \sigma_f(u, p) : \nabla v_f + \int_{\Omega_s} \sigma_s(d) : \nabla v_s \\ \qquad \qquad \qquad = \int_{\Phi_{t_k}(\Omega_f)} f_f^k \cdot v_f + \int_{\Omega_s} f_s^k \cdot v_s, \quad \forall (v_f, v_s) \in W_u, \\ \int_{\Phi_{t_k}(\Omega_f)} q \text{div}(u) = 0, \quad \forall q \in L^2(\Phi_{t_k}(\Omega_f)). \end{array} \right. \quad (4.39)$$

Problem (4.39) admits a unique solution that we still denote by (u_f^k, p_f^k, d_s^k) (see Section A.2). Moreover, $\sigma_f(u_f^k, p_f^k)$ belongs to $(H_{\text{div}}(\Phi_{t_k}(\Omega_f)))^n$, $\sigma_s(d_s^k)$ belongs to $(H_{\text{div}}(\Omega_s))^n$ and we can give a weak sense to the second transmission condition in (4.38c). Let X stands for either Ω_f or Ω_s and let η be the exterior normal vector to X . Let $\Upsilon = (H_{00}^{1/2}(\Gamma))^n$ be the image of $(H_{\partial X \setminus \Gamma}^1(X))^n$ by the trace operator on the interface Γ , i.e. the space of functions in $(H^{1/2}(\Gamma))^n$ whose extension by zero on $\partial X \setminus \Gamma$ belongs to $(H^{1/2}(\partial X))^n$.

Then, for all σ in $(H_{\text{div}}(X))^n$, we have the following Stokes formula:

$$\int_X \sigma : \nabla v + \int_X \text{div}(\sigma) \cdot v = \langle \gamma_\eta(\sigma), v \rangle_{\Upsilon', \Upsilon}, \quad \forall v \in (H_{\partial X \setminus \Gamma}^1(X))^n. \quad (4.40)$$

where Υ' is the dual space of Υ and γ_η is the trace normal operator on Γ . Then, the second transmission condition in (4.38c) is satisfied in the following sense:

$$\langle \gamma_{n_s}(\sigma_s(d_s^k)), v \rangle_{\Upsilon', \Upsilon} = - \langle \gamma_{n_f}(\Pi_f(u_f^k \circ \Phi_{t_k}, p_f^k \circ \Phi_{t_k})), v \rangle_{\Upsilon', \Upsilon}, \quad \forall v \in \Upsilon. \quad (4.41)$$

Similarly, we define $\Upsilon^k = (H_{00}^{1/2}(\Phi_{t_k}(\Gamma)))^n$ which enables to also write Stokes formulas for a tensor σ in $\Phi_{t_k}(\Omega_f)$ and in $\Phi_{t_k}(\Omega_s)$.

Now, we present the smooth extension method applied to problem (4.38). Formally, it writes: find g in $(V_s^k)'$ such that the solution of the following problem,

$$\left\{ \begin{array}{l} \text{find } u : \Omega \rightarrow \mathbb{R}^n, p : \Omega \rightarrow \mathbb{R} \text{ and } d : \Omega_s \rightarrow \mathbb{R}^n \text{ such that,} \\ -\text{div}(\sigma_f(u, p)) = \overline{f_f^k}^\Omega + \overline{g}^\Omega, \quad \text{in } \Omega, \\ \text{div}(u) = 0, \quad \text{in } \Omega, \\ u = 0, \quad \text{in } \partial\Omega, \\ -\text{div}(\sigma_s(d)) = f_s^k, \quad \text{in } \Omega_s, \\ d = 0, \quad \text{on } \Gamma_s, \\ \sigma_s(d)n_s = \Pi_f(u \circ \Phi_{t_k}, p \circ \Phi_{t_k})n_s, \quad \text{on } \Gamma \end{array} \right. \quad (4.42a)$$

$$\left. \begin{array}{l} -\text{div}(\sigma_s(d)) = f_s^k, \quad \text{in } \Omega_s, \\ d = 0, \quad \text{on } \Gamma_s, \\ \sigma_s(d)n_s = \Pi_f(u \circ \Phi_{t_k}, p \circ \Phi_{t_k})n_s, \quad \text{on } \Gamma \end{array} \right\} \quad (4.42b)$$

satisfies the equality,

$$u \circ \Phi_{t_k} = \frac{1}{\delta t}(d - d_s^{k-1}), \text{ on } \Gamma.$$

Let v be in $(\mathcal{D}(\Omega))^n$ and suppose that u , p and d are sufficiently regular. Moreover, we assume for the moment that g belongs to $(L^2(\Phi_{t_k}(\Omega_s)))^n$ in order to do formal computations. Formally, we multiply the first equation in (4.42a) by v and the first equation in (4.42b) by $v|_{\Omega_s}$, and integrate respectively over Ω and Ω_s . After an integration by part and using the Neumann condition on Γ , we find

$$\begin{aligned} \int_{\Omega} \sigma_f(u, p) : \nabla v &= \int_{\Phi_{t_k}(\Omega_f)} f_f^k \cdot v + \int_{\Phi_{t_k}(\Omega_s)} g \cdot v, \\ \int_{\Omega_s} \sigma_s(d) : \nabla v|_{\Omega_s} &= \int_{\Omega_s} f_s^k \cdot v|_{\Omega_s} + \int_{\Gamma} (\Pi_f(u \circ \Phi_{t_k}, p \circ \Phi_{t_k}) n_s) \cdot v. \end{aligned}$$

Moreover, we remark that

$$\begin{aligned} &\int_{\Gamma} (\Pi_f(u \circ \Phi_{t_k}, p \circ \Phi_{t_k}) n_s) \cdot v \\ &= \int_{\Omega_s} \operatorname{div}(\Pi_f(u \circ \Phi_{t_k}, p \circ \Phi_{t_k})) \cdot v|_{\Omega_s} + \int_{\Omega_s} \Pi_f(u \circ \Phi_{t_k}, p \circ \Phi_{t_k}) : \nabla v|_{\Omega_s}, \\ &= - \int_{\Omega_s} \det(\nabla \Phi_{t_k})(g \circ \Phi_{t_k}) \cdot v|_{\Omega_s} + \int_{\Omega_s} \Pi_f(u \circ \Phi_{t_k}, p \circ \Phi_{t_k}) : \nabla v|_{\Omega_s}, \\ &= - \int_{\Phi_{t_k}(\Omega_s)} g \cdot (v|_{\Omega_s} \circ \Phi_{t_k}^{-1}) + \int_{\Omega_s} \Pi_f(u \circ \Phi_{t_k}, p \circ \Phi_{t_k}) : \nabla v|_{\Omega_s}. \end{aligned}$$

Thus, we define the weak formulation of the smooth extension problem (4.42), which makes sense for g in $(V_s^k)'$, as the problem of finding a suitable control g in $(V_s^k)'$, such that the solution of the following problem,

$$\left\{ \begin{array}{l} \text{find } u \in H_0^1(\Omega), p \in L_0^2(\Omega) \text{ and } d \in V_s \text{ such that} \\ \int_{\Omega} \sigma_f(u, p) : \nabla v_f = \int_{\Phi_{t_k}(\Omega_f)} f_f^k \cdot v_f|_{\Phi_{t_k}(\Omega_f)} \\ \quad + \langle g, v_f|_{\Phi_{t_k}(\Omega_s)} \rangle_{(V_s^k)', V_s^k}, \quad \forall v_f \in H_0^1(\Omega), \\ \int_{\Omega} q \operatorname{div}(u) = 0, \quad \forall q \in L_0^2(\Omega), \\ \int_{\Omega_s} \sigma_s(d) : \nabla v_s = \int_{\Omega_s} f_s^k \cdot v_s - \langle g, v_s \circ \Phi_{t_k}^{-1} \rangle_{(V_s^k)', V_s^k} \\ \quad + \int_{\Omega_s} \Pi_f(u \circ \Phi_{t_k}, p \circ \Phi_{t_k}) : \nabla v_s, \quad \forall v_s \in V_s, \end{array} \right. \quad (4.43)$$

verifies the equality

$$u \circ \Phi_{t_k} = \frac{1}{\delta t}(d - d_s^{k-1}), \text{ on } \Gamma. \quad (4.44)$$

For every $f_f^k \in (L^2(\Phi_{t_k}(\Omega_f)))^n$ and every $g \in (V_s^k)'$, there exists a unique solution to the Stokes problem appearing in problem (4.43), denoted by (u^g, p^g) (see [Boyer and Fabrie, 2012]). On the other hand, for all $f_s^k \in (L^2(\Omega_s))^n$, the weak problem of linear elasticity that appears in (4.43) also admits a unique solution in V_s , denoted by d^g (see [Ciarlet, 1988]). In the following theorem, we state the existence of a control g such that the solution of (4.43) satisfies the equality (4.44) and explain how to recover the solution of the initial fluid-structure problem (4.39).

Theorem 4.10. *Let Ω be a domain that satisfies Assumption (H_4) . Consider f_f^k in $(L_2(\Phi_{t_k}(\Omega_f)))^n$ and f_s^k in $(L_2(\Omega_s))^n$. Then, there exists a function g in $(V_s^k)'$ such that the solution (u^g, p^g, d^g) of problem (4.43) satisfies (4.44). Moreover, we can recover the solution of the fluid-structure problem (4.39):*

$$\begin{aligned} (u_f^k, p_f^k) &= (u_{|\Phi_{t_k}(\Omega_f)}^g, p_{|\Phi_{t_k}(\Omega_f)}^g), \\ d_s^k &= d^g. \end{aligned}$$

The proof of Theorem 4.10 relies on the construction of extensions for the functions u_f^k and p_f^k to the whole domain Ω , which is what we have done for the Stokes transmission problem. Hence, the proof of Theorem 4.10 directly follows from the one of Theorem 4.7. This is detailed in Section A.2.

As before, the problem of finding a control such that the solution of (4.42) verifies (4.44) can be formulated as an optimization problem on the following cost function, defined for any $k \geq 0$,

$$\begin{aligned} J_k &: V_{s,k}' \rightarrow \mathbb{R}^+ \\ g &\mapsto \frac{1}{2} \int_{\Gamma} |u^g \circ \Phi_{t_k} - \frac{1}{\delta t} (d^g - d_s^{k-1})|^2, \end{aligned} \quad (4.45)$$

where u^g and d^g are the velocity of the fluid and the displacement of the structure that solve problem (4.43) at time t_k . The function d_s^{k-1} is the displacement of the structure that solves problem (4.38) at time t_{k-1} . Yet, the minimization of this cost function is equivalent to the minimization of the real-valued function,

$$\begin{aligned} (H_0^1(\Omega))^n \times V_s &\rightarrow \mathbb{R}^+ \\ (u, d) &\mapsto \frac{1}{2} \int_{\Gamma} |u \circ \Phi_{t_k} - \frac{1}{\delta t} (d - d_s^{k-1})|^2, \end{aligned}$$

under the constraint that u and d are the velocity of the fluid and the displacement of the structure that solve problem (4.43). Then, to this constrained optimization problem, we can associate the following Lagrangian function, defined from

$$(V_s^k)' \times ((H_0^1(\Omega))^n \times L_0^2(\Omega) \times V_s) \times ((H_0^1(\Omega))^n \times L_0^2(\Omega) \times V_s),$$

to \mathbb{R} by,

$$\begin{aligned} \mathcal{L}_k(g, (u, p, d), (\lambda_f, \pi, \nu_s)) &= \\ &\frac{1}{2} \int_{\Gamma} |u \circ \Phi_{t_k} - \frac{1}{\delta t} (d - d_s^{k-1})|^2 + \int_{\Omega} \sigma_f(u, p) : \nabla \lambda_f - \int_{\Omega} \pi \operatorname{div}(u) \\ &+ \int_{\Omega_s} \sigma_s(d) : \nabla \nu_s - \int_{\Omega_s} \Pi_f(u \circ \Phi_{t_k}, p \circ \Phi_{t_k}) : \nabla \nu_s \\ &- \int_{\Phi_{t_k}(\Omega_f)} f_f^k \cdot \lambda_f - \langle g, \lambda_f \rangle_{(V_s^k)', V_s^k} - \int_{\Omega_s} f_s^k \cdot \nu_s + \langle g, \nu_s \circ \Phi_{t_k}^{-1} \rangle_{(V_s^k)', V_s^k}. \end{aligned} \quad (4.46)$$

Again, this Lagrangian function can be used to compute the gradient of J_k and show that the minimization of J_k is equivalent to the problem of finding a suitable control g such that the solution of (4.43) satisfies (4.44). For that purpose, we introduce the adjoint problem

of (4.43),

$$\left\{ \begin{array}{l} \text{find } \nu_s \in V_s, \lambda_f \in (H_0^1(\Omega))^n \text{ and } \pi \in L_0^2(\Omega) \text{ such that,} \\ \int_{\Omega_s} \sigma_s(\nu_s) : \nabla v_s = \frac{1}{\delta t} \int_{\Gamma} (u^g \circ \Phi_{t_k} - \frac{1}{\delta t} (d^g - d_s^{k-1})) \cdot v_s, \quad \forall v_s \in V_s, \\ \int_{\Omega} \sigma_f(\lambda_f, \pi) : \nabla v_f = 2\mu_f \int_{\Phi_{t_k}(\Omega_s)} D(\nu_s \circ \Phi_{t_k}^{-1}) : D(v_f) \\ \quad - \int_{\Gamma} (u^g \circ \Phi_{t_k} - \frac{1}{\delta t} (d^g - d_s^{k-1})) \cdot v_f \circ \Phi_{t_k}, \quad \forall v_f \in (H_0^1(\Omega))^n, \\ \int_{\Omega} q \operatorname{div}(\lambda_f) = \int_{\Phi_{t_k}(\Omega_s)} q \operatorname{div}(\nu_s \circ \Phi_{t_k}^{-1}), \quad \forall q \in L_0^2(\Omega). \end{array} \right. \quad (4.47)$$

Problem (4.47) admits a unique solution that we denote $(\nu^g, \lambda^g, \pi^g)$. Then, the existence and the characterization of the gradient of J_k is given in the following theorem,

Theorem 4.11. *The mapping $g \in (V_s^k)' \mapsto J_k(g) \in \mathbb{R}^+$ is differentiable and its gradient $\nabla J_k(g)$ in $(V_s^k)''$ is given by,*

$$\langle \nabla J_k(g), \delta g \rangle_{(V_s^k)'', (V_s^k)'} = \left\langle \delta g, \nu^g \circ \Phi_{t_k}^{-1} - \lambda_{\Phi_{t_k}(\Omega_s)}^g \right\rangle_{(V_s^k)', (V_s^k)}, \quad \forall \delta g \in V_s', \quad (4.48)$$

where λ^g and ν^g satisfy the adjoint problem (4.47).

Moreover, the equivalence between the smooth extension problem and its formulation as a minimization problem can also be stated in the case of a fluid-structure interaction problem.

Theorem 4.12. *A control g in $(V_s^k)'$ is a minimizer of J_k if and only if the solution of (4.43) satisfies (4.44).*

Proofs of Theorem 4.11 and Theorem 4.12 can be easily adapted from the ones already done for the Stokes transmission problem. However, the change of domains between the structure in reference configuration and the fluid in current configuration can be confusing. For that matter, all proofs are detailed in Section A.2.

The formulation of the fluid-structure interaction problem as a control problem and as a minimization problem enables us to numerically solve these equations with a fictitious domain approach. Here, we apply this method to the numerical simulation of the bending of an elastic beam in a viscous fluid subjected to shear boundary condition. The initial geometry of the problem is represented in Figure 4.13: Ω_f is the rectangle $[0, 2] \times [0, 1]$ in \mathbb{R}^2 and Ω_s is a rectangular beam of length L_c and of radius r_c . This beam is anchored at the bottom of Ω_f , at positions $(x_c - r_c, 0)$ and $(x_c + r_c, 0)$. We consider periodic boundary conditions on the left and right boundaries of the fluid domain and imposed a shear condition on the top, given by

$$u_{bc}(x) = (3, 0), \quad \forall x \in [0, 1].$$

On the bottom boundaries of the fluid and solid domains, homogeneous Dirichlet boundary conditions are considered. No external force is considered and constant values are chosen for the fluid viscosity, $\mu_f = 1$, the Young's modulus of the solid material, $E_s = 10^5$, and its Poisson's ratio, $\nu_s = 0.49$. The Lamé coefficients μ_s and λ_s are then given by

$$\begin{aligned} \mu_s &= \frac{E_s}{2(1 + \nu_s)}, \\ \lambda_s &= \frac{\nu_s E_s}{((1 + \nu_s)(1 - 2\nu_s))}. \end{aligned}$$

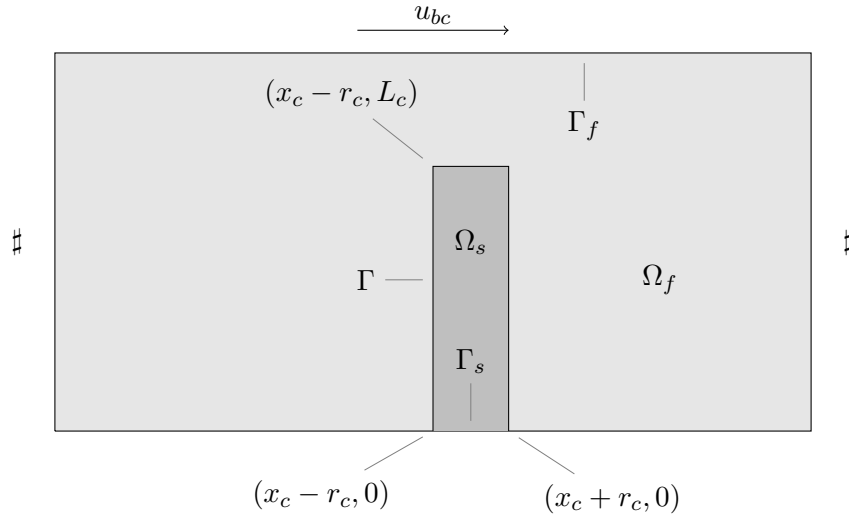


Figure 4.13 – Two dimensional representation of the initial geometry for the fluid-structure problem.

For the parameters of the beam, we choose $x_c = 1$, $r_c = 0.05$ and $L_c = 0.65$. The final time of the simulation is set to $T = 0.5$.

The solution given by the Smooth Extension method is obtained following Algorithm 4.1 and using the L-BFGS algorithm (see [Nocedal, 1980]). The resolution of the two different Stokes problems appearing in the minimization process is done using Mini elements, while the resolution of the two elasticity problems is done using $P1$ elements. Fluid problems are solved on a fixed mesh representing the whole domain Ω and elasticity problems are solve on a fixed mesh representing Ω_s , i.e. in the solid reference configuration. Moreover, the fluid mesh does not conform with the solid boundary. We compare this solution to the one obtained with conformal meshes and using a Lagrangian multiplier to ensure the continuity of the fluid and solid velocities through the interface Γ . With this method, an Arbitrary Lagrangian-Eulerian (ALE) methodology (see [Boilevin-Kayl et al., 2019]) is used to ensure the mesh conformity when the beam bends and prevent cells from overlapping within the fluid mesh. However, if the quality of the fluid mesh is too poor, one needs to remesh it (this is done using the Mmg remeshing software [Dapogny et al., 2014]). In the following, this method will be referred as the ALE method.

In this test case, the fluid-structure system attains a stationary state, where the beam is at equilibrium in a deformed configuration, which is well caught by both the ALE and the Smooth Extension methods (see Figure 4.14). To study the robustness of the Smooth Extension method, we coarsen the fluid mesh and observe the consequences on the dynamic of the system. To do so we define the *coarsening ratio of the fluid mesh* as the ratio of the number of nodes in the reference fluid mesh used in the ALE method divided by the number of nodes of the fluid mesh used in the Smooth Extension method. For example, a coarsening ratio of 1 means that the two fluid meshes have the same number of nodes, whereas a ratio of 0.5 means that the fluid mesh used in the Smooth Extension method has half as many nodes than the reference fluid mesh used for the ALE method. Then, in Figure 4.14, we observe that the coarser is the fluid mesh, the farther is the stationary state from the equilibrium state obtained with the ALE method. In order to quantify this error, we consider the $L^1(\Omega)$ distance between the position of the beam obtained with the ALE

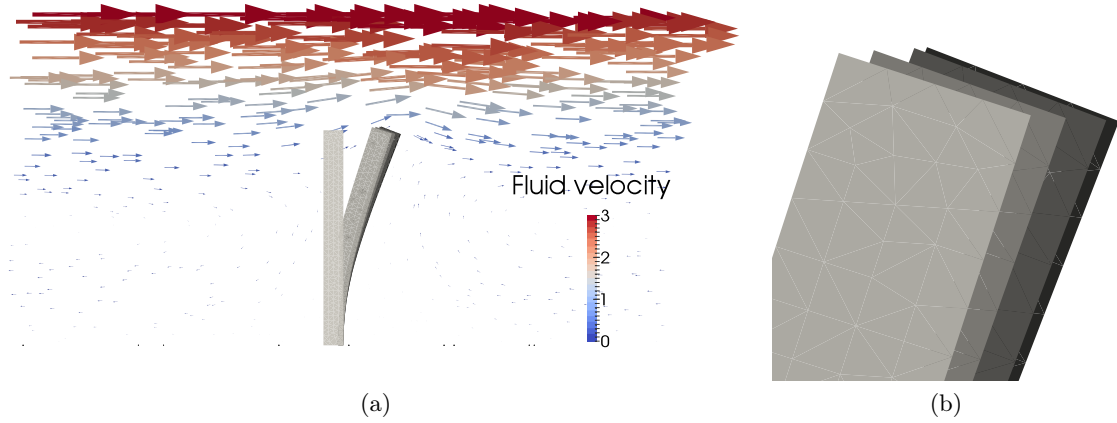


Figure 4.14 – Comparison of the stationary states obtained through the Smooth Extension method and the ALE method (a). The darkest grey mesh represents the equilibrium position of the beam obtained with the ALE method. The lightest grey mesh represents the initial position of the beam. The other three meshes represent the equilibrium positions of the beam obtained with the Smooth Extension method for different coarsening ratios (0.99, 0.71, 0.46): the lighter is the colour the coarser is the fluid mesh. Zoom on the tips of the beams (b).

method and the one obtained with the Smooth Extension method at time t , defined by

$$d_{SEM}^{ALE}(t) = \frac{\int_{\Omega} |\chi_{\Omega_s^{SEM}(t)} - \chi_{\Omega_s^{ALE}(t)}|}{\int_{\Omega} |\chi_{\Omega_s^{SEM}(t)}| + \int_{\Omega} |\chi_{\Omega_s^{ALE}(t)}|},$$

where $\chi_{\Omega_s^{SEM}(t)}$ is a $L^2(\Omega)$ function which has value 1 inside the solid current domain $\Omega_s^{SEM}(t)$ obtained with the Smooth Extension method, and 0 otherwise. Similarly, $\chi_{\Omega_s^{ALE}(t)}$ is a $L^2(\Omega)$ function which has value 1 inside the solid current domain $\Omega_s^{ALE}(t)$ obtained with the ALE method, and 0 otherwise. Consequently, this distance is 0 if the two domains are the same and 1 if they do not overlap. Moreover, for a final time $T > 0$, we also consider the global norm in time of d_{SEM}^{ALE} defined by

$$\|d_{SEM}^{ALE}\| = \frac{1}{T} \int_0^T |d_{SEM}^{ALE}(t)| dt,$$

which is 0 if the two domains $\Omega_s^{ALE}(t)$ and $\Omega_s^{SEM}(t)$ are identical for all t in $[0, T]$ and 1 if they never overlap. Then, we compute the distance d_{SEM}^{ALE} in function of the time for different coarsening ratios to study their influence on the dynamic of the system when using the Smooth Extension method. This is represented in Figure 4.15a, where we observe that, for all coarsening ratios, the distance d_{SEM}^{ALE} increases in time to reach a constant value when the stationary state is attained. This result corroborates and quantifies what we observed on Figure 4.14, i.e. that the error on the equilibrium position of the beam seems to increase when the coarsening ratio decreases, but stays relatively low considering the coarsening of the fluid mesh. To go further, we plot in Figure 4.15b the global norm in time of d_{SEM}^{ALE} in function of the coarsening ratio. In addition to the already mentioned fact that

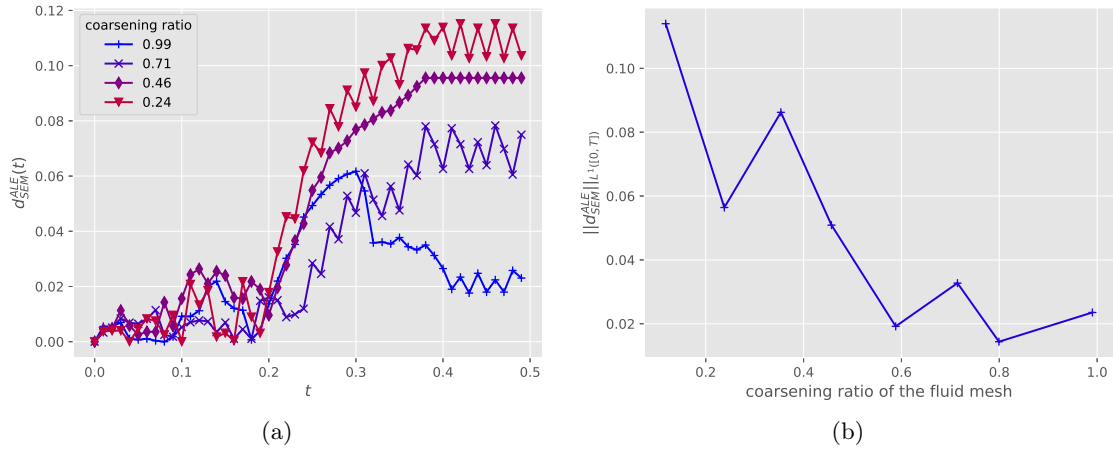


Figure 4.15 – Distance d_{SEM}^{ALE} between the two solid configuration Ω_s^{SEM} and Ω_s^{ALE} in function of the time (a). Global norm in time $\|d_{SEM}^{ALE}\|$ in function of the coarsening ratio of the fluid mesh in the Smooth Extension method (b).

the error tends to increase when the coarsening ratio decreases, we remark that the error in time is just above 0.1 for a coarsening ratio of 0.12, which implies that the coarsening of the fluid mesh in the Smooth Extension method does not drastically change the time dynamic of the bending of the beam in this test case.

All these results suggest that the Smooth Extension method is well suited for time dependent problems involving a moving structure in a viscous fluid, where the fluid mesh is fixed, possibly Cartesian and coarser than the structure mesh.

4.5 Conclusion

In this chapter we have presented a numerical strategy for the resolution of transmission problems with non-conformal meshes and which preserves optimal rates of convergence in space. It is based on a control formulation of the transmission problem, namely the Smooth Extension formulation, whose numerical resolution can be done by minimizing a particular objective function. This method allows the use of standard finite element functional spaces along with fixed structured or unstructured meshes and pre-existing finite element solvers and optimization algorithms.

This smooth extension method has been derived in the particular case of the transmission Laplace problem with only two subdomains and considering Dirichlet boundary conditions. Other boundary conditions could also be considered with no additional difficulty, provided that the initial transmission problem is well-posed. The same methodology should also work for transmission problems with more than two subdomains. In addition, we have shown that the Smooth Extension method can be applied to a wide variety of transmission problems, even the ones with totally different operators, such as the fluid-structure interaction problem studied in Subsection 4.4.2.

The Smooth Extension method has been compared to a standard numerical method for different test cases and has shown to give good approximations of the solutions for each one of them. However, some numerical aspects, such as the use of fast solvers on Cartesian

meshes or the choice of the optimization algorithm appearing in the minimization process, should be explored further.

Chapitre 5

Conclusion et perspectives

Dans cette thèse, nous avons étudié l'interaction de structures élancées, élastiques et actives avec un fluide homogène, incompressible et visqueux à bas nombre de Reynolds. En particulier, trois axes de recherche ont été abordés : la modélisation mathématique du phénomène bio-physique, l'analyse théorique des problèmes mathématiques issus de la modélisation et leur résolution numérique.

Dans le Chapitre 2, nous avons présenté un modèle pour les déformations de structures dont l'activité provient de contraintes de cisaillement internes, qui s'inscrit dans le contexte de la mécanique des milieux continus. Comme nous l'avons mis en évidence, ce formalisme permet de représenter une grande diversité de déformations, qualitativement proches de celles observées chez les cils bronchiques ou les flagelles de spermatozoïdes. En couplant les équations de l'élasticité active avec les équations de Stokes, nous avons étudié le problème d'interaction fluide-structure discrétisé en temps d'un point de vue mathématique, puis sous un angle plus expérimental avec la simulation numérique directe du système. Avec un scénario d'activité engendrant des déformations phénoménologiquement proches de celles d'un cil eucaryote, nous avons alors observé l'importance des effets induits par les forces hydrodynamiques du fluide sur les déformations de la structure et de l'action du cil sur le déplacement du fluide environnant.

Dans le Chapitre 3, nous avons étudié le problème d'interaction fluide-structure quasi-statique mettant en jeu une structure active et un fluide de Stokes et avons montré l'existence et l'unicité d'une solution forte locale en temps pour des données petites. La preuve de ce résultat s'appuie sur un procédé de point-fixe de Banach, pour lequel des résultats intermédiaires sur le problème fluide et le problème d'élasticité ont été démontrés.

Dans le Chapitre 4, nous avons développé une méthode de prolongement régulier pour la résolution de problèmes de transmission, qui conserve l'ordre de convergence optimal de la méthode des éléments finis. Cette méthode a été validée pour les problèmes de transmission de Laplace et de Stokes, ainsi que pour un problème d'interaction fluide-structure avec une structure passive dont le déplacement vérifie les équations de l'élasticité linéarisée.

Pour conclure, nous présentons quelques développements qui s'inscrivent dans la continuité du travail réalisé dans ce manuscrit.

Structures actives et problèmes inverses

Le modèle introduit dans le Chapitre 2 permet *a priori* tout type de déformations pour les structures actives. Dans l'objectif d'appliquer ce travail à la modélisation de véritables cils eucaryotes, une piste envisageable serait d'utiliser la paramétrisation du déplacement d'un cil définie dans [Fulford and Blake, 1986] afin de déterminer, par la résolution de

problèmes inverses, les contraintes internes de la structure. Notre modèle d'interaction fluide-structure est d'ailleurs particulièrement intéressant pour cette étude, car il permet la prise en compte complète de l'interaction fluide-structure, qui est importante ici puisque la paramétrisation dans [Fulford and Blake, 1986] a été réalisée à partir d'images obtenues par microscopes pour un cil battant dans un fluide visqueux.

Dans le cadre du modèle que nous avons développé, se pose la question de l'identification d'un scénario d'activité interne qui permettrait de retrouver, dans un fluide de référence, les déformations du cil obtenues avec cette paramétrisation. La formulation du problème inverse associé à cette question peut nécessiter un certain nombre d'hypothèses, à préciser, sur la classe des activités internes admissibles.

Pour comprendre les mécanismes internes de l'activité des cils

Les scénarios considérés dans le Chapitre 2 pour le tenseur des contraintes actives Σ^* dépendent uniquement du temps et de la variable d'espace. Un autre axe de recherche serait de considérer des contraintes internes qui prennent également en compte les déformations de la structure, par exemple au travers du gradient du déplacement ∇d_s . En effet, comme nous en avons discuté dans la Sous-section 1.2.4, plusieurs modèles considèrent les déformations locales de la structure dans la modélisation des contraintes de cisaillement internes. En particulier, ces classes de modèles permettent de mettre en évidence l'émergence de synchronisation entre plusieurs cils battant initialement avec un décalage de phase, ce qui est bien observé dans la nature. Un modèle simple que nous pourrions envisager serait d'écrire, en reprenant les notations du Chapitre 2, les contraintes actives sous la forme

$$\Sigma^*(t, x, d_s(t)) = (\Sigma_a(t, x) + \Sigma_d(d_s(t)))e_a \otimes e_a, \quad t \geq 0, \quad x \in \Omega_s, \quad (5.1)$$

où Σ_a est le scénario d'activité introduit dans la Section 2.2 et Σ_d est une fonction à valeurs réelles qui dépend du déplacement de la structure à l'instant t . Du point de vue de l'analyse mathématique, la prise en compte de ce terme correspond à l'ajout d'un terme non linéaire dans les équations de l'élasticité active, dont l'étude dépend bien évidemment de la forme de la fonction Σ_d choisie.

Applications à d'autres micro-particules actives

Avec le formalisme que nous avons introduit tout au long de cette thèse, l'étude d'autres types de micro-nageurs, biologiques et biomimétiques, est parfaitement envisageable. La modélisation de micro-algues, bactéries ou spermatozoïdes pourrait facilement être réalisée, en attachant par exemple les cils et flagelles à un ellipsoïde, rigide ou élastique, représentant le corps du micro-organisme. Encore une fois, notre modélisation dans le cadre de la théorie des milieux continus nous permettrait de considérer les interactions entre le fluide et les micro-nageurs de façon précise. L'objectif ultime serait alors de pouvoir observer des phénomènes d'émergence de dynamiques collectives dans des suspensions de micro-nageurs à l'échelle des cils et des flagelles, ce qui est difficile car nécessiterait la prise en compte d'un grand nombre de nageurs, l'utilisation de solveurs fluide et structure particulièrement efficaces et une gestion des conditions de transmissions adaptée. La méthode de prolongement régulier développée dans le Chapitre 4 pourrait être adaptée à la résolution numérique de ces problèmes.

Vers une méthode de résolution numérique rapide

Concernant la méthode de prolongement régulier, nous travaillons actuellement à l'extension de la méthode à des structures élastiques complètement immergées dans le fluide (pour la simulation de suspensions de particules élastiques passives ou actives) et à des structures élancées dont le déplacement vérifie les équations non linéaires de l'élasticité (pour la simulation de cils eucaryotes). Ce travail est en lien avec la perspective d'application de nos travaux à la simulation de suspensions de micro-nageurs énoncée précédemment.

De plus, un autre projet à court terme que nous avons pour la méthode de prolongement régulier concerne son implémentation sur maillages cartésiens et avec des solveurs utilisant des algorithmes de transformées de Fourier rapides. En effet, les méthodes de domaine fictif, comme celle que nous avons développée, se prêtent bien à l'utilisation de ce type de techniques, qui permettent des gains de temps considérables pour la résolution numérique.

Des questions mathématiques ouvertes

Parmi les problèmes mathématiques que nous avons traités dans cette thèse, certaines questions n'ont pas été abordées et pourront être envisagées dans des travaux de recherche futurs. En particulier, l'étude du problème d'interaction fluide-structure stationnaire faite dans le Chapitre 2 concerne des modèles d'élasticité linéarisée. L'extension aux équations non linéaires de l'élasticité pourraient être envisagée. Pour le problème quasi-statique étudié dans le Chapitre 3, nous avons supposé que les forces extérieures exercées sur le fluide sont nulles et que la structure est dans sa position d'équilibre initialement. L'étude du problème général avec des forces fluides et une structure initialement déformée est donc une question ouverte. En particulier, l'étude du système où la structure n'est pas à l'équilibre à l'instant initial pourrait être une première étape pour étudier l'existence de solutions fortes globales en temps.

Enfin, concernant les résultats du Chapitre 4, l'analyse numérique de la méthode de prolongement régulier est une perspective importante de ce travail, qui permettrait de justifier mathématiquement les observations numériques de convergence optimale de la méthode.

Appendix A

Proofs of theorems related to the smooth extension method

A.1 Proofs of theorems related to the Stokes transmission problem

This appendix is dedicated to the proofs of all results stated in Subsection 4.4.1. In particular, we are interested in showing the existence of the control g , in giving an explicit formula for the gradient of \tilde{J} and, finally, in proving the equivalence between the minimisation of \tilde{J} and the resolution of the Stokes transmission problem.

We follow the order of the previous enumeration and start with the proof of Theorem 4.7.

Proof of Theorem 4.7. We can construct two extension operators E_u and E_p that extend \bar{w}_1 into the whole space $(H_0^1(\Omega))^n$ (and such that $E_u\bar{w}_1$ is divergence-free) and \bar{p}_1 into the whole space $L_0^2(\Omega)$. Indeed, consider the operators defined by

$$\begin{aligned} E_u\bar{w}_1 &= \begin{cases} \bar{w}_1 & \text{in } \Omega_1 \\ \bar{w}_2 & \text{in } \Omega_2 \end{cases}, \\ E_p\bar{p}_1 &= \begin{cases} \bar{p}_1 & \text{in } \Omega_1 \\ \bar{p}_2 & \text{in } \Omega_2 \end{cases}. \end{aligned}$$

Since (\bar{w}_1, \bar{w}_2) belongs to \mathcal{W} , the function $E_u\bar{w}_1$ is an extension of \bar{w}_1 which belongs to $(H_0^1(\Omega))^n$. Moreover, it satisfies $\text{div}(E_u\bar{w}_1) = 0$ because both \bar{w}_1 and \bar{w}_2 are divergence-free. Similarly, since (\bar{p}_1, \bar{p}_2) belongs to Q , the function $E_p\bar{p}_1$ is an extension of \bar{p}_1 which belongs to $L_0^2(\Omega)$. Furthermore, $\mu_1\nabla(E_u\bar{w}_1) - (E_p\bar{p}_1)I$ belongs to $(H_{\text{div}}(\Omega))^n$.

Then, we construct a suitable control g in W_2' such that

$$\begin{aligned} \langle g, v \rangle_{W_2', W_2} &= \mu_1 \int_{\Omega_2} \nabla(E_u\bar{w}_1)|_{\Omega_2} : \nabla v - \int_{\Omega_2} \bar{p}_1|_{\Omega_2} \text{div}(v) \\ &\quad + \langle \gamma_{n_1}(\sigma_E), v \rangle_{\Upsilon', \Upsilon}, \end{aligned} \quad \forall v \in W_2, \quad (\text{A.1})$$

where we define $\sigma_E = \mu_1\nabla(E_u\bar{w}_1) - (E_p\bar{p}_1)I$. Using the Stokes formula (4.27) and the definition (A.1), it follows that the extensions $E_u\bar{w}_1$ and $E_p\bar{p}_1$ satisfy

$$\begin{aligned} \mu_1 \int_{\Omega} \nabla(E_u\bar{w}_1) : \nabla v_1 - \int_{\Omega} (E_p\bar{p}_1) \text{div}(v_1) \\ &= \int_{\Omega_1} f_1 \cdot v_1|_{\Omega_1} + \langle g, v_1|_{\Omega_2} \rangle_{W_2', W_2}, \quad \forall v_1 \in H_0^1(\Omega) \\ \int_{\Omega} q_1 \text{div}(E_u\bar{w}_1) &= 0, \quad \forall q_1 \in L_0^2(\Omega). \end{aligned}$$

Similarly, using (4.27), (A.1) and the weak transmission condition (4.28), (\bar{w}_2, \bar{p}_2) satisfies

$$\begin{aligned} & \mu_2 \int_{\Omega_2} \nabla \bar{w}_2 : \nabla v_2 - \int_{\Omega_2} \bar{p}_2 \operatorname{div}(v_2) \\ = & \int_{\Omega_2} f_2 \cdot v_2 + \mu_1 \int_{\Omega_2} \nabla (E_u u_1)|_{\Omega_2} : \nabla v_2 - \langle g, v_2 \rangle_{W_2', W_2} - \int_{\Omega_2} (E_p \bar{p}_1|_{\Omega_2}) \operatorname{div}(v_2), \forall v_2 \in W_2, \end{aligned}$$

Finally, we conclude that $((E_u \bar{w}_1, E_p \bar{p}_1), (\bar{w}_2, \bar{p}_2))$ is the solution of problem (4.30). Thus,

$$((w_1^g, p_1^g), (w_2^g, p_2^g)) = ((E_u \bar{w}_1, E_p \bar{p}_1), (\bar{w}_2, \bar{p}_2))$$

and, by construction, the equality (4.31) is satisfied. This proves the first part of the theorem.

Now, suppose that g is a control such that the equality (4.31) is satisfied. In particular, the equality $w_{1|\Gamma}^g = w_{2|\Gamma}^g$ implies that $(w_{1|\Omega_1}^g, w_2^g)$ belongs to the space \mathcal{W} . Let us define the following Hilbert space:

$$\tilde{\mathcal{W}} = \{(v_1, v_2) \in (H_0^1(\Omega))^n \times W_2; v_{1|\Omega_1} = v_2\}.$$

As the unique solution of problem (4.30), the couples (w_1^g, p_1^g) and (w_2^g, p_2^g) satisfy, in particular, for all (v_1, v_2) in $\tilde{\mathcal{W}}$ and for all (q_1, q_2) in $L_0^2(\Omega) \times L^2(\Omega_2)$, the equations

$$\begin{aligned} \mu_1 \int_{\Omega} \nabla w_1^g : \nabla v_1 - \int_{\Omega} p_1^g \operatorname{div}(v_1) &= \int_{\Omega} f_1 \cdot v_{1|\Omega_1} + \langle g, v_{1|\Omega_2} \rangle_{W_2', W_2}, \\ \int_{\Omega} q \operatorname{div}(w_1^g) &= 0, \\ \mu_2 \int_{\Omega_2} \nabla w_2^g : \nabla v_2 - \int_{\Omega_2} p_2^g \operatorname{div}(v_2) &= \int_{\Omega_2} f_2 \cdot v_2 - \langle g, v_2 \rangle_{W_2', W_2} \\ &+ \mu_1 \int_{\Omega_2} \nabla w_1^g : \nabla v_2 - \int_{\Omega_2} p_1^g \operatorname{div}(v_2), \\ \int_{\Omega_2} q_{|\Omega_2} \operatorname{div}(w_2^g) &= 0. \end{aligned} \tag{A.2}$$

Then, summing equations in (A.2), it follows that $((w_{1|\Omega_1}^g, w_2^g), (p_{1|\Omega_1}^g, p_2^g))$ satisfies

$$\begin{aligned} \mu_1 \int_{\Omega_1} \nabla w_{1|\Omega_1}^g : \nabla v_{1|\Omega_1} - \int_{\Omega_1} p_{1|\Omega_1}^g \operatorname{div}(v_{1|\Omega_1}) + \mu_2 \int_{\Omega_2} \nabla w_2^g : \nabla v_2 - \int_{\Omega_2} p_2^g \operatorname{div}(v_2) \\ = \int_{\Omega_1} f_1 \cdot v_1 + \int_{\Omega_2} f_2 \cdot v_2, \quad \forall (v_1, v_2) \in \tilde{\mathcal{W}}, \\ \int_{\Omega_1} q_{1|\Omega_1} \operatorname{div}(w_{1|\Omega_1}^g) + \int_{\Omega_2} q_2 \operatorname{div}(w_2^g) = 0, \quad \forall (q_1, q_2) \in L_0^2(\Omega) \times L^2(\Omega_2). \end{aligned}$$

Because the test function v_1 belongs to $H_0^1(\Omega)$ and because $v_2 = v_{1|\Omega_1}$, we can redefine the pressures p_1^g and p_2^g up to a constant, by

$$\begin{aligned} \tilde{p}_1^g &= p_1^g - \frac{1}{|\Omega|} \left(\int_{\Omega_2} p_2^g + \int_{\Omega_1} p_{1|\Omega_1}^g \right), \\ \tilde{p}_2^g &= p_2^g - \frac{1}{|\Omega|} \left(\int_{\Omega_2} p_2^g + \int_{\Omega_1} p_{1|\Omega_1}^g \right), \end{aligned}$$

such that $(\tilde{p}_{1|\Omega_1}^g, \tilde{p}_2^g)$ belongs to the space Q . Moreover, for all (v_1, v_2) in \mathcal{W} we can extend v_1 in the whole space $H_0^1(\Omega)$ using v_2 , as we did it for \bar{w}_1 and \bar{w}_2 . We still denote $E_u v_1$

this extension. Similarly, for all (q_1, q_2) in Q , we can extend q_1 in the whole space $L_0^2(\Omega)$ and we still denote $E_p q_1$ this extension. Then, the couple $(E_u v_1, v_2)$ belongs to \tilde{W} , the couple $(E_p q_1, q_2)$ belongs to $L_0^2(\Omega) \times L^2(\Omega_2)$ and, finally, $((w_{1|\Omega_1}^g, w_2^g), (\tilde{p}_{1|\Omega_1}^g, \tilde{p}_2^g))$, satisfies the equations

$$\begin{aligned} \mu_1 \int_{\Omega_1} \nabla w_{1|\Omega_1}^g : \nabla v_1 - \int_{\Omega_1} \tilde{p}_{1|\Omega_1}^g \operatorname{div}(v_1) + \mu_2 \int_{\Omega_2} \nabla w_2^g : \nabla v_2 - \int_{\Omega_2} \tilde{p}_2^g \operatorname{div}(v_2) \\ = \int_{\Omega_1} f_1 \cdot v_1 + \int_{\Omega_2} f_2 \cdot v_2, \quad \forall (v_1, v_2) \in \mathcal{W}, \\ \int_{\Omega_1} q_{1|\Omega_1} \operatorname{div}(w_{1|\Omega_1}^g) + \int_{\Omega_2} q_2 \operatorname{div}(w_2^g) = 0, \quad \forall (q_1, q_2) \in Q. \end{aligned}$$

Thus, $((w_{1|\Omega_1}^g, w_2^g), (\tilde{p}_{1|\Omega_1}^g, \tilde{p}_2^g))$ is the unique solution of the initial Stokes transmission problem (4.26), which proves that we can recover the solution of the Stokes transmission problem from the solution of the smooth extension problem. \square

We continue with the proof of Theorem 4.8, i.e. we show the existence of the gradient of \tilde{J} and give an explicit formula to compute it.

Proof of Theorem 4.8. We start by computing the derivatives of the Lagrangian function $\tilde{\mathcal{L}}$ with respect to u_1 , p_1 , u_2 and p_2 , to justify the adjoint equations written in (4.34). These computations are similar to the ones made in the proof of Lemma 4.1 and we have

$$\begin{aligned} \left\langle \frac{\partial \tilde{\mathcal{L}}}{\partial u_1}, \delta u_1 \right\rangle_{(H^{-1}(\Omega))^n, (H_0^1(\Omega))^n} &= \int_{\Gamma} (u_1 - u_2) \cdot \delta u_1 + \mu_1 \int_{\Omega} \nabla \lambda_1 : \nabla \delta u_1 \\ &\quad - \int_{\Omega} \pi_1 \operatorname{div}(\delta u_1) - \mu_1 \int_{\Omega_2} \nabla \lambda_2 : \nabla \delta u_1, \quad \forall \delta u_1 \in (H_0^1(\Omega))^n, \end{aligned}$$

$$\begin{aligned} \left\langle \frac{\partial \tilde{\mathcal{L}}}{\partial u_2}, \delta u_2 \right\rangle_{W_2', W_2} &= - \int_{\Gamma} (u_1 - u_2) \cdot \delta u_2 + \mu_2 \int_{\Omega_2} \nabla \lambda_2 : \nabla \delta u_2 \\ &\quad - \int_{\Omega_2} \pi_2 \operatorname{div}(\delta u_2), \quad \forall \delta u_2 \in W_2, \end{aligned}$$

$$\left\langle \frac{\partial \tilde{\mathcal{L}}}{\partial p_1}, \delta p_1 \right\rangle_{L^2(\Omega), L^2(\Omega)} = - \int_{\Omega} \delta p_1 \operatorname{div}(\lambda_1) + \int_{\Omega_2} \delta p_1 \operatorname{div}(\lambda_2), \quad \forall \delta p_1 \in L_0^2(\Omega),$$

$$\left\langle \frac{\partial \tilde{\mathcal{L}}}{\partial p_2}, \delta p_2 \right\rangle_{L^2(\Omega_2), L^2(\Omega)} = - \int_{\Omega_2} \delta p_2 \operatorname{div}(\lambda_2), \quad \forall \delta p_2 \in L^2(\Omega_2).$$

Then, taking $(u_1, p_1) = (w_1^g, p_1^g)$ and $(u_2, p_2) = (w_2^g, p_2^g)$, we can deduce that the adjoint

problem associated to the direct problem (4.30) is,

$$\left\{ \begin{array}{l} \text{find } (\lambda_1, \pi_1) \in (H_0^1(\Omega))^n \times L_0^2(\Omega) \text{ and } (\lambda_2, \pi_2) \in W_2 \times L^2(\Omega) \text{ such that} \\ \left\langle \frac{\partial \tilde{\mathcal{L}}}{\partial u_1}, v_1 \right\rangle_{(H^{-1}(\Omega))^n, (H_0^1(\Omega))^n} = 0, \quad \forall v_1 \in (H_0^1(\Omega))^n, \\ \left\langle \frac{\partial \tilde{\mathcal{L}}}{\partial p_1}, q_1 \right\rangle_{L^2(\Omega), L^2(\Omega)} = 0, \quad \forall q_1 \in L_0^2(\Omega), \\ \left\langle \frac{\partial \tilde{\mathcal{L}}}{\partial u_2}, v_2 \right\rangle_{W_2', W_2} = 0, \quad \forall v_2 \in W_2, \\ \left\langle \frac{\partial \tilde{\mathcal{L}}}{\partial p_2}, q_2 \right\rangle_{L^2(\Omega_2), L^2(\Omega)} = 0, \quad \forall q_2 \in L^2(\Omega_2). \end{array} \right. \quad (\text{A.3})$$

Thus, the adjoint problem for the Stokes transmission problem is indeed the weak problem written in (4.34). Problem (4.34) consists in two Stokes problems, whose well-posedness derives from well-known results about the Stokes equations (see [Boyer and Fabrie, 2012]). We denote $((\omega_1^g, \pi_1^g), (\omega_2^g, \pi_2^g))$ its unique solution in $((H_0^1(\Omega))^n \times L_0^2(\Omega)) \times (W_2 \times L^2(\Omega_2))$.

The differentiability of \tilde{J} relies on the same arguments that the ones used in the proof of Theorem 4.3. Likewise, taking $(u_1, p_1) = (\omega_1^g, p_1^g)$ and $(u_2, p_2) = (\omega_2^g, p_2^g)$, the Lagrangian (4.33) reduces to

$$\tilde{\mathcal{L}}(g, ((\omega_1^g, p_1^g), (\omega_2^g, p_2^g)), ((\lambda_1, \pi_1), (\lambda_2, \pi_2))) = \tilde{J}(g), \quad \forall g \in W_2'.$$

Differentiating this previous inequality with respect to g using the chain rule and taking

$$(\lambda_1, \pi_1) = (\omega_1^g, \pi_1^g) \text{ and } (\lambda_2, \pi_2) = (\omega_2^g, \pi_2^g),$$

we find that, for all δg in W_2' ,

$$\left\langle \nabla \tilde{J}, \delta g \right\rangle_{W_2'', W_2} = \left\langle \frac{\partial \tilde{\mathcal{L}}}{\partial g}(g, ((\omega_1^g, p_1^g), (\omega_2^g, p_2^g)), ((\omega_1^g, \pi_1^g), (\omega_2^g, \pi_2^g))), \delta g \right\rangle_{W_2'', W_2'}.$$

Moreover, the differentiate of $\tilde{\mathcal{L}}$ with respect to g , $\frac{\partial \tilde{\mathcal{L}}}{\partial g} \in W_2''$, is defined such that, for all δg in W_2' ,

$$\left\langle \frac{\partial \tilde{\mathcal{L}}}{\partial g}(g, ((u_1, p_1), (u_2, p_2)), ((\lambda_1, \pi_1), (\lambda_2, \pi_2))), \delta g \right\rangle_{W_2'', W_2'} = \langle \delta g, \lambda_2 - \lambda_1|_{\Omega_2} \rangle_{W_2', W_2}$$

Finally, the gradient of \tilde{J} is given by,

$$\left\langle \nabla \tilde{J}, \delta g \right\rangle_{W_2'', W_2} = \langle \delta g, \lambda_2 - \lambda_1|_{\Omega_2} \rangle_{W_2', W_2}, \quad \forall \delta g \in W_2'.$$

□

Now, let us show the equivalence between the minimisation of \tilde{J} and the research of a suitable control such that the solution of (4.30) satisfies the conditions (4.31).

Proof of Theorem 4.9. The reciprocal statement is straightforward. If, for a given g , the solution of (4.30) satisfies the condition (4.31) then, $\tilde{J}(g) = 0$.

Now, let g be a minimiser of \tilde{J} . It follows that one has

$$\left\langle \delta g, \omega_2^g - \omega_{1|\Omega_2}^g \right\rangle_{W_2', W_2} = 0, \quad \forall \delta g \in W_2',$$

which means that $\omega_{1|\Omega_2}^g = \omega_2^g$ and the couple $(\omega_{1|\Omega_1}^g, \omega_2^g)$ belongs to \mathcal{W} . Yet, the functions $\omega_1^g, \omega_2^g, \pi_1^g$ and π_2^g satisfy the equations in problem (4.34). In particular, for all (v_1, v_2) in $\tilde{\mathcal{W}}$ and for all (q_1, q_2) in $L_0^2(\Omega) \times L^2(\Omega_2)$, where

$$\tilde{\mathcal{W}} = \{(v_1, v_2) \in (H_0^1(\Omega))^n \times W_2; v_{1|\Omega_2} = v_2\},$$

these equations write,

$$\begin{aligned} \mu_2 \int_{\Omega_2} \nabla \omega_2^g : \nabla v_2 - \int_{\Omega_2} \pi_2^g \operatorname{div}(v_2) &= \int_{\Gamma} (w_1^g - w_2^g) \cdot v_1, \\ \int_{\Omega_2} q_2 \operatorname{div}(\omega_2^g) &= 0, \\ \mu_1 \int_{\Omega} \nabla \omega_1^g : \nabla v_1 - \int_{\Omega} \pi_1^g \operatorname{div}(v_1) &= - \int_{\Gamma} (w_1^g - w_2^g) \cdot v_1 + \mu_1 \int_{\Omega_2} \nabla \omega_2^g : \nabla v_{1|\Omega_2}, \\ \int_{\Omega} q_1 \operatorname{div}(\omega_1^g) &= \int_{\Omega_2} q_{1|\Omega_2} \operatorname{div}(\omega_2^g). \end{aligned} \tag{A.4}$$

Summing the first equation in (A.4) with the third one and summing the second equation with the fourth one and using the fact that $\omega_{1|\Omega_2}^g = \omega_2^g$, we find that

$$\begin{aligned} \mu_1 \int_{\Omega_1} \nabla \omega_{1|\Omega_1}^g : \nabla v_{1|\Omega_1} - \int_{\Omega_1} \pi_{1|\Omega_1}^g \operatorname{div}(v_{1|\Omega_1}) + \mu_2 \int_{\Omega_2} \nabla \omega_2^g : \nabla v_2 - \int_{\Omega_2} (\pi_2^g + \pi_{1|\Omega_2}^g) \operatorname{div}(v_2) \\ = 0, \quad \forall (v_1, v_2) \in \tilde{\mathcal{W}}, \\ \int_{\Omega_1} q_{1|\Omega_1} \operatorname{div}(\omega_{1|\Omega_1}^g) + \int_{\Omega_2} q_2 \operatorname{div}(\omega_2^g) = 0, \quad \forall (q_1, q_2) \in L_0^2(\Omega) \times L^2(\Omega_2). \end{aligned}$$

Moreover, because the test function v_1 belongs to $(H_0^1(\Omega))^n$, we can redefine the pressure π_1^g up to a constant by

$$\tilde{\pi}_1^g = \pi_1^g - \frac{1}{|\Omega|} \int_{\Omega_2} \pi_2^g$$

such that $(\tilde{\pi}_{1|\Omega_1}^g, \pi_2^g + \tilde{\pi}_{1|\Omega_2}^g)$ belongs to the space \mathcal{Q} . Moreover, let (v_1, v_2) be in \mathcal{W} . We can construt an extension of v_1 in the whole space $(H_0^1(\Omega))^n$ using v_2 , as in the proof of Theorem 4.7 and we still denote $E_u v_1$ this extension. Likewise, for all (q_1, q_2) in \mathcal{Q} , we can extend q_1 in the whole space $L_0^2(\Omega)$ and we still denote $E_p q_1$ this extension. Then, the couple $(E_u v_1, v_2)$ belongs to $\tilde{\mathcal{W}}$, the couple $(E_p q_1, q_2)$ belongs to $L_0^2(\Omega) \times L^2(\Omega_2)$ and it follows that $((\omega_{1|\Omega_1}^g, \omega_2^g), (\tilde{\pi}_{1|\Omega_1}^g, \pi_2^g + \tilde{\pi}_{1|\Omega_2}^g))$ satisfies the equations

$$\begin{aligned} \mu_1 \int_{\Omega_1} \nabla \omega_{1|\Omega_1}^g : \nabla v_1 - \int_{\Omega_1} \tilde{\pi}_{1|\Omega_1}^g \operatorname{div}(v_1) + \mu_2 \int_{\Omega_2} \nabla \omega_2^g : \nabla v_2 - \int_{\Omega_2} (\pi_2^g + \tilde{\pi}_{1|\Omega_2}^g) \operatorname{div}(v_2) \\ = 0, \quad \forall (v_1, v_2) \in \mathcal{W}, \\ \int_{\Omega_1} q_1 \operatorname{div}(\omega_{1|\Omega_1}^g) + \int_{\Omega_2} q_2 \operatorname{div}(\omega_2^g) = 0, \quad \forall (q_1, q_2) \in \mathcal{Q}. \end{aligned}$$

We conclude that $((\omega_{1|\Omega_1}^g, \omega_2^g), (\tilde{\pi}_{1|\Omega_1}^g, \pi_2^g + \tilde{\pi}_{1|\Omega_2}^g))$ is solution of a Stokes problem similar to (4.26) but with no external force and, thus, is the zero of $\mathcal{W} \times \mathcal{Q}$. Then, the first equation in (4.34) becomes

$$\int_{\Gamma} (w_1^g - w_2^g) \cdot v_2 = 0, \quad \forall v_2 \in \tilde{W}_2,$$

where

$$\tilde{W}_2 = \{v \in W_2; \operatorname{div}(v) = 0\}.$$

Besides, $w_{1|\Gamma}^g$ and $w_{2|\Gamma}^g$ belongs to the space

$$W_\Gamma = \{v \in H_{00}^{1/2}(\Gamma); \int_\Gamma v = 0\},$$

because $\operatorname{div}(w_{1|\Omega_1}^g) = 0$ and $\operatorname{div}(w_2^g) = 0$, and for all v_2 in W_Γ we can construct an extension of v_2 in the whole space \tilde{W}_2 , according to Bogovskii's result in [Bogovski, 1979]. In particular, taking $v_2 = w_{1|\Omega_1}^g - w_2^g$ in W_Γ , it follows that

$$\int_\Gamma |w_1^g - w_2^g|^2 = 0,$$

which means that $w_{1|\Gamma}^g = w_{2|\Gamma}^g$ and the equality (4.31) is satisfied. \square

A.2 Proofs of theorems related to the fluid-structure interaction problem

This appendix is dedicated to the proofs of all results stated in Subsection 4.4.2. In particular, we are interested in proving the well-posedness of Problem (4.39), in showing the existence of the control g , in giving an explicit formula for the gradient of J_k and, finally, in proving the equivalence between the minimisation of J_k and the resolution of the fluid-structure interaction problem.

We follow the order of the previous enumeration and start with the well-posedness of Problem (4.39). To study Problem (4.39), we do a change in variable on the displacement d_s^k , in order to work on a velocity-velocity formulation of the fluid-structure problem. We introduce the velocity of the structure at time t_k ,

$$u_s^k = \frac{1}{\delta t}(d_s^k - d_s^{k-1}).$$

Because Problem (4.39) is linear, it is completely equivalent to the problem where d_s^k has been replaced with $\delta u_s^k + d_s^{k-1}$:

$$\left\{ \begin{array}{l} \text{find } (u_f, u_s) \in W_u \text{ and } p \in L^2(\Phi_{t_k}(\Omega_f)) \text{ such that} \\ a((u_f, u_s), (v_f, v_s)) - (B(v_f, v_s), p)_{L^2(\Phi_{t_k}(\Omega_f))} = L(v_f, v_s), \quad \forall (v_f, v_s) \in W_u, \\ (B(u_f, u_s), q)_{L^2(\Phi_{t_k}(\Omega_f))} = 0, \quad \forall q \in L^2(\Phi_{t_k}(\Omega_f)), \end{array} \right. \quad (\text{A.5})$$

where $(\cdot, \cdot)_{L^2(\Phi_{t_k}(\Omega_f))}$ denotes the scalar product in $L^2(\Phi_{t_k}(\Omega_f))$ and a , L and B are defined by

$$\begin{aligned} a((u_f, u_s), (v_f, v_s)) &= 2\mu_f \int_{\Phi_{t_k}(\Omega_f)} D(u_f) : D(v_f) + 2\delta_t \mu_s \int_{\Omega_s} D(u_s) : D(v_s) \\ &\quad + \delta_t \lambda_s \int_{\Omega_s} \operatorname{div}(u_s) \operatorname{div}(v_s), \quad \forall (u_f, u_s), (v_f, v_s) \in W_u, \end{aligned} \quad (\text{A.6})$$

$$\begin{aligned} L(v_f, v_s) &= -2\mu_s \int_{\Omega_s} D(d_s^{k-1}) : D(v_s) - \lambda_s \int_{\Omega_s} \operatorname{div}(d_s^{k-1}) \operatorname{div}(v_s) \\ &\quad + \int_{\Phi_{t_k}(\Omega_f)} f_f \cdot v_f + \int_{\Omega_s} f_s \cdot v_s, \quad \forall (v_f, v_s) \in W_u, \\ B(v_f, v_s) &= \operatorname{div}(v_f), \quad \forall (v_f, v_s) \in W_u. \end{aligned}$$

This is a saddle-point problem, whose well-posedness can be proved using results from [Brezzi, 1974]. Using the well-known Cauchy-Schwartz and Korn inequalities, we show that the bilinear form a is continuous and coercive and that the linear form L is continuous. The operator B is also linear and continuous. It remains to show that B is surjective from W_u to $L^2(\Phi_{t_k}(\Omega_f))$. Indeed, let q be in $L^2(\Phi_{t_k}(\Omega_f))$. We can easily extend q in the whole space $L_0^2(\Omega)$; it is sufficient to take

$$E_p q = \begin{cases} q & \text{in } \Phi_{t_k}(\Omega_f), \\ \frac{-1}{|\Phi_{t_k}(\Omega_s)|} \int_{\Phi_{t_k}(\Omega_f)} q & \text{in } \Phi_{t_k}(\Omega_s). \end{cases} \quad (\text{A.7})$$

Then, $E_p q$ belongs to $L_0^2(\Omega)$ and Bogovskii's result in [Bogovski, 1979] implies that there exists \tilde{u} in $H_0^1(\Omega)$ such that $\text{div}(\tilde{u}) = E_p q$. Finally, we define $v_f = \tilde{u}|_{\Phi_{t_k}(\Omega_f)}$ and $v_s = \tilde{u}|_{\Phi_{t_k}(\Omega_s)}$ and it follows that the couple $(v_f, v_s \circ \Phi_{t_k}^{-1})$ belongs to W_u and satisfies $B(v_f, v_s \circ \Phi_{t_k}^{-1}) = \text{div}(v_f) = q$. This proves the surjectivity of the operator B . Thus, problem (A.5), and consequently problem (4.39), are well-posed.

We now give a proof of Theorem 4.10.

Proof of Theorem 4.10. We can construct two extension operators, still denoted E_u and E_p , that extend u_f^k into the whole space $(H_0^1(\Omega))^n$ (and stays divergence-free) and p_f^k into the whole space $L_0^2(\Omega)$. Indeed, for the pressure, consider the operator defined in (A.7). Then, the extension of the pressure $E_p p_f^k$ belongs to $L_0^2(\Omega)$. Now, because the fluid is incompressible, we have that

$$0 = \int_{\Phi_{t_k}(\Omega_f)} \text{div}(u_f^k) = \int_{\Phi_{t_k}(\Gamma)} u_f^k \cdot n_f^k.$$

Thus, using one more time Bogovskii's result, there exists \tilde{u}_f in $H^1(\Phi_{t_k}(\Omega_s))$ such that

$$\text{div}(\tilde{u}_f) = 0, \quad \tilde{u}_f|_{\Phi_{t_k}(\Gamma)} = u_f^k|_{\Phi_{t_k}(\Gamma)} \quad \text{and} \quad \tilde{u}_f|_{\Phi_{t_k}(\Gamma_s)} = 0.$$

Then, the extension of the fluid velocity, $E_u u_f^k$, is defined such that

$$E_u u_f^k = \begin{cases} u_f^k & \text{in } \Phi_{t_k}(\Omega_f) \\ \tilde{u}_f & \text{in } \Phi_{t_k}(\Omega_s) \end{cases}.$$

The extension $E_u u_f^k$ belongs to $(H_0^1(\Omega))^n$, is divergence-free and satisfies the equality

$$E_u u_f^k \circ \Phi_{t_k} = \frac{1}{\delta t} (d_s^k - d_s^{k-1}) \quad \text{on } \Gamma.$$

Furthermore, $\sigma_f(E_u u_f^k, E_p p_f^k)$ belongs to $(L^2(\Omega))^{n \times n}$.

Now, we construct a suitable control g in $(V_s^k)'$ such that

$$\begin{aligned} \langle g, v \rangle_{(V_s^k)', V_s^k} &= \int_{\Phi_{t_k}(\Omega_s)} \sigma_f(E_u u_f^k, E_p p_f^k) : \nabla v \\ &+ \left\langle \gamma_{n_f^k}(\sigma_f(E_u u_f^k, E_p p_f^k)), v \right\rangle_{(\Upsilon^k)', \Upsilon^k}, \quad \forall v \in V_s^k, \end{aligned} \quad (\text{A.8})$$

where n_f^k is the unit exterior normal vector to $\partial\Phi_{t_k}(\Omega_f)$. Using the Stokes formula (4.40) and the definition (A.8), it follows that the extensions $E_u u_f^k$ and $E_p p_f^k$ satisfy

$$\begin{aligned} \int_{\Omega} \sigma_f(E_u u_f^k, E_p p_f^k) : \nabla v_f &= \int_{\Phi_{t_k}(\Omega_f)} f_f^k \cdot v_f|_{\Phi_{t_k}(\Omega_f)} \\ &\quad + \left\langle g, v_f|_{\Phi_{t_k}(\Omega_s)} \right\rangle_{(V_s^k)', V_s^k}, \quad \forall v_f \in (H_0^1(\Omega))^n, \\ \int_{\Omega} q \operatorname{div}(E_u u_f^k) &= 0, \quad \forall q \in L_0^2(\Omega). \end{aligned}$$

Similarly, using (4.40), (A.8) and the weak transmission condition (4.41), d_s^k satisfies

$$\begin{aligned} \int_{\Omega_s} \sigma_s(d_s^k) : \nabla v_s &= \int_{\Omega_s} f_s^k \cdot v_s - \langle g, v_s \circ \Phi_{t_k}^{-1} \rangle_{(V_s^k)', V_s^k} \\ &\quad + \int_{\Omega_s} \Pi_f(E_u u_f^k \circ \Phi_{t_k}, E_p p_f^k \circ \Phi_{t_k}) : \nabla v_s, \quad \forall v_s \in V_s. \end{aligned}$$

Finally, we conclude that $(E_u u_f^k, E_p p_f^k, d_s^k)$ is the solution of problem (4.43). Thus,

$$(u^g, p^g, d^g) = (E_u u_f^k, E_p p_f^k, d_s^k)$$

and condition (4.44) is satisfied by construction. This proves the first part of the theorem.

Now, suppose that g is a control such that the equality (4.44) is satisfied. In particular, this implies that the couple $(u_{|\Phi_{t_k}(\Omega_f)}^g, d^g)$ belongs to the space W_d . Let us define the following Hilbert space:

$$\tilde{W}_u = \{(v_f, v_s) \in (H_0^1(\Omega))^n \times V_s; (v_f \circ \Phi_{t_k})|_{\Omega_s} = v_s\}.$$

As the unique solution of problem (4.43), the triplet (u^g, p^g, d^g) satisfies, in particular for all (v_f, v_s) in \tilde{W}_u and for all q in $L_0^2(\Omega)$, the equations

$$\begin{aligned} \int_{\Omega} \sigma_f(u^g, p^g) : \nabla v_f &= \int_{\Phi_{t_k}(\Omega_f)} f_f \cdot v_f + \langle g, v_f \rangle_{(V_s^k)', V_s^k}, \\ \int_{\Omega} q \operatorname{div}(u^g) &= 0, \\ \int_{\Omega_s} \sigma_s(d^g) : \nabla v_s &= \int_{\Omega_s} f_s \cdot v_s - \langle g, v_f \rangle_{(V_s^k)', V_s^k} + \int_{\Phi_{t_k}(\Omega_s)} \sigma_f(u^g, p^g) : \nabla v_f. \end{aligned} \tag{A.9}$$

Then adding the first and the third equations in (A.9) and using the fact that u^g is divergence-free, it follows that the triplet $(u_{|\Phi_{t_k}(\Omega_f)}^g, p_{|\Phi_{t_k}(\Omega_f)}^g, d^g)$ satisfies

$$\begin{aligned} \int_{\Phi_{t_k}(\Omega_f)} \sigma_f(u^g, p^g) : \nabla v_f + \int_{\Omega_s} \sigma_s(d^g) : \nabla v_s \\ &= \int_{\Phi_{t_k}(\Omega_f)} f_f \cdot v_f + \int_{\Omega_s} f_s \cdot v_s, \quad \forall (v_f, v_s) \in \tilde{W}_u, \\ \int_{\Phi_{t_k}(\Omega_f)} q \operatorname{div}(u^g) &= 0, \quad \forall q \in L_0^2(\Omega). \end{aligned}$$

Moreover, for all (v_f, v_s) in W_u , we can extend v_f in the whole space $(H_0^1(\Omega))^n$ as we did it for u_f^k and we denote $E_u v_f$ this extension. Similarly, for all q in $L_0^2(\Phi_{t_k}(\Omega_f))$, we extend q in the whole space $L_0^2(\Omega)$ and we denote $E_p q$ this extension. Then, the couple $(E_u v_f, v_s)$

belongs to \tilde{W}_u , $E_p q$ belongs to $L_0^2(\Omega)$ and, finally, the triplet $(u|_{\Phi_{t_k}(\Omega_f)}^g, p|_{\Phi_{t_k}(\Omega_f)}^g, d^g)$ satisfies the equations

$$\begin{aligned} \int_{\Phi_{t_k}(\Omega_f)} \sigma_f(u|_{\Phi_{t_k}(\Omega_f)}^g, p|_{\Phi_{t_k}(\Omega_f)}^g) : \nabla v_f + \int_{\Omega_s} \sigma_s(d^g) : \nabla v_s \\ = \int_{\Phi_{t_k}(\Omega_f)} f_f \cdot v_f + \int_{\Omega_s} f_s \cdot v_s, \quad \forall (v_f, v_s) \in W_u, \\ \int_{\Phi_{t_k}(\Omega_f)} q \operatorname{div}(u|_{\Phi_{t_k}(\Omega_f)}^g) = 0, \quad \forall q \in L^2(\Phi_{t_k}(\Omega_f)). \end{aligned}$$

Thus, the triplet $(u|_{\Phi_{t_k}(\Omega_f)}^g, p|_{\Phi_{t_k}(\Omega_f)}^g, d^g)$ is the unique solution of the initial fluid-structure problem (4.39), which proves that we can recover the solution of the fluid-structure interaction problem from the solution of its smooth extension formulation. \square

Since there exists at least one suitable control g for the smooth extension problem, we can hope to obtain it by a minimisation process on the function J_k . This is actually possible according to Theorem 4.11, which states that J_k is differentiable with respect to g and gives a characterisation of its gradient. Here, we prove this result.

Proof of Theorem 4.11. On the first hand, the differentiation of the Lagrangian function \mathcal{L}_k , defined in (4.46), with respect to u , p , d and g follows the same process that the one explained for the Laplace and Stokes transmission problems. Here, we only give the expressions of these different derivatives:

$$\begin{aligned} \left\langle \frac{\mathcal{L}_k}{\partial u}, \delta u \right\rangle_{H^{-1}(\Omega), H_0^1(\Omega)} &= \int_{\Phi_{t_k}(\Omega_f)} \sigma_f(\lambda_f, \pi) : \nabla \delta u \\ &\quad - 2\mu_f \int_{\Phi_{t_k}(\Omega_s)} D(\nu_s \circ \Phi_{t_k}^{-1}) : D(\delta u) \\ &\quad + \int_{\Gamma} (u \circ \Phi_{t_k} - \frac{1}{\delta t} (d - d^{k-1})) \cdot (\delta u \circ \Phi_{t_k}), \quad \forall \delta u \in (H_0^1(\Omega))^n, \\ \left\langle \frac{\mathcal{L}_k}{\partial p}, \delta p \right\rangle_{L^2(\Omega), L^2(\Omega)} &= - \int_{\Omega} \delta p \operatorname{div}(\lambda_f) + \int_{\Omega_s} \delta p \operatorname{div}(\nu_s \circ \Phi_{t_k}^{-1}), \quad \forall \delta p \in L_0^2(\Omega), \\ \left\langle \frac{\mathcal{L}_k}{\partial d}, \delta d \right\rangle_{V'_s, V_s} &= \int_{\Omega_s} \sigma_s(\nu_s) : \nabla \delta d \\ &\quad - \frac{1}{\delta t} \int_{\Gamma} (u \circ \Phi_{t_k} - \frac{1}{\delta t} (d - d^{k-1})) \cdot \delta d, \quad \forall \delta d \in V_s, \\ \left\langle \frac{\mathcal{L}_k}{\partial g}, \delta g \right\rangle_{V''_{s,k}, V'_{s,k}} &= \left\langle \delta g, \nu_s \circ \Phi_{t_k}^{-1} - \lambda_f|_{\Phi_{t_k}(\Omega_s)} \right\rangle_{(V_s^k)', V_s^k}, \quad \forall \delta g \in V'_{s,k}. \end{aligned}$$

They enable us, in particular, to recover the adjoint equations, written in (4.47). Problem (4.47) consists in a linear elasticity problem and a Stokes problem, whose well-posedness derives from the same arguments that we already used. We denote by $(\nu^g, \lambda^g, \pi^g)$ its unique solution.

On the other hand, the differentiability of J_k relies on the same arguments that the ones used in the proof of Theorem 4.3 and the fact that the transformation Φ_{t_k} is sufficiently regular. Then, replacing (u, p, d) in the Lagrangian function (4.46), by the solution (u^g, p^g, d^g) of the smooth extension problem (4.43), the Lagrangian (4.46) reduces to

$$\mathcal{L}_k(g, (u^g, p^g, d^g), (\lambda_f, \pi, \nu_s)) = J_k(g), \quad \forall g \in (V_s^k)'.$$

Differentiating with respect to g using the chain rule and replacing the triplet (λ_f, π, ν_s) by the solution $(\lambda^g, \pi^g, \nu^g)$ of the adjoint problem (4.47), the gradient of J_k is finally given by,

$$\langle \nabla J_k(g), \delta g \rangle_{(V_s^k)'', (V_s^k)'} = \left\langle \delta g, \nu_k^g \circ \Phi_{t_k}^{-1} - \lambda_{k|\Phi_{t_k}(\Omega_s)}^g \right\rangle_{(V_s^k)', V_s^k}, \quad \forall \delta g \in (V_s^k)'. \quad \square$$

With this explicit expression of the gradient of J_k , we can now state the equivalence between the research of a suitable control such that the solution of the smooth extension problem (4.43) satisfies the condition (4.44) and the minimisation of J_k . This is the result of Theorem 4.12, that we prove in the following.

Proof of Theorem 4.12. On the one hand, if for a given g in $(V_s^k)'$, the solution (u^g, p^g, d^g) of the smooth extension problem (4.43) satisfies the condition (4.44), then

$$J_k(g) = 0.$$

On the other hand, suppose that g is a minimiser of J_k . Then, the adjoints λ^g and ν^g satisfy the equality,

$$\left\langle \delta g, \nu^g \circ \Phi_{t_k}^{-1} - \lambda_{|\Phi_{t_k}(\Omega_s)}^g \right\rangle_{(V_s^k)', V_s^k} = 0, \quad \forall \delta g \in (V_s^k)',$$

which corresponds to the fact that g is a zero for the gradient of J_k . It follows, in particular, that,

$$\nu^g \circ \Phi_{t_k}^{-1} = \lambda_{|\Phi_{t_k}(\Omega_s)}^g, \quad (\text{A.10})$$

and the couple $(\lambda_{|\Phi_{t_k}(\Omega_f)}^g, \nu^g)$ belongs to the space W_u . Yet, λ^g , π^g and ν^g satisfy the adjoint equations in (4.47). In particular, for all (v_f, v_s) in \hat{W}_u and for all q in $L_0^2(\Omega)$, where

$$\hat{W}_u = \{(v_f, v_s) \in (H_0^1(\Omega))^n \times V_s; \operatorname{div}(v_f) = 0, (v_f \circ \Phi_{t_k})|_{\Omega_s} = v_s\},$$

these equations write

$$\begin{aligned} \mu_s \int_{\Omega_s} \sigma_s(\nu^g) : \nabla v_s &= \frac{1}{\delta t} \int_{\Gamma} (u^g \circ \Phi_{t_k} - \frac{1}{\delta t} (d^g - d_s^{k-1})) \cdot v_s, \\ 2\mu_f \int_{\Phi_{t_k}(\Omega_f)} D(\lambda^g) : D(v_f) - \int_{\Omega} \pi^g \operatorname{div}(v_f) &= - \int_{\Gamma} (u^g \circ \Phi_{t_k} - \frac{1}{\delta t} (d^g - d_s^{k-1})) \cdot v_s, \\ \int_{\Phi_{t_k}(\Omega_f)} q \operatorname{div}(\lambda^g) &= 0, \end{aligned} \quad (\text{A.11})$$

Multiplying the first equation in (A.11) by δt and summing it with the second one, we obtain that,

$$2\mu_f \int_{\Phi_{t_k}(\Omega_f)} D(\lambda_{|\Phi_{t_k}(\Omega_f)}^g) : D(v_f) + \delta t \mu_s \int_{\Omega_s} \sigma_s(\nu^g) : \nabla v_s = 0, \quad \forall (v_f, v_s) \in \hat{W}_u. \quad (\text{A.12})$$

Moreover, let (v_f, v_s) be in W_u . We can construct an extension of v_f in the whole space $(H_0^1(\Omega))^n$, denoted $E_u v_f$, such that $\operatorname{div}(E_u v_f) = 0$ and $((E_u v_f) \circ \Phi_{t_k})|_{\Gamma} = v_s|_{\Gamma}$, as we did it in the proof of Theorem 4.10. Then, the couple $(E_u v_f, v_s)$ belongs to \hat{W}_u and it follows that the couple $(\lambda_{|\Phi_{t_k}(\Omega_f)}^g, \nu^g)$ satisfies the equation

$$2\mu_f \int_{\Phi_{t_k}(\Omega_f)} D(\lambda_{|\Phi_{t_k}(\Omega_f)}^g) : D(v_f) + \delta t \mu_s \int_{\Omega_s} \sigma_s(\nu^g) : \nabla v_s = 0, \quad \forall (v_f, v_s) \in W_u.$$

We conclude that $(\lambda_{|\Phi_{t_k}^g(\Omega_f)}^g, \nu^g)$ is solution of the problem

$$\begin{cases} \text{find } (\lambda, \nu) \text{ in } W_u \text{ such that,} \\ a((\lambda, \nu), (v_f, v_s)) = 0, \quad \forall (v_f, v_s) \in W_u, \end{cases} \quad (\text{A.13})$$

where the bilinear continuous and coercive form a has been defined in (A.6), which admits the zero of W_u as unique solution. Then, the first equation in (4.47) becomes

$$\int_{\Gamma} \left(u^g \circ \Phi_{t_k} - \frac{1}{\delta_t} (d^g - d_s^{k-1}) \right) \cdot v_s = 0, \quad \forall v_s \in V_s.$$

Moreover, for all v_s in $(H_{00}^{1/2}(\Gamma))^n$ we can construct an extension of v_s in the whole space V_s .

In particular, taking $v_s = (u^g \circ \Phi_{t_k})_{|\Gamma} - \frac{1}{\delta_t} (d_{|\Gamma}^g - d_{s|\Gamma}^{k-1})$, it follows that

$$\int_{\Gamma} |(u^g \circ \Phi_{t_k})_{|\Gamma} - \frac{1}{\delta_t} (d_{|\Gamma}^g - d_{s|\Gamma}^{k-1})|^2 = 0,$$

which means that $(u^g \circ \Phi_{t_k})_{|\Gamma} = \frac{1}{\delta_t} (d_{|\Gamma}^g - d_{s|\Gamma}^{k-1})$ and the equality (4.44) is satisfied. \square

Appendix B

Transformation of the Stokes equations into the reference configuration

The present appendix is dedicated to justify the change of variables mentioned in Chapter 2, Chapter 3 and Chapter 4 in order to write the fluid equations into their reference configuration. The presentation of the different results and demonstrations given in the following are largely inspired by [Ciarlet, 1988] and [Le Dret, 2003].

B.1 Deformations

Let Ω be a domain in \mathbb{R}^n ($n = 2$ or 3), i.e. a bounded open connected subset of \mathbb{R}^n with a Lipschitz boundary. The points x contained in $\bar{\Omega}$ are the material points of a solid body which lies at rest. The domain Ω is said to be the *reference configuration* of that solid. When forces are applied to the body, it deforms. The material point initially placed at x is sent to the position $y = \Phi(x)$, where Φ is a mapping from $\bar{\Omega}$ to \mathbb{R}^n , called the *deformation* of the solid body. Then, the subset $\Phi(\Omega)$ of \mathbb{R}^n is the *deformed configuration* of the solid. From a mathematical point of view, the transformation from one configuration to the other is just a change of variables.

In the following, it is assumed that the deformations are sufficiently regular that what is written makes sense. We should also consider that deformations are globally injective in such a way as to prohibit the interpenetration of the material but not necessarily self-contacts on the boundary. Moreover, elastic deformations should preserve the orientation. Note that if Φ is sufficiently regular (e.g. a C^1 -diffeomorphism) $\Phi(\Omega)$ is also a domain of \mathbb{R}^n .

The matrix $\nabla\Phi$, where each entry is defined by

$$(\nabla\Phi)_{ij} = \partial_j\Phi_i,$$

is called the *deformation gradient* and represents the differential of the mapping Φ in the sense that

$$\Phi(x+h) = \Phi(x) + \nabla\Phi(x)h + o(\|h\|),$$

for x and $x+h$ in Ω .

The orientation preserving condition can be explicitly written by mean of the deformation gradient, with the condition that

$$\det(\nabla\Phi(x)) > 0,$$

in Ω . If Φ is of class C^1 , this condition also implies that Φ is locally a C^1 -diffeomorphism, due to the local inversion Theorem.

B.2 Transformation from the deformed configuration to the reference configuration

The purpose of this section is to write the transformation of an equation in conservative form (e.g. the Stokes equations (2.11)) from the deformed configuration $\Phi(\Omega)$ to the reference configuration Ω . To that aim, we start by recalling some well-known identities on the gradient deformation $\nabla\Phi$, then we explain how the deformation transforms the volumes with scalar and vector functions in divergence form.

B.2.1 Preliminaries

Let Φ be an orientation preserving C^1 -diffeomorphism that is twice differentiable. For all x in Ω , one has $\Phi^{-1}(\Phi(x)) = x$. Differentiating this equality using the chain rule we find the following fundamental identity:

$$\nabla_x \Phi(x) \nabla_y \Phi^{-1}(y) = I \implies (\nabla_x \Phi(x))^{-1} = \nabla_y \Phi^{-1}(y), \forall x \in \Omega, \quad (\text{B.1})$$

where we denote $y = \Phi(x)$.

If A is a matrix in $\mathbb{R}^{n \times n}$, we denote by $\text{cof}(A)$ the *cofactor matrix* associated to A , i.e. the matrix defined such that

$$A \text{cof}(A)^T = \text{cof}(A)^T A = \det(A)I.$$

Concerning the cofactor matrix associated to the gradient deformation, we have the following remarkable property called the *Piola identity*.

Proposition B.1. *Let Φ be a twice differentiable deformation. Then*

$$\text{div}(\text{cof}(\nabla\Phi)) = 0, \quad (\text{B.2})$$

where the divergence operator of a matrix is given by

$$(\text{div}(A))_i = \partial_j A_{ij}, \text{ for all } i, j \text{ in } \{1, \dots, n\}.$$

Proof. Let us begin with the case $n = 2$. The cofactor matrix writes

$$\text{cof}(\nabla\Phi) = \begin{pmatrix} \partial_2 \Phi_2 & -\partial_1 \Phi_2 \\ -\partial_2 \Phi_1 & \partial_1 \Phi_1 \end{pmatrix}$$

and it simply follows that

$$\text{div}(\text{cof}(\nabla\Phi)) = \begin{pmatrix} \partial_1 \partial_2 \Phi_2 - \partial_2 \partial_1 \Phi_2 \\ -\partial_1 \partial_2 \Phi_1 + \partial_2 \partial_1 \Phi_1 \end{pmatrix} = \begin{pmatrix} 0 \\ 0 \end{pmatrix}.$$

For the case $n = 3$, the first line of $\text{cof}(\nabla\Phi)$ is given by

$$\begin{aligned} (\text{cof}(\nabla\Phi))_{11} &= \partial_2(\Phi_2 \partial_3 \Phi_3) - \partial_3(\Phi_2 \partial_2 \Phi_3), \\ (\text{cof}(\nabla\Phi))_{12} &= \partial_3(\Phi_2 \partial_1 \Phi_3) - \partial_1(\Phi_2 \partial_3 \Phi_3), \\ (\text{cof}(\nabla\Phi))_{13} &= \partial_1(\Phi_2 \partial_2 \Phi_3) - \partial_2(\Phi_2 \partial_1 \Phi_3). \end{aligned}$$

We remark that the first line of the cofactor matrix is formed by the components of the curl of the vector

$$(\Phi_2 \partial_1 \Phi_3, \Phi_2 \partial_2 \Phi_3, \Phi_2 \partial_3 \Phi_3)^T.$$

Thus, the divergence of the first line of $\text{cof}(\nabla\Phi)$ is zero and this is also true for the two other lines. \square

B.2.2 Transformation of volumes

We recall the standard formula for change of variables for volume integrals.

Proposition B.2. *Let Ω be a domain in \mathbb{R}^n and let Φ be an orientation-preserving C^1 -diffeomorphism from Ω to \mathbb{R}^n . For all integrable scalar function f in $\Phi(\Omega)$, we have the change of variables formula*

$$\int_{\Phi(\Omega)} f(y)dy = \int_{\Omega} f \circ \Phi(x) \det(\nabla\Phi(x))dx. \quad (\text{B.3})$$

The interested reader could find a proof of this formula in [Briane and Pages, 2018], for example. Moreover, from this result we directly obtain the following corollary for the change of variables of the product of two functions.

Corollary B.1. *Let Ω be a domain in \mathbb{R}^n and let Φ be an orientation-preserving C^1 -diffeomorphism from Ω to \mathbb{R}^n . For all scalar functions f and v in $\Phi(\Omega)$, such that the product fv is integrable in $\Phi(\Omega)$, we have the change of variables formula*

$$\int_{\Phi(\Omega)} f(y)v(y)dy = \int_{\Omega} (f \circ \Phi(x))(v \circ \Phi(x)) \det(\nabla\Phi(x))dx.$$

B.2.3 Transformation of the divergence of a vector function

Proposition B.3. *Let Ω be a domain in \mathbb{R}^n and let Φ be an orientation-preserving C^1 -diffeomorphism from Ω to \mathbb{R}^n . For all differentiable vector function f from $\Phi(\Omega)$ to \mathbb{R}^n , such that $\text{div}(f)$ is integrable in $\Phi(\Omega)$, we have the formula*

$$\int_{\Phi(\Omega)} \text{div}(f(y))dy = \int_{\Omega} \text{div}(\text{cof}(\nabla\Phi(x))^T f \circ \Phi(x))dx. \quad (\text{B.4})$$

Proof. Using the formula for change of variables (B.3), we have that

$$\begin{aligned} \int_{\Phi(\Omega)} \text{div}_y(f(y))dy &= \int_{\Omega} \text{div}_{\Phi(x)}(f \circ \Phi(x)) \det(\nabla_x\Phi(x))dx, \\ &= \int_{\Omega} \sum_{i=1}^n \frac{\partial f_i \circ \Phi(x)}{\partial \Phi_i(x)} \det(\nabla_x\Phi(x))dx, \\ &= \int_{\Omega} \sum_{i,j=1}^n \frac{\partial f_i \circ \Phi(x)}{\partial x_j} \frac{\partial x_j}{\partial \Phi_i(x)} \det(\nabla_x\Phi(x))dx, \\ &= \int_{\Omega} \sum_{i,j=1}^n (\nabla_x f \circ \Phi)_{ij}(x) (\nabla_y \Phi^{-1}(y))_{ji} \det(\nabla_x\Phi(x))dx. \end{aligned}$$

Then, using the identity (B.1), it follows that

$$\begin{aligned} \int_{\Phi(\Omega)} \text{div}_y(f(y))dy &= \int_{\Omega} \nabla_x(f \circ \Phi)(x) : (\nabla_x\Phi(x))^{-T} \det(\nabla_x\Phi(x))dx, \\ &= \int_{\Omega} \nabla(f \circ \Phi) : \text{cof}(\nabla\Phi) \end{aligned}$$

Yet, on the other side, we have in Ω

$$\begin{aligned}
& \operatorname{div}(\operatorname{cof}(\nabla\Phi(x))^T f \circ \Phi(x)) \\
&= \sum_{i=1}^n \frac{\partial(\operatorname{cof}(\nabla\Phi(x))^T f \circ \Phi(x))_i}{\partial x_i}, \\
&= \sum_{i=1}^n \frac{\partial}{\partial x_i} \left(\sum_{j=1}^n (\operatorname{cof}(\nabla\Phi(x))^T)_{ij} f_j \circ \Phi(x) \right), \\
&= \sum_{j=1}^n \sum_{i=1}^n \left(\frac{\partial(\operatorname{cof}(\nabla\Phi(x))^T)_{ij}}{\partial x_i} f_j \circ \Phi(x) + (\operatorname{cof}(\nabla\Phi(x))^T)_{ij} \frac{\partial f_j \circ \Phi(x)}{\partial x_i} \right), \\
&= \sum_{j=1}^n f_j \circ \Phi_j(x) \sum_{i=1}^n \frac{\partial(\operatorname{cof}(\nabla\Phi(x)))_{ji}}{\partial x_i} + \sum_{i,j=1}^n (\operatorname{cof}(\nabla\Phi(x))^T)_{ij} (\nabla f \circ \Phi(x))_{ji}, \\
&= (f \circ \Phi(x)) \cdot \operatorname{div}(\operatorname{cof}(\nabla\Phi(x))) + \operatorname{cof}(\nabla\Phi(x))^T : \nabla(f \circ \Phi)(x)^T,
\end{aligned}$$

and using the Piola identity (B.2),

$$\begin{aligned}
\operatorname{div}(\operatorname{cof}(\nabla\Phi(x))^T f \circ \Phi(x)) &= \operatorname{cof}(\nabla\Phi(x))^T : \nabla(f \circ \Phi)(x)^T, \\
&= \operatorname{cof}(\nabla\Phi(x)) : \nabla(f \circ \Phi)(x),
\end{aligned}$$

in Ω , which proves formula (B.4). □

Corollary B.2. *Let Ω be a domain in \mathbb{R}^n and let Φ be an orientation-preserving C^1 -diffeomorphism from Ω to \mathbb{R}^n . For all differentiable vector function f from $\Phi(\Omega)$ to \mathbb{R}^n and for all scalar function v from $\Phi(\Omega)$ to \mathbb{R} , such that the product $\operatorname{div}(f)v$ is integrable in $\Phi(\Omega)$, we have the formula*

$$\int_{\Phi(\Omega)} \operatorname{div}(f(y))v(y)dy = \int_{\Omega} \operatorname{div}(\operatorname{cof}(\nabla\Phi(x))^T (f \circ \Phi(x)))(v \circ \Phi(x))dx.$$

Within the proof of Proposition B.3, we also prove the following remarkable identity.

Corollary B.3. *For all differentiable vector function f from $\Phi(\Omega)$ to \mathbb{R}^n , we have*

$$\operatorname{div}_x(\operatorname{cof}(\nabla_x\Phi(x))^T (f \circ \Phi)(x)) = \det(\nabla_x\Phi(x))\operatorname{div}_{\Phi(x)}(f \circ \Phi(x)). \quad (\text{B.5})$$

B.2.4 Transformation of the divergence of a matrix function

Proposition B.4. *Let Ω be a domain in \mathbb{R}^n and let Φ be an orientation-preserving C^1 -diffeomorphism from Ω to \mathbb{R}^n . For all differentiable matrix function σ from $\Phi(\Omega)$ to $\mathbb{R}^{n \times n}$, such that $\operatorname{div}(\sigma)$ is integrable in $\Phi(\Omega)$, we have the formula*

$$\int_{\Phi(\Omega)} \operatorname{div}(\sigma(y))dy = \int_{\Omega} \operatorname{div}(\sigma \circ \Phi(x)\operatorname{cof}(\nabla\Phi(x)))dx. \quad (\text{B.6})$$

Proof. For each component i of $\operatorname{div}(\sigma)$, we have

$$\begin{aligned}
\int_{\Phi(\Omega)} (\operatorname{div}(\sigma(y)))_i dy &= \int_{\Phi(\Omega)} \sum_{j=1}^n \frac{\partial\sigma_{ij}(y)}{\partial y_j} dy, \\
&= \int_{\Phi(\Omega)} \operatorname{div}(\sigma^{l_i}(y))dy,
\end{aligned}$$

where σ^{li} is the (column) vector whose coefficients are the components of the line i of σ . Then, using formula (B.4) it comes, for all i in $\{1, \dots, n\}$,

$$\int_{\Phi(\Omega)} \operatorname{div}(\sigma^{li}(y))dy = \int_{\Omega} \operatorname{div}(\operatorname{cof}(\nabla\Phi(x))^T \sigma^{li} \circ \Phi(x))dx.$$

Yet, for all i in $\{1, \dots, n\}$, if we denote $A = \operatorname{cof}(\nabla\Phi)$ and $b = \sigma^{li} \circ \Phi$, the divergence term in the previous equality term writes (using Einstein summation rule),

$$\begin{aligned} \operatorname{div}(\operatorname{cof}(\nabla\Phi)^T \sigma^{li} \circ \Phi) &= \operatorname{div}(A^T b), \\ &= \partial_j (A^T b)_j, \\ &= \partial_j (A_{jk}^T b_k), \\ &= \partial_j (b_k A_{kj}), \\ &= \partial_j ((\sigma \circ \Phi)_{ik} \operatorname{cof}(\nabla\Phi)_{kj}), \\ &= \partial_j (\sigma \circ \Phi \operatorname{cof}(\nabla\Phi))_{ij}, \\ &= (\operatorname{div}(\sigma \circ \Phi \operatorname{cof}(\nabla\Phi)))_i, \end{aligned}$$

and this proves formula (B.6). □

Corollary B.4. *Let Ω be a domain in \mathbb{R}^n and let Φ be an orientation-preserving C^1 -diffeomorphism from Ω to \mathbb{R}^n . For all differentiable matrix function σ from $\Phi(\Omega)$ to $\mathbb{R}^{n \times n}$ and for all vector function v from $\Phi(\Omega)$ to \mathbb{R}^n , such that the scalar product $\operatorname{div}(\sigma) \cdot v$ is integrable in $\Phi(\Omega)$, we have the formula*

$$\int_{\Phi(\Omega)} \operatorname{div}(\sigma(y)) \cdot v(y)dy = \int_{\Omega} \operatorname{div}(\sigma \circ \Phi(x) \operatorname{cof}(\nabla\Phi(x))) \cdot (v \circ \Phi(x))dx.$$

B.2.5 The Piola transform

In the change of variables formula (B.6), we made use of the tensor field $\sigma \circ \Phi \operatorname{cof}(\nabla\Phi)$, defined in the reference configuration Ω . This transformation of the tensor σ is called the *Piola transform* and is defined in the following.

Definition B.1. Let σ be a tensor field from $\Phi(\Omega)$ to $\mathbb{R}^{n \times n}$. The Piola transform of σ is the tensor field defined in Ω by

$$\Phi_* \sigma(x) = (\sigma \circ \Phi(x)) \operatorname{cof}(\nabla\Phi(x)), \text{ in } \Omega.$$

A remarkable property of the Piola transform concerns its divergence.

Proposition B.5. *For all tensor field $\sigma : \Phi(\Omega) \rightarrow \mathbb{R}^{n \times n}$, we have*

$$\operatorname{div}_x(\Phi_* \sigma)(x) = \det(\nabla\Phi(x)) \operatorname{div}_{\Phi(x)}(\sigma(\Phi(x))), \text{ in } \Omega. \quad (\text{B.7})$$

Proof. We use the formula for the divergence of a matrix product:

$$\operatorname{div}(AB) = \operatorname{div}_B A + A \operatorname{div}(B)$$

for all regular matrices A and B , where the operator div_B is defined component by component by

$$(\operatorname{div}_B)_i = B_{ij} \partial_j, \text{ for all } i \text{ in } \{1, \dots, n\}.$$

Thus, we have that

$$\operatorname{div}_x(\Phi_*\sigma)(x) = \operatorname{div}_{x,\operatorname{cof}(\nabla\Phi)}(\sigma \circ \Phi)(x) + (\sigma \circ \Phi)(x)\operatorname{div}_x(\operatorname{cof}(\nabla\Phi(x))).$$

The second term is zero, according to Piola identity (B.2). For the first term, on proceed component by component. For i in $\{1, \dots, n\}$, we have

$$\begin{aligned} (\operatorname{div}_{x,\operatorname{cof}(\nabla\Phi)}(\sigma \circ \Phi))_i(x) &= \operatorname{cof}(\nabla\Phi)_{kj}(x) \frac{\partial(\sigma \circ \Phi)_{ik}}{\partial x_j}(x), \\ &= \operatorname{cof}(\nabla\Phi)_{kj}(x) \frac{\partial\sigma_{ik}}{\partial y_l}(\Phi(x)) \frac{\partial\Phi_l}{\partial x_j}(x), \\ &= (\nabla\Phi)_{lj}(x) \operatorname{cof}(\nabla\Phi)_{jk}^T(x) \frac{\partial\sigma_{ik}}{\partial y_l}(\Phi(x)), \\ &= \det(\nabla\Phi(x)) \delta_{lk} \frac{\partial\sigma_{ik}}{\partial y_l}(\Phi(x)), \\ &= \det(\nabla\Phi(x)) \frac{\partial\sigma_{il}}{\partial y_l}(\Phi(x)), \\ &= \det(\nabla\Phi(x)) (\operatorname{div}_y\sigma)_i(\Phi(x)). \end{aligned}$$

□

B.3 Application to the transformation of the Stokes equations

Let Ω be a domain in \mathbb{R}^n and let Φ be an orientation-preserving C^1 -diffeomorphism from Ω to \mathbb{R}^n . The Stokes equations are usually written in Eulerian coordinates, i.e. in the deformed configuration $\Phi(\Omega)$. For example, the Stokes problem with homogeneous Dirichlet boundary conditions writes

$$\left\{ \begin{array}{l} \text{find } u : \Phi(\Omega) \rightarrow \mathbb{R}^n \text{ and } p : \Phi(\Omega) \rightarrow \mathbb{R} \text{ such that} \\ -\operatorname{div}(\sigma_f) = f, \quad \text{in } \Phi(\Omega), \\ \operatorname{div}(u) = 0, \quad \text{in } \Phi(\Omega), \\ u = 0, \quad \text{on } \partial\Phi(\Omega). \end{array} \right. \quad (\text{B.8})$$

where σ_f is the fluid stress tensor defined in $\Phi(\Omega)$ by

$$\begin{aligned} \sigma_f &= 2\mu_f D(u) - pI, \\ D(u) &= \frac{1}{2}(\nabla u + \nabla u^T), \end{aligned}$$

and μ_f is the viscosity of the fluid.

Proposition B.6. *Let $w = u \circ \Phi$ and $q = p \circ \Phi$ be the velocity and the pressure of the fluid written in the reference fluid domain Ω . We also define the matrices F and G wich write*

$$\begin{aligned} F &= \nabla\Phi^{-1}\operatorname{cof}(\nabla\Phi), \\ G &= \operatorname{cof}(\nabla\Phi). \end{aligned}$$

Then, the Stokes equations (B.8) written in the reference configuration are

$$\left\{ \begin{array}{l} \text{find } w : \Omega \rightarrow \mathbb{R}^n \text{ and } q : \Omega \rightarrow \mathbb{R} \text{ such that} \\ -\operatorname{div}(\Pi_f) = \det(\nabla\Phi) f \circ \Phi, \quad \text{in } \Omega, \\ \operatorname{div}(G^T w) = 0, \quad \text{in } \Omega, \\ w = 0, \quad \text{on } \partial\Omega. \end{array} \right. \quad (\text{B.9})$$

where Π_f is the Piola transform of σ , i.e. the fluid stress tensor written in the reference configuration, defined in Ω by

$$\begin{aligned}\Pi_f &= \sigma_f \circ \Phi \operatorname{cof}(\nabla \Phi), \\ &= \mu_f (\nabla w F + \nabla \Phi^{-T} \nabla w G) - qG, \\ &= \mu_f ((F \nabla) w + \nabla \Phi^{-T} \nabla w G) - qG.\end{aligned}$$

Proof. The proof is straightforward using formulas (B.5) and (B.7). Indeed, we have in Ω ,

$$\begin{aligned}\operatorname{div}_x(\Pi_f(x)) &= \operatorname{div}_x(\Phi_* \sigma_f(x)), \\ &= \det(\nabla \Phi(x)) \operatorname{div}_{\Phi(x)}(\sigma_f(\Phi(x))), \\ &= -\det(\nabla \Phi(x)) f \circ \Phi(x)\end{aligned}$$

and

$$\begin{aligned}\operatorname{div}_x(G(x)^T w(x)) &= \operatorname{div}_x(\operatorname{cof}(\nabla \Phi(x))(u \circ \Phi)(x)), \\ &= \det(\nabla \Phi(x)) \operatorname{div}_{\Phi(x)}(u \circ \Phi(x)) = 0.\end{aligned}$$

Moreover, we verify that the expression of Π_f is correct. By definition of the Piola transform, we have

$$\begin{aligned}\Pi_f(x) &= \sigma_f \circ \Phi(x) \operatorname{cof}(\nabla_x \Phi(x)), \\ &= (\mu_f (\nabla_{\Phi(x)}(u \circ \Phi)(x) + (\nabla_{\Phi(x)}(u \circ \Phi)(x))^T) - p \circ \Phi(x) I) G(x).\end{aligned}$$

Yet, using the chain rule it follows that

$$\begin{aligned}\nabla_{\Phi(x)}(u \circ \Phi)(x) &= \nabla_x(u \circ \Phi)(x) \nabla_x \Phi(x)^{-1}, \\ &= \nabla_x w(x) \nabla_x \Phi(x)^{-1}\end{aligned}$$

Then,

$$\begin{aligned}\Pi_f(x) &= \mu_f (\nabla_x w(x) \nabla_x \Phi(x)^{-1} + \nabla_x \Phi(x)^{-T} \nabla_x w(x)^T) G(x) - q(x) G(x), \\ &= \mu_f (\nabla_x w(x) F(x) + \nabla_x \Phi(x)^{-T} \nabla_x w(x) G(x)) - q(x) G(x).\end{aligned}$$

Finally, for all sufficiently regular matrix field A and vector field u , we have that $(A \nabla) u = (\nabla u) A^T$. Since the matrix F is symmetric, it follows that

$$\Pi_f(x) = \mu_f ((F(x) \nabla_x) w(x) + \nabla_x \Phi(x)^{-T} \nabla_x w(x) G(x)) - q(x) G(x).$$

□

Bibliography

- [Adams and Fournier, 2003] Adams, R. A. and Fournier, J. J. (2003). *Sobolev spaces*, volume 140. Academic Press.
- [Afzelius and Eliasson, 1983] Afzelius, B. and Eliasson, R. (1983). Male and female infertility problems in the immotile-cilia syndrome. *European Journal of Respiratory Diseases. Supplement*, 127:144–147.
- [Alauzet et al., 2016] Alauzet, F., Fabrèges, B., Fernández, M., and Landajuela, M. (2016). Nitsche-XFEM for the coupling of an incompressible fluid with immersed thin-walled structures. *Computer Methods in Applied Mechanics and Engineering*, 301:300–335.
- [Alouges and Di Fratta, 2018] Alouges, F. and Di Fratta, G. (2018). Parking 3-sphere swimmer I. Energy minimizing strokes. *Discrete And Continuous Dynamical Systems*, 23(4):1797–1817.
- [Ambrosi and Pezzuto, 2012] Ambrosi, D. and Pezzuto, S. (2012). Active stress vs. active strain in mechanobiology: constitutive issues. *Journal of Elasticity*, 107(2):199–212.
- [Atamian et al., 1991] Atamian, C., Dinh, Q., Glowinski, R., He, J., and Périaux, J. (1991). Control approach to fictitious-domain methods. Application to fluid dynamics and electro-magnetics. In *Proceedings of the Fourth International Symposium on Domain Decomposition Methods for Partial Differential Equations*, R. Glowinski, Y. Kuznetsov, G. Meurant, J. Périaux, and OB Widlund, eds., SIAM, Philadelphia, pages 275–309.
- [Atamian and Joly, 1993] Atamian, C. and Joly, P. (1993). Une analyse de la méthode des domaines fictifs pour le problème de Helmholtz extérieur. *ESAIM: Mathematical Modelling and Numerical Analysis*, 27(3):251–288.
- [Baaijens, 2001] Baaijens, F. P. (2001). A fictitious domain/mortar element method for fluid-structure interaction. *International Journal for Numerical Methods in Fluids*, 35(7):743–761.
- [Babič, 1953] Babič, V. M. (1953). On the extension of functions. *Uspekhi Matematicheskikh Nauk*, 8(2(54)):111–113.
- [Behzadan and Holst, 2015] Behzadan, A. and Holst, M. (2015). Multiplication in Sobolev spaces, revisited. *arXiv preprint arXiv: 1512. 07379*.
- [Berg, 2002] Berg, H. C. (2002). How Spiroplasma might swim. *Journal of Bacteriology*, 184(8):2063–2064.
- [Bertoluzza et al., 2011] Bertoluzza, S., Ismail, M., and Maury, B. (2011). Analysis of the fully discrete fat boundary method. *Numerische Mathematik*, 118(1):49–77.
- [Blake, 1971a] Blake, J. R. (1971a). Infinite models for ciliary propulsion. *Journal of Fluid Mechanics*, 49(2):209–222.
- [Blake, 1971b] Blake, J. R. (1971b). A spherical envelope approach to ciliary propulsion. *Journal of Fluid Mechanics*, 46(1):199–208.

- [Bogen et al., 1980] Bogen, D. K., Rabinowitz, S. A., Needleman, A., McMahon, T. A., and Abelmann, W. H. (1980). An analysis of the mechanical disadvantage of myocardial infarction in the canine left ventricle. *Circulation Research*, 47(5):728–741.
- [Bogovski, 1979] Bogovski, M. E. (1979). Solution of the first boundary value problem for an equation of continuity of an incompressible medium. *Doklady Akademii Nauk SSSR*, 248(5):10371040.
- [Boilevin-Kayl et al., 2019] Boilevin-Kayl, L., Fernández, M. A., and Gerbeau, J.-F. (2019). Numerical methods for immersed FSI with thin-walled structures. *Computers and Fluids*, 179:744–763.
- [Boulakia, 2003] Boulakia, M. (2003). Existence of weak solutions for the motion of an elastic structure in an incompressible viscous fluid. *Comptes Rendus Mathématique*, 336(12):985–990.
- [Boulakia, 2007] Boulakia, M. (2007). Existence of weak solutions for the three-dimensional motion of an elastic structure in an incompressible fluid. *Journal of Mathematical Fluid Mechanics*, 9(2):262–294.
- [Boulakia et al., 2012] Boulakia, M., Schwindt, E. L., and Takahashi, T. (2012). Existence of strong solutions for the motion of an elastic structure in an incompressible viscous fluid. *Interfaces and Free Boundaries*, 14(3):273–306.
- [Boulakia et al., 2018] Boulakia, M., Takahashi, T., and Guerrero, S. (2018). Well-posedness for the coupling between a viscous incompressible fluid and an elastic structure. *HAL preprint <https://hal.inria.fr/hal-01939464/>*.
- [Boyer and Fabrie, 2005] Boyer, F. and Fabrie, P. (2005). *Éléments d’analyse pour l’étude de quelques modèles d’écoulements de fluides visqueux incompressibles*, volume 52. Springer Science and Business Media.
- [Boyer and Fabrie, 2012] Boyer, F. and Fabrie, P. (2012). *Mathematical tools for the study of the incompressible Navier-Stokes equations and related models*, volume 183. Springer Science and Business Media.
- [Brezis, 1999] Brezis, H. (1999). *Analyse fonctionnelle: théorie et applications*, volume 91. Dunod Paris.
- [Brezzi, 1974] Brezzi, F. (1974). On the existence, uniqueness and approximation of saddle-point problems arising from Lagrangian multipliers. *Revue Française d’Automatique, Informatique, Recherche Opérationnelle. Analyse Numérique*, 8(R2):129–151.
- [Briane and Pages, 2018] Briane, M. and Pages, G. (2018). *Théorie de l’intégration*. De Boeck supérieur.
- [Brokaw, 1966] Brokaw, C. J. (1966). Bend propagation along flagella. *Nature*, 209(5019):161–163.
- [Brokaw, 1971] Brokaw, C. J. (1971). Bend propagation by a sliding filament model for flagella. *Journal of Experimental Biology*, 55(2):289–304.
- [Brokaw, 1972] Brokaw, C. J. (1972). Computer simulation of flagellar movement: I. demonstration of stable bend propagation and bend initiation by the sliding filament model. *Biophysical Journal*, 12(5):564–586.
- [Brokaw, 1975] Brokaw, C. J. (1975). Molecular mechanism for oscillation in flagella and muscle. *Proceedings of the National Academy of Sciences*, 72(8):3102–3106.
- [Brokaw, 1985] Brokaw, C. J. (1985). Computer simulation of flagellar movement. VI. Simple curvature-controlled models are incompletely specified. *Biophysical Journal*, 48(4):633–642.

- [Brokaw, 2001] Brokaw, C. J. (2001). Simulating the effects of fluid viscosity on the behaviour of sperm flagella. *Mathematical Methods in the Applied Sciences*, 24(17-18):1351–1365.
- [Brokaw, 2002] Brokaw, C. J. (2002). Computer simulation of flagellar movement VIII. Coordination of dynein by local curvature control can generate helical bending waves. *Cell Motility and the Cytoskeleton*, 53(2):103–124.
- [Brokaw, 2005] Brokaw, C. J. (2005). Computer simulation of flagellar movement IX. Oscillation and symmetry breaking in a model for short flagella and nodal cilia. *Cell Motility and the Cytoskeleton*, 60(1):35–47.
- [Camner et al., 1983] Camner, P., Mossberg, B., and Afzelius, B. A. (1983). Measurements of tracheobronchial clearance in patients with immotile-cilia syndrome and its value in differential diagnosis. *European Journal of Respiratory Diseases. Supplement*, 127:57–63.
- [Cartan, 1967] Cartan, H. (1967). *Calcul différentiel*. Hermann, Paris.
- [Chateau et al., 2017] Chateau, S., Favier, J., D’ortona, U., and Poncet, S. (2017). Transport efficiency of metachronal waves in 3D cilium arrays immersed in a two-phase flow. *Journal of Fluid Mechanics*, 824:931–961.
- [Chatelin, 2013] Chatelin, R. (2013). *Méthodes numériques pour l’écoulement de Stokes 3D: fluides à viscosité variable en géométrie complexe mobile; application aux fluides biologiques*. PhD thesis, Université de Toulouse, Université Toulouse III-Paul Sabatier, <http://thesesups.ups-tlse.fr/2398/>.
- [Chatelin and Poncet, 2016] Chatelin, R. and Poncet, P. (2016). A parametric study of mucociliary transport by numerical simulations of 3d non-homogeneous mucus. *Journal of Biomechanics*, 49(9):1772 – 1780.
- [Chavent, 2010] Chavent, G. (2010). *Nonlinear least squares for inverse problems: theoretical foundations and step-by-step guide for applications*. Springer Science and Business Media.
- [Ciarlet, 1988] Ciarlet, P. G. (1988). *Three-dimensional elasticity*, volume 1 of *Mathematical elasticity*. North-Holland.
- [Cortez, 2001] Cortez, R. (2001). The method of regularized stokeslets. *SIAM Journal on Scientific Computing*, 23(4):1204–1225.
- [Costabel et al., 2010] Costabel, M., Dauge, M., and Nicaise, S. (2010). *Corner Singularities and Analytic Regularity for Linear Elliptic Systems. Part I: Smooth domains*. HAL preprint <https://hal.archives-ouvertes.fr/hal-00453934/>.
- [Court, 2017] Court, S. (2017). Existence of 3D strong solutions for a system modeling a deformable solid inside a viscous incompressible fluid. *Journal of Dynamics and Differential Equations*, 29:737–782.
- [Coutand and Shkoller, 2005] Coutand, D. and Shkoller, S. (2005). Motion of an elastic solid inside an incompressible viscous fluid. *Archive for Rational Mechanics and Analysis*, 176(1):25–102.
- [Coutand and Shkoller, 2006] Coutand, D. and Shkoller, S. (2006). The interaction between quasilinear elastodynamics and the Navier-Stokes equations. *Archive for Rational Mechanics and Analysis*, 179(3):303–352.
- [Dapogny et al., 2014] Dapogny, C., Dobrzynski, C., and Frey, P. (2014). Three-dimensional adaptive domain remeshing, implicit domain meshing, and applications to free and moving boundary problems. *Journal of Computational Physics*, 262:358–378.

- [Dauplain et al., 2008] Dauplain, A., Favier, J., and Bottaro, A. (2008). Hydrodynamics of ciliary propulsion. *Journal of Fluids and Structures*, 24(8):1156 – 1165.
- [Decoene et al., 2018] Decoene, A., Martin, S., and Maury, B. (2018). Direct simulation of rigid particles in a viscoelastic fluid. *Journal of Non-Newtonian Fluid Mechanics*, 260:1–25.
- [Desjardins et al., 2001] Desjardins, B., Esteban, M. J., Grandmont, C., and Le Tallec, P. (2001). Weak solutions for a fluid-elastic structure interaction model. *Revista Matemática Complutense*, 14(2):523–538.
- [Dillon and Fauci, 2000] Dillon, R. H. and Fauci, L. J. (2000). An integrative model of internal axoneme mechanics and external fluid dynamics in ciliary beating. *Journal of Theoretical Biology*, 207(3):415–430.
- [Dillon et al., 2003] Dillon, R. H., Fauci, L. J., and Omoto, C. (2003). Mathematical modeling of axoneme mechanics and fluid dynamics in ciliary and sperm motility. *Dynamics of Continuous Discrete and Impulsive Systems Series A*, 10:745–758.
- [Ding et al., 2014] Ding, Y., Nawroth, J. C., McFall-Ngai, M. J., and Kanso, E. (2014). Mixing and transport by ciliary carpets: a numerical study. *Journal of Fluid Mechanics*, 743:124–140.
- [dos Santos, 2007] dos Santos, N. D. (2007). *Numerical methods for fluid-structure interaction problems with valves*. PhD thesis, Université Pierre et Marie Curie-Paris VI, <https://tel.archives-ouvertes.fr/tel-00521654v2>.
- [Dresdner et al., 1980] Dresdner, R., Katz, D., and Berger, S. (1980). The propulsion by large amplitude waves of uniflagellar micro-organisms of finite length. *Journal of Fluid Mechanics*, 97(3):591–621.
- [Dreyfus et al., 2005] Dreyfus, R., Baudry, J., Roper, M. L., Fermigier, M., Stone, H. A., and Bibette, J. (2005). Microscopic artificial swimmers. *Nature*, 437(7060):862.
- [Du et al., 2003] Du, Q., Gunzburger, M. D., Hou, L. S., and Lee, J. (2003). Analysis of a linear fluid-structure interaction problem. *Discrete and Continuous Dynamical Systems*, 9(3):633–650.
- [Eloy and Lauga, 2012] Eloy, C. and Lauga, E. (2012). Kinematics of the most efficient cilium. *Physical Review Letters*, 109(3):038101.
- [Fabrèges, 2012] Fabrèges, B. (2012). *A smooth extension method for the simulation of fluid/particles flows*. PhD thesis, Université Paris Sud - Paris XI, <https://tel.archives-ouvertes.fr/tel-00763895>.
- [Fabrèges et al., 2013] Fabrèges, B., Gouarin, L., and Maury, B. (2013). A smooth extension method. *Comptes Rendus Mathématique*, 351(9):361–366.
- [Fournié and Lozinski, 2014] Fournié, M. and Lozinski, A. (2014). A fictitious domain approach for fluid-structure interactions based on the extended finite element method. *ESAIM: Proceedings and Surveys*, 45:308–317.
- [Fournié and Lozinski, 2017] Fournié, M. and Lozinski, A. (2017). Stability and optimal convergence of unfitted extended finite element methods with Lagrange multipliers for the stokes equations. In *Geometrically Unfitted Finite Element Methods and Applications*, pages 143–182. Springer.
- [Fulford and Blake, 1986] Fulford, G. and Blake, J. (1986). Muco-ciliary transport in the lung. *Journal of Theoretical Biology*, 121(4):381–402.
- [Galdi, 1999] Galdi, G. P. (1999). On the steady self-propelled motion of a body in a viscous incompressible fluid. *Archive for Rational Mechanics and Analysis*, 148(1):53–88.

- [Girault and Glowinski, 1995] Girault, V. and Glowinski, R. (1995). Error analysis of a fictitious domain method applied to a Dirichlet problem. *Japan Journal of Industrial and Applied Mathematics*, 12(3):487–514.
- [Girault et al., 2001] Girault, V., Glowinski, R., López, H., and Vila, J.-P. (2001). A boundary multiplier/fictitious domain method for the steady incompressible Navier-Stokes equations. *Numerische Mathematik*, 88(1):75–103.
- [Grandmont, 2002] Grandmont, C. (2002). Existence for a three-dimensional steady state fluid-structure interaction problem. *Journal of Mathematical Fluid Mechanics*, 4(1):76–94.
- [Gray and Hancock, 1955] Gray, J. and Hancock, G. (1955). The propulsion of sea-urchin spermatozoa. *Journal of Experimental Biology*, 32(4):802–814.
- [Grisvard, 2011] Grisvard, P. (2011). *Elliptic problems in nonsmooth domains*. SIAM.
- [Gueron and Levit-Gurevich, 1998] Gueron, S. and Levit-Gurevich, K. (1998). Computation of the internal forces in cilia: application to ciliary motion, the effects of viscosity, and cilia interactions. *Biophysical Journal*, 74(4):1658–1676.
- [Gueron and Levit-Gurevich, 2001] Gueron, S. and Levit-Gurevich, K. (2001). A three-dimensional model for ciliary motion based on the internal 9+2 structure. *Proceedings of the Royal Society of London. Series B: Biological Sciences*, 268(1467):599–607.
- [Hancock, 1953] Hancock, G. (1953). The self-propulsion of microscopic organisms through liquids. *Proceedings of the Royal Society of London. Series A. Mathematical and Physical Sciences*, 217(1128):96–121.
- [Hecht, 2012] Hecht, F. (2012). New development in FreeFem++. *Journal of Numerical Mathematics*, 20(3-4):251–266.
- [Higdon, 1979] Higdon, J. (1979). The hydrodynamics of flagellar propulsion: helical waves. *Journal of Fluid Mechanics*, 94(2):331–351.
- [Hines and Blum, 1978] Hines, M. and Blum, J. (1978). Bend propagation in flagella. I. Derivation of equations of motion and their simulation. *Biophysical Journal*, 23(1):41–57.
- [Holwill and Satir, 1987] Holwill, M. E. J. and Satir, P. (1987). Generation of propulsive forces by cilia and flagella. *Cytomechanics*, pages 120–130.
- [Janela et al., 2005] Janela, J., Lefebvre, A., and Maury, B. (2005). A penalty method for the simulation of fluid-rigid body interaction. In *ESAIM: Proceedings*, volume 14, pages 115–123. EDP Sciences.
- [Johnson and Brokaw, 1979] Johnson, R. and Brokaw, C. J. (1979). Flagellar hydrodynamics. a comparison between resistive-force theory and slender-body theory. *Biophysical journal*, 25(1):113–127.
- [Johnson, 1977] Johnson, R. E. (1977). *Slender-body theory for Stokes flow and flagellar hydrodynamics*. PhD thesis, California Institute of Technology, <https://thesis.library.caltech.edu/1435/>.
- [King and Pazour, 2009] King, S. M. and Pazour, G. J. (2009). *Cilia: motors and regulation*, volume 92. Academic Press.
- [Kukavica and Tuffaha, 2012] Kukavica, I. and Tuffaha, A. (2012). Solutions to a fluid-structure interaction free boundary problem. *Discrete and Continuous Dynamical Systems*, 32(4):1355–1389.
- [Lacouture, 2016] Lacouture, L. (2016). *Modélisation et simulation du mouvement de structures fines dans un fluide visqueux: application au transport mucociliaire*. PhD thesis, Paris Saclay, <https://tel.archives-ouvertes.fr/tel-01366885/>.

- [Laitinen et al., 1985] Laitinen, L., Heino, M., Laitinen, A., Kava, T., and Haahtela, T. (1985). Damage of the airway epithelium and bronchial reactivity in patients with asthma 1–3. *American Review of Respiratory Disease*, 131(4):599–606.
- [Lauga and Eloy, 2013] Lauga, E. and Eloy, C. (2013). Shape of optimal active flagella. *Journal of Fluid Mechanics*, 730.
- [Le Dret, 2003] Le Dret, H. (2003). Méthodes mathématiques en élasticité. *Notes de cours de DEA, Université Pierre et Marie Curie*, <https://www.ljll.math.upmc.fr/MathModel/enseignement/polycopies/ledret-elasticite.pdf>.
- [Lighthill, 1952] Lighthill, M. J. (1952). On the squirming motion of nearly spherical deformable bodies through liquids at very small Reynolds numbers. *Communications on Pure and Applied Mathematics*, 5(2):109–118.
- [Lighthill, 1976] Lighthill, M. J. (1976). Flagellar hydrodynamics. *SIAM Review*, 18(2):161–230.
- [Logg et al., 2012] Logg, A., Mardal, K.-A., and Wells, G. (2012). *Automated solution of differential equations by the finite element method: The FEniCS book*, volume 84. Springer Science and Business Media.
- [Lozinski, 2016] Lozinski, A. (2016). A new fictitious domain method: Optimal convergence without cut elements. *Comptes Rendus Mathématique*, 354(7):741–746.
- [Lubliner and Blum, 1971] Lubliner, J. and Blum, J. (1971). Model for bend propagation in flagella. *Journal of Theoretical Biology*, 31(1):1 – 24.
- [Ludwig, 1930] Ludwig, W. (1930). Zur theorie der flimmerbewegung (dynamik, nutzeffekt, energiebilanz). *Zeitschrift für vergleichende Physiologie*, 13(3):397–504.
- [Lukens et al., 2010] Lukens, S., Yang, X., and Fauci, L. (2010). Using Lagrangian coherent structures to analyze fluid mixing by cilia. *Chaos: An Interdisciplinary Journal of Nonlinear Science*, 20(1):017511.
- [Machin, 1958] Machin, K. (1958). Wave propagation along flagella. *Journal of Experimental Biology*, 35(4):796–806.
- [Machin, 1963] Machin, K. (1963). The control and synchronization of flagellar movement. *Proceedings of the Royal Society of London. Series B. Biological Sciences*, 158(970):88–104.
- [Maury, 2009] Maury, B. (2009). Numerical analysis of a finite element/volume penalty method. *SIAM Journal on Numerical Analysis*, 47(2):1126–1148.
- [Mitran, 2007] Mitran, S. M. (2007). Metachronal wave formation in a model of pulmonary cilia. *Computers and structures*, 85(11):763–774.
- [Moës and Belytschko, 2002] Moës, N. and Belytschko, T. (2002). X-FEM, de nouvelles frontières pour les éléments finis. *Revue Européenne des Eléments*, 11(2-4):305–318.
- [Murase, 1992] Murase, M. (1992). *The dynamics of cellular motility*. John Wiley and Sons.
- [Nečasová et al., 2011] Nečasová, Š., Takahashi, T., and Tucsnak, M. (2011). Weak solutions for the motion of a self-propelled deformable structure in a viscous incompressible fluid. *Acta Applicandae Mathematicae*, 116(3):329–352.
- [Nocedal, 1980] Nocedal, J. (1980). Updating quasi-Newton matrices with limited storage. *Mathematics of computation*, 35(151):773–782.
- [Oevermann and Klein, 2006] Oevermann, M. and Klein, R. (2006). A Cartesian grid finite volume method for elliptic equations with variable coefficients and embedded interfaces. *Journal of Computational Physics*, 219(2):749–769.

- [Osterman and Vilfan, 2011] Osterman, N. and Vilfan, A. (2011). Finding the ciliary beating pattern with optimal efficiency. *Proceedings of the National Academy of Sciences*, 108(38):15727–15732.
- [Panfilov et al., 2005] Panfilov, A. V., Keldermann, R., and Nash, M. (2005). Self-organized pacemakers in a coupled reaction-diffusion-mechanics system. *Physical Review Letters*, 95(25):258104.
- [Payan and Ohayon, 2017] Payan, Y. and Ohayon, J. (2017). *Biomechanics of living organs: hyperelastic constitutive laws for finite element modeling*. Academic Press.
- [Perret, 1998] Perret, B. (1998). *Étude de quelques méthodes de domaine fictif et applications aux ondes électromagnétiques*. PhD thesis.
- [Peskin, 2002] Peskin, C. S. (2002). The immersed boundary method. *Acta numerica*, 11:479–517.
- [Pezzuto et al., 2014] Pezzuto, S., Ambrosi, D., and Quarteroni, A. (2014). An orthotropic active-strain model for the myocardium mechanics and its numerical approximation. *European Journal of Mechanics-A/Solids*, 48:83–96.
- [Purcell, 1977] Purcell, E. M. (1977). Life at low Reynolds number. *American Journal of Physics*, 45(1):3–11.
- [Raymond and Vanninathan, 2014] Raymond, J.-P. and Vanninathan, M. (2014). A fluid-structure model coupling the Navier-Stokes equations and the Lamé system. *Journal de Mathématiques Pures et Appliquées*, 102(3):546 – 596.
- [San Martín et al., 2008] San Martín, J., Scheid, J.-F., Takahashi, T., and Tucsnak, M. (2008). An initial and boundary value problem modeling of fish-like swimming. *Archive for Rational Mechanics and Analysis*, 188(3):429–455.
- [Sanderson and Sleight, 1981] Sanderson, M. and Sleight, M. (1981). Ciliary activity of cultured rabbit tracheal epithelium: beat pattern and metachrony. *Journal of Cell Science*, 47(1):331–347.
- [Shen et al., 1975] Shen, J., Tam, P., Shack, W., and Lardner, T. (1975). Large amplitude motion of self-propelling slender filaments at low Reynolds numbers. *Journal of Biomechanics*, 8(3):229 – 236.
- [Smith et al., 2008] Smith, D. J., Gaffney, E. A., and Blake, J. R. (2008). Modelling mucociliary clearance. *Respiratory Physiology and Neurobiology*, 163(1):178–188.
- [Smith, 2004] Smith, N. P. (2004). A computational study of the interaction between coronary blood flow and myocardial mechanics. *Physiological Measurement*, 25(4):863.
- [Tawada and Oosawa, 1972] Tawada, K. and Oosawa, F. (1972). Responses of Paramecium to temperature change. *The Journal of Protozoology*, 19(1):53–57.
- [Taylor, 1951] Taylor, G. (1951). Analysis of the swimming of microscopic organisms. In *Proceedings of the Royal Society of London A: Mathematical, Physical and Engineering Sciences*, volume 209, pages 447–461. The Royal Society.
- [Taylor, 1952] Taylor, G. (1952). The action of waving cylindrical tails in propelling microscopic organisms. *Proceedings of the Royal Society of London. Series A. Mathematical and Physical Sciences*, 211(1105):225–239.
- [Taylor, 1967] Taylor, G. (1967). Film notes for low-Reynolds number flows. Technical report, National Committee for fluid mechanics films.
- [Tomas, 1997] Tomas, L. (1997). An error estimate for a fictitious domain formulation using volumic Lagrange multipliers of a Dirichlet problem. *Comptes Rendus de l'Academie des Sciences Series I Mathematics*, 325(7):793–796.

- [Wheatley et al., 1996] Wheatley, D. N., Wang, A. M., and Strugnell, G. E. (1996). Expression of primary cilia in mammalian cells. *Cell Biology International*, 20(1):73–81.
- [Yang et al., 2008] Yang, X., Dillon, R. H., and Fauci, L. J. (2008). An integrative computational model of multiciliary beating. *Bulletin of Mathematical Biology*, 70(4):1192–1215.
- [Yu, 2005] Yu, Z. (2005). A DLM/FD method for fluid/flexible-body interactions. *Journal of Computational Physics*, 207(1):1–27.

Contents

1	Introduction	1
1.1	Sur la vie à bas nombre de Reynolds	1
1.1.1	Mécanique des fluides à bas nombre de Reynolds	2
1.1.2	Zoologie des déformations des cils et flagelles	4
1.1.3	Mécanismes de déformation des cils eukaryotes	6
1.1.4	Motivations et applications	8
1.2	Modélisation mathématique des cils et flagelles	9
1.2.1	Le modèle historique de Taylor	9
1.2.2	Les débuts de l'étude du mouvement des cils	9
1.2.3	Modèles à mouvement imposé	10
1.2.4	Modélisation de l'activité interne des cils	12
1.2.5	Étude mathématique de problèmes d'interaction fluide-structure avec structures actives	15
1.2.6	Positionnement de la thèse	16
1.3	Résultats principaux	17
1.3.1	Résumé du Chapitre 2	17
1.3.2	Résumé du Chapitre 3	20
1.3.3	Résumé du Chapitre 4	23
2	A continuum active structure model for the interaction of cilia with a viscous fluid	29
2.1	Introduction	29
2.2	A continuum active structure model	32
2.2.1	The active-stress method	32
2.2.2	The problem of active elasticity	32
2.2.3	Application to cilia-like structures	33
2.2.4	Examples of internal activity	34
2.3	A coupled fluid-structure interaction problem with cilia-like structures	39
2.3.1	Description of the model	40
2.3.2	The discrete-in-time fluid-structure interaction problem	42
2.3.3	Existence and uniqueness of a weak solution to the linearized fluid-structure interaction problem	44
2.3.4	A saddle-point formulation for the fluid-active structure interaction problem	47
2.4	Numerical simulations of active structures in a viscous fluid	49
2.4.1	Description of the method	49
2.4.2	Influence of the fluid viscosity	51

2.4.3	Interaction of two cilia in a viscous fluid	57
2.4.4	Discussion	59
3	Existence and uniqueness for a quasi-static interaction problem between a viscous fluid and an active structure	63
3.1	Introduction	63
3.2	Notations and preliminaries	68
3.2.1	Technical lemma	68
3.2.2	Assumptions and preliminary results	69
3.3	Main result	71
3.4	Structure equations	74
3.5	Fluid equations	78
3.6	Fixed point procedure. Proof of Theorem 3.1	80
3.7	More general conditions on the data	87
4	A smooth extension method for transmission problems	89
4.1	Introduction	89
4.2	Presentation of the method	90
4.2.1	The smooth extension formulation	91
4.2.2	Formulation as an optimization problem	95
4.2.3	On convergence rates for the numerical method	100
4.2.4	Particular case for strictly included domains	104
4.3	Validation of the method	107
4.3.1	Numerical procedure for the smooth extension method	108
4.3.2	Test case 1: the transmission Laplace problem in the unit square . .	108
4.3.3	Test case 2: the transmission Laplace problem with a spherical inclusion	112
4.3.4	Test case 3: the transmission Laplace problem in a L-shape domain .	114
4.4	Extension to other coupled problems	114
4.4.1	The Stokes transmission problem	116
4.4.2	A fluid-structure interaction problem	121
4.5	Conclusion	131
5	Conclusion et perspectives	133
A	Proofs of theorems related to the smooth extension method	137
A.1	Proofs of theorems related to the Stokes transmission problem	137
A.2	Proofs of theorems related to the fluid-structure interaction problem	142
B	Transformation of the Stokes equations into the reference configuration	149
B.1	Deformations	149
B.2	Transformation from the deformed configuration to the reference configuration	150
B.2.1	Preliminaries	150
B.2.2	Transformation of volumes	151
B.2.3	Transformation of the divergence of a vector function	151
B.2.4	Transformation of the divergence of a matrix function	152
B.2.5	The Piola transform	153
B.3	Application to the transformation of the Stokes equations	154
	Bibliography	157
	Contents	165

<i>Contents</i>	167
List of Figures	169
List of Tables	173

List of Figures

1.1	Aperçu général de quelques micro-organismes possédant des cils ou des flagelles et autres organismes associés. Image tirée de [Lighthill, 1976]. Les micro-organismes possédant des cils sont représentés à l'intérieur du cercle au centre de la figure.	5
1.2	Cils bronchiques (a) et <i>Chlamydomonas reinhardtii</i> (b).	7
1.3	Schéma représentant la coupe transversale d'un cil eucaryotes.	7
2.1	Bending of an elongated elastic structure with the internal activity given by (2.5) at different times: $t = 0\text{s}$ (a), $t = 0.012\text{s}$ (b), and $t = 0.025\text{s}$ (c). The activity scenario Σ_a is plotted, with the set of parameters be given in Table 2.1.	35
2.2	Deformation of an elongated structure subjected to the internal activity defined by (2.6) at different times: $t = 0\text{s}$ (a), $t = 0.012\text{s}$ (b), $t = 0.025\text{s}$ (c) and $t = 0.037\text{s}$ (d). The activity scenario Σ_a is represented with the set of parameters be given in Table 2.2.	36
2.3	Elongated structure subjected to the internal activity defined by (2.7) inducing cilia-like deformations at different time: $t = 0\text{s}$ (a), $t = 0.015\text{s}$ (b), $t = 0.035\text{s}$ (c), $t = 0.050\text{s}$ (d), $t = 0.050\text{s}$ (h), $t = 0.065\text{s}$ (g), $t = 0.085\text{s}$ (f), and $t = 0.1\text{s}$ (e). The activity scenario Σ_a is represented with the set of parameters be given in Table 2.3.	38
2.4	Elongated three-dimensional structure subjected to the internal activity defined by (2.8) inducing twirling at different time: $t = 0\text{s}$ (a), $t = 0.052\text{s}$ (b), $t = 0.082\text{s}$ (c), $t = 0.107\text{s}$ (f), and $t = 0.128\text{s}$ (e). The activity scenario Σ_a in represented with the set of parameters be given in Table 2.4.	39
2.5	One cilium beating in a viscous fluid of viscosity $\mu_f = 0.01\text{pN} \cdot \mu\text{m} \cdot \text{s}$ at different times: $t = 0.091\text{s}$ (a), $t = 0.110\text{s}$ (b), $t = 0.120\text{s}$ (c), and $t = 0.166\text{s}$ (d). The activity scenario of the structure is given by (2.7).	53
2.6	One cilium beating in a viscous fluid at time $t = 0.128\text{s}$ (left) and at time $t = 0.171\text{s}$ (right) for different values of the fluid viscosity: $\mu_f = 0.01\text{pN} \cdot \mu\text{m}^{-1} \cdot \text{s}$ (a, b), $\mu_f = 0.02\text{pN} \cdot \mu\text{m}^{-1} \cdot \text{s}$ (c, d) and $\mu_f = 0.04\text{pN} \cdot \mu\text{m}^{-1} \cdot \text{s}$ (e, f). The activity scenario of the structure is given by (2.7).	54
2.7	Mean deformation of the solid as a function of the time for different values of the fluid viscosity (in $\text{pN} \cdot \mu\text{m}^{-2} \cdot \text{s}$).	55
2.8	Time average of the solid deformation as a function of the viscosity of the fluid. 56	
2.9	Mean horizontal velocity of the fluid in function of the time for different values of the fluid viscosity (in $\text{pN} \cdot \mu\text{m}^{-2} \cdot \text{s}$).	56

2.10	Time average of the horizontal fluid velocity in function of the viscosity of the fluid (a) and horizontal velocity of the fluid as a function of the height for different values of the viscosity (b).	57
2.11	Two cilia beating in a viscous fluid with $\mu_f = 0.01\text{pN} \cdot \mu\text{m}^{-2} \cdot \text{s}$ at $t = 0.788\text{s}$ (a) and $t = 0.83\text{s}$ (b). The cilia are anchored at $x_{c_1} = 7.5$ and $x_{c_2} = 12.5$. The phase shift between the two cilia is $\delta\phi = 0.075\text{s}$	58
2.12	Trajectories of the two cilia summits for different values of the phase shift between their activity scenario: $\delta\phi = 0.025$ (a) and $\delta\phi = 0.075$ (b).	59
2.13	Horizontal velocity of the fluid as a function of the height for different values of the phase shift (a) and time average of the horizontal fluid velocity in function of the phase shift (b).	60
2.14	Horizontal velocity of the fluid as a function of the height for different values of the distance between the two cilia (a) and time average of the horizontal fluid velocity in function of the distance (b).	60
2.15	Three-dimensional simulation of a cilium-like structure in a viscous fluid. . .	61
3.1	Two-dimensional example of the geometry of the fluid-structure problem. . .	65
4.1	Two-dimensional example of a geometry considered for the proof of the smooth extension.	102
4.2	Construction of the function ξ_0 and its regular extension, $\tilde{\xi}_0$	103
4.3	Two dimensional representation of the geometry for the Laplace transmission problems (4.1).	109
4.4	Numerical solution for the Laplace problem (4.1) with $\mu_1 = 1$, $\mu_2 = 10$, $f_1 = 1$, $f_2 = 1$ and $x_\Gamma = 0.57$. We compare the reference solution \bar{u} obtained with the standard finite element method on a fine mesh (a) to the one obtained through the smooth extension method (c). The fields u_1^g (b) and u_2^g (d) are superposed (c) to show the continuity through the interface Γ despite the use of non-conformal meshes. For the SEM, the mesh is 16×16	110
4.5	Rates of convergence in space for the finite element method ($P1$ elements) applied to the resolution of the Laplace problem (4.1) with $\mu_1 = 1$, $\mu_2 = 10$, $f_1 = 1$, $f_2 = 1$ and $x_\Gamma = 0.57$. The solution with a conformal mesh (a) is compare to the one with a non-conformal mesh (b)	111
4.6	Rates of convergence in space for the smooth extension method applied to the resolution of the Laplace transmission problem with homogeneous boundary conditions (4.1) , with $\mu_1 = 1$, $\mu_2 = 10$, $f_1 = 1$, $f_2 = 2$ and $x_\Gamma = 0.67$	112
4.7	Two dimensional representation of the geometry for the Laplace transmission problem (4.17).	113
4.8	Rates of convergence in space for the smooth extension method applied to the resolution of the Laplace transmission problem with a strictly included subdomain Ω_2 (4.17), for $\mu_1 = 1$, $\mu_2 = 10$, $f_1 = 1$, $f_2 = 2$, $(x_c, y_c) = (0.62, 0.43)$ and $r_c = 0.2$	113
4.9	Two dimensional representation of the geometry for the Laplace transmission problem (4.1) in a L-shape domain.	114
4.10	Rates of convergence in space for the smooth extension method applied to the resolution of the Laplace transmission problem (4.1) in a L-shape domain.	115
4.11	Two dimensional representation of the geometry for the Stokes transmission problem.	120

- 4.12 Representation of the solution for the Stokes transmission problem (4.24) with $\mu_1 = 1$, $\mu_2 = 10$, $f_1 = (1, 0)$, $f_2 = (1, 0)$, $\alpha_\Gamma = 0.25$ and $\beta_\Gamma = 0.5$. On the top, we compare the magnitude of the fluid velocity obtained with a standard finite element method (a) and with the smooth extension method (b). On the bottom, we compare the pressure of the fluid computed with the classical finite element method (c) and the smooth extension method (d). The interface Γ is highlighted with a white curve. 122
- 4.13 Two dimensional representation of the initial geometry for the fluid-structure problem. 129
- 4.14 Comparison of the stationary states obtained through the Smooth Extension method and the ALE method (a). The darkest grey mesh represents the equilibrium position of the beam obtained with the ALE method. The lightest grey mesh represents the initial position of the beam. The other three meshes represent the equilibrium positions of the beam obtained with the Smooth Extension method for different coarsening ratios (0.99, 0.71, 0.46): the lighter is the colour the coarser is the fluid mesh. Zoom on the tips of the beams (b). 130
- 4.15 Distance d_{SEM}^{ALE} between the two solid configuration Ω_s^{SEM} and Ω_s^{ALE} in function of the time (a). Global norm in time $\|d_{SEM}^{ALE}\|$ in function of the coarsening ratio of the fluid mesh in the Smooth Extension method (b). . . 131

List of Tables

2.1	Set of parameters for the bending scenario of activity.	35
2.2	Set of parameters for the flapping scenario of activity.	36
2.3	Set of parameters for the non symmetric scenario of activity.	37
2.4	Set of parameters for the twirling scenario of activity in three space dimensions.	39
4.1	Comparison of the rates of convergence between the finite element method (FEM) with a conformal mesh, the FEM with a non-conformal mesh and the smooth extension method (SEM) with a non-conformal mesh for different test cases.	115

Titre : Structures actives dans un fluide visqueux : modélisation, analyse mathématique et simulations numériques

Mots Clefs : Équations aux dérivées partielles, Interaction fluide-structure, Élasticité active, Écoulement visqueux.

Résumé : Le transport de micro-organismes et de fluides biologiques au moyen de cils et flagelles est un phénomène universel que l'on retrouve chez presque tous les êtres vivants. Le but de cette thèse est la modélisation, l'analyse mathématique et la simulation numérique de problèmes d'interaction fluide-structure qui font intervenir des structures actives, capables de se déformer d'elles-mêmes grâce à des contraintes internes, et un fluide à faible nombre de Reynolds, modélisé par les équations de Stokes. Le Chapitre 2 traite de la modélisation de ces structures actives en considérant la loi de Saint Venant-Kirchhoff dans les équations de l'élasticité et en ajoutant un terme d'activité au second tenseur de contraintes de Piola-Kirchhoff. Les équations fluide et structures sont couplées à l'interface fluide-structure et l'étude mathématique d'un problème linéarisé et discrétisé en temps est ensuite réalisée. Une reformulation sous forme d'un problème point-selle est proposée et utilisée pour la simulation numérique du problème. Le Chapitre 3 s'intéresse à l'analyse du problème d'interaction fluide-structure quasi-statique avec une structure active, pour lequel nous montrons l'existence et l'unicité, pour des données petites, d'une solution forte localement en temps. Le Chapitre 4 présente une nouvelle méthode de type domaine fictif (la *méthode de prolongement régulier*) pour la résolution numérique de problèmes de transmission. La méthode est d'abord développée pour un problème de transmission de Laplace, puis étendue aux problèmes de transmission de Stokes et d'interaction fluide-structure.

Title: Active structures in a viscous fluid: model, mathematical analysis and numerical simulations

Keys words: Partial differential equations, Fluid-structure interaction, Active elasticity, Viscous flow.

Abstract: The transport of microorganisms and biological fluids by means of cilia and flagella is an universal phenomenon found in almost all living beings. The aim of this thesis is to model, analyze and simulate mathematical fluid-structure interaction problems involving active structures, capable of deforming themselves through internal stresses, and a low Reynolds number fluid, modeled by Stokes equations. In Chapter 2, these active structures are modeled as elastic materials satisfying Saint Venant-Kirchhoff law for elasticity whose activity comes from the addition of an activity term to the second Piola-Kirchhoff stress tensor. Elasticity and Stokes equations are coupled on the fluid-structure interface and the mathematical study of the linearized problem discretized in time is realized. Then, the problem is formulated as a saddle-point problem which is used for numerical simulations. Chapter 3 focuses on the analysis of a quasi-static fluid-structure with an active structure, for which we show existence and uniqueness, for small data, of a strong solution locally in time. Chapter 4 presents a new fictitious domain method (the *smooth extension method*) for the numerical resolution of transmission problems. The method is first developed for a Laplace transmission problem and further extended to Stokes transmission and fluid-structure interaction problems.

